NASA Conference Publication 10132

High-Speed Research: Sonic Boom Volume I

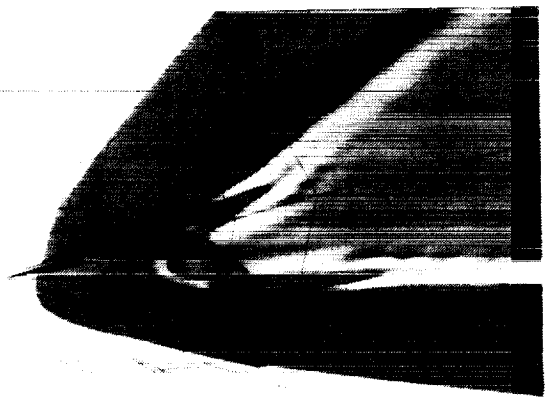

Proceedings of a conference sponsored by the National Aeronautics and Space Administration, Washington, D.C., and held at Ames Research Center, Moffett Field, California May 12–14, 1993

NASA Conference Publication 10132

High-Speed Research: Sonic Boom Volume I

Edited by
Thomas A. Edwards
Aerothermodynamics Branch
Ames Research Center
Moffett Field, California

Proceedings of a conference spnsored by the National Aeronautics and Space Administration, Washington, D.C., and held at Ames Research Center, Moffett Field, California May 12–14, 1993

National Aeronautics and Space Administration

Ames Research Center
Moffett Field, California 94035-1000

1994

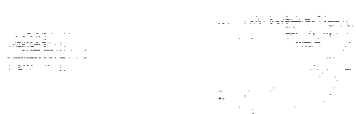

CONTENTS

Preface

Volume I

The second High Speed Research Program Sonic Boom Workshop was held at NASA Ames Research Center May 12-14, 1993. The purpose of this workshop was to provide a forum for government, industry and university participants to present and discuss progress in their research. The workshop was organized into three sessions dealing with atmospheric propagation, acceptability and configuration design. Attendance at the workshop was by invitation only.

This volume of the workshop proceedings includes papers on atmospheric propagation and acceptability studies. Significant progress is noted in these areas in the time since the previous workshop a year earlier. In particular, several papers demonstrate an improved capability to model the effect of atmospheric turbulence on sonic booms. This is a key issue in determining the stability and, ultimately, the acceptability, of shaped sonic booms. In the area of acceptability, the PLdB metric has withstood considerable scrutiny and is validated as a loudness metric for a wide variety of sonic boom shapes. The differential loudness of asymmetric sonic booms is better understood, too.

Progress in Modeling Atmospheric Propagation of Sonic Booms

Allan D. Pierce
The Pennsylvania State University
Graduate Program in Acoustics
157 Hammond Building
University Park, PA, 16802

Presentation at NASA HSR Sonic Boom Workshop
NASA Ames Research Center
May 12-14, 1993

The improved simulation of sonic boom propagation through the real atmosphere requires greater understanding of how the transient acoustic pulses popularly termed sonic booms are affected by humidity and turbulence. A realistic atmosphere is invariably somewhat turbulent, and may be characterized by an ambient fluid velocity v and sound speed c that vary from point to point. The absolute humidity will also vary from point to point, although possibly not as irregularly. What is ideally desired is a relatively simple scheme for predicting the probable spreads in key sonic boom signature parameters. Such parameters could be peak amplitudes, rise times, or gross quantities obtainable by signal processing that correlate well with annoyance or damage potential. The practical desire for the prediction scheme is that it require a relatively small amount of knowledge, possibly of a statistical nature, concerning the atmosphere along the propagation path from the aircraft to the ground. The impact of such a scheme, if developed, implemented, and verified, would be that it would give the persons who make planning decisions a tool for assessing the magnitude of environmental problems that might result from any given overflight or sequence of overflights.

Realistic Sonic Boom Propagation Problem

- Turbulent atmosphere
  - diffraction by smaller turbulent eddies
  - focusing and defocusing by larger turbulent eddies
- Molecular relaxation important
  - Humidity controls molecular relaxation
- Nonlinear distortion
  - tendency toward waveform steepening
  - stretching of waveform
  - more rapid elimination of very narrow spikes
  - overtaking of closely-spaced shocks

PENNSTATE

The technical approach that has been followed by the author and some of his colleagues is to formulate a hierarchy of simple approximate models based on fundamental physical principles and then to test these models against existing data.

For propagation of sonic booms and of other types of acoustic pulses in nonturbulent model atmospheres, there exists a basic overall theoretical model that has evolved as an outgrowth of geometrical acoustics. This theoretical model depicts the sound as propagating within ray tubes in a manner analogous to sound in a waveguide of slowly varying cross-section. Propagation along the ray tube is quasi-one-dimensional, and a wave equation for unidirectional wave propagation is used. A nonlinear term is added to this equation to account for nonlinear steepening, and the formulation has been carried through to allow for spatially varying sound speed, ambient density, and ambient wind velocities. The model intrinsically neglects diffraction, so it cannot take into account what has previously been mentioned in the literature as possibly important mechanisms for turbulence-related distortion. The model as originally developed could predict an idealized N-waveform which often agrees with data in terms of peak amplitude and overall positive phase duration. It is possible, moreover, to develop simple methods based on the physics of relaxation processes for incorporating molecular relaxation into the quasi-one-dimensional model of nonlinear propagation along ray tubes.

Simpler Propagation Models

- Propagation along ray tubes
  - stratified atmosphere
  - turbulence ignored
  - spiking and roundening effects not predicted
- Model can account for
  - gross magnification and demagnification
  - nonlinear distortion
  - molecular relaxation contribution to rise times

PENNSTATE

There are currently two methods that are in use for carrying out such an incorporation of relaxation phenomena into propagation predictions; one is a numerical algorithm that arose out of the 1973 doctoral dissertation by Pestorius, which carries forward the propagation along a ray tube as an alternating sequence of two basic types of steps. In one step one has linear propagation of a Fourier superposition of frequency components, and each frequency component is shifted in phase and attenuated in an appropriate manner with propagation along a given distance interval. In the other step, the nonlinear distortion is carried out according to inviscid weak shock theory through the same distance interval.

The author and his colleagues, on the other hand, have been working with an explicit set of approximate partial differential equations analogous to Burgers' equation, an early version of which can be found in the author's 1981 textbook. One very simple model that has been used by the author and his colleagues is what is termed the asymptotic quasi-steady theory of sonic boom waveforms.

Solution Techniques

- Transient evolution using Pestorius algorithm
  - split-step algorithm
  - nonlinear distortion step
  - molecular relaxation step using Fourier transforms
- Asymptotic quasi-steady theory
  - basic waveform shape predicted with neglect of molecular relaxation
  - rise-phase corrected for molecular relaxation
  - correction based on local humidity, temperature, and net pressure jump in shock

PENNSTATE

The asymptotic quasi-steady theory predicts an explicit waveform shape near the leading shock, given the waveform peak amplitude and the local humidity and temperature. The model incorporates modecular relaxation, which is slower for dryer air and consequently a cause of sharper bangs in humid air.

This can alternately be termed the "steady-state" model or the "quasi-frozen waveform" model. The terminology is not ideal, and one must first understand the detailed assumptions involved before adopting any conceptions about what the terminology implies. The ideas involved go back to early papers by G. I. Taylor and Richard Becker on the structure of shock waves, only here the mechanisms of interest are molecular relaxation rather than viscosity or thermal conduction. The first tenet of the theory is that molecular relaxation is important only in the rise phase of waveforms. Such seems justified because the characteristic times, such as positive phase duration, associated with other portions of the waveform are invariably much longer than the characteristic relaxation times for molecular relaxation. During most of the time at which the waveform is being received, it is reasonable to assume that the air is in complete quasi-static thermodynamic equilibrium. Molecular relaxation is a nonequilibrium thermodynamic phenomenon and is important only when pressure is changing rapidly, with characteristic times of the order of a few milliseconds or less.

Molecular-relaxation correction

- Rise-phase prediction near $t = t_{\text{sh}}$:

$$p = (\Delta p)_{\text{sh}} f_{\text{rise}}(t - t_{\text{sh}}, \text{parameters})$$

$$f_{\text{rise}}(\tau, \text{parameters}) \to 0 \quad \text{as} \quad \tau \to -\infty$$

$$f_{\text{rise}}(\tau, \text{parameters}) \to (\Delta p)_{\text{sh}} \quad \text{as} \quad \tau \to +\infty$$

- parameters are $(\Delta p)_{\text{sh}}$, temperature, and humidity

- Composite expression:

$$\begin{aligned} p =& p_{\text{basic}}(t) H(t_{\text{sh}} - t) \\ &+ (\Delta p)_{\text{sh}} f_{\text{rise}}(t - t_{\text{sh}}, \text{parameters}) \\ &+ \left[p_{\text{basic}}(t) - (\Delta p)_{\text{sh}}\right] H(t - t_{\text{sh}}) \end{aligned}$$

PENNSTATE

A second hypothesis, which is related to the first, but which requires extensive analysis for its justification, is that the rise phase of the waveform is determined solely by the peak overpressure of the shock and the local properties of the atmosphere. Strictly speaking, one expects the waveform received at a local point to be the result of a gradual evolution that took place over the entire propagation path, so it depends in principle on the totality of the atmospheric properties along the path. However, an N-wave shape, or at least the positive phase portion, is often established fairly close to the source (i.e., the flight trajectory in the case of sonic boom generation) relative to the overall propagation distance. With increasing propagation distance, the peak overpressure decreases, but does so very slowly, and the positive phase duration increases, but also does so very slowly. There is a net loss of energy from the wave and the loss takes place almost entirely within the rise phases of the shocks. However, the manner in which the peak overpressure decreases and the positive phase duration increases is virtually independent of the energy loss mechanism.

One should note in particular that the model based on the asymptotic quasi-steady theory predicts rise times.

Rise-time prediction

- $(\Delta t)_{\text{rise}}$ is time interval for $f_{\text{rise}}(t - t_{\text{sh}}, \text{parameters})$ to rise from 0.1 to 0.9.
- parameters are $(\Delta p)_{\text{sh}}$, temperature, and humidity
- $(\Delta t)_{\text{rise}}$ is function of "parameters"

$$(\Delta t)_{\text{rise}} = F([\Delta p]_{\text{sh}}, \text{temperature}, \text{humidity})$$

where F is "universal" function.

PENNSTATE

The viewgraph here sketches the principal ideas that are embodied in calculating the rise-phase of a sonic boom profile according to the quasi-static theory. The parameter ξ in the diagram is $x - v_{sh}t$. Ahead of the shock the overpressure p is asymptotically zero, and the theory predicts the manner in which it approaches zero. Behind the shock p asymptotically approaches the net shock overpressure P_{sh}, and here again the theory predicts the manner in which this asymptotic limit is achieve. For points in between one must must numerically solve a set of coupled ordinary nonlinear differential equations. One interesting aspect of the solution is that the nitrogen relaxation is only important is the later portion of this rise phase.

Early rise phase: O_2 relaxation dominates
Later rise phase: N_2 relaxation dominates

The theoretical rise phase is determined using asymptotic and numerical solution methods:

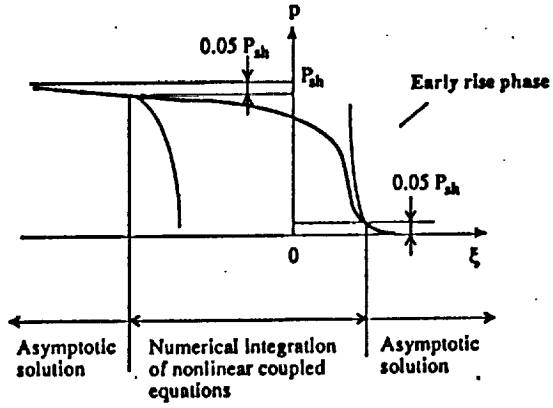

PENNSTATE

Kang carried out detailed comparisons of the predictions of the frozen-profile model with actual waveforms of sonic booms, recorded by the US Air Force in the Mojave Desert in 1987. The original comparison reported in Kang's doctoral thesis, unfortunately, was flawed because the reflection at the ground was incorrectly taken into account. (That such may have been the case was first suggested to the author by Gerry McAninch as a result of a conversation with Alan Wenzel.)

Waveforms measured during flight tests

at ground level

- $(\Delta t)_{\text{rise}}$ can be measured for each data sample.
- Theory predicts

$$(\Delta t)_{\text{rise}} = F([\Delta p]_{\text{sh}}, \text{temperature}, \text{humidity})$$

  where F is "universal" function.

- For comparison of data with theory, what value of $[\Delta p]_{\text{sh}}$ does one use in the "universal function" F?
- Theory is based on idealization of plane wave propagating in one direction through unbounded medium. Measurements were made on the ground

PENNSTATE

The corrected procedure takes the ground as rigid and the reflection process as linear, so that the waveform at the ground has the same time dependence as the incident wave, only the amplitude is twice as great. The theoretical predictions based on accumulated nonlinear effects for a unidirectional propagating wave are applicable to the so-inferred incident wave.

Rigid ground idealization:

- $$p_{\text{ground}} = 2p_{\text{inc}}; \qquad (\Delta p)_{\text{sh,grnd}} = 2(\Delta p)_{\text{sh,inc}}$$
- Theory predicts a function F, where

  $$(\Delta t)_{\text{rise}} = F\big([\Delta p]_{\text{sh,inc}}, \text{temperature}, \text{humidity}\big)$$

  decreases with increasing (Δp) roughly as $(\Delta p)^{-1}$
- Previous comparisons were erroneously based on above with argument taken as $[\Delta p]_{\text{sh,grnd}}$ rather than $(1/2)[\Delta p]_{\text{sh,grnd}}$
- Using a (Δp) that is too large by a factor of 2 means you tend to underpredict the rise time.

PENNSTATE

This summarizes the comparison of rise time data with the asymptotic quasi-steady-state theory. The overpressures on the horizontal axis are those actually observed in waveforms recorded at the ground. The theoretical curve is derived assuming that the incident wave's overpressure is one-half of what is measured. All of the data was taken at times when the humidity and temperature were very nearly the same, so one theoretical curve suffices for the entire data set. The data was taken in 1987 in the Mojave desert, with various airplanes, flying at various altitudes and with various Mach numbers. The relative humidity was 24% and the temperature at the ground was 33° C.

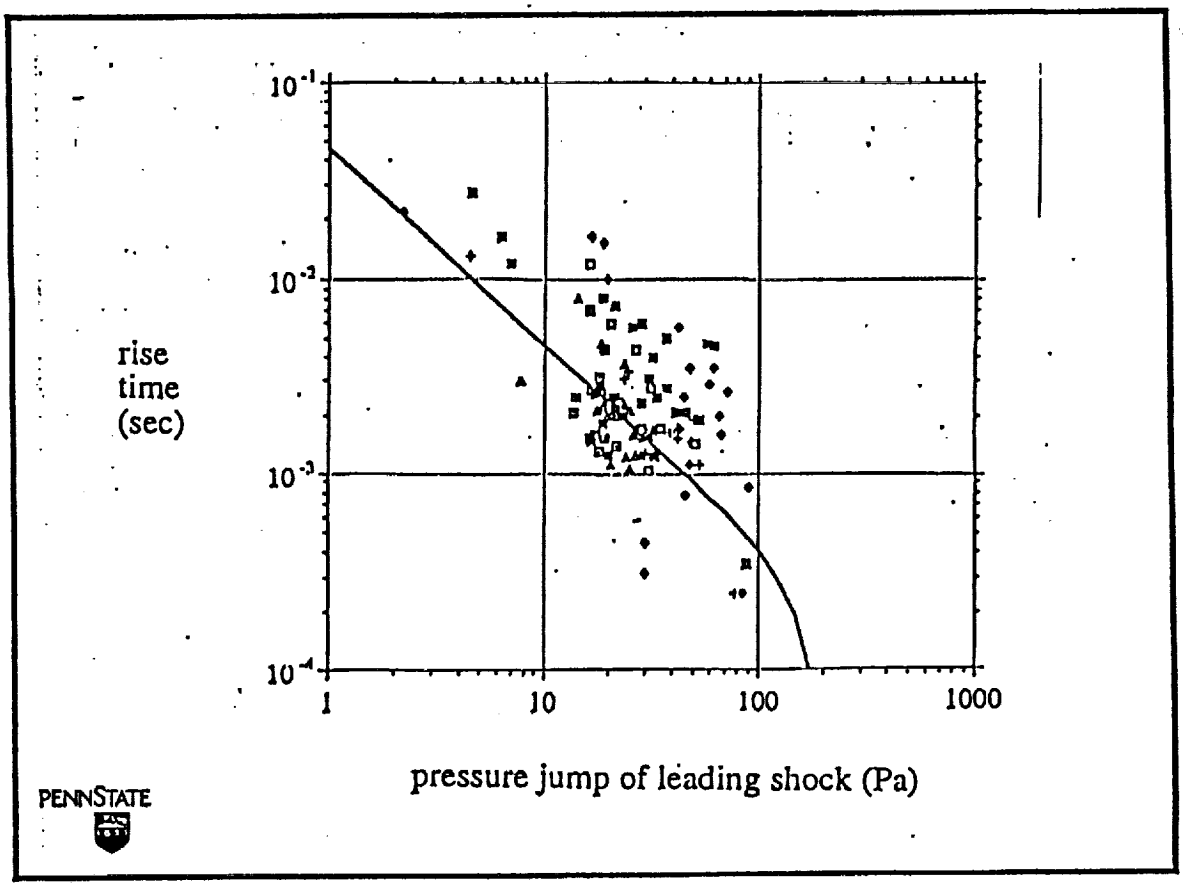

The overall result of the comparison, with ground reflection taken into account as here described, is that the theoretically predicted rise times are roughly the same as the average rise time of the experimental waveforms under conditions of the same incident waveform pressure amplitude and the same atmospheric humidity.

Inferences from updated theory-data comparison:

- Relaxation theory predicts rise times of correct order of magnitude
- Theoretical predictions of rise times tend (but not in all cases) to be lower than observed in field data
- Turbulence is major factor in rise times.

PENNSTATE

The rise phase structure of the waveform is basically a tug-of-war between nonlinear steepening and molecular relaxation. When the boom passes through a region where the molecular relaxation is weaker, the nonlinear steepening causes the waveform to sharpen up and causes the rise time to decrease until the mechanisms balance each other out. One can associate a characteristic adjustment time with this restoration of the balance between the two mechanisms. The quasi-steady hypothesis used in the simpler models hypothesis rests on the assertion that this characteristic adjustment time is substantially less than any characteristic time it takes for the waveform to propagate over a path segment within which the relevant atmospheric properties (especially the absolute humidity) change appreciably. A current question regarding the closely related and competing effects of molecular relaxation and nonlinear steepening is just how resilient is the steady-state model.

Raspet has referred to the characteristic distance over which recovery from a perturbation to the asymptotic waveform takes place as the healing distance.

Concept of healing distance:

- Suppose rise phase of waveform slightly perturbed from asymptotic quasi-steady-state form
- For further propagation through a homogeneous medium, the perturbation dies out
- Rise phase eventually evolves to asymptotic form that depends on x and t only in combination $x - V_{\mathrm{sh}}t$.
- What is characteristic additional propagation distance for the perturbation to die out?

PENNSTATE

The question of the magnitude of the healing distance has been answered tentatively by detailed numerical computations of transient evolution of waveforms over large propagation distances by Raspet and others, with the apparent prediction that it takes propagation distances of several kilometers (the value depending on the peak amplitude) for the waveform to recover from slight perturbations in the steady-state shape. Even more so than is the case for the rise time, there is room for considerable arbitrariness in the definition of this healing distance. The present author suspects that one can devise a meaningful definition for which the numerical value of this healing distance is less than a kilometer for representative cases of interest.

That the latter speculation has some credibility can be seen at once when one considers that a typical value for the pertinent relaxation time is about 1 ms (corresponding to the relaxation time of N_2 in air with 50% relative humidity). The waveform moves with roughly the sound speed, which is of the order of 340 m/s, and a pressure amplitude of 50 Pa would move with an additional speed increment of $\beta P/\rho_0 c = (1.2)50/400 = 0.15$ m/s. If such a peak lags a zero-crossing by a distance of $(.001)(340)$ m, then the distance for it to overtake the zero-crossing in the absence of any dissipation effect is approximately $(.001)(340)^2/0.15$ or 0.8 km. To put such an estimate in perspective, one can contrast this with a distance of 11 km for a typical height of the tropopause and with a representative distance of 15 km for a ray trajectory from the aircraft flight track to the ground. The numbers sometimes mentioned for the thickness of the atmosphere's turbulent boundary layer, on the other hand, are much smaller, on the order of 1 to 2 km.

Order of magnitude of healing distance:

- Take pertinent relaxation time as 1 ms
- Waveform moves with speed $c \approx 340$ m/s
- Pressure amplitude of 50 Pa moves with additional speed increment of

$$\beta(\Delta p)/\rho_0 c = (1.2)(50)/(400) = 0.15\,\text{m/s}$$

- Propagation distance for peak to overtake zero crossing in absence of dissipation:

$$(0.001)(340)^2/0.15 \approx 0.8\,\text{km}$$

PENNSTATE

Kang and the author some time ago initiated a systematic study of the tendency toward the steady-state profile in which the analysis was based more on analytic considerations rather than lengthy numerical case studies. In this theory the steady-state profile provides a framework whereby perturbations to the profile can be regarded as a superposition of natural eigenfunctions of fixed shape as seen by someone moving with the nominal shock speed. Each such natural eigenfunction has its own natural decay time which results as an eigenvalue in the theory. The task then emerges of systematically determining these eigenfunctions and the associated eigenvalues.

Eigenfunctions and characteristic healing distances:

- Propagation equations are

$$\frac{\partial u}{\partial t} + c\frac{\partial u}{\partial x} + \beta u\frac{\partial u}{\partial x} - \delta'_{\rm cl}\frac{\partial^2 u}{\partial x^2} + \sum_{\nu}(\Delta c)_\nu \frac{\partial u_\nu}{\partial x} = 0$$

$$\frac{\partial u_\nu}{\partial t} + \frac{1}{\tau_\nu}u_\nu = \frac{\partial u}{\partial t}$$

  where $p = \rho_0 x u$.

- Steady state solution is

$$u = F(\xi); \quad u_\nu = F_\nu(\xi)$$

  where $\xi = x - V_{\rm sh}t$.

- Take perturbed solution to be of form

PENNSTATE

$$u = F(\xi) + \psi(\xi)e^{-\lambda x}; \quad u_\nu = F_\nu(\xi) + \psi_\nu(\xi)e^{-\lambda x}$$

This summarizes the mathematical problem that ideally should be solved to determine a sequence of healing distances. One expects the so-posed eigenvalue problem to have several solutions that correspond to real eigenfunctions. The structure of the problem is still to be studied, and one does not have any orthogonality theorems as yet regarding different eigenvector functions. However, a crude solution can be found if one replaces the governing equations by Burgers' equation with an effective bulk viscosity.

Equations governing healing eigenfunctions:

- $$u = F(\xi) + \psi(\xi)e^{-\lambda x}; \quad u_\nu = F_\nu(\xi) + \psi_\nu(\xi)e^{-\lambda x}$$

  are inserted into propagation equations; one keeps only linear terms in the ψ's, with result in matrix form

  $$[\mathcal{L}]\{\psi\} = \lambda[\mathcal{M}]\{\psi\} + \lambda^2[\mathcal{N}]\{\psi\}$$

  where $[\mathcal{L}]$, $[\mathcal{M}]$, and $[\mathcal{N}]$ are 3-by-3 matrices made up of linear operators, each possibly involving differentiation with respect to ξ and the steady state profile functions $F(\xi)$, $F_1(\xi)$, $F_2(\xi)$

- $\{\psi\}$ is an eigenfunction array (ψ, ψ_1, ψ_2)
- Nontrivial solution (boundary condition of ψ's equal to zero at $\xi = \pm\infty$) exists only for special values of λ.
- Special values of λ construed as eigenvalues and as reciprocals of characteristic healing distances.

PENNSTATE

Predictions of healing distance based on effective bulk viscosity:

- $$L_{\text{heal}} = 16\frac{\delta_{\text{appar}}}{c}\left(\frac{\rho c^2}{\beta(\Delta p)_{\text{sh}}}\right)^2$$

$$\delta_{\text{appar}} = \frac{\mu_{\text{bulk}}}{2\rho} + \cdots$$

- Tisza's equivalence:

$$\mu_{\text{bulk}} \approx 2\rho c(\Delta c)_\nu \tau_\nu$$

- so we infer

$$L_{\text{heal}} = 16c\tau_\nu\left(\frac{(\Delta c)_\nu}{c}\right)\left(\frac{\rho c^2}{\beta(\Delta p)_{\text{sh}}}\right)^2$$

PENNSTATE

Representative numerical values based on effective bulk viscosity:

- $$L_{\text{heal}} = 16c\tau_\nu\left(\frac{(\Delta c)_\nu}{c}\right)\left(\frac{\rho c^2}{\beta(\Delta p)_{\text{sh}}}\right)^2$$

- Typical numerical values (O_2 relaxation)

$$(\Delta p)_{\text{sh}} = 50\,\text{Pa}; \quad \frac{\rho c^2}{\beta(\Delta p)_{\text{sh}}} = 2300$$

$$\frac{(\Delta c)_\nu}{c} = 3 \times 10^{-4}; \quad \tau_\nu = 10^{-5}\,\text{s}$$

- so we infer $L_{\text{heal}} \sim 250\,\text{m}$
- But you can get much larger values using parameters for N_2 relaxation.

PENNSTATE

The author and his colleagues have recently been exploring various methods for computation of sonic boom propagation through turbulent atmospheres and have obtained a generalization of the Burgers equation which has some similarities to the KZK equation and to the NPE equation of McDonald and Kuperman. The equation can be regarded as a string of "small terms" tacked onto the inviscid linear Burgers equation, with individual terms accounting for nonlinear steepening, viscous attenuation, refraction, molecular relaxation, and diffraction.

The Penn State Univ Propagation Equation (PSUPE):

- Generalization of Burgers equation (which really should be called the Cole equation, as inferred from Cal Tech literature of late 1940's by ADP)
- Term for diffraction by smaller turbulent eddies
- Molecular relaxation term
- Nonlinear steepening term
- Turbulence can be simulated using Fourier transforms (series) with random number algorithms used in selection of coefficients.
- Larger scale turbulence and ambient atmospheric stratification can be incorporated in multiplicative Blokhintzev factor (roughly same as $1/\sqrt{A}$, where A is ray tube area) which varies with distance along central ray.

PENNSTATE

Pestorius had a good idea

- Basic Pestorius algorithm alternated between nonlinear distortion (NL) and absorption-dispersion (AD) steps
- Noise-Con 93 paper by ADP shows that this is rigorously correct in limit of small step sizes Δx. Taking limit yields partial differential equation

$$\frac{\partial u}{\partial x} + \frac{1}{c}\frac{\partial u}{\partial t} = \mathcal{M}_{\mathrm{NL}}\{u\} + \mathcal{M}_{\mathrm{AD}}\{u\}$$

  where right-side terms are same as appear in PSUPE.
- Why not use same idea to handle the diffraction term?

PENNSTATE

Concluding remarks

- Solving PSUPE to realistically simulate sonic boom statistics will require major theoretical innovations in computational acoustics. (But so what?)
- Two doctoral theses presently in progress at Penn State on alternate approaches to solving PSUPE
  - Kirchhoff integral for the diffraction step.
  - Finite-difference algorithms using flux-corrected transport methods of Boris and McDonald.
- Another idea being pursued by the present author independently is that the healing eigenfunctions are natural basis set for a variational (or Galerkin) formulation which reduces the dimensionality of the problem, and which leads to simpler ways of decomposing messy waveforms encountered in field data.

PENNSTATE

N94-28190

Implications for High Speed Research: The Relationship Between Sonic Boom Signature Distortion and Atmospheric Turbulence

Victor W. Sparrow and Thomas A. Gionfriddo
The Pennsylvania State University
Graduate Program in Acoustics
157 Hammond Building
University Park PA, 16802

Presentation at NASA HSR Sonic Boom Workshop
NASA Ames Research Center
May 12-14, 1993

Good morning. My name is Dr. Victor W. Sparrow of the Penn State University Graduate Program in Acoustics. The Graduate Program in Acoustics is a Department in the Penn State College of Engineering. My co-author is Tom Gionfriddo, a graduate student at Penn State who finished up his M.S. degree in Acoustics early in the Fall of 1992. Much of the work I will be presenting today is the result of Tom's effort on his master's thesis.

The topic I will be discussing today is Implications for High Speed Research: The Relationship Between Sonic Boom Signature Distortion and Atmospheric Turbulence. But before we get to these implications, let us review a little history concerning previous research on sonic boom waveform distortion.

Implications for High Speed Research:
The Relationship Between Sonic Boom Signature Distortion and Atmospheric Turbulence

Victor W. Sparrow and Thomas A. Gionfriddo
Graduate Program in Acoustics
The Pennsylvania State University

Presentation at NASA HSR Sonic Boom Workshop
NASA Ames Research Center
May 12–14, 1993

PENNSTATE

In 1968 Dr. Allan Pierce hypothesized that the cause of sonic boom distortion, which takes the form of spiked or rounded waveforms, was due to atmospheric turbulence. This was a theoretical result, and was not widely accepted at the time due to the lack of experimental evidence.

In 1973 Ribner, Morris, and Chu performed laboratory experiments which showed that one could cause sonic boom shaped waves to spike or become rounded, if the waves were propagated through a turbulent jet. This laboratory result gave some evidence that turbulence could, in fact, be the cause of sonic boom waveform distortion in the atmosphere. Others also performed similar laboratory experiments.

In the mid to late 1970's, however, the role of molecular relaxation absorption in sonic boom propagation had not yet been established. The relative importance of molecular relaxation and atmospheric turbulence for sonic boom distortion was not clear.

- In 1968 Pierce hypothesized (Ref. 1) that the cause of sonic boom distortions, such as spiked or rounded waveforms, was due to atmospheric turbulence.
- In 1973 Ribner, Morris, and Chu found in the laboratory (Ref. 2) that sonic boom shaped acoustic waves indeed were distorted in a turbulent jet, producing both spiked and rounded waveforms.
- However, the relative importance of atmospheric turbulence and molecular relaxation effects had yet to be established.

PENNSTATE

By the early 1980's the theory for molecular relaxation absorption in the atmosphere was fairly well understood. The two dominant process are Oxygen and Nitrogen relaxation, with humidity (water vapor) being the next most important process. The result of the theory is that molecular relaxation cannot cause the spikes on sonic boom waves, although they can round sonic boom waves somewhat. It is thought that the rounding effect is insufficient to explain observed distorted waveforms, however.

After the molecular relaxation theory was understood, it became the common notion that atmospheric turbulence is primarily responsible for sonic boom distortion. This is an assumption which most workers in sonic boom propagation have adopted, since the spiking and rounding could not be due to molecular relaxation. Most of the talks during the rest of this session make this assumption.

- By the early 1980's molecular relaxation was fairly well understood. Molecular relaxation cannot cause spikes on sonic boom waves.
- Thus, most researchers in sonic boom propagation have assumed that turbulence must be responsible for sonic boom distortion.
- Most of the talks in this session make such an assumption.

PENNSTATE

Until recently this assumption has not been tested statistically. Such a test would provide a firm foundation for much of the ongoing work on sonic boom propagation through turbulence at a number of NASA Contractor sites, including The University of Mississippi, The University of Texas at Austin, Penn State University, Wyle Laboratories, etc.

One supposes here that an originally undistorted sonic boom propagating through turbulence should, on average, be more distorted as it propagates through more turbulence.

However,

until recently this assumption has not been tested statistically with real sonic boom data and real atmospheric turbulence.

One supposes that a sonic boom propagating through more turbulence should, on average, be more distorted.

PENNSTATE

Therefore, the purpose our research study is was to test the above hypothesis rigorously. That is, the specific purpose is to see if increasing travel distances through turbulence is correlated with increasing sonic boom wave distortion. This paper documents the results of our study.

In this study it is assumed that the strength of the atmospheric turbulence is somewhat uniform, and it is the travel distance of booms through the turbulence that is important. This assumption is necessary due to the absence of direct turbulence measurements to complement the sonic boom experimental data which will be used to test the hypothesis.

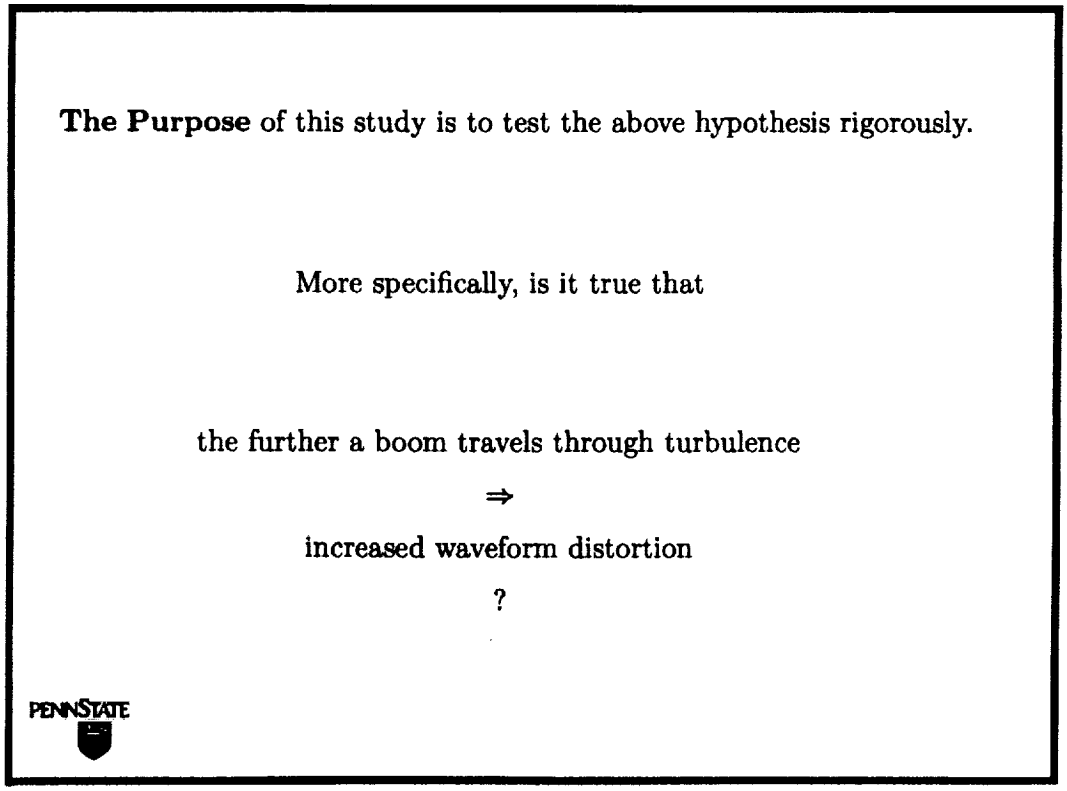

In this study there were two primary tasks. The first was to develop an algorithm for quantifying the distortion in a sonic boom. Such an algorithm should be somewhat automatic, with minimal human intervention. Once the algorithm was developed, it was used to test the previously mentioned hypothesis. This hypothesis testing was the second task. Using readily available sonic boom data, we statistically tested whether there was a correlation between the sonic boom distortion and the distance a boom traveled through atmospheric turbulence.

In this study we

A. Developed an algorithm to quantify the distortion in a sonic boom waveform.

B. Tested the correlation between this distortion and the distance a boom traveled through atmospheric turbulence.

PENNSTATE

The terminology that is used in our paper is described here. The booms have a maximum shock overpressure after some rise time. This maximum shock overpressure is called the bow shock. The duration is then defined as the time as waveform slopes off to the minimum shock overpressure at the tail shock. For most of the booms examined, the duration was between 75 and 200 milliseconds, and the amplitudes varied between 30 and 200 pascals. Most booms have a subsonic fundamental frequency in the range of 6 to 10 hertz. Our definition of rise time is from 10% to 90% of the maximum shock overpressure.

SONIC BOOM WAVEFORM TERMINOLOGY

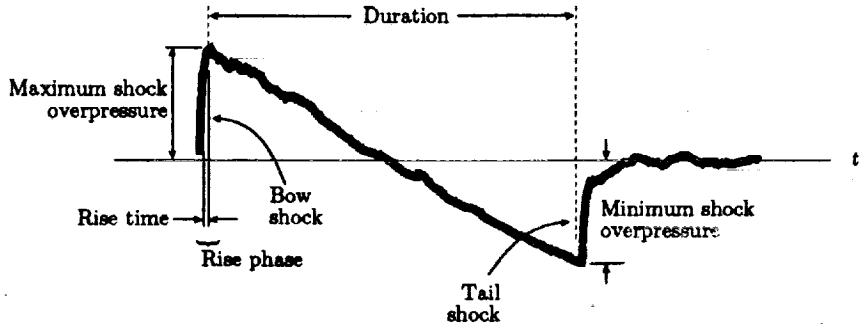

Duration typically 75-200 ms, amplitude 30-200 Pa

Subsonic fundamental ~ 6-10 Hz

Rise time is time from 10% to 90% of maximum shock overpressure

Why annoying? Rise phase structure important

Sonic booms can be distorted in many ways as they propagate through the atmosphere. Here a large number of sonic booms were collected into categories, and a representative waveform example is shown from each category. The waves which were the most undistorted were called Classic N. Waveforms showing one large peak were called Peaked. Many of waveforms have two distinct peaks, and were called Double-peaked. Some waveforms had many peaks, and these were called Multi-peaked. The U-wave category was defined as those waves having very large spikes on both the bow and tail shocks, the spikes dominating all features. The Rounded waveform category had rounded bow and tail shocks. All other waveforms, which could not be classified in one of the previous categories, were called Messy (for lack of a better term).

DATA CLASSIFICATION BY WAVEFORM SHAPE

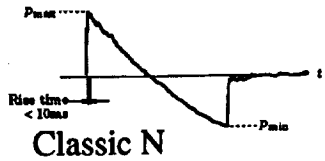

Classic N

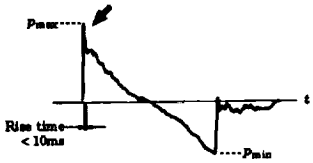

Peaked

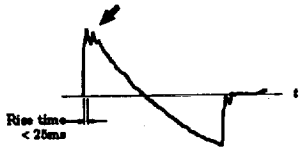

Double-peaked

Multi-peaked

U-wave

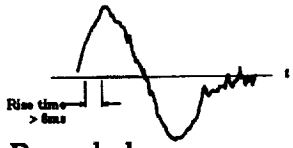

Rounded

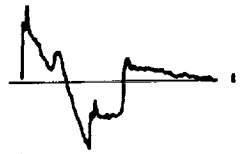

Messy
(for lack of a better term)

Because of the great variability in the distortions a sonic boom wave can undergo, an automatic numerical procedure was developed for quantifying the distortion in a sonic boom wave. The first component of this quantification is to find a basis for comparison. Since one usually puts microphones on the ground, and measures the sonic boom wave only after it has been distorted, it is necessary to estimate the wave shape of the sonic boom *before* it was distorted.

The assumption made here is that before any waveform distortions occurred that the sonic boom wave had the shape of a perfect N-wave with zero rise times on both bow and tail shocks. The energy in the distorted sonic boom is measured, and then it is assumed that the undistorted ideal N-wave has the same energy. Obviously, this is an approximation.

Given this information the proper maximum overpressure, duration, and start time offset of the ideal N-wave is automatically computed. Additional details on the elaborate algorithm used to calculate the parameters for the ideal N-wave, given the distorted sonic boom wave, are available in the M.S. thesis of Gionfriddo (Ref. 3).

WAVEFORM DISTORTION ANALYSIS:
COMPARE DATA TO IDEAL N-WAVE MODEL

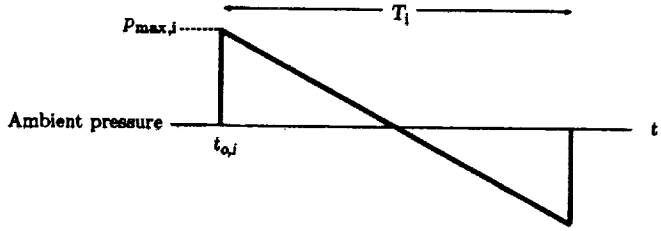

Model of the sonic boom signature just prior to entering the TBL.

Ideal N-wave and the recorded data have equal acoustic energy.

The ideal N-wave is superimposed on the same time axis as the recorded data.

The proper maximum overpressure, duration, and start time offset of the ideal N-wave must be determined.

It is desired to have Classic N data with the lowest mean- squared deviation for any waveshape. Therefore, Classic N data are used as a reference for superimposing the ideal N-wave correctly over the recorded data.

Here is a typical recorded sonic boom wave with its ideal N-wave superimposed.

To quantify the distortion in the measured waveform, the notion of a mean-squared deviation is used, defined below. The functions $p_{ideal}[n]$ and $p_{recorded}[n]$ are both assumed to be digitized data. For the example waveform shown here, the mean-squared deviation is 0.075.

EXAMPLE OF RECORDED BOOM WITH IDEAL N-WAVE SUPERIMPOSED

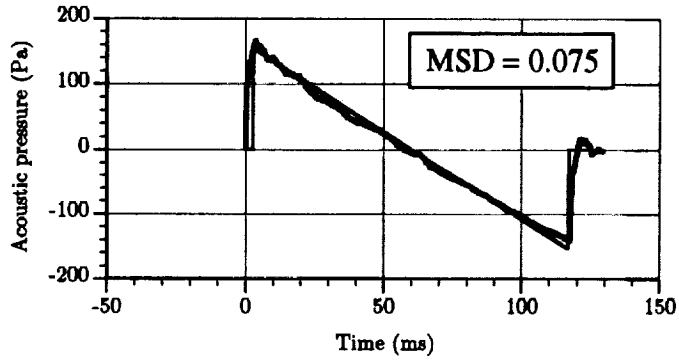

MEASURE OF WAVEFORM DISTORTION: MEAN-SQUARED DEVIATION

The *mean-squared deviation* (MSD) is defined as:

$$MSD = \frac{\Sigma (p_{ideal}[n] - p_{recorded}[n])^2}{\Sigma (p_{ideal}[n])^2}$$

Here are two more sonic boom waveforms with superimposed ideal N-waves. The upper waveform is a Peaked sonic boom wave, and it shows a mean-squared deviation of 0.095. The lower waveform is a Rounded waveform, having a much larger mean-squared deviation of 0.23.

TWO MORE EXAMPLES OF RECORDED BOOMS WITH IDEAL N-WAVES SUPERIMPOSED:

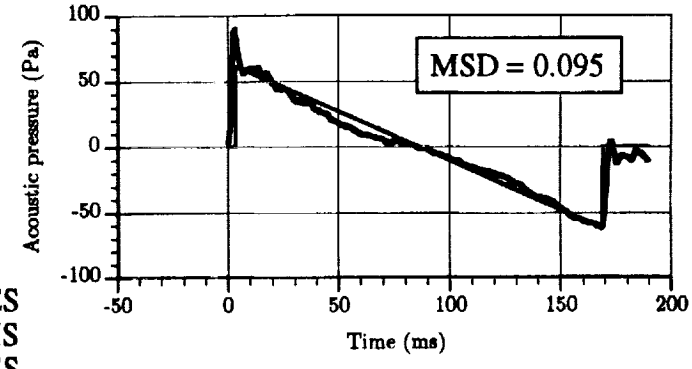

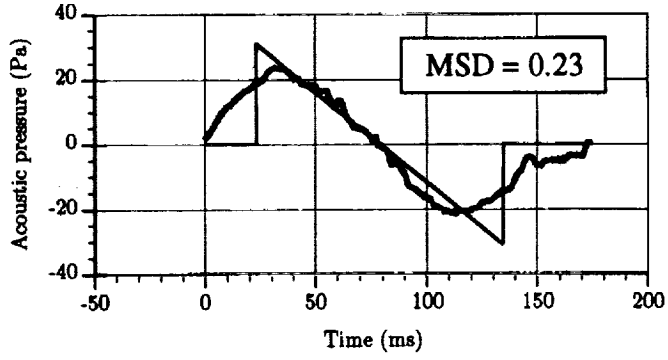

The particular sonic boom data we analyzed was taken near Edwards Air Force Base in the late summer of 1987 by the U. S. Air Force. Autonomous Boom Event Analyzer Recorder (BEAR) systems took data over several days from a wide variety of supersonic aircraft: F-4, F-14, F-15, F-16, F-18, SR-71, T-38, AT-38, and F-111D. The recorders were placed at the mile markers along a road in the area. The aircraft were to fly perpendicular to the road over a specific flight track. From 44 aircraft flights, over 500 data files were obtained for analysis. The specific position of where the aircraft overflew the road was recorded, and this information has been taken into account in our analysis.

MOJAVE DESERT SONIC BOOM ACQUISITION SCHEMATIC

F-4, F-14, F-15, F-16, F-18, SR-71, T-38, AT-38, and F-111D aircraft

Lateral array of thirteen Boom Event Analyzer Recorder (BEAR) systems

Flight track perpendicular to array

44 Flights ~ 500 data files

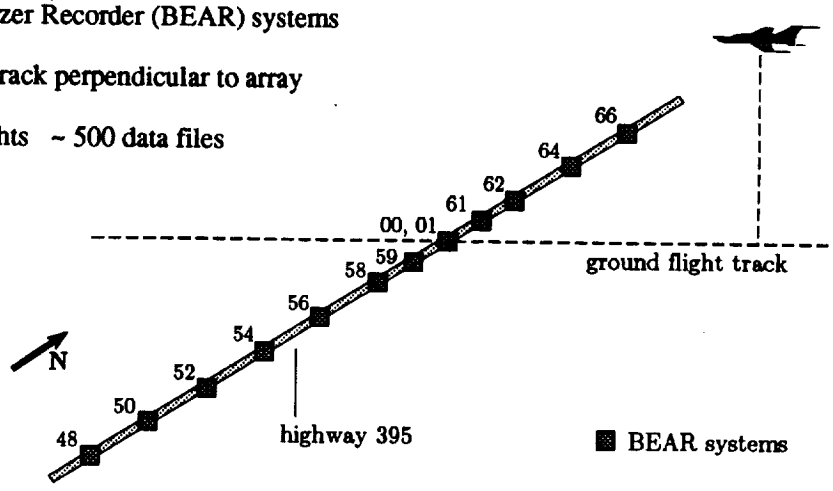

To determine the path length a sonic boom will traverse through the turbulent boundary layer near the earth's surface, a short exercise in three-dimensional solid geometry is needed. Knowing the altitude of the aircraft, its Mach number, the lateral ground distance of the receiving microphone from the aircraft's actual flight track, and the thickness of the boundary layer, this path length can be obtained. The path length is shown as a dark solid line in the diagram.

PATH LENGTH THROUGH THE TURBULENT BOUNDARY LAYER

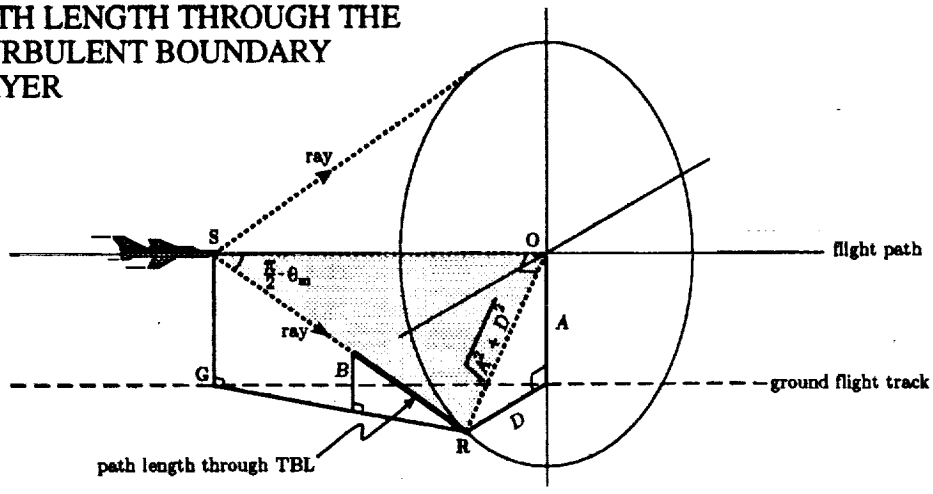

Function of:
- altitude
- Mach number
- lateral ground distance
- TBL thickness

The turbulent boundary layer is defined as the thickness of the mixing layer of the planetary boundary layer. One may assume that the turbulence in the mixing layer is somewhat evenly distributed and homogeneous.

To determine the thickness of this layer, a numerical model by A. K. Blackadar was employed. The numerical model takes into account information from rawinsonde launches, surface weather data, satellite cloud photos, and soil parameters for the site of the sonic boom tests. Blackadar's model provides daily profiles to 2000 m height for temperature, water content, wind, and boundary layer thickness.

PATH LENGTH THROUGH THE TURBULENT BOUNDARY LAYER (CONTINUED)

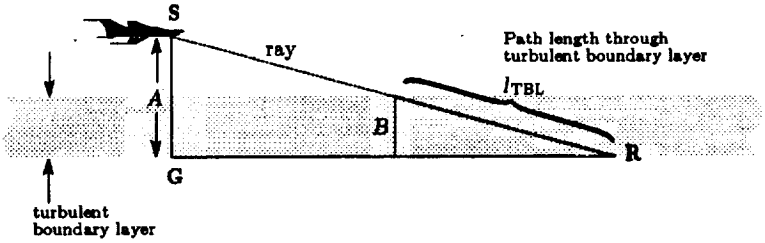

TBL thickness estimated using numerical model by A. K. Blackadar (PSU meteorology)

Input atmospheric information from rawinsonde launches, surface weather station, satellite cloud photos, soil parameters

Model provides diurnal profiles to 2000 m for temperature, water content, wind, and TBL thickness

For the days of the tests, 3 - 8 August 1987, profiles of the turbulent boundary layer thickness were obtained from the Blackadar model. One can see the thickness of the boundary layer generally grew during the day between 7:00 AM and 2:00 PM. Because of the meteorological conditions present, the boundary layer grew much more on 3 August and 4 August than it did on the other days of the tests.

TURBULENT BOUNDARY LAYER THICKNESS
ESTIMATION USING BLACKADAR MODEL

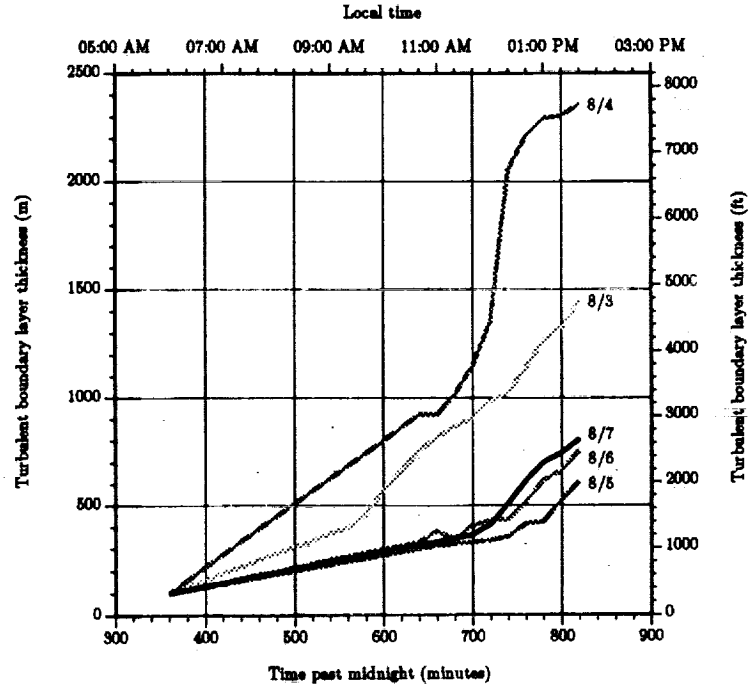

Before continuing, the analysis procedure will be summarized. On one track the BEAR sonic boom data was obtained and calibrated. From this data pressure versus time plots were obtained, which were subsequently sorted into waveshape categories. Given these plots, the sonic boom distortion quantification algorithm was run, and mean-squared deviations from the computer generated corresponding ideal N-waves were obtained for all the the waveforms.

On the other track, the aircraft flight parameters and geometry were combined with the meteorological data and subsequent predictions of the boundary layer height from Blackadar's model. From this information the path length through the turbulence was found for *each* recorded sonic boom waveform.

It was then possible to determine if a statistical correlation existed between the mean-squared deviation and the path length the sonic boom traveled through the turbulence.

ANALYSIS PROCEDURE

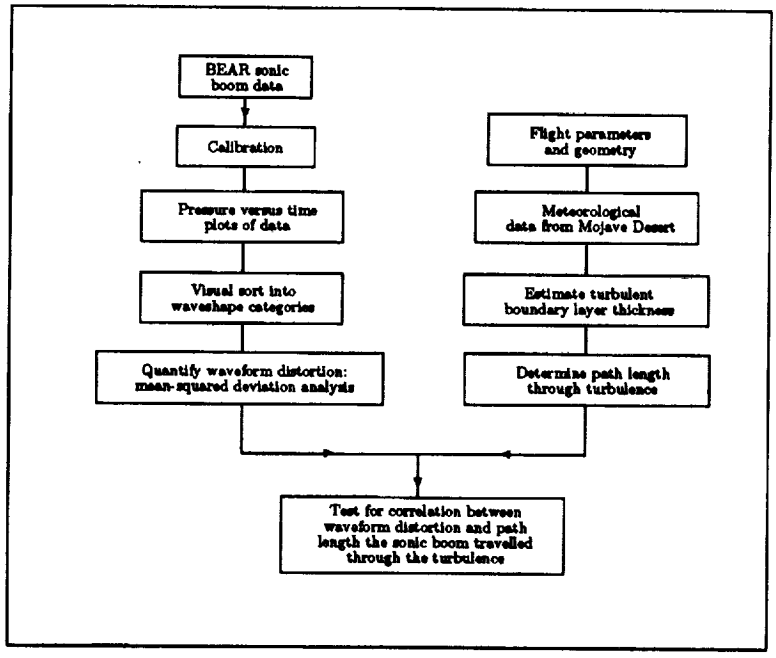

During the analysis procedure it became immediately apparent that those waveforms which were either shaped as a Classic N-waves, or were nearly shaped as such, were primarily manifest only in the early morning hours.

This result leads us to believe that as the turbulent boundary layer grew through the day, that the number of undistorted waveforms decreased. This result is averaging over all of the usable observation data.

SIMPLE DEMONSTRATION: FRACTION OF RECORDED SONIC BOOM WAVEFORMS THAT ARE LEAST-DISTORTED

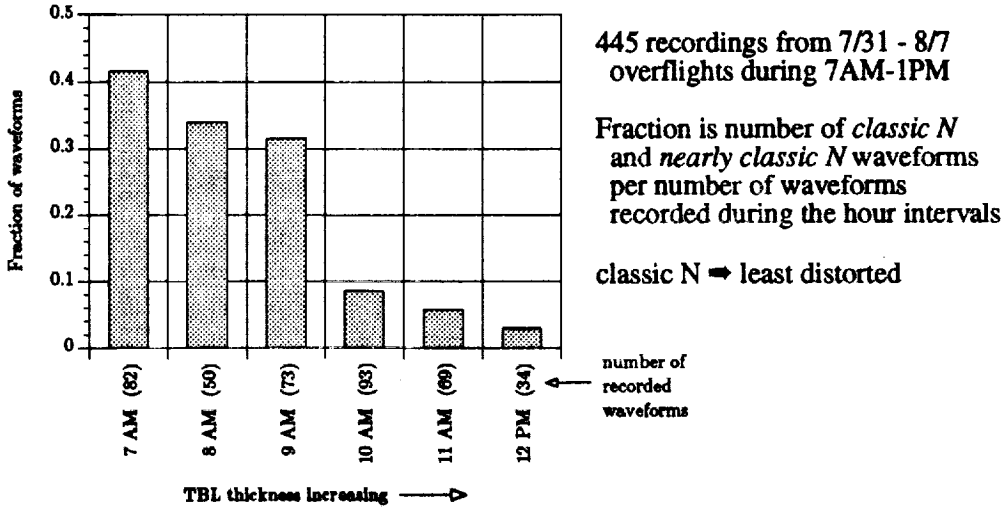

445 recordings from 7/31 - 8/7 overflights during 7AM-1PM

Fraction is number of *classic N* and *nearly classic N* waveforms per number of waveforms recorded during the hour intervals

classic N ➡ least distorted

This is a plot of the mean-squared deviation as a function of altitude (or roughly Mach number, since faster planes generally flew higher). It is apparent that increased altitude and speed imply decreased waveform distortion and a decreased spread of data points. Now higher and faster flying planes generally will have shorter propagation paths through the turbulent boundary layer, which can be shown from simple geometry. Thus, it appears as if longer propagation paths through the turbulence result in larger mean-squared deviations, i.e., more distorted waveforms.

ALTITUDE AND MACH NUMBER INFLUENCE UPON WAVEFORM DISTORTION

Increased altitude and speed ➡ decreased waveform distortion and decreased spread of data points

F-18, F-15, SR-71, F-4, and F-16 data

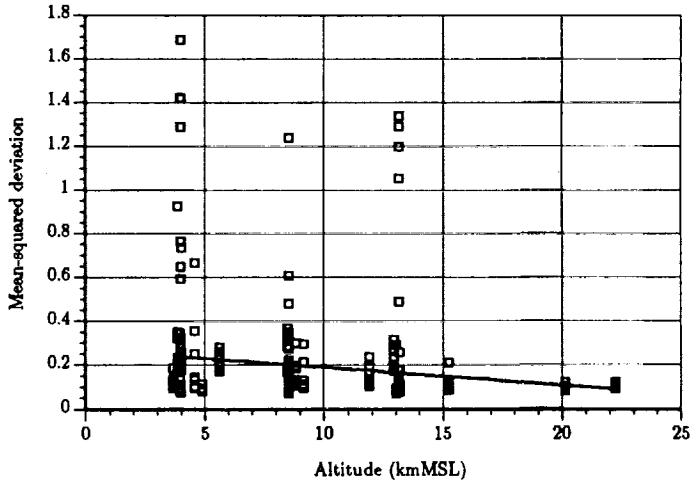

Here are some results listed by plane type of the linear correlation coefficients between the mean-squared deviation and the path length through the turbulent boundary layer. It is seen that there is strong correlation in some cases (F-18 and F-15) and fair correlation in the others. This also gives us some evidence that increasing distortion is correlated with increasing path length through the turbulence.

The F-4 and F-16 data have the lowest correlations and the lowest altitudes. For these cases the sonic boom signatures probably did not have time to develop into an N-wave by the time it began to interact with the turbulence. The other aircraft types flown had too few data points to draw any statistical conclusions.

We also are currently working on obtaining correlation coefficients grouped by altitude and mach number as well as by plane type, to determine how these factors interrelate.

CORRELATION COEFFICIENTS FOR
MEAN-SQUARED DEVIATION AND
TBL PATH LENGTH

Aircraft type	Correlation coefficient: MSD vs TBL path length	Number of samples
F-18	0.712	62
F-15	0.591	75
SR-71	0.398	48
F-4	0.324	46
F-16	0.318	65

(Linear regression correlation coefficients)

Strong correlation in some cases, fair correlation in others

F-4 and F-16 have lowest correlations and the lowest altitudes
- Sonic boom signature before TBL probably not N-wave
- Less distance for nonlinear steepening to work before TBL

The conclusions of this study are the following: a strong linear correlation exists between the mean-squared deviation and path length through the turbulence for the F-18 and F-15 sonic boom data. Fair correlation exists for the SR-71, F-4, and F-16 data. An increase in altitude and speed results in decreased waveform distortion and a small deviation between distortion values. Looking at the waveform classification results, the large percentage of Classic N-wave data during each day's early flights seems to correspond with the thin boundary layer at that time.

Conclusions:

- A strong linear correlation exists between mean-squared deviation and path length through the turbulence for F-18 and F-15 sonic boom data.
- Fair correlation exists for SR-71, F-4, and F-16 data.
- An increase in altitude and speed results in decreased waveform distortion and a smaller deviation between distortion values.
- Looking at waveform classification results, the large percentage of classic N wave data during early flights seems to correspond with the thin boundary layer at that time.

PENNSTATE

The implications of this study for high speed research are the following: Increased interaction between real atmospheric turbulence and actual sonic boom data does imply more distorted waveforms. The common assumption prevailing in the sonic boom propagation community for the last several years has been validated statistically. And most importantly, it is now clear that atmospheric turbulence will determine how well a shaped sonic boom will remain shaped as it propagates to the ground. We are now led to believe that higher and faster aircraft having shaped sonic booms will, on average, have more shaped boom preserved than will aircraft flying at lower altitudes and slower speeds, since flying higher and faster minimizes the path length through the turbulence.

Implications for High Speed Research:

- Increased interaction between real atmospheric turbulence and actual sonic booms does imply more distorted waveforms.
- This common assumption has been validated statistically.
- *Most Importantly:* Atmospheric turbulence primarily will determine how well a shaped sonic boom will remain shaped as it propagates to the ground.

PENNSTATE

The authors would like to thank Dr. Allan D. Pierce and Dr. Richard Raspet for numerous discussions. This research was supported by NASA Langley Research Center, under grant NAG-1-1365, administered by Dr. G. L. McAninch, Scientific Officer.

References

1. "Spikes on sonic-boom pressure waveforms," Allan D. Pierce, J. Acoust. Soc. Am., **44** 1052-1061 (1968).
2. "Laboratory simulation of development of superbooms by atmospheric turbulence," H. S. Ribner, P. J. Morris, and W. H. Chu, J. Acoust. Soc. Am., **53** 926–928 (1973).
3. "Quantification of sonic boom distortions from propagation through atmospheric turbulence," Thomas A. Gionfriddo, M.S. Thesis, The Pennsylvania State University, December 1992.

PENNSTATE

Implications for High Speed Research: The Relationship Between Sonic Boom Signature Distortion and Atmospheric Turbulence

Victor W. Sparrow and Thomas A. Gionfriddo
The Pennsylvania State University
Graduate Program in Acoustics
157 Hammond Building
University Park PA, 16802

Presentation at NASA HSR Sonic Boom Workshop
NASA Ames Research Center
May 12-14, 1993

Good morning. My name is Dr. Victor W. Sparrow of the Penn State University Graduate Program in Acoustics. The Graduate Program in Acoustics is a Department in the Penn State College of Engineering. My co-author is Tom Gionfriddo, a graduate student at Penn State who finished up his M.S. degree in Acoustics early in the Fall of 1992. Much of the work I will be presenting today is the result of Tom's effort on his master's thesis.

The topic I will be discussing today is Implications for High Speed Research: The Relationship Between Sonic Boom Signature Distortion and Atmospheric Turbulence. But before we get to these implications, let us review a little history concerning previous research on sonic boom waveform distortion.

Implications for High Speed Research:
The Relationship Between Sonic Boom Signature Distortion and Atmospheric Turbulence

Victor W. Sparrow and Thomas A. Gionfriddo
Graduate Program in Acoustics
The Pennsylvania State University

Presentation at NASA HSR Sonic Boom Workshop
NASA Ames Research Center
May 12–14, 1993

PENNSTATE

In 1968 Dr. Allan Pierce hypothesized that the cause of sonic boom distortion, which takes the form of spiked or rounded waveforms, was due to atmospheric turbulence. This was a theoretical result, and was not widely accepted at the time due to the lack of experimental evidence.

In 1973 Ribner, Morris, and Chu performed laboratory experiments which showed that one could cause sonic boom shaped waves to spike or become rounded, if the waves were propagated through a turbulent jet. This laboratory result gave some evidence that turbulence could, in fact, be the cause of sonic boom waveform distortion in the atmosphere. Others also performed similar laboratory experiments.

In the mid to late 1970's, however, the role of molecular relaxation absorption in sonic boom propagation had not yet been established. The relative importance of molecular relaxation and atmospheric turbulence for sonic boom distortion was not clear.

- In 1968 Pierce hypothesized (Ref. 1) that the cause of sonic boom distortions, such as spiked or rounded waveforms, was due to atmospheric turbulence.
- In 1973 Ribner, Morris, and Chu found in the laboratory (Ref. 2) that sonic boom shaped acoustic waves indeed were distorted in a turbulent jet, producing both spiked and rounded waveforms.
- However, the relative importance of atmospheric turbulence and molecular relaxation effects had yet to be established.

PENNSTATE

By the early 1980's the theory for molecular relaxation absorption in the atmosphere was fairly well understood. The two dominant process are Oxygen and Nitrogen relaxation, with humidity (water vapor) being the next most important process. The result of the theory is that molecular relaxation cannot cause the spikes on sonic boom waves, although they can round sonic boom waves somewhat. It is thought that the rounding effect is insufficient to explain observed distorted waveforms, however.

After the molecular relaxation theory was understood, it became the common notion that atmospheric turbulence is primarily responsible for sonic boom distortion. This is an assumption which most workers in sonic boom propagation have adopted, since the spiking and rounding could not be due to molecular relaxation. Most of the talks during the rest of this session make this assumption.

- By the early 1980's molecular relaxation was fairly well understood. Molecular relaxation cannot cause spikes on sonic boom waves.
- Thus, most researchers in sonic boom propagation have assumed that turbulence must be responsible for sonic boom distortion.
- Most of the talks in this session make such an assumption.

PENNSTATE

Until recently this assumption has not been tested statistically. Such a test would provide a firm foundation for much of the ongoing work on sonic boom propagation through turbulence at a number of NASA Contractor sites, including The University of Mississippi, The University of Texas at Austin, Penn State University, Wyle Laboratories, etc.

One supposes here that an originally undistorted sonic boom propagating through turbulence should, on average, be more distorted as it propagates through more turbulence.

However,

until recently this assumption has not been tested statistically with real sonic boom data and real atmospheric turbulence.

One supposes that a sonic boom propagating through more turbulence should, on average, be more distorted.

PENNSTATE

Therefore, the purpose our research study is was to test the above hypothesis rigorously. That is, the specific purpose is to see if increasing travel distances through turbulence is correlated with increasing sonic boom wave distortion. This paper documents the results of our study.

In this study it is assumed that the strength of the atmospheric turbulence is somewhat uniform, and it is the travel distance of booms through the turbulence that is important. This assumption is necessary due to the absence of direct turbulence measurements to complement the sonic boom experimental data which will be used to test the hypothesis.

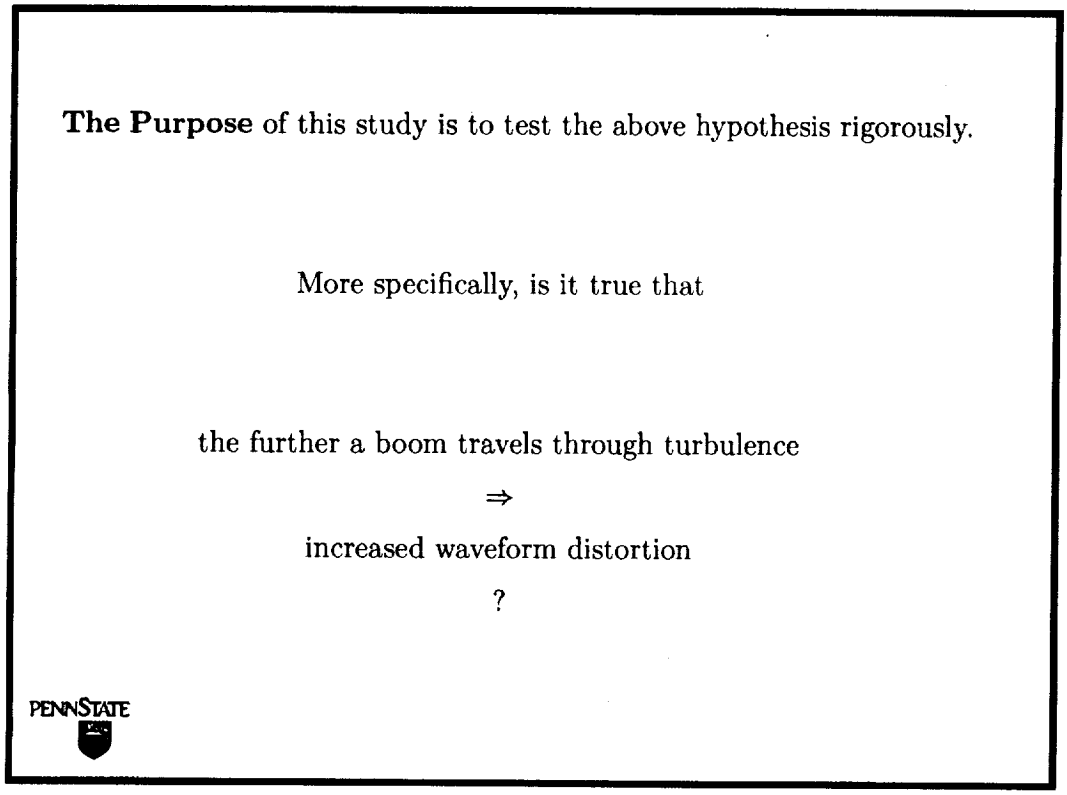

In this study there were two primary tasks. The first was to develop an algorithm for quantifying the distortion in a sonic boom. Such an algorithm should be somewhat automatic, with minimal human intervention. Once the algorithm was developed, it was used to test the previously mentioned hypothesis. This hypothesis testing was the second task. Using readily available sonic boom data, we statistically tested whether there was a correlation between the sonic boom distortion and the distance a boom traveled through atmospheric turbulence.

In this study we

A. Developed an algorithm to quantify the distortion in a sonic boom waveform.

B. Tested the correlation between this distortion and the distance a boom traveled through atmospheric turbulence.

PENNSTATE

The terminology that is used in our paper is described here. The booms have a maximum shock overpressure after some rise time. This maximum shock overpressure is called the bow shock. The duration is then defined as the time as waveform slopes off to the minimum shock overpressure at the tail shock. For most of the booms examined, the duration was between 75 and 200 milliseconds, and the amplitudes varied between 30 and 200 pascals. Most booms have a subsonic fundamental frequency in the range of 6 to 10 hertz. Our definition of rise time is from 10% to 90% of the maximum shock overpressure.

SONIC BOOM WAVEFORM TERMINOLOGY

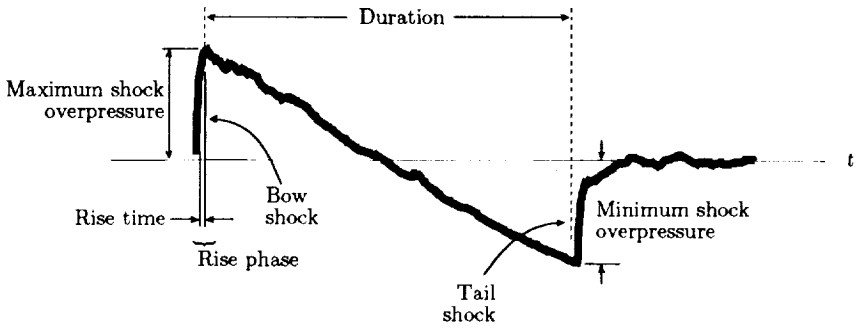

Duration typically 75-200 ms, amplitude 30-200 Pa

Subsonic fundamental ~ 6-10 Hz

Rise time is time from 10% to 90% of maximum shock overpressure

Why annoying? Rise phase structure important

Sonic booms can be distorted in many ways as they propagate through the atmosphere. Here a large number of sonic booms were collected into categories, and a representative waveform example is shown from each category. The waves which were the most undistorted were called Classic N. Waveforms showing one large peak were called Peaked. Many of waveforms have two distinct peaks, and were called Double-peaked. Some waveforms had many peaks, and these were called Multi-peaked. The U-wave category was defined as those waves having very large spikes on both the bow and tail shocks, the spikes dominating all features. The Rounded waveform category had rounded bow and tail shocks. All other waveforms, which could not be classified in one of the previous categories, were called Messy (for lack of a better term).

DATA CLASSIFICATION BY WAVEFORM SHAPE

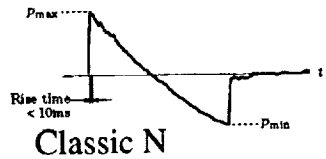

Classic N

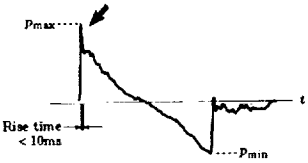

Peaked

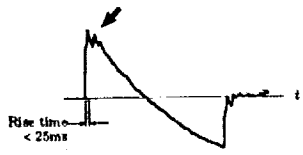

Double-peaked

Multi-peaked

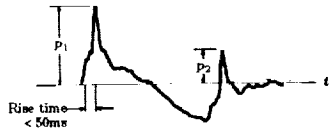

U-wave

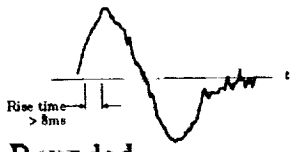

Rounded

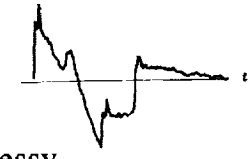

Messy
(for lack of a better term)

Because of the great variability in the distortions a sonic boom wave can undergo, an automatic numerical procedure was developed for quantifying the distortion in a sonic boom wave. The first component of this quantification is to find a basis for comparison. Since one usually puts microphones on the ground, and measures the sonic boom wave only after it has been distorted, it is necessary to estimate the wave shape of the sonic boom *before* it was distorted.

The assumption made here is that before any waveform distortions occurred that the sonic boom wave had the shape of a perfect N-wave with zero rise times on both bow and tail shocks. The energy in the distorted sonic boom is measured, and then it is assumed that the undistorted ideal N-wave has the same energy. Obviously, this is an approximation.

Given this information the proper maximum overpressure, duration, and start time offset of the ideal N-wave is automatically computed. Additional details on the elaborate algorithm used to calculate the parameters for the ideal N-wave, given the distorted sonic boom wave, are available in the M.S. thesis of Gionfriddo (Ref. 3).

WAVEFORM DISTORTION ANALYSIS:
COMPARE DATA TO IDEAL N-WAVE MODEL

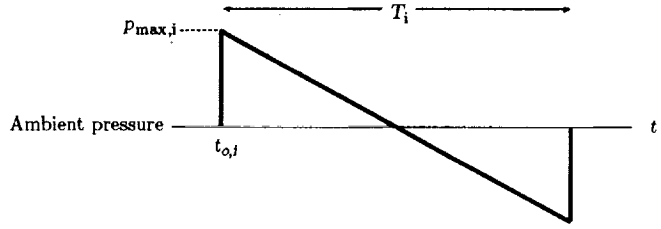

Model of the sonic boom signature just prior to entering the TBL.

Ideal N-wave and the recorded data have equal acoustic energy.

The ideal N-wave is superimposed on the same time axis as the recorded data.

The proper maximum overpressure, duration, and start time offset of the ideal N-wave must be determined.

It is desired to have Classic N data with the lowest mean- squared deviation for any waveshape. Therefore, Classic N data are used as a reference for superimposing the ideal N-wave correctly over the recorded data.

Here is a typical recorded sonic boom wave with its ideal N-wave superimposed.

To quantify the distortion in the measured waveform, the notion of a mean-squared deviation is used, defined below. The functions $p_{ideal}[n]$ and $p_{recorded}[n]$ are both assumed to be digitized data. For the example waveform shown here, the mean-squared deviation is 0.075.

EXAMPLE OF RECORDED BOOM WITH IDEAL N-WAVE SUPERIMPOSED

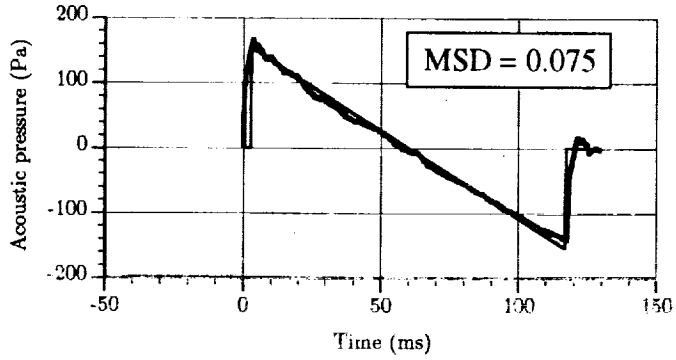

MEASURE OF WAVEFORM DISTORTION: MEAN-SQUARED DEVIATION

The *mean-squared deviation* (MSD) is defined as:

$$MSD = \frac{\sum (p_{ideal}[n] - p_{recorded}[n])^2}{\sum (p_{ideal}[n])^2}$$

Here are two more sonic boom waveforms with superimposed ideal N-waves. The upper waveform is a Peaked sonic boom wave, and it shows a mean-squared deviation of 0.095. The lower waveform is a Rounded waveform, having a much larger mean-squared deviation of 0.23.

TWO MORE EXAMPLES OF RECORDED BOOMS WITH IDEAL N-WAVES SUPERIMPOSED:

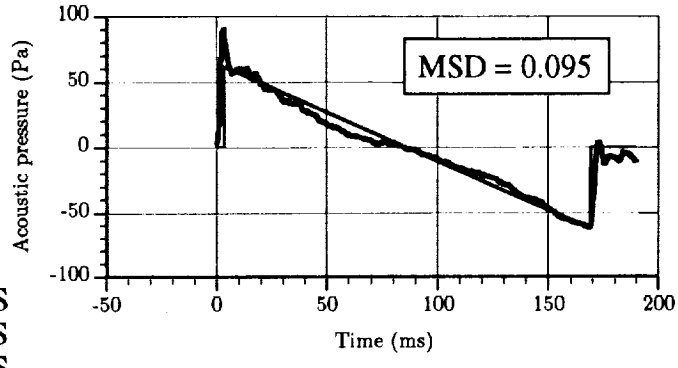

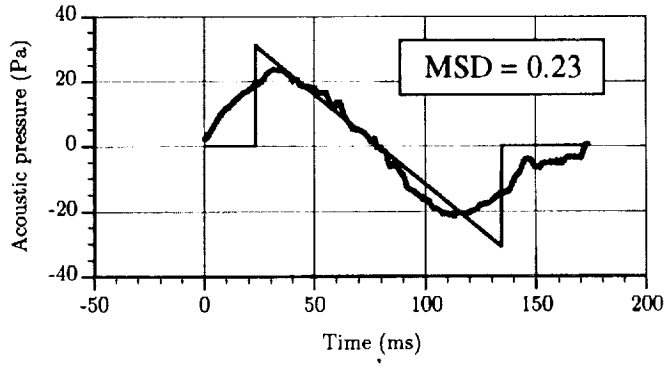

The particular sonic boom data we analyzed was taken near Edwards Air Force Base in the late summer of 1987 by the U. S. Air Force. Autonomous Boom Event Analyzer Recorder (BEAR) systems took data over several days from a wide variety of supersonic aircraft: F-4, F-14, F-15, F-16, F-18, SR-71, T-38, AT-38, and F-111D. The recorders were placed at the mile markers along a road in the area. The aircraft were to fly perpendicular to the road over a specific flight track. From 44 aircraft flights, over 500 data files were obtained for analysis. The specific position of where the aircraft overflew the road was recorded, and this information has been taken into account in our analysis.

MOJAVE DESERT SONIC BOOM ACQUISITION SCHEMATIC

F-4, F-14, F-15, F-16, F-18, SR-71, T-38, AT-38, and F-111D aircraft

Lateral array of thirteen Boom Event Analyzer Recorder (BEAR) systems

Flight track perpendicular to array

44 Flights ~ 500 data files

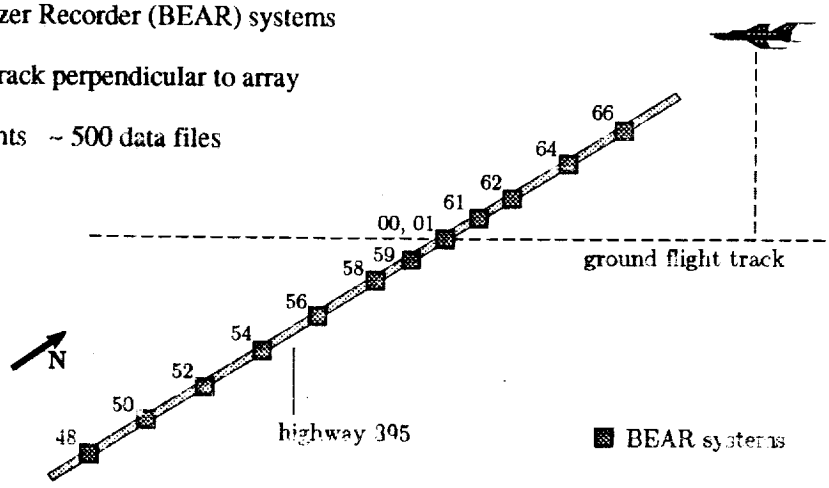

To determine the path length a sonic boom will traverse through the turbulent boundary layer near the earth's surface, a short exercise in three-dimensional solid geometry is needed. Knowing the altitude of the aircraft, its Mach number, the lateral ground distance of the receiving microphone from the aircraft's actual flight track, and the thickness of the boundary layer, this path length can be obtained. The path length is shown as a dark solid line in the diagram.

PATH LENGTH THROUGH THE TURBULENT BOUNDARY LAYER

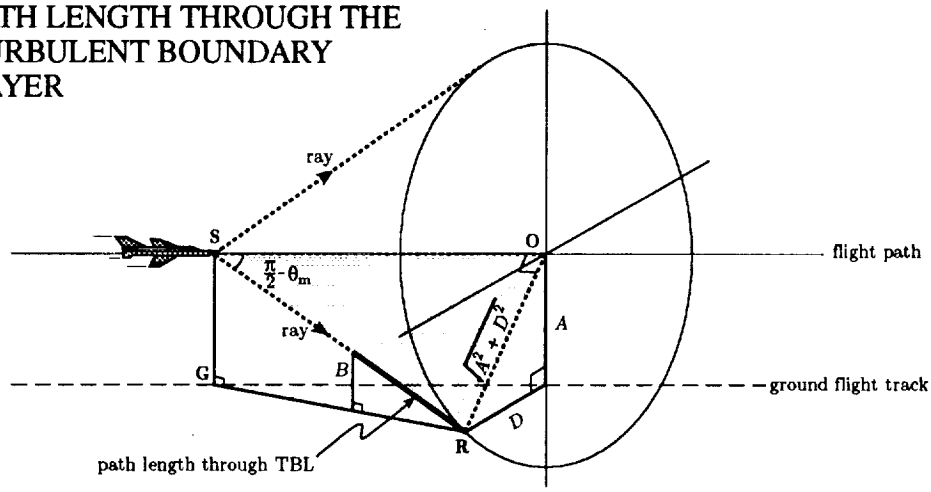

Function of:
- altitude
- Mach number
- lateral ground distance
- TBL thickness

The turbulent boundary layer is defined as the thickness of the mixing layer of the planetary boundary layer. One may assume that the turbulence in the mixing layer is somewhat evenly distributed and homogeneous.

To determine the thickness of this layer, a numerical model by A. K. Blackadar was employed. The numerical model takes into account information from rawinsonde launches, surface weather data, satellite cloud photos, and soil parameters for the site of the sonic boom tests. Blackadar's model provides daily profiles to 2000 m height for temperature, water content, wind, and boundary layer thickness.

PATH LENGTH THROUGH THE TURBULENT BOUNDARY LAYER (CONTINUED)

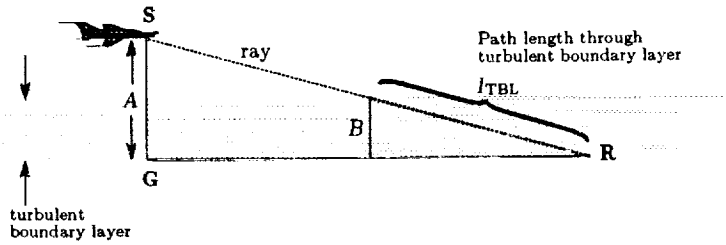

TBL thickness estimated using numerical model by A. K. Blackadar (PSU meteorology)

Input atmospheric information from rawinsonde launches, surface weather station, satellite cloud photos, soil parameters

Model provides diurnal profiles to 2000 m for temperature, water content, wind, and TBL thickness

For the days of the tests, 3 - 8 August 1987, profiles of the turbulent boundary layer thickness were obtained from the Blackadar model. One can see the thickness of the boundary layer generally grew during the day between 7:00 AM and 2:00 PM. Because of the meteorological conditions present, the boundary layer grew much more on 3 August and 4 August than it did on the other days of the tests.

TURBULENT BOUNDARY LAYER THICKNESS
ESTIMATION USING BLACKADAR MODEL

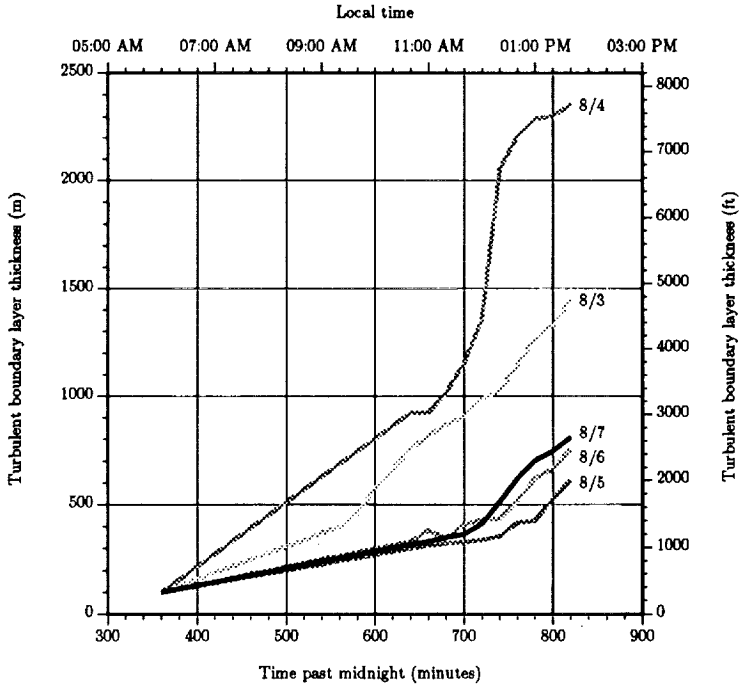

Before continuing, the analysis procedure will be summarized. On one track the BEAR sonic boom data was obtained and calibrated. From this data pressure versus time plots were obtained, which were subsequently sorted into waveshape categories. Given these plots, the sonic boom distortion quantification algorithm was run, and mean-squared deviations from the computer generated corresponding ideal N-waves were obtained for all the the waveforms.

On the other track, the aircraft flight parameters and geometry were combined with the meteorological data and subsequent predictions of the boundary layer height from Blackadar's model. From this information the path length through the turbulence was found for *each* recorded sonic boom waveform.

It was then possible to determine if a statistical correlation existed between the mean-squared deviation and the path length the sonic boom traveled through the turbulence.

ANALYSIS PROCEDURE

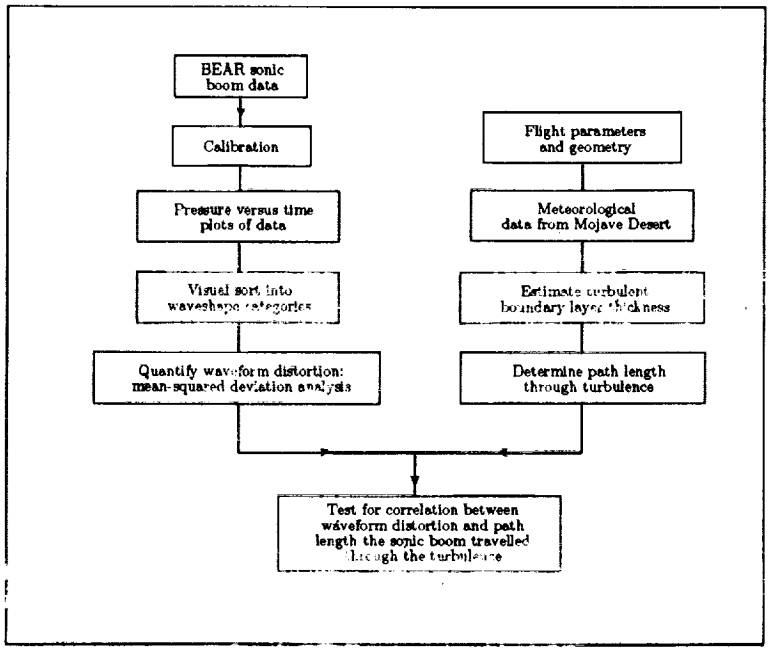

During the analysis procedure it became immediately apparent that those waveforms which were either shaped as a Classic N-waves, or were nearly shaped as such, were primarily manifest only in the early morning hours.

This result leads us to believe that as the turbulent boundary layer grew through the day, that the number of undistorted waveforms decreased. This result is averaging over all of the usable observation data.

SIMPLE DEMONSTRATION: FRACTION OF RECORDED SONIC BOOM WAVEFORMS THAT ARE LEAST-DISTORTED

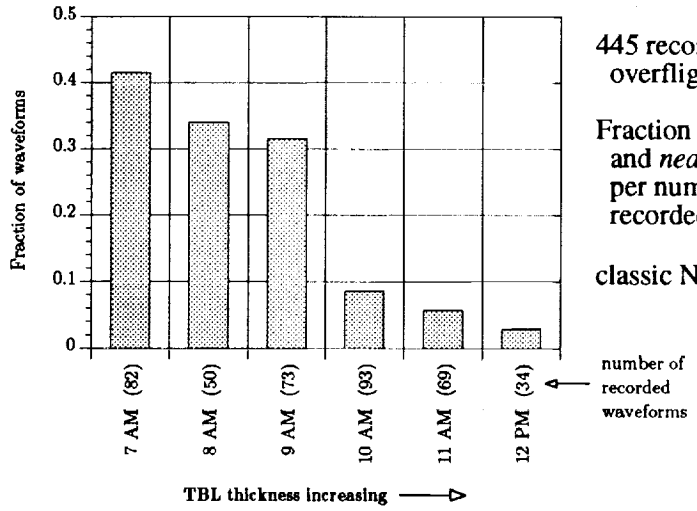

445 recordings from 7/31 - 8/7 overflights during 7AM-1PM

Fraction is number of *classic N* and *nearly classic N* waveforms per number of waveforms recorded during the hour intervals

classic N ➡ least distorted

This is a plot of the mean-squared deviation as a function of altitude (or roughly Mach number, since faster planes generally flew higher). It is apparent that increased altitude and speed imply decreased waveform distortion and a decreased spread of data points. Now higher and faster flying planes generally will have shorter propagation paths through the turbulent boundary layer, which can be shown from simple geometry. Thus, it appears as if longer propagation paths through the turbulence result in larger mean-squared deviations, i.e., more distorted waveforms.

ALTITUDE AND MACH NUMBER INFLUENCE UPON WAVEFORM DISTORTION

Increased altitude and speed ➡ decreased waveform distortion and decreased spread of data points

F-18, F-15, SR-71, F-4, and F-16 data

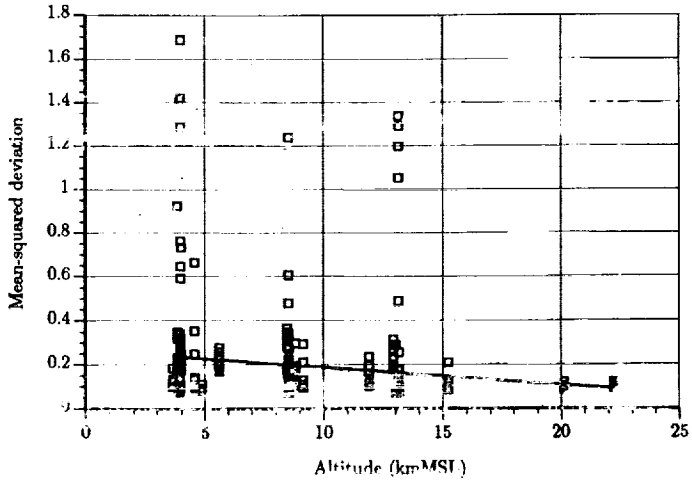

Here are some results listed by plane type of the linear correlation coefficients between the mean-squared deviation and the path length through the turbulent boundary layer. It is seen that there is strong correlation in some cases (F-18 and F-15) and fair correlation in the others. This also gives us some evidence that increasing distortion is correlated with increasing path length through the turbulence.

The F-4 and F-16 data have the lowest correlations and the lowest altitudes. For these cases the sonic boom signatures probably did not have time to develop into an N-wave by the time it began to interact with the turbulence. The other aircraft types flown had too few data points to draw any statistical conclusions.

We also are currently working on obtaining correlation coefficients grouped by altitude and mach number as well as by plane type, to determine how these factors interrelate.

CORRELATION COEFFICIENTS FOR
MEAN-SQUARED DEVIATION AND
TBL PATH LENGTH

Aircraft type	Correlation coefficient: MSD vs TBL path length	Number of samples
F-18	0.712	62
F-15	0.591	75
SR-71	0.398	48
F-4	0.324	46
F-16	0.318	65

(Linear regression correlation coefficients)

Strong correlation in some cases, fair correlation in others

F-4 and F-16 have lowest correlations and the lowest altitudes
- Sonic boom signature before TBL probably not N-wave
- Less distance for nonlinear steepening to work before TBL

The conclusions of this study are the following: a strong linear correlation exists between the mean-squared deviation and path length through the turbulence for the F-18 and F-15 sonic boom data. Fair correlation exists for the SR-71, F-4, and F-16 data. An increase in altitude and speed results in decreased waveform distortion and a small deviation between distortion values. Looking at the waveform classification results, the large percentage of Classic N-wave data during each day's early flights seems to correspond with the thin boundary layer at that time.

Conclusions:

- A strong linear correlation exists between mean-squared deviation and path length through the turbulence for F-18 and F-15 sonic boom data.
- Fair correlation exists for SR-71, F-4, and F-16 data.
- An increase in altitude and speed results in decreased waveform distortion and a smaller deviation between distortion values.
- Looking at waveform classification results, the large percentage of classic N wave data during early flights seems to correspond with the thin boundary layer at that time.

PENNSTATE

The implications of this study for high speed research are the following: Increased interaction between real atmospheric turbulence and actual sonic boom data does imply more distorted waveforms. The common assumption prevailing in the sonic boom propagation community for the last several years has been validated statistically. And most importantly, it is now clear that atmospheric turbulence will determine how well a shaped sonic boom will remain shaped as it propagates to the ground. We are now led to believe that higher and faster aircraft having shaped sonic booms will, on average, have more shaped boom preserved than will aircraft flying at lower altitudes and slower speeds, since flying higher and faster minimizes the path length through the turbulence.

Implications for High Speed Research:

- Increased interaction between real atmospheric turbulence and actual sonic booms does imply more distorted waveforms.
- This common assumption has been validated statistically.
- *Most Importantly:* Atmospheric turbulence primarily will determine how well a shaped sonic boom will remain shaped as it propagates to the ground.

PENNSTATE

The authors would like to thank Dr. Allan D. Pierce and Dr. Richard Raspet for numerous discussions. This research was supported by NASA Langley Research Center, under grant NAG-1-1365, administered by Dr. G. L. McAninch, Scientific Officer.

References

1. "Spikes on sonic-boom pressure waveforms," Allan D. Pierce, J. Acoust. Soc. Am., **44** 1052-1061 (1968).
2. "Laboratory simulation of development of superbooms by atmospheric turbulence," H. S. Ribner, P. J. Morris, and W. H. Chu, J. Acoust. Soc. Am., **53** 926–928 (1973).
3. "Quantification of sonic boom distortions from propagation through atmospheric turbulence," Thomas A. Gionfriddo, M.S. Thesis, The Pennsylvania State University, December 1992.

PENNSTATE

N94-28191

Interaction of the Sonic Boom with Atmospheric Turbulence

Zvi Rusak

Mechanical Engineering, Aeronautical Engineering and Mechanics,

Julian D. Cole

Department of Mathematical Sciences,

Rensselaer Polytechnic Institute

Troy, NY 12180-3590

Abstract

Theoretical research has been carried out to study the effect of free-stream turbulence on sonic boom pressure fields. A new transonic small-disturbance model to analyze the interactions of random disturbances with a weak shock has been developed. The model equation has an extended form of the classic small-disturbance equation for unsteady transonic aerodynamics. An alternative approach shows that the pressure field may be described by an equation that has an extended form of the classic nonlinear acoustics equation that describes the propagation of sound beams with narrow angular spectrum. The model shows that diffraction effects, nonlinear steepening effects, focusing and caustic effects and random induced vorticity fluctuations interact simultaneously to determine the development of the shock wave in space and time and the pressure field behind it. A finite-difference algorithm to solve the mixed-type elliptic-hyperbolic flows around the shock wave has also been developed. Numerical calculations of shock wave interactions with various deterministic and random fluctuations will be presented in a future report.

Contents

1 Introduction

Experimental data exists showing the pressure profiles of sonic booms, created by the passage of a distant supersonic aircraft, can be drastically affected by free-stream atmospheric turbulence.[1-5] The usual N-wave or a shaped sonic boom profile can randomly exhibit either large pressure peaks with short rise times or rounded profiles with longer rise times or messy pressure signatures. Recent laboratory model experiments to study the effect of turbulence on the rise time and wave form of N-waves have shown similar results.[6] The interaction of the sonic boom with the atmospheric turbulence, specifically in the atmospheric boundary layer relatively near the ground, may result sometimes in higher, and may be unacceptable loudness levels.[7] Therefore, in order to get reasonable estimates of the sonic boom performance of various designs of a future supersonic transport airplane it is essential to understand the basic interactions of the atmospheric turbulence with shock waves.

The basic analysis of the distortion of sonic bangs by atmospheric turbulence was given by Crow.[8] Using a first-order acoustic scattering theory, Crow showed that the pressure perturbation behind the shock is related to the interaction of the shock with the disturbances it encounters while moving in the atmosphere. The pressure profile can be calculated by a surface integral over a paraboloid of dependence, whose focus is the observation point and whose directix is the shock front. By describing the turbulent eddies in the Kolmogorov inertial subrange, it was found that the mean-square pressure perturbation behind the shock changes like $(\Delta p)^2(t_c/t)^{7/6}$ where (Δp) is the pressure jump across the shock, (t) is time after the shock passes an observation point and (t_c) is a critical time predicted in terms of meteorological conditions. Crow's analysis predicts reasonable average values of the pressure fluctuations for times (t) comparable to (t_c).

The singularity in the pressure perturbations near the shock front (when $t \rightarrow 0$) was analyzed by Plotkin and George[9]. A second-order acoustic scattering theory was used to describe shock rounded signatures. The average of the diffraction effects was approximated as a dissipation term.

The thickening of the shock is explained as a balance between nonlinear steepening effects and the dissipative effect of the turbulent scattering of acoustic energy out of the incident shock. Rise time predictions of this theory show some correlation with experimental data. On the other hand, Ffowcs Williams and Howe[10] examined the approaches that describe the possibility of a turbulent thickening of weak shock waves and reached a conclusion that atmospheric turbulence cannot be the cause of shock thickening. They suggested that weak shocks may attain a dispersed profile due to non-equilibrium gas effects.

It should be emphasized here that the scattering analyses of References 8-10 considered small turbulent perturbations against the shock strength, whereas in the case of the interaction of the sonic boom with atmospheric turbulence the flow random fluctuations may be of the same order of the shock weak strength and may strongly distort the shock front. The above analyses also did not account for shock jump conditions that must be satisfied in an inviscid analysis across any shock surface. The approximation made in Reference 9 of the average diffraction effects described as a dissipative term is also unclear.

A different approach was taken by Pierce[11,12]. He interpreted the spikes observed on sonic boom pressure waveforms as being due to the simultaneous focusing and diffraction of a nearly planar N-wave by an inhomogeneous layer in the atmosphere. The shock front develops ripples that are transformed into folds in the front when the shock passes vertices of caustics. This mechanism results in a fine structure of very small pressure jumps that correspond to the various segments of the folded wavefront. Pierce[12] derived a stochastic model of a sharp shock propagating through a turbulent atmosphere to substantiate the very small discrete structure of sonic boom profiles.

Pierce model[11,12], however, neglects nonlinear effects that become significant specifically near a caustic vertex as was shown by Cramer and Seebass[13] and Gill and Seebass[14]. Cramer and Seebass[13] described the focusing of a very weak and slightly concave shock wave by the unsteady transonic small-disturbance flow equation. Gill and Seebass[14] derived an

approximate analytical solution of the steady transonic small-disturbance problem for the nonlinear behavior of a weak compression wave with a finite rise time near a caustic. They calculated the reflected shock wave from a caustic and provided an estimate of its strength. The experimental results of Sturtevant and Kulkarny[15] also show that focusing effects are specifically significant for weak shock waves as occurs in the case of the sonic boom signatures.

Sparrow and Pierce[15] have recently presented a simple statistical prediction for how often sonic booms propagating in the earth's boundary layer will encounter caustics. The theory is based on describing the variation of ray tube areas of a sound wave propagating in a turbulent medium by a generic harmonic oscillator equation. For realistic realizations of atmospheric turbulence the model predicts that sonic booms will exhibit spikes with the occurrence of caustics after a very short distance of travel in the random medium, thus agreeing with the predictions of Pierce[11,12].

In a recent paper, Pierce[17] has derived a model equation to describe the development of sonic boom signatures in an atmospheric turbulence. The equation has been constructed by suing logical physical considerations only. It extends geometrical acoustic approximations to include convection at the wave speed, diffraction effects, molecular relaxation, classical dissipation and nonlinear steepening effects. The atmospheric turbulence enters through an effective speed of sound which varies randomly in time and space. However, since this theory has not been developed consistently from the fluid dynamic equations, Pierce[17] raised questions whether all the effects are necessary in his suggested model and how to accomplish a numerical or analytical solution to the problem.

Related with the problem of the sonic boom interaction with turbulence is the basic question of the interaction of a shock wave with a vortical flow and specifically with a vortex or a train of eddies[18-21]. The research of the later problem was basically motivated by the interest to reduce the noise and vibrations produced by high-speed supersonic vehicles. For these problems, the interaction of relatively strong shock waves with turbulent jets or wakes is a significant source of noise. The shock-vortex system is a

basic element of these more complex interactions[21]. It can also shed light on the sonic boom interaction with atmospheric turbulence, specifically when the shocks are weak and vortex strength is comparable with the shock strength.

Experimental results of shock-vortex systems[18-21] revealed curved, diffracted shocks as well as complicate structures of reflected curved shock waves from the incident shock front due to the vortex induced flow field. The pressure field behind the shock contains regions of compressions and rarefactions that produce acoustic waves. Similar shock structures were also observed by Sturtevant and Kulkarny[15] who investigated the focusing of weak curved shock waves. Of specific interest are Dosanjh and Weeks[19] measurements of the interaction of a shock wave with a vortex street. The shock front is distorted by the wake flow which probably results in a focusing process, while the vortex street is rapidly dissolved by the shock.

The analyses of the shock-vortex interaction are limited to linear perturbation theories only.[22-26] These analyses considered the jump conditions across a shock surface and predicted the development of vorticity waves, entropy waves and acoustic waves behind the shock front.[22-24] The acoustic wave was approximated by a quadrupolar[26] or as a sum of monopole, dipole and quadrupole acoustic sources. However, since all of these theories are linear, they cannot account for any nonlinear effects due to shock large distortions, focusing and caustic effects or nonlinear steepening effects that are found in experiments[18-20] or in recent numerical simulations of shock-vortex interactions.[27-29]

The review of experimental and theoretical investigations of the interaction of shock waves with free stream vortical or turbulent flows shows that this complex nonlinear interaction is still an open problem.[27] Specifically, the improved simulation of sonic boom propagation through the real atmosphere requires a better understanding of the interaction of sonic boom with atmospheric turbulence.[16]

The analysis of the experimental data and the theoretical approaches shows that in the case of the sonic boom, the shock waves near ground

are very weak, but still stronger than any acoustic wave. Also, flow fluctuations due the atmospheric turbulence can become comparable to the shock weak strength such that locally the shock strength can be strongly reduced or magnified and the shock wave front can be distorted significantly. Therefore, linearized acoustics and its second-order scattering problem, or first-order linear theories of shock-vorticity interaction do not represent correctly the development of the weak shock and the pressure field behind it (see also Section 2). However, in a coordinate system moving with the basic weak shock, the problem may fit the transonic framework.

This paper presents a new transonic small-disturbance model that has been developed to describe the interactions of random fluctuations with a weak shock wave. The model equation is found to have an extended form of the classic nonlinear acoustics equation that describes the propagation of sound beams with narrow angular spectrum (KKZ equation).[30,31] The model shows that diffraction effects, nonlinear steepening effects, focusing and caustic effects and random induced vorticity fluctuations interact simultaneously to determine the development of the shock wave in space and time and the pressure field behind it. A finite-difference algorithm to solve the mixed-type elliptic-hyperbolic flows around the shock wave is also presented. The results of the numerical calculations will be presented in a future report. It is expected to find solutions that will describe both peaked or rounded or messy pressure signatures as were recorded in experiments.

2 The Breakdown of the Linearized Theory

2.1 The Linearized Theory

An inviscid and a non heat conducting flow is assumed. A normal shock with a uniform supersonic oncoming stream and a uniform subsonic outgoing flow is considered. The upstream flow ahead of he shock is characterized by a speed (U_{0a}) in the x- direction, pressure (p_{0a}) and density (ρ_{0a}) and the downstream flow behind the shock by (U_{0b}), (p_{0b}) and (ρ_{0b}) respectively.

Assuming the shock front is given by the $x = 0$ plane, the jump conditions across a normal shock[32] show that:

$$\rho_{0a}U_{0a} = \rho_{0b}U_{0b}$$

$$\rho_{0a}U_{0a}^2 + p_{0a} = \rho_{0b}U_{0b}^2 + p_{0b} \tag{1}$$

$$\frac{1}{2}\rho_{0a}U_{0a}^3 + \frac{\gamma}{\gamma-1}p_{0a}U_{0a} = \frac{1}{2}\rho_{0b}U_{0b}^3 + \frac{\gamma}{\gamma-1}p_{0b}U_{0b}$$

Small disturbances are considered in each of the uniform streams. The velocity vector ($\underset{\sim}{V}$), pressure (P), density (ρ) and vorticity ($\underset{\sim}{\omega}$) are given ahead ($j = a$) and behind the shock ($j = b$) by:

$$\underset{\sim}{V}_j = U_{0j}(\underset{\sim}{e}_x + \epsilon \underset{\sim}{v}_{1j} + \cdots)$$

$$P_j = P_{0j}(1 + \epsilon p_{1j} + \cdots) \tag{2}$$

$$\rho_j = \rho_{0j}(1 + \epsilon \rho_{1j} + \cdots)$$

$$\underset{\sim}{\omega}_j = \epsilon \underset{\sim}{\omega}_{1j} + \cdots, \qquad \underset{\sim}{\omega}_{1j} = \nabla \times \underset{\sim}{v}_{1j}$$

Here $\underset{\sim}{v}_{1j}, p_{1j}, \rho_{1j}$ are functions of (x, y, z, t). An axial coordinate moving with the uniform speed is considered in each region, $\xi_j = x - U_{0j}t, \tau = U_{0j}t$. The substitution into the continuity, momentum and energy equations results to the leading order in ($\underset{\sim}{\nabla} = \frac{\partial}{\partial \xi_j}\underset{\sim}{e}_x + \frac{\partial}{\partial y}\underset{\sim}{e}_y + \frac{\partial}{\partial z}\underset{\sim}{e}_z$):

$$\frac{\partial \rho_{1j}}{\partial \tau} + \underset{\sim}{\nabla} \cdot \underset{\sim}{v}_{1j} = 0$$

$$\frac{\partial \underset{\sim}{v}_{1j}}{\partial \tau} + \frac{1}{\gamma M_{0j}^2}\underset{\sim}{\nabla} p_{1j} = 0 \tag{3}$$

$$\frac{\partial p_{1j}}{\partial \tau} + \gamma(\underset{\sim}{\nabla} \cdot \underset{\sim}{v}_{1j}) = 0$$

Equations (3) result in:

$$\frac{\partial p_{1j}}{\partial \tau} = \gamma \frac{\partial \rho_{1j}}{\partial \tau}, \qquad \frac{\partial \underset{\sim}{\omega}_{1j}}{\partial \tau} = 0, \qquad M_{0j}^2 \frac{\partial^2 p_{1j}}{\partial \tau^2} - \nabla^2 p_{1j} = 0 \tag{4}$$

where $M_{0j} = U_{0j}/c_{0j}$ and $c_{0j}^2 = \gamma p_{0j}/\rho_{0j}$. Equations (4) show that $\underset{\sim}{\omega}_{1j} = \underset{\sim}{\omega}_{1j}(\xi_j, y, z)$ and that the pressure perturbation p_{1j} is described by the acoustics equation. Therefore, the first order disturbance flow can be split into a linear combination of rotational and irrotational parts: $\underset{\sim}{v}_{1j} = \underset{\sim}{v}_{1j\omega} + \underset{\sim}{v}_{1j0}$. The rotational part can be described essentially by incompressible flow equations:

$$\underset{\sim}{\nabla} \cdot \underset{\sim}{v}_{1j\omega} = 0, \qquad \underset{\sim}{\nabla} \times \underset{\sim}{v}_{1j\omega} = \underset{\sim}{\omega}_{1j}(\xi_j, y, z) \tag{5a}$$

The irrotational (potential) part may be described by acoustics equations relative to the basic flow in each region:

$$\underset{\sim}{v}_{1j0} = \underset{\sim}{\nabla}\phi_j, \qquad p_{1j} = -\gamma M_{0j}^2 \frac{\partial \phi_j}{\partial \tau}, \qquad M_{0j}^2 \frac{\partial^2 \phi_j}{\partial \tau^2} - \nabla^2 \phi_j = 0 \tag{5b}$$

The first-order perturbation theory also considers the distortion of the shock front. Assuming that the perturbed shock front is given by $x - \epsilon g_1(y, z, t) = 0$, the exact jump condition across the shock[32] result to the leading order in a set of conditions that must be satisfied along the $x = 0$ plane for any (y, z, t):

$$\rho_{1a}(0, y, z, t) + u_{1a}(0, y, z, t) - \frac{g_{1t}}{U_{0a}} = \rho_{1b}(0, y, z, t) + u_{1b}(0, y, z, t) - \frac{g_{1t}}{U_{0b}}$$

$$U_{0a}\left(\rho_{1a}(0, y, z, t) + 2u_{1a}(0, y, z, t)) + \frac{1}{\gamma M_{0a}^2} p_{1a}(0, y, z, t)\right) =$$

$$= U_{0b}\left(\rho_{1b}(0, y, z, t) + 2u_{1b}(0, y, z, t) + \frac{1}{\gamma M_{0b}^2} p_{1b}(0, y, z, t)\right)$$

$$U_{0a}^2\Big(\rho_{1a}(0,y,z,t)+3u_{1a}(0,y,z,t)+\frac{2}{(\gamma-1)M_{0a}^2}(p_{1a}(0,y,z,t)+$$

$$+u_{1a}(0,y,z,t))-\frac{g_{1t}}{U_{0a}}\left(1+\frac{2/\gamma}{(\gamma-1)M_{0a}^2}\right)\Big)$$

$$=U_{0b}^2\Big(\rho_{1b}(0,y,z,t)+3u_{1b}(0,y,z,t)+\frac{2}{(\gamma-1)M_{0b}^2}(p_{1b}(0,y,z,t)+$$

$$+u_{1b}(0,y,z,t))-\frac{g_{1t}}{U_{0b}}\left(1+\frac{2/\gamma}{(\gamma-1)M_{0b}^2}\right)\Big)$$

$$U_{0a}(v_{1a}(0,y,z,t)+g_{1y})=U_{0b}(v_{1b}(0,y,z,t)+g_{1y})$$

$$U_{0a}(w_{1a}(0,y,z,t)+g_{1z})=U_{0b}(w_{1b}(0,y,z,t)+g_{1z}) \tag{6}$$

Here $g_{1t}=\partial g_1/\partial t$ and (u_{1j},v_{1j},w_{1j}) are the components of the velocity perturbation $\underset{\sim}{v}_{1j}$. The linearized jump conditions in Eqs. (6) include the entropy increase produced by the shock. It can be shown from Eqs. (5) and (6) that, using the solution of the downstream equations for the disturbance flow, the shock conditions are adequate to describe the flow downstream and the disturbed motion of the shock wave for given upstream disturbances.

2.2 One Dimensional Flow

In the case of a one-dimensional flow, the rotational part vanishes identically and the solution of the acoustics equation ahead ($j=a$) and behind ($j=b$)

the shock is given by:

$$
\begin{aligned}
u_{1j} &= F\left(\xi_j - \frac{\tau}{M_{0j}}\right) + G\left(\xi_j + \frac{\tau}{M_{0j}}\right) \\
p_{1j} &= \gamma M_{0j}\left(F\left(\xi_j - \frac{\tau}{M_{0j}}\right) - G\left(\xi_j + \frac{\tau}{M_{0j}}\right)\right) \\
\rho_{1j} &= M_{0j}\left(F\left(\xi_j - \frac{\tau}{M_{0j}}\right) - G\left(\xi_j + \frac{\tau}{M_{0j}}\right) + \rho_{sj}(\xi_j)\right)
\end{aligned}
\tag{7}
$$

where F and G are arbitrary functions that describe the upstream and downstream acoustic waves. Here ρ_s is an arbitrary function that describes entropy waves that are convected with the flows (the entropy first-order disturbance is given by $S_j - S_{0j} = \epsilon s_{1j} = -\epsilon c_p M_{0j}\rho_{sj}(\xi_j)$, where S_j is the entropy in region j, $S_{0j} = c_v \ln(P_{0j}/\rho_{0j}^{\gamma})$ and c_v, c_p are the specific heat constants). Assuming that no upstream acoustic waves can develop, specifically not in the flow behind the shock then $G \equiv 0$. Then the shock jump conditions (6) provide a system of 3 linear equations for the solution of the downstream acoustic and entropy waves $F_b(\xi_b - \frac{\tau}{M_{0b}})$ and $\rho_{sb}(\xi_b)$ and the shock position rate of change in time $g_{1t}(t)$ in terms of the given acoustic and entropy perturbations $F_a(\xi_a - \frac{\tau}{M_{0a}})$ and $\rho_{sa}(\xi_a)$ in the upstream flow. Let,

$$
\begin{aligned}
F_{a0} &= F_a(-(U_{0a} + c_{0a})t), \qquad \rho_{sa0} = \rho_{sa}(-U_{0a}t) \\
F_{b0} &= F_b(-(U_{0b} + c_{0b})t). \qquad \rho_{sb0} = \rho_{sb}(-U_{0b}t)
\end{aligned}
\tag{8}
$$

then from Eqs. (6) - (8) we get:

$$(1+M_{0b})F_{b0}+M_{0b}\rho_{sb0}+\left(\frac{U_{0b}}{U_{0a}}-1\right)\frac{g_{1t}}{U_{0b}}=(1+M_{0a})F_{a0}+M_{0a}\rho_{sa0}$$

$$\left(2+M_{0b}+\frac{1}{M_{0b}}\right)F_{b0}+M_{0b}\rho_{sb0}=\frac{U_{0a}}{U_{0b}}\left(\left(2+M_{0a}+\frac{1}{M_{0a}}\right)F_{a0}+M_{0a}\rho_{sa0}\right)$$

$$\left(3+M_{0b}+\frac{2}{(\gamma-1).M_{0b}^2}(1+\gamma.M_{0b})\right)F_{b0}+M_{0b}\rho_{sb0}+$$

$$+\left(\frac{U_{0a}}{U_{0b}}\left(1+\frac{2/\gamma}{(\gamma-1).M_{0a}^2}\right)-1-\frac{2/\gamma}{(\gamma-1).M_{0b}^2}\right)\frac{g_{1t}}{U_{0b}}=$$

$$=\frac{U_{0a}^2}{U_{0b}^2}\left(\left(3+M_{0a}+\frac{2}{(\gamma-1).M_{0a}^2}(1+\gamma M_{0a})\right)F_{a0}+M_{0a}\rho_{sa0}\right) \qquad (9)$$

The determinant of the system (9) may be written in the form $\Delta = (M_{0a}^2-1)fn(M_{0a}^2)$. Therefore, the solution of Eqs. (9) shows that the shock front motion and the perturbed flow behind it may be described by:

$$\begin{aligned}
x &= \frac{\epsilon}{M_{0a}^2-1}\tilde{g}_1(t;M_{0a}) \\
u_{1b} &= U_{0b}\left(1+\frac{\epsilon}{M_{0a}^2-1}\tilde{u}_1(x,t;M_{0a})+\cdots\right) \\
p_{1b} &= P_{0b}\left(1+\frac{\epsilon}{M_{0a}^2-1}\tilde{p}_1(x,t;M_{0a})+\cdots\right) \qquad (10) \\
\rho_{1b} &= \rho_{0b}\left(1+\frac{\epsilon}{M_{0a}^2-1}\tilde{\rho}_1(x,t;M_{0a})+\cdots\right)
\end{aligned}$$

The functions $\tilde{g}_1, \tilde{u}_1, \tilde{p}_1, \tilde{\rho}_1$ can be expressed in terms of the given flow perturbations ahead of the shock wave. In principle, these expressions may

enable a spectral characterization of the pressure fluctuations and the turbulence downstream of the shock wave in terms of the spectral characterization of the incoming turbulence. However, Eqs. (10) show that the linear approach is a non-uniform approach when the shock wave is very weak $M_{0_a}^2 \rightarrow 1^+$ and the flow fluctuations are of the same order of the shock strength, $\epsilon \sim (M_{0_a}^2 - 1)$, as is the case of the interaction of the sonic boom with atmospheric turbulence. A similar nonuniformity is also expected from the analysis of two- or three-dimensional flows. However, this uniformity problem leads to a different approach to study the interaction of a weak shock with comparable random fluctuations in the flow.

3 A Transonic Small Disturbance Model

The analysis of the linearized problem of the interaction of a weak shock with small disturbances shows that it is an invalid approach when the flow perturbations are of the order of the shock strength. Therefore, a different approach has been developed to study the interaction of weak shocks with comparable random fluctuations in the flow. In a coordinate system moving with a basic given weak shock, the problem may fit the transonic theory framework. A transonic small-disturbance model is developed to analyze the flow across a basic weak shock running in the $(-x)$ direction. A coordinate system attached to the basic shock is considered. The velocity vector $(\underset{\sim}{V})$, pressure (P), density (ρ) and vorticity $(\underset{\sim}{\omega})$ are described every where in the flow by:

$$\begin{aligned}
\underset{\sim}{V} &= U_\infty \{ \underset{\sim}{i}(1 + \epsilon^{2/3}u + \epsilon u_1 + \epsilon^{4/3}u_2 + \cdots) \\
&\quad + \underset{\sim}{j}(\epsilon v_1 + \epsilon^{4/3}v_2 + \cdots) + \underset{\sim}{k}(\epsilon w_1 + \epsilon^{4/3}w_2 + \cdots)\} \\
P &= p_\infty(1 + \epsilon^{2/3}p + \epsilon p_1 + \epsilon^{4/3}p_2 + \cdots) \qquad (11) \\
\rho &= \rho_\infty(1 + \epsilon^{2/3}\rho + \epsilon\rho_1 + \epsilon^{4/3}\rho_2 + \cdots)
\end{aligned}$$

$$\underset{\sim}{\omega} = \epsilon^{2/3}(\underset{\sim}{j}w_y + \underset{\sim}{k}w_z) + \epsilon(\underset{\sim}{i}\omega_{x1} + \underset{\sim}{j}\omega_{y1} + \underset{\sim}{k}\omega_{z1}) + \cdots$$

where $U_\infty = a_\infty(1 + \frac{K}{2}\epsilon^{2/3})$ is the speed of the basic shock ($K > 0$) and $a_\infty, p_\infty, \rho_\infty$ are the speed of sound, pressure and density of the unperturbed flow ahead of the shock. $(\epsilon^{2/3})$ represents the scale of strength of the basic weak shock where $\epsilon \ll 1$. A rescaling of the x-coordinate and time (t) has also been considered: $x^* = \frac{x}{\epsilon^{1/3}}$ and $t^* = ta_\infty\epsilon^{1/3}$, such that each of the terms in (11) is a function of (x^*, y, z, t^*). The rescaling in x means a stretching of the picture of the flow around the basic shock in order to capture the basic nonlinear effects that occur in the flow across the shock. The rescaling in time accounts for low-frequency unsteady perturbations in the flow. The constant K reflects that the speed of the basic shock wave is a little higher than the speed of sound, ahead of the shock. The substitution of Eqs. (11) into the continuity, momentum and energy equations results to the leading orders in:

$$\begin{cases} \dfrac{\partial}{\partial x^*}(\rho + u) = 0 \\ \dfrac{\partial}{\partial x^*}(\rho_1 + u_1) = 0 \\ \dfrac{\partial \rho}{\partial t^*} + \dfrac{\partial}{\partial x^*}(u_2 + \rho_2 + \rho u) + \dfrac{\partial v_1}{\partial y} + \dfrac{\partial w_1}{\partial z} = 0 \end{cases} \tag{12}$$

$$\begin{cases} \dfrac{\partial}{\partial x^*}(\gamma u + p) = 0 \\ \dfrac{\partial}{\partial x^*}(\gamma u_1 + p_1) = 0 \\ \dfrac{\partial u}{\partial t^*} + \dfrac{\partial u_2}{\partial x^*} + (u + \rho + K)\dfrac{\partial u}{\partial x^*} + \dfrac{1}{\gamma}\dfrac{\partial p_2}{\partial x^*} = 0 \end{cases} \tag{13}$$

$$\begin{cases} \dfrac{\partial v_1}{\partial x^*} = -\dfrac{1}{\gamma}\dfrac{\partial p}{\partial y} \\ \dfrac{\partial w_1}{\partial x^*} = -\dfrac{1}{\gamma}\dfrac{\partial p}{\partial z} \end{cases} \tag{14}$$

$$\frac{\partial p}{\partial t^*} - \gamma\frac{\partial \rho}{\partial t^*} + \rho\frac{\partial p}{\partial x^*} - \gamma p\frac{\partial \rho}{\partial x^*} + \frac{\partial p_2}{\partial x^*} - \gamma\frac{\partial \rho_2}{\partial x^*} = 0 \tag{15}$$

$$\frac{\partial \omega_y}{\partial x^*} = 0, \qquad \frac{\partial \omega_z}{\partial x^*} = 0 \tag{16}$$

From the equation of state and the definition of entropy it can be shown that the temperature T_m and entropy S are given by:

$$\begin{aligned} T_m &= T_\infty(1 + \epsilon^{2/3}T + \cdots) \\ S &= S_\infty(1 + \epsilon^{2/3}s + \cdots) \end{aligned} \tag{17a}$$

where

$$\begin{aligned} T_\infty &= p_\infty/R\rho_\infty, \qquad S_\infty = c_v \ln\left(\frac{p_\infty}{\rho_\infty^\gamma}\right) \\ T &= p - \rho, \qquad s = \frac{c_v}{S_\infty}(p - \gamma\rho) \end{aligned} \tag{17b}$$

Equations (12) through (17) result in:

$$u + \rho = f(y, z, t^*) \tag{18a}$$

$$\gamma u + p = g(y, z, t^*) \tag{18b}$$

$$-2\frac{\partial u}{\partial t^*} + (-K - f + g - (\gamma + 1)u)\frac{\partial u}{\partial x^*} + \frac{\partial v_1}{\partial y} + \frac{\partial w_1}{\partial z} = -\frac{1}{\gamma}\frac{\partial g}{\partial t^*} \tag{18c}$$

$$\omega_y = \frac{\partial u}{\partial z} - \frac{\partial w_1}{\partial x^*} = \frac{1}{\gamma}\frac{\partial g}{\partial z} \tag{18d}$$

$$-\omega_z = \frac{\partial u}{\partial y} - \frac{\partial v_1}{\partial x^*} = \frac{1}{\gamma}\frac{\partial g}{\partial y} \tag{18e}$$

$$T = g - f - (\gamma - 1)u, \qquad s = \frac{c_v}{S_\infty}(g - \gamma f) \tag{18f}$$

where f and g are random induced fluctuations due to the free turbulence. The function g is related to the vorticity fluctuations in the flow. Equations (18) show that the axial perturbation (u), pressure perturbation (p) and density perturbation (ρ), that are of order of the shock strength ($\epsilon^{2/3}$), interact with the transverse velocity perturbations v_1 and w_1, that are of a smaller scale (ϵ).

The substitution of $u = g/\gamma + \bar{u}$ in (18c), (18d) and (18e) results in a problem for solving a velocity potential function $\phi(x^*, y, z, t^*)$ where:

$$\bar{u} = \frac{\partial \phi}{\partial x^*}, \qquad v_1 = \frac{\partial \phi}{\partial y}, \qquad w_1 = \frac{\partial \phi}{\partial z}, \qquad p = -\gamma\frac{\partial \phi}{\partial x^*} \tag{19a}$$

$$2\phi_{x^*t^*} + \left(K + \frac{g}{\gamma} + f + (\gamma + 1)\phi_{x^*}\right)\phi_{x^*x^*} - (\phi_{yy} + \phi_{zz}) = -\frac{1}{\gamma}\frac{\partial g}{\partial t^*} \tag{19b}$$

In a conservative form Eq. (19b) is given by:

$$\left(2\phi_{x^*} + \frac{1}{\gamma}g\right)_{t^*} + ((K + g/\gamma + f)\phi_{x^*} + (\gamma + 1)\phi_{x^*}^2/2))_{x^*} - (\phi_y)_y - (\phi_z)_z = 0 \tag{19c}$$

The exact shock jump conditions (Ref. 32) must be satisfied along any shock surface $x^* - h(y, z, t^*) = 0$ that may appear in the solution. To the leading orders they result in:

$$[f] = 0, \qquad [g] = 0 \tag{20a}$$

$$-2[\phi_{x^*}]\frac{\partial h}{\partial t^*}+(K+g+f)[\phi_{x^*}]+(\gamma+1)\left[\frac{\phi_{x^*}^2}{2}\right]+[\phi_y]\frac{\partial h}{\partial y}+[\phi_z]\frac{\partial h}{\partial z}=0 \quad (20b)$$

$$[\phi_y]+[\phi_{x^*}]\frac{\partial h}{\partial y}=0 \qquad [\phi_z]+[\phi_{x^*}]\frac{\partial h}{\partial z}=0. \quad (20c)$$

where $[a]$ represents the jump across the shock property a, $[a]=a_B-a_A$. Equations (20a) show that to the leading order there is no jump in entropy across the shock, $[S]=0$. Equations (11) and (18) also show that the local Mach number M_ℓ at any point in the flow is given by:

$$M_\ell^2-1=\epsilon^{2/3}u^*, \qquad u^*=\left\{(\gamma+1)\phi_{x^*}+K+f+\frac{g}{\gamma}\right\} \quad (21)$$

The flow is locally supersonic when $(\gamma+1)\phi_{x^*}+K+f+\frac{g}{\gamma}>0$, sonic when $(\gamma+1)\phi_{x^*}+K+f+\frac{g}{\gamma}=0$, and subsonic when $(\gamma+1)\phi_{x^*}+K+f+\frac{g}{\gamma}<0$. Equations (19) and (20) are an extended version of the classic unsteady small-disturbance equation for transonic aerodynamics (Cole and Cook[33]). The only changes are due to the random terms g and f. Starting from given functions for f and g and initial conditions that describe a given basic shock, Eqs. (19) and (20) can be integrated in space and time to describe the development of the shock wave and pressure field behind it. A numerical algorithm to solve these equations is described in Section 4.

An alternative approach may be found by taking a x^*- derivative of (18c) and using Eqs. (18a) and (14). The pressure perturbation (p) satisfies the equation:

$$\frac{\partial}{\partial x^*}\left(\frac{\partial p}{\partial t^*}+\frac{K+f+g/\gamma}{2}-\frac{\gamma+1}{2\gamma}p\frac{\partial p}{\partial x^*}\right)=\frac{1}{2}\left(\frac{\partial^2 p}{\partial y^2}+\frac{\partial^2 p}{\partial z^2}\right) \quad (22)$$

Equation (22) is an extended version of the classic KKZ equation that describes the propagation of nonlinear sound beams with narrow angular spectrum in an inviscid fluid (Zabolotskaya et al.[30], Kuznetsov[31]). Eq. (22) also has a similar form to the model equation that has been recently developed by Pierce[17] using logical considerations only.

Equations (19) and (22) show that diffraction effects, nonlinear steepening, focusing and caustic effects and random induced fluctuations due to turbulence interact simultaneously to determine the development of the shock wave in space and time and the pressure field behind it. Turbulence tends to change the local speed of sound in the flow across the shock and through this effect to reduce or to magnify the strength of the jump along the basic shock (see Eq. (21)) or to distort the shock front. These changes may result in unsteady motion of the shock front or in caustic vertices or in reflected shocks behind the incident wave that can produce the variety of pressure signatures of sonic booms that are measured in experiments.

4 Finite Difference Scheme

A finite difference algorithm to solve the unsteady mixed-type elliptic-hyperbolic flow around the shock wave has been developed. Murman and Cole[34] and Cole and Cook[33] techniques are used. A fully conservative scheme that is based on the conservative form (Eq. 19c) is used. In this way the difference equations also contain the shock relations (Eqs. (20)).

Consider a uniform finite difference mesh $(\Delta x^*, \Delta y, \Delta z, \Delta t^*)$ in space and time, with points (x^*, y, z, t^*) labeled by (i, j, k, n). The results can be easily generalized to a variable mesh. Eq. (19c) can be expressed in a conservative flux form for a box centered on a mesh point (i, j, k). Therefore,

$$\begin{aligned}
&\frac{1}{\Delta t^*}\left\{\left(2\phi_{x^*}+\frac{1}{\gamma}g\right)_{(i,j,k,n)}-\left(2\phi_{x^*}+\frac{1}{\gamma}g\right)_{(i,j,k,n-1)}\right\}+\\
&+\frac{1}{\Delta x^*}\left\{\left(\left(K^*+\frac{1}{\gamma}g+f\right)\phi_{x^*}+(\gamma+1)\phi_{x^*}^2/2\right)_{(i+\frac{1}{2},j,k,n)}\right.\\
&\left.-\left(\left(K^*+\frac{1}{\gamma}g+f\right)\phi_{x^*}+(\gamma+1)\phi_{x^*}^2/2\right)_{(i-\frac{1}{2},j,k,n)}\right\}\\
&-\frac{1}{\Delta y}\left\{(\phi_y)_{(i,j+\frac{1}{2},k,n)}-(\phi_y)_{(i,j-\frac{1}{2},k,n)}\right\}-\frac{1}{\Delta z}\left\{(\phi_z)_{(i,j,k+\frac{1}{2},n)}-(\phi_z)_{(i,j,k-\frac{1}{2},n)}\right\}=0
\end{aligned} \tag{23}$$

(ϕ_y) and (ϕ_z) are always calculated from a centered expression. However, the approximation of (ϕ_x) strongly depends on whether locally, at a point, the flow is subsonic, supersonic, sonic or it is a shock point. Extending References 33, 34 methodologies to our case and using Eq. (21), a centered approximation and a backward expression are given for u^*:

$$u^{*c}_{(i,j,k,n)} = K + f(j,k,n) + \frac{1}{\gamma} g(j,k,n) + \frac{\gamma+1}{2\Delta x^*}(\phi(i+1,j,k,n) - \phi(i-1,j,k,n))$$

$$u^{*b}_{(i,j,k,n)} = K + f(j,k,n) + \frac{1}{\gamma} g(j,k,n) + \frac{\gamma+1}{2\Delta x^*}(\phi(i,j,k,n) - \phi(i-2,j,k,n)) \qquad (24)$$

The local type of the flow is determined by the following table:[33,34]

condition	u^{*c}	u^{*b}	local flow is
1	< 0	< 0	subsonic
2	> 0	> 0	supersonic
3	> 0	< 0	a sonic point
4	< 0	> 0	a shock point

Table 1

Eq. (23) is developed in a specific form according to the local type of the flow. When the flow is locally subsonic, an elliptic difference form is used:

$$
\begin{aligned}
G(i,j,k,n) &= \frac{1}{\Delta x^* \Delta t^*}(\phi(i+1,j,k,n) - \phi(i-1,j,k,n-1)) \\
&\quad -\frac{2}{\Delta t^*}\phi_{x^*}(i,j,k,n-1) + \frac{1}{\gamma \Delta t^*}(g(j,k,n) - g(j,k,n-1)) \\
&\quad +\left\{K + f(j,k,n) + \frac{1}{\gamma}g(j,k,n)\right. \\
&\quad \left. +\frac{\gamma+1}{2\Delta x^*}(\phi(i+1,j,k,n) - \phi(i-1,j,k,n))\right\} \cdot \\
&\quad \frac{\phi(i+1,j,k,n) - 2\phi(i,j,k,n) + \phi(i-1,j,k,n)}{(\Delta x^*)^2} \\
&\quad -\frac{1}{(\Delta y)^2}(\phi(i,j+1,k,n) - 2\phi(i,j,k,n) + \phi(i,j-1,k,n)) \\
&\quad -\frac{1}{(\Delta z)^2}(\phi(i,j,k+1,n) - 2\phi(i,j,k,n) + \phi(i,j,k-1,n)) = 0.
\end{aligned}
\tag{25}
$$

When the flow is locally supersonic, a hyperbolic difference form is used:

$$
\begin{aligned}
G(i,j,k,n) &= \frac{2}{\Delta x^* \Delta t^*}(\phi(i,j,k,n) - \phi(i-1,j,k,n)) - \\
&\quad -\frac{2}{\Delta t^*}\phi_{x^*}(i,j,k,n-1) + \frac{1}{\gamma \Delta t^*}(g(i,j,k,n) - g(i,j,k,n-1))
\end{aligned}
$$

$$+\left\{K + f(j,k,n) + \frac{1}{\gamma}g(j,k,n)\right.$$

$$\left.+\frac{\gamma+1}{2\,\Delta\, x^*}(\phi(i,j,k,n) - \phi(i-2,j,k,n))\right\} \cdot$$

$$\frac{\phi(i,j,k,n) - 2\phi(i-1,j,k,n) + \phi(i-2,j,k,n)}{(\Delta x^*)^2}$$

$$-\frac{1}{(\Delta y)^2}(\phi(i,j+1,k,n) - 2\phi(i,j,k,n) + \phi(i,j-1,k,n))$$

$$-\frac{1}{(\Delta z)^2}(\phi(i,j,k+1,n) - 2\phi(i,j,k,n) + \phi(i,j,k-1,n)) = 0. \tag{26}$$

When the flow is locally sonic, $(\gamma+1)\phi_{x^*} + K + f + \frac{1}{\gamma}g = 0$. Then the sonic point difference form is:

$$\begin{aligned} G(i,j,k,n) \;=\; & \frac{1}{(\Delta y)^2}(\phi(i,j+1,k,n) - 2\phi(i,j,k,n) + \phi(i,j-1,k,n)) \\ & +\frac{1}{(\Delta z)^2}(\phi(i,j,k+1,n) - 2\phi(i,j,k,n) + \phi(i,j,k-1,n)) \\ & -\frac{1}{(\gamma+1)\,\Delta\, t^*}\left(\frac{\gamma-1}{\gamma}(g(j,k,n) - g(j,k,n-1))\right. \\ & \left.-2(f(j,k,n) - f(j,k,n-1))\right) = 0. \end{aligned} \tag{27}$$

When locally there is a shock point, a shock point difference operator is used where the flux ahead of the shock may be approximated by a backward

formula and the flux behind the shock by a centered formula.

$$
\begin{aligned}
G(i,j,k,n) \quad = \quad & \frac{1}{\Delta x^* \, \Delta t^*}(\phi(i+1,j,k,n) - \phi(i-1,j,k,n)) \\
& - \frac{2}{\Delta t^*}\phi_{x^*}(i,j,k,n-1) + \frac{1}{\gamma \, \Delta t^*}(g(j,k,n) - g(j,k,n-1)) \\
& + \left\{ K + f(j,k,n) + \frac{1}{\gamma} g(j,k,n) \right. \\
& + \frac{\gamma+1}{2 \, \Delta x^*}(\phi(i+1,j,k,n) - \phi(i,j,k,n) + \phi(i-1,j,k,n) \\
& \left. + \phi(i-2,j,k,n)) \right\} \cdot \\
& \cdot \frac{\phi(i+1,j,k,n) - \phi(i,j,k,n) - \phi(i-1,j,k,n) + \phi(i-2,j,k,n)}{(\Delta x^*)^2} \\
& - \frac{1}{(\Delta y)^2}(\phi(i,j+1,k,n) - 2\phi(i,j,k,n) + \phi(i,j-1,k,n)) - \\
& - \frac{1}{(\Delta z)^2}(\phi(i,j,k+1,n) - 2\phi(i,j,k,n) + \phi(i,j,k-1,n)) = 0.
\end{aligned}
\tag{28}
$$

Starting from initial conditions that describe a given shock wave in the space for $t = 0$ (or $n = 0$), and given the functions $f(y,z,t)$ and $g(y,z,t)$, equations (25) through (28) can be applied for $n = 1$ at any mesh point according to Table 1. They can be solved by an iterative point or line - or plane - relaxation algorithm until at any point $\max|G(i,j,k,1)| < \delta$ where δ is a given small tolerance of convergence. Then $\phi_{x^*}(i,j,k,1)$ can be calculated at any mesh point and the process is restarted for the next time step. In this way the shock motion and pressure field behind it can be integrated in space and time and the effect of various deterministic and

random fluctuations f and g can be studied. Numerical calculations of various examples are underway and will be presented in a future report.

5 Conclusions

The review of the theoretical studies of the interaction of shock waves with free stream vortical flows or turbulence shows that this complex nonlinear interaction is still an open problem to analyze. The analysis of the linearized problem of the interaction of a weak shock with relatively small disturbances shows that it is an invalid approach when the perturbations are of the order of shock strength. However, in a coordinate system moving with the basic weak shock, the problem may fit the transonic theory framework.

A new transonic small-disturbance model has been developed where a rescaling of the axial coordinate and time has been considered to capture the basic nonlinear effects that occur in the flow across the shock. This model results in two alternative approaches: (1) an equation for solving a velocity potential function that is described by an extended version of the classic small-disturbance equation for unsteady transonic aerodynamics;[33] and (2) a nonlinear equation to describe the pressure field that is similar to the model equation recently presented by Pierce[17] using logical considerations only. This equation also has extended form of the classic equation that describes the propagation of nonlinear sound beams with narrow angular spectrum.[30,31]

Both approaches show that diffraction effects, nonlinear steepening, focusing and caustic effects and random induced turbulence fluctuations interact simultaneously to determine the development of the shock wave in space and time and the pressure field behind it. Turbulence fluctuations tend to change the local speed of sound in the flow across the shock and through this effect to reduce or magnify the strength of the basic shock.

A finite difference scheme that uses Murman and Cole[34] finite-difference

techniques for solving mixed-type elliptic-hyperbolic flows with shock waves has also been presented. Numerical calculations of the interaction of shock waves with various deterministic and random fluctuations will be presented in a future report. We will also look for analytical methods to identify the basic relations between given turbulence properties and the development of the shock waves and the pressure field behind it. It is expected to find solutions that will describe both peaked or rounded or messy pressure signatures as were recorded in experiments. We also intend to extend the model to include humidity and winds effects that are also known to have a significant effect on sonic boom pressure peaks and rise times.

Acknowledgements

This work was carried out with the support of NASA Langley Research Center under Award NAG-1-1362. The authors would like to acknowledge Dr. G. L. McAninch for funding and monitoring this research.

References

[1] Hubbard, H. H., Maglieri, D. J., Huckel, V. and Hilton, D. A., "Ground Measurements of Sonic Boom Pressures for the Altitude Range of 10,000 to 75,000 feet," NASA TR R-198, July 1964.

[2] Maglieri, D. J., "Sonic Boom Flight Research - Some Effects of Airplane Operations and the Atmosphere on Sonic Boom Signatures," in *Sonic Boom Research*, Edited by Seebass, A. R., NASA SP-147, April 1967.

[3] Garrick, I. E. and Maglieri, D. J., "A Summary of Results on Sonic Boom Pressure-Signature Variations Associated with Atmospheric Conditions," NASA TN D-4588, May 1968.

[4] Downing, M. J., "Lateral Spread of Sonic Boom Measurements from U.S. Air Force Boomfile Flight Tests," NASA CP-3172, Feb. 1992, pp. 117-135.

[5] Willshire, Jr., W. L. and Devilbiss, D. W., "Preliminary Results from the White Sands Missile Range Sonic Boom Propagation Experiment," NASA CP-3172, Feb. 1992, pp. 137- 149.

[6] Lipkens, B. and Blackstock, D.T., "Model Experiment to Study the Effect of Turbulence on Risetime and Waveform of N Waves," NASA CP-3172, Feb. 1992, pp. 97-107.

[7] Leatherwood, J. D. and Sullivan, B. M., "Subjective Loudness response to Simulated Sonic Booms," NASA CP-3172, Feb. 1992, pp. 151-170.

[8] Crow, S. C., "Distortion of Sonic Bangs by Atmospheric Turbulence," *J. Fluid Mechanics*, vol. 37, part 3, 1969, pp. 529-563.

[9] Plotkin, K. J. and George, A. R., "Propagation of Weak Shock Waves Through Turbulence," *J. Fluid Mechanics*, vol. 54, part 3, 1972, pp. 449-467.

[10] Ffowcs Williams, J. E. and Howe, M. S., "On the Possibility of Turbulent Thickening of Weak Shock Waves," *J. Fluid Mechanics*, vol. 58, part 3, 1973, pp. 461-480.

[11] Pierce, A. D., "Spikes on Sonic-Boom Pressure Waveforms," *J. Acoustical Society of America*, vol. 44, no. 4, 1968, pp. 1052-1061.

[12] Pierce, A. D., "Statistical Theory of Atmospheric Turbulence Effects on Sonic-Boom Rise Times," *J. Acoustical Society of America*, vol. 49, no. 3 (part 2), 1971, pp. 906-924.

[13] Cramer, M. S. and Seebass, A. R., "Focusing of Weak Shock Waves at an Arête," *J. Fluid Mechanics*, vol. 88, part 2, 1978, pp. 209-222.

[14] Gill, M. and Seebass, A. R., "Nonlinear Acoustic Behavior at a Caustic: An Approximate Analytical Solution," AIAA Paper 73-1037, AIAA Aeroacoustics Conference, Seattle, Wash., 1973.

[15] Sturtevant, B. and Kulkarny, V. A., "The Focusing of Weak Shock Waves," *J. Fluid Mechanics*, vol. 73, 1976, pp. 651-671.

[16] Sparrow, V. W. and Pierce, A. D., "Simulations of Sonic Boom Ray Tube Area Fluctuations for Propagation Through Atmospheric Turbulence Including Caustics via a Monte Carlo Method," NASA CP-3172, Feb. 1992, pp. 49-62.

[17] Pierce, A. D., "Wave Equations and Computational Models for Sonic Boom Propagation Through a Turbulent Atmosphere," NASA CP-3172, Feb. 1992, pp. 31-48.

[18] Hollingsworth, M. A. and Richards, E. J., "A Schlieren Study of the Interaction Between a Vortex and a Shock Wave in a Shock Tube," A.R.C. Rept. 17985, FM2323, 1955.

[19] Dosanjh, D. S. and Weeks, T. M., "Interaction of a Starting Vortex as Well as a Vortex Street with a Traveling Shock Wave," *AIAA J.*, vol. 3, 1965, pp. 216-223.

[20] Naumann, A. and Hermanns, E., "On the Interaction Between a Shock Wave and a Vortex Field," in *Noise Mechanisms*, AGARD CP-131, 1973, pp. 23-1.

[21] Ribner, H. S., "Spectra of Noise and Amplified Turbulence Emanating from Shock-Turbulence Interaction," *AIAA J.*, vol. 25, 1987, pp. 436.

[22] Kovasnay, L. S. G., "Turbulence in Supersonic Flow," *Journal of the Aeronautical Sciences*, vol. 20, 1953, pp. 657-674.

[23] Moore, F. K., "Unsteady Oblique Interaction of a Shock Wave with a Plane Disturbance," NACA Report 1165, 1954.

[24] Ribner, H. S., "Shock-Turbulence Interaction and the Generation of Noise," NACA Report 1233, 1955.

[25] Chang, C. T., "Interaction of a Plane Shock and Oblique Plane Disturbances with Special Reference to Entropy Waves," *Journal of the Aeronautical Sciences*, vol. 24, 1957, pp. 675-682.

[26] Ribner, H. S., "Cylindrical Sound Wave Generated by Shock-Vortex Interaction," *AIAA J.*, vol. 23, no. 11, 1985, pp. 1708-1715.

[27] Zang, T. A., Hussaini, M. Y. and Bushnell, D. M., "Numerical Computations of Turbulence Amplification in Shock- Wave Interactions," *AIAA J.*, vol. 22, no. 1, 1984, pp. 13-21.

[28] Meadows, K. R., Kumar, A. and Hussaini, M. Y., "Computational Study on the Interaction Between a Vortex and a Shock Wave," *AIAA J.*, vol. 29, no. 2, 1991, pp. 174-179.

[29] Ellzey, J. L., Picone, M. and Oran, E. S., "The Interaction of a Shock with a Compressible Vortex," Naval Research Laboratory M.R. 6919, 1992.

[30] Zabolotskaya, E.A. and Khorkhlov, R.V., *Akust. Zhurnal* 15, 1, 1969, pp. 40.

[31] Kuznetsov, V. P., *Akust. Zhurnal* 6, 4, 1970, pp. 548.

[32] Courant, R. and Friedrichs, K. O., "Supersonic Flow and Shock Waves," *Interscience Publishers, Inc.* N.Y., pp. 297-302.

[33] Cole, J. D. and Cook, L. P., *Transonic Aerodynamics*, North-Holland, 1986.

[34] Murman, E. M. and Cole, J. D., "Calculation of Plane Steady Transonic Flows," *AIAA J.*, vol. 9, pp. 114-121.

Sonic Boom Propagation through Turbulence; A Ray Theory Approach

Leick D. Robinson
Applied Research Laboratories
The University of Texas at Austin

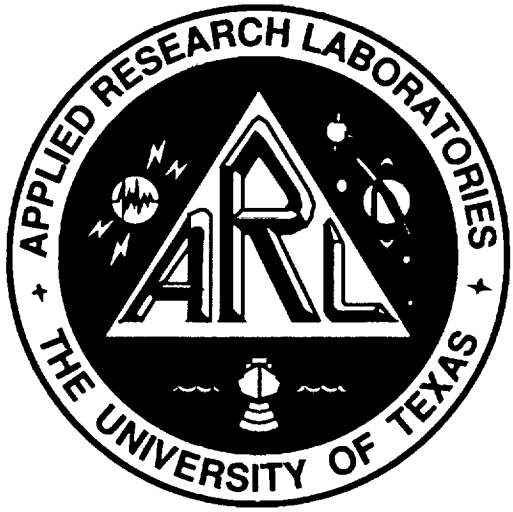

Presentation at NASA HSR Sonic Boom Workshop
NASA Ames Research Center
May12-14, 1993

In this work, a ray theory approach is used to examine the propagation of sonic booms through a turbulent ground layer, and to make predictions about the received waveform. The rays are not propagated one at a time, as is typical in ray theory; instead, sufficient rays to represent a continuous wave front are propagated together. New rays are interpolated as needed to maintain the continuity of the wave front. In order to predict the received boom signature, the wave front is searched for eigenrays after it has propagated to the receiver.

OVERVIEW

- **Rays describing a wave front propagate through an instantaneous "snapshot" of the turbulence.**
- **Turbulence produces focusing and defocusing of portions of the wave front, which results in caustic formation, wave front "folding", and multiple eigenray paths to the receiver.**
- **The eigenrays to the receiver are identified.**
- **The respective arrival times and ray tube areas of the eigenrays, along with the identification of caustics, generate the predicted waveform at the receiver.**
- **If repeated many times, this generates a statistical description of the predicted wave form characteristics.**

The Comte-Bellot turbulence model (Ref. 1) is used to generate an instantaneous "snapshot" of the turbulent field. The transient acoustic wave is assumed to be sufficiently short in duration such that the time-dependance of the turbulent field may be neglected.

Turbulence Model
(Comte-Bellot '91)

Instantaneous realization of incompressible, isotropic turbulence is represented by a sum of Fourier modes:

$$w(x) = \sum_{j=1}^{N} a_j \cos(k_j \cdot x + \phi_j)$$

where directions of a_j and k_j are random with the provision that

$$(a_j \cdot k_j) = 0 \text{ for each } j$$

For a given mode k_j, the magnitude $|a_j|$ is given by

$$|a_j| \sim \sqrt{E(k)\,\delta k}$$

δk is the separation between modes.
The spectral energy density $E(k)$ is given by the Von Kármán model:

$$E(k) \sim \frac{k^4}{\left(k^2 + \frac{1}{L_0^2}\right)^{17/6}} \exp(-2.25\,(\eta k)^{4/3})$$

L_0 = integral length scale
η = Kolmogorov scale

The magnitude of the rms velocity is related by

$$|v_{rms}| = \frac{1}{2} \sum_{j=1}^{N} |a|^2$$

In this model, we use60 Fourier modes logarithmically distributed between wavenumbers 10^{-2} and 10 (m^{-1}). The integral length scale was chosen to be 100m, as was the thickness of the turbulent layer. The rms wind velocity was chosen to be 1 m/s. This corresponds to a mild turbulent layer, such as might be found in the morning on a clear day. These values are used for all of the remaining figures and discussions.

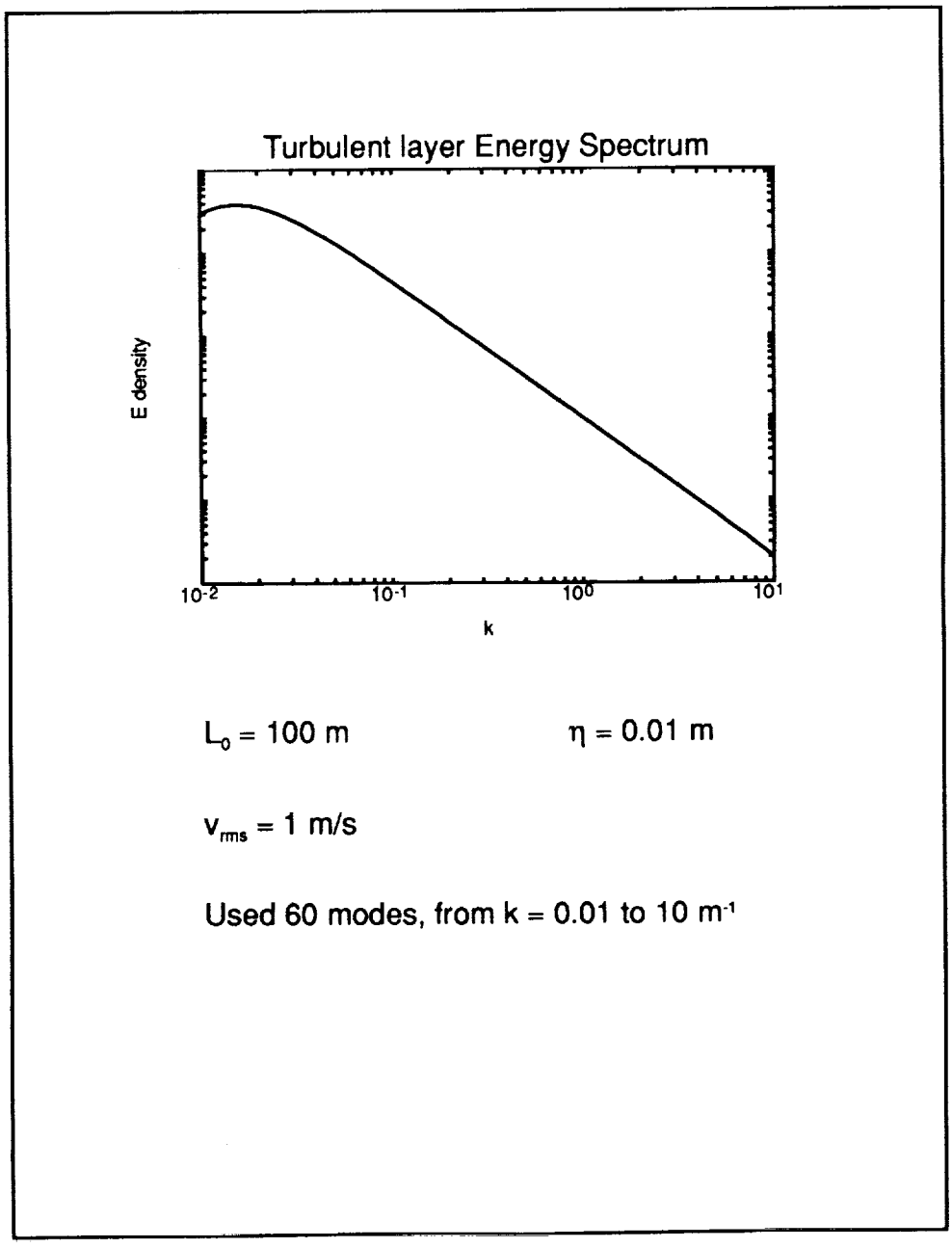

A number of rays, with the same starting conditions, are propagated through different realizations or "snapshots" of the turbulent field. Each ray will be displaced by the turbulence away from the undistorted ray path, which in this case would be represented by a horizontal line.

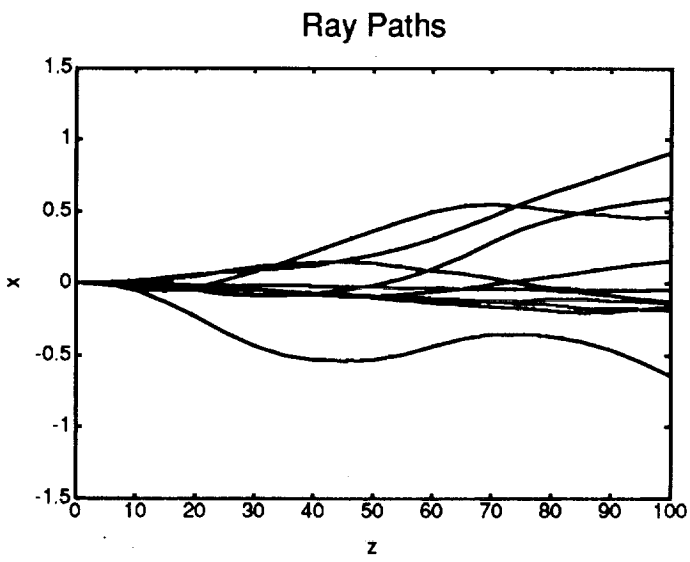

- Each ray represents a different realization of the turbulent layer.
- The turbulence displaces each ray from the horizontal (undistorted) ray path.

If a large number of rays are propagated through different turbulence realizations, a pattern or distribution of ray displacement may be developed. In our case, 95% of the rays fall within a circle of radius 2 meters around the zero-turbulence ray path. By symmetry arguments, this means that any eigenrays have a 95% probability of starting within 2 meters of the zero-turbulence eigenray. This statistical approach allows us to drastically reduce our eigenray search area to a feasible quantity.

Ray displacement distribution after 100 m propagation

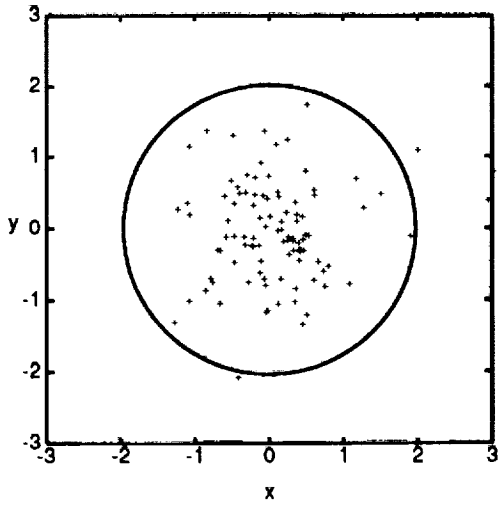

• 95% of the rays fall within a circle of radius 2 m

The development of the ray tube area along the ray paths gives an indication of how much the turbulent field is distorting the wave fronts. A ray crossing the horizontal as indicates that the ray has passed through a caustic at that point.

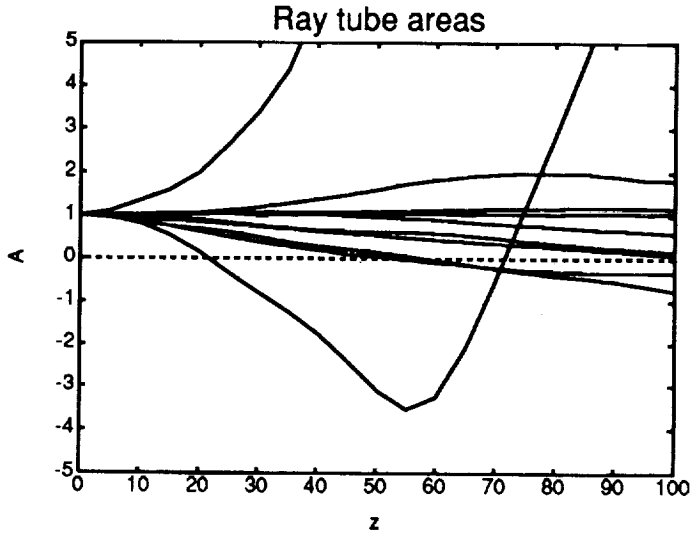

- Each ray represents a different realization of the turbulent layer.
- Crossing the horizontal axis indicates that the ray has encountered a caustic.

In this figure, a linear "slice" of a wavefront is propagated through 100 m of turbulence. In this case, the distortion is slight and no caustics are observed.

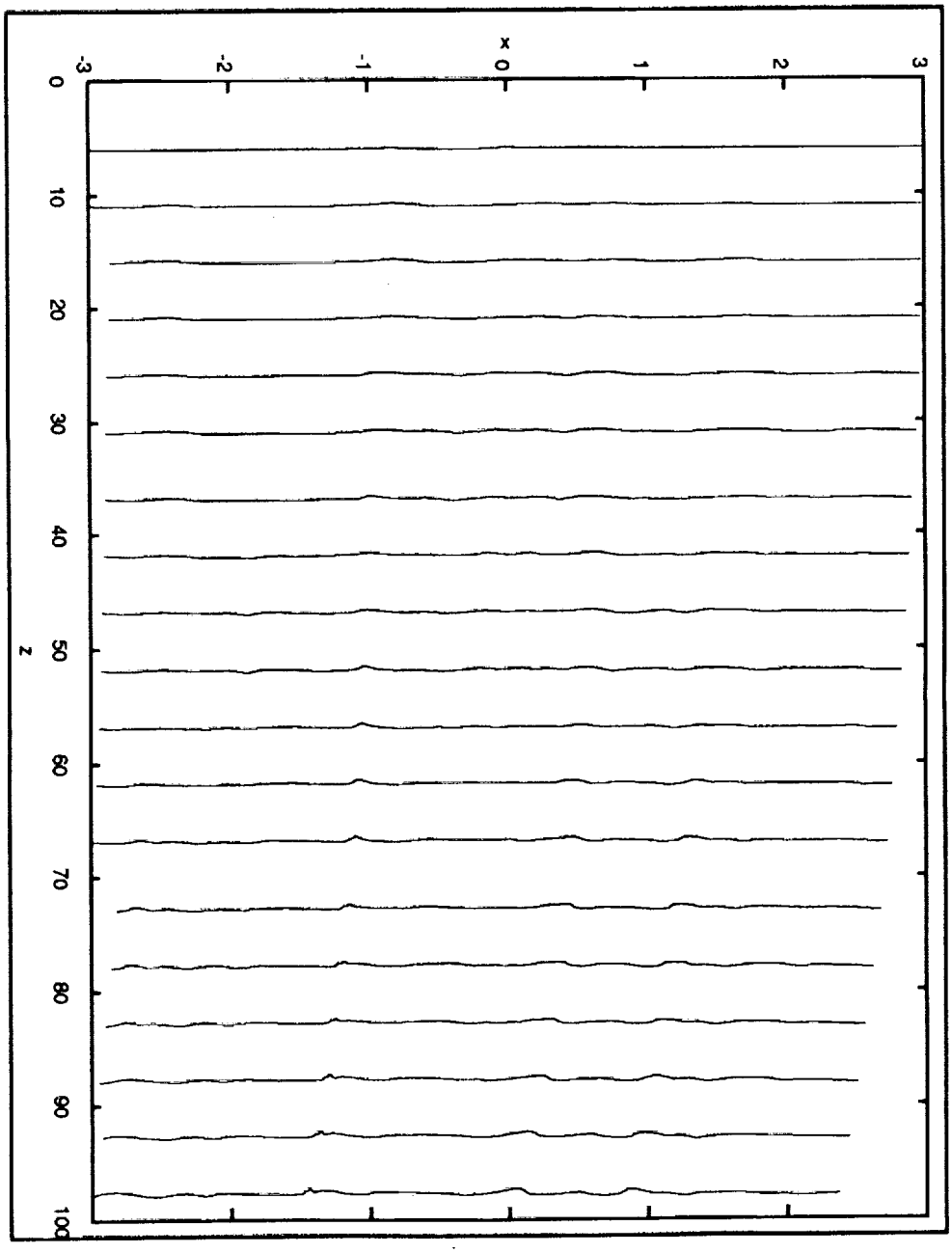

Again, a linear "slice" of the wavefront is propagated through a realization of turbulence. Although the statistical parameters are unchanged, in this case, the turbulence has a marked effect on the wavefronts. After 20 m, caustics begin to form which eventually overlap, producing, in the end, a highly folded wave front, with multiple eigenrays to the receiver.

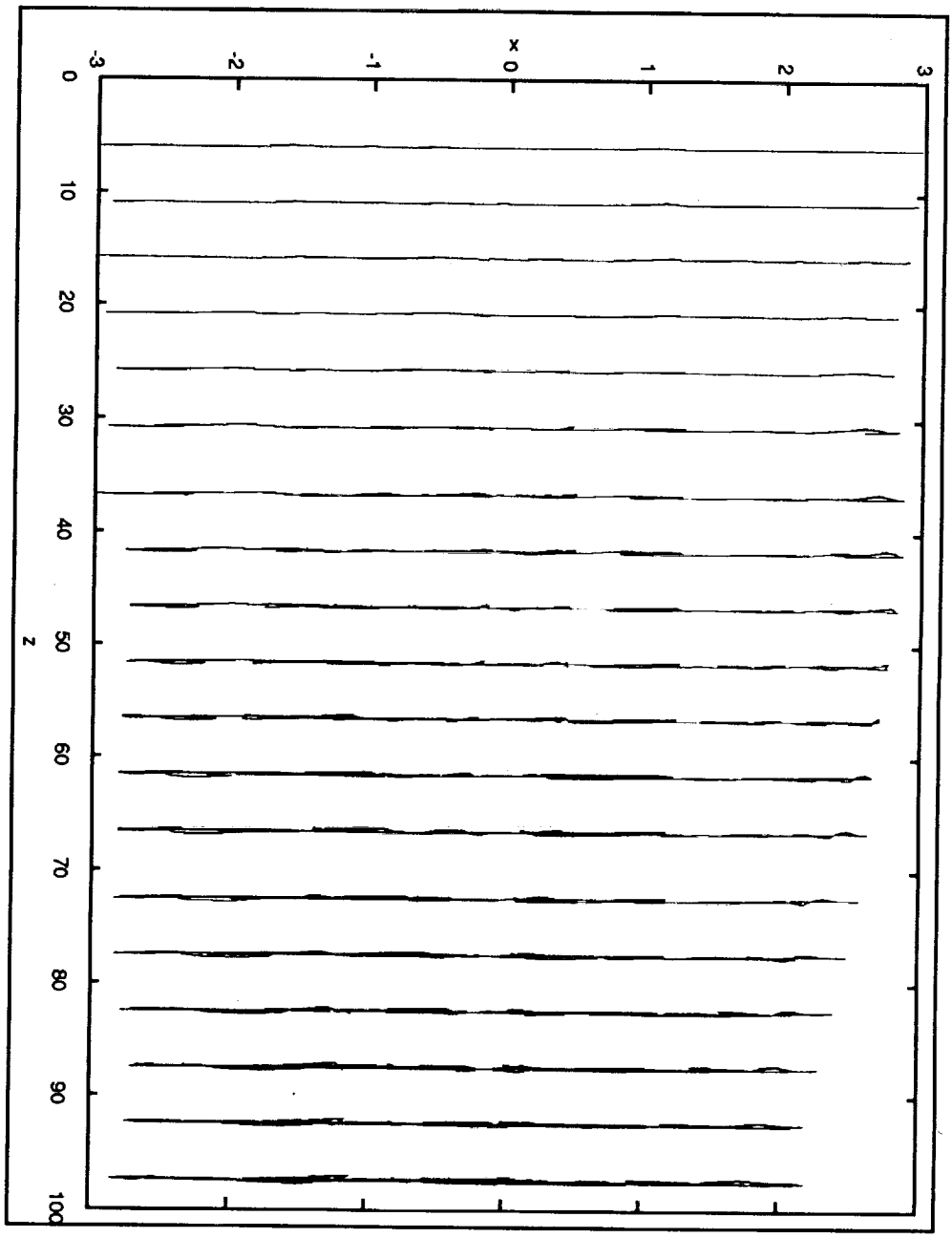

It must be remembered that the wavefront distortion is three-dimensional. The two plots below show the distortion of the original wavefront "slice" in the previous two figures, show in the plane normal to the direction of propagation. Note that the second figure shows considerable distortion due to the presence of numerous caustics.

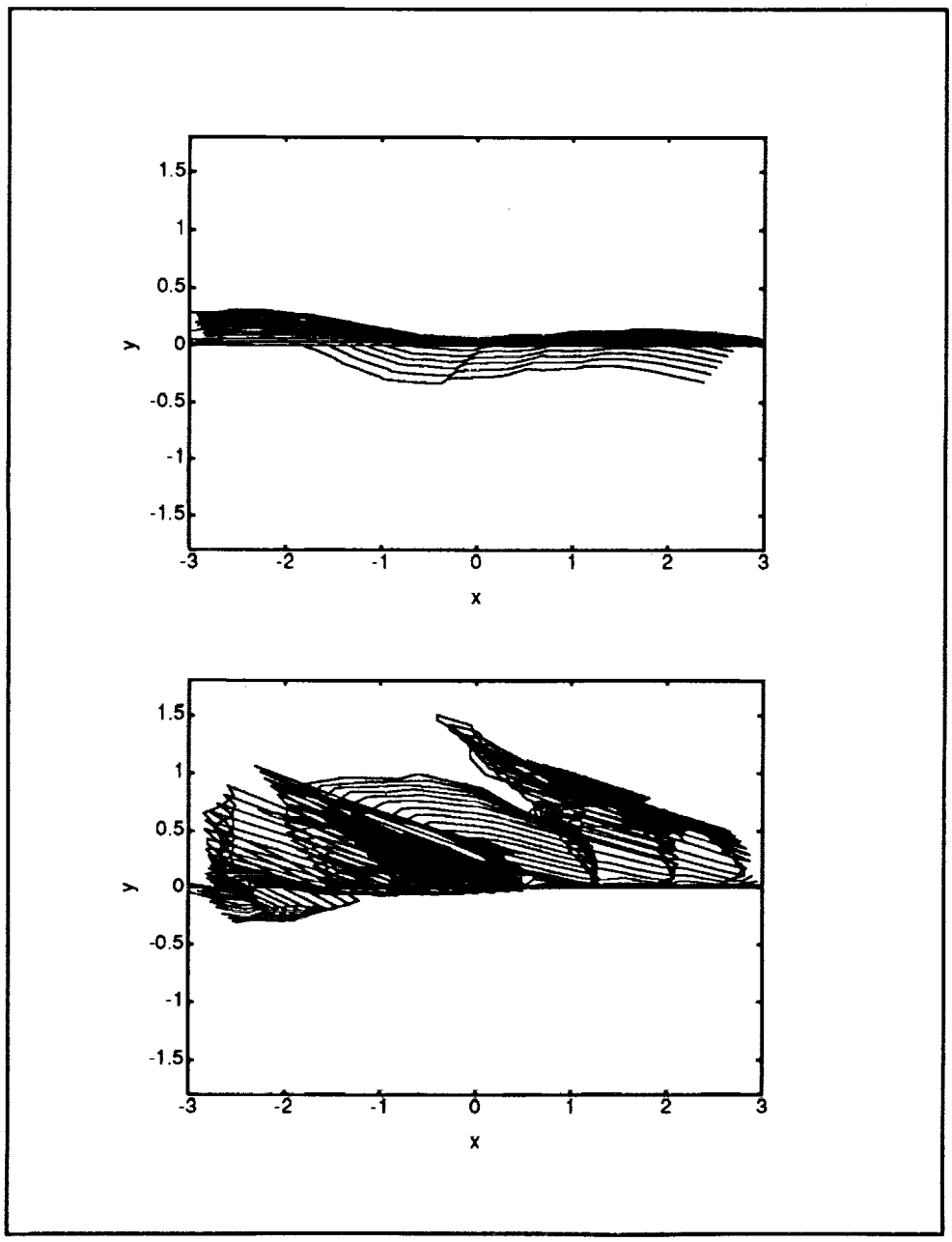

For four realizations of the turbulent field, the wave fronts were propagated, eigenrays were found, and the resultant waveforms were calculated. The initial waveform was generated by the ZEPHYRUS model (Ref. 2); it represents a typical sonic boom waveform in the absence of turbulence. The next two plots demonstrate theresulting waveforms when the wave front is spreading, or defocusing, and when the wave front is focusing, but has not formed a caustic. The last plot displays the U wave resulting from multiple eigenrays, some of which have passed through one or more caustics.

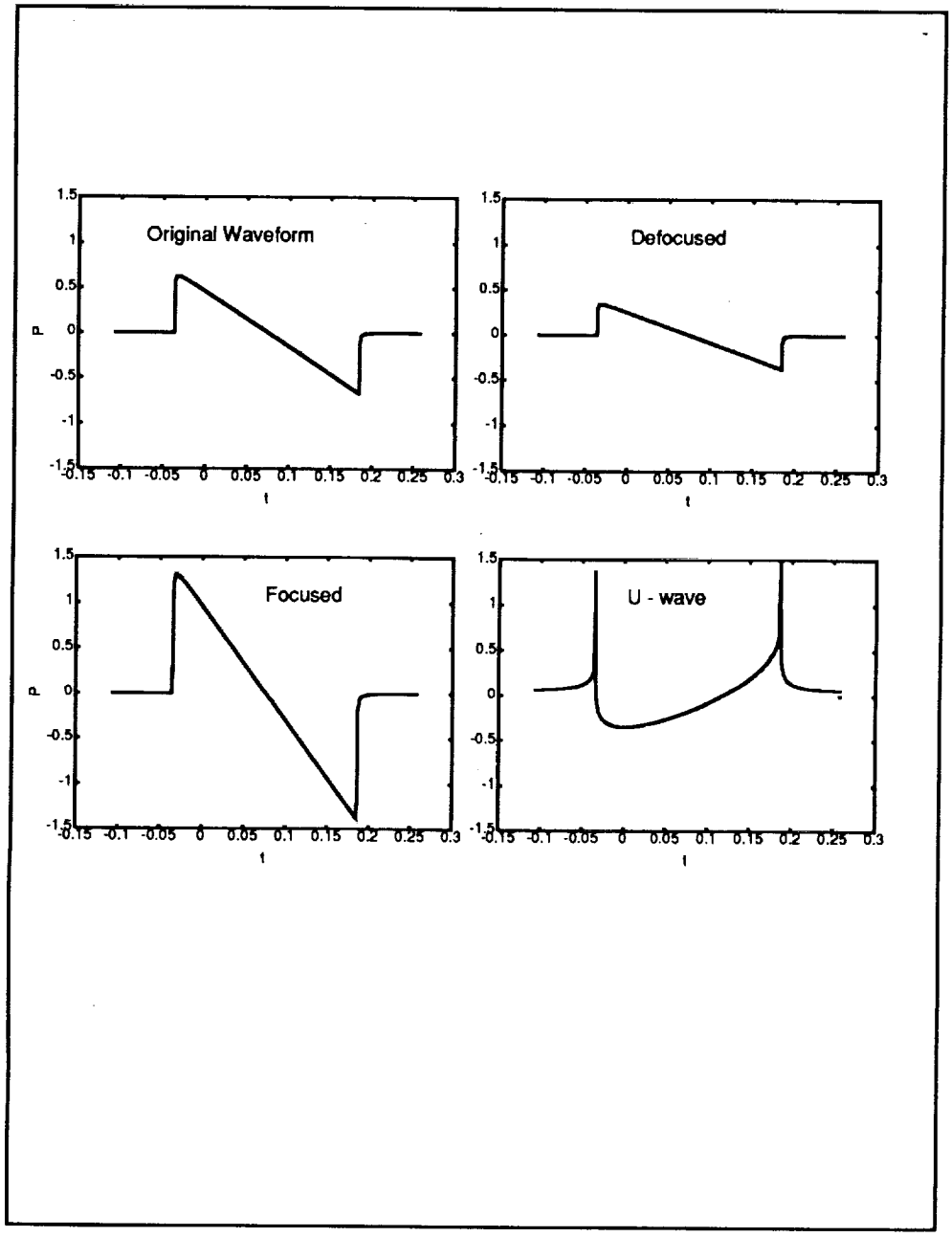

In nonlinear geometric acoustics, the effects of self-refraction may usually be ignored. Although nonlinear effects may displace a ray from the small-signal ray path, the properties of the wave front is usually slowly varying in the plane of the wave front and so, the equivalent nonlinear wave front is virtually identical to the original. As we've seen, however, in the case of propagation through turbulence, we've seen that the wave fronts may become very distorted and so the assumptions that lead to neglecting self-refraction must be examined more closely. This is most easily tested by comparing the same ray with and without the nonlinear correction. We first start with the nonlinear ray path equations given below.

Nonlinear Ray Equations

The ray path equations may be modified to include self-refraction as follows:

$$\frac{d\mathbf{x}}{dt} = \left[(\mathbf{W} + \mathbf{u}') + \frac{\left(c_0 + \frac{P'\alpha}{c_0^2}\right)\mathbf{p}}{(1 - \mathbf{W}\cdot\mathbf{p} - \mathbf{u}'\cdot\mathbf{p})} \right]$$

$$\frac{d\mathbf{p}}{dt} = \left[\left(\sum_i - p_i \nabla'(W_i + u'_i) \right) - \frac{\left(c_0 + \frac{P'\alpha}{c_0^2}\right)\nabla'\left(c_0 + \frac{P'\alpha}{c_0^2}\right)|\mathbf{p}|^2}{(1 - \mathbf{W}\cdot\mathbf{p} - \mathbf{u}'\cdot\mathbf{p})} \right]$$

where

$$\alpha = \frac{(\beta - 1)\, c_0}{\rho_0}$$

p is the slowness vector

P' and **u'** are the acoustical overpressure and particle velocity

and ∇' is the spatial operator in retarded time coordinates:

$$\nabla' = \nabla + \mathbf{p}\frac{\partial}{\partial t}$$

The simplest wave front property to calculate is the ray tube area. When we compare the results for a number of different turbulence realizations, we see that the ray tubes with and without the nonlinear correction give almost the same result. This indicates that, for these environments, the wave fronts remain sufficiently smooth that we may continue to ignore the effects of self-refraction.

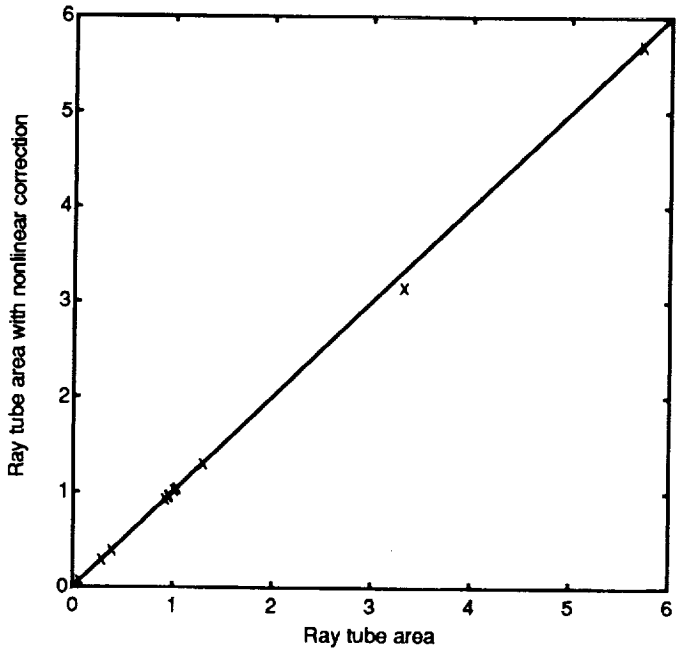

- Initial 200 Pa acoustic overpressure
- The nonlinear correction to the ray paths makes little difference.

The ray theory approach has been demonstrated to be a useful tool for the investigation of propagation through turbulence. The next step will likely be to attempt prediction for more severe turbulence, to see if waveforms of more complex structure that have been observed, such as multiply peaked or rounded, can be simulated by this method.
It is fortunate that the nonlinear distortion of the ray paths may be neglected, as this simplifies the goal of sonic boom prediction.

Conclusions

- **A ray theory approach provides a useful tool for investigating the properties of propagation through turbulence.**
- **Wavefront folding and multiple eigenrays are good candidates for explaining some of the structure commonly observed in sonic booms.**
- **Nonlinear distortion of the ray paths may be safely ignored.**

References

(1) Karweit, M., Blanc-Benon, P., Juvé, D., and Comte-Bellot, G. (1991). "Simulation of the propagation of an acoustic wave through a turbulent velocity field: A study of phase variance," J. Acoust. Soc. Am. 89, pp. 52-62.

(2) Robinson, Leick D.: *Sonic Boom Propagation through an Inhomogeneous, Windy Atmosphere*, Ph.D. dissertation, The University of Texas at Austin, December 1991.

The propagation of spark-produced N waves through turbulence

Bart Lipkens

Applied Research Laboratories
Mechanical Engineering Dept.
The University of Texas at Austin

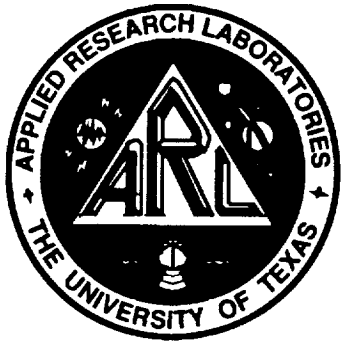

Work supported by NASA Langley

Presentation at NASA HSR Sonic Boom Workshop
NASA Ames Research Center
May 12-14, 1993

A model experiment was designed and built to simulate the propagation of sonic booms through atmospheric turbulence. The setup of the model experiment is described briefly. Measurements of the N waves after they propagated across the turbulent velocity field reveal the same waveform distortion and change in rise time as for sonic booms.

The data from the model experiment is used to test sonic boom models. Some models yield predictions for the waveform distortion, while others give estimates of the rise time of the sonic booms.

A new theoretical model for the propagation of plane N waves through a turbulent medium is described.

Introduction.

- model experiment: - successful in simulating the propagation of sonic booms through atmospheric turbulence
  - setup and results

- model experiment data is used to test sonic boom models
  - waveform distortion models
  - rise time prediction models

- new theoretical model for the propagation of plane N waves through a turbulent medium

In the model experiment the N waves are generated by a spark source. The spark-produced N wave is a spherically spreading wave, but it is also possible to create a locally plane N wave by inserting a paraboloidal reflector. The mirror is positioned so that the spark gap is at the focus of the paraboloidal reflector.

A plane jet generates the turbulent velocity field. A centrifugal fan blows air into a plenum chamber. The jet is formed when the air exits the chamber through the nozzle. The jet nozzle velocity is controlled by a Variac variable voltage controller and by adjusting the width of the nozzle. The plane jet characteristics are measured by hot-wire anemometry.

The N waves are measured by a wide band condensor microphone. Rise times as small as 0.45 μs can be measured.

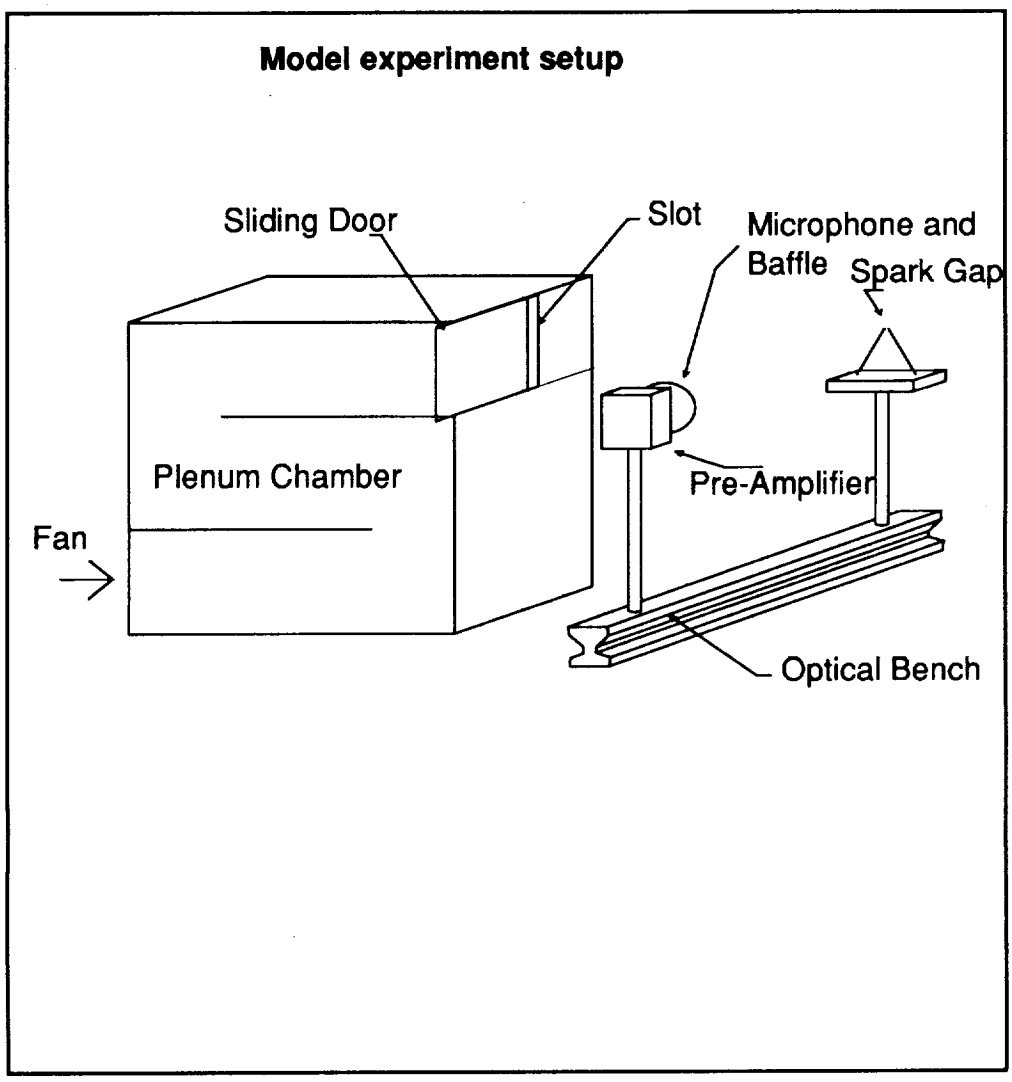

Examples of waveform distortion are shown. The upper left signature is that of a reference plane N wave recorded in the absence of turbulence. All other signatures represent waveforms measured after the plane N waves propagated through the turbulent velocity field. The distortion of the waveforms is similar as observed for sonic boom signatures. The distortion of the wavefront is most pronounced near the front and tail shocks. The fact that the distortion of the tail shock has the same pattern as that of the front shock is an indication that the turbulence is frozen during passage of the N wave. Variations in waveform from peaked to rounded and U-shaped are apparent. Double-peaked and multiple-peaked waveforms and messy wave shapes are also represented.

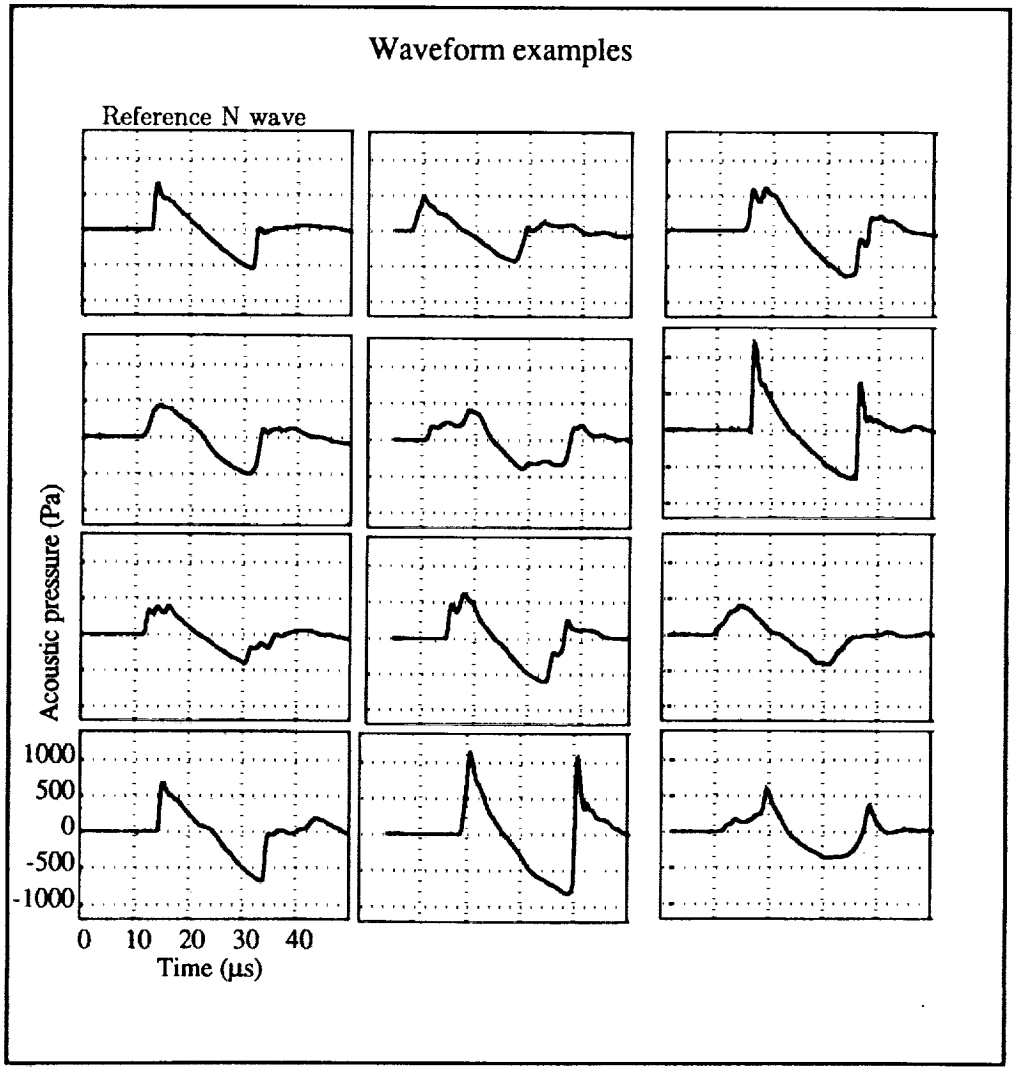

The first sonic boom model we review is Crow's waveform distortion model (Ref. 1). Crow's model is based on first order scattering theory. He modeled the sonic boom as a step shock of strength Δp. The mean-squared pressure perturbation equals $\langle p_S^2 \rangle = \Delta p^2 \, (t_c/t)^{7/6}$, where t_c is a critical time that is a function of the turbulence characteristics. The graph presents an example of the variance of an N wave for a value of $t_c = 2$ ms. A finite, very large value is obtained for the mean-squared pressure perturbation near the shock. Since the theory is a first-order scattering theory, both the incident and the scattered wave propagate at the ambient speed of sound c_0. However, from geometric acoustics we know that some ray paths might exist along which the actual propagation speed is faster than the ambient speed of sound. If we want to compare Crow's prediction with experimental data, then we have to shift the time origin of each sample waveform so that it begins at the time of shock arrival.

Testing of previous models

1. Crow's distortion model

- step shock : $\langle \psi^2(t) \rangle = (t_c/t)^{7/6}$ $\qquad \psi(t) = p^S/\Delta p,$

$$t_c = \frac{1}{c_0} (\sec\theta)^{11/7} \left[\int_0^{h_f} 1.33 \, c_0^{-2} h^{5/6} \epsilon_u^{2/3} dh \right]^{6/7}$$

- Result of rms scattered pressure ($t_C = 2$ ms)

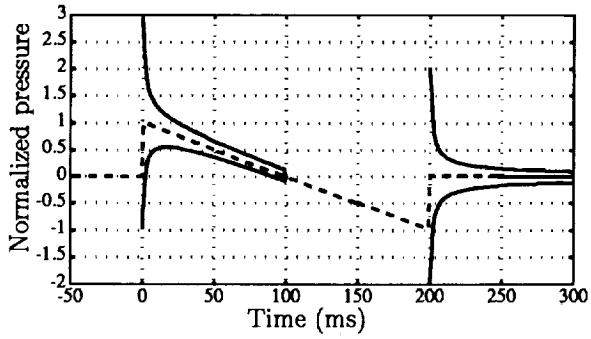

- Problems: $< \psi^2(0) > \approx 10^8$
  - incident wave of form f(x + c_0 t)
  - shock arrival time?
  - comparison with experiment?

Plotkin (Ref. 2) showed that an incident wave of arbitrary structure can be represented as a sum of infinitesimal step shocks. When the incident wave is modeled as a ramp shock instead of a step shock, an upper bound for the maximum pressure perturbation can be found, which is given by $\langle p_S^2 \rangle^{1/2} = \frac{12}{5} \Delta p \left(\frac{t_c}{t_0}\right)^{7/12}$, where t_0 is the rise time of the ramp shock.

Lipkens (Ref. 3) extended this model for an N wave. The rms pressure perturbation is presented in the first graph for an N wave with a rise time of 1 μs and a critical time of 0.33 μs. In order to calculate the rms pressure perturbation for the measured waveforms of the model experiment, we shifted the time origin of each waveform so that the times corresponding to 50 % of peak pressure all coincide.

A comparison between the measured distortion and Crow's prediction is presented in the lower graph. The measured distortion has the same general behavior as Crow's prediction, but the maximum pressure perturbation according to Crow's prediction is larger than the measured one by a factor of more than ten.

- Plotkin (1971): extension of Crow's model for a ramp shock
  - incident wave of arbitrary structure: sum of infinitesimal steps
  - upper bound for rms pressure perturbation

$$\left\langle (p_S)^2 \right\rangle_{\max}^{1/2} = \frac{12}{5} A \left(\frac{t_c}{t_0}\right)^{7/12}$$

- extension to N wave

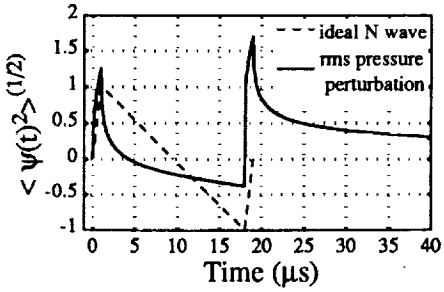

- measurements: shift each waveform --> 50 % peak pressure times coincide

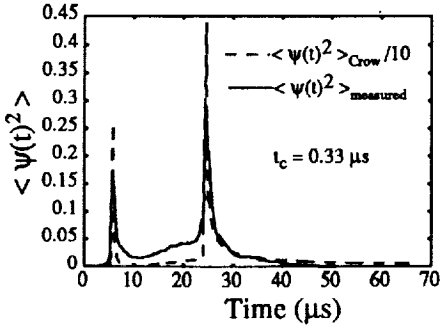

It is now widely accepted that molecular relaxation, especially that of nitrogen, is responsible for the large rise time of sonic booms. Controversy still exists whether turbulence has a pronounced effect on rise time. When a theory for the propagation of shock waves and transients through a turbulent medium is developed, it is important to incorporate the effect of shock arrival time correctly. The rise time of the stochastic mean of a set of waveforms represents an insignificant upper bound to the average of the rise times of each individual waveform. The graph shows a simple example that demonstrates that the rise time of the stochastic mean waveform of five step shocks, each having a rise time of 1 μs, is more than tenfold the average of the rise time of the individual realizations.

Rise time prediction models

- Turbulence cause of large rise time? What mechanism?

- Question of shock arrival time

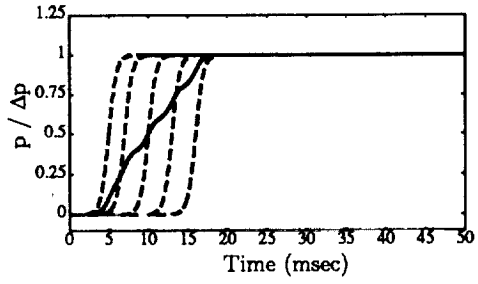

Pierce's model (Ref. 4) is based on the mechanism of wavefront folding at a caustic. If at a certain instant turbulence causes a ripple to develop on the shock front, a caustic is formed when the wavefront is propagated according to geometric acoustics. Inside the caustic three segments of the shock front arrive instead of one. Pierce argued that this process could occur many times if the turbulence intensity is large. A receiver then "sees" many segments of a multifolded wavefront at slighly different arrival times. The result is that instead of a sharp shock front a shock is received that consists of many smaller shocks at different arrival times. The overall result is a rounded shock front. The lower graph shows the mean waveform calculated according to Pierce's theory. Again, t_c is Crow's critical time.

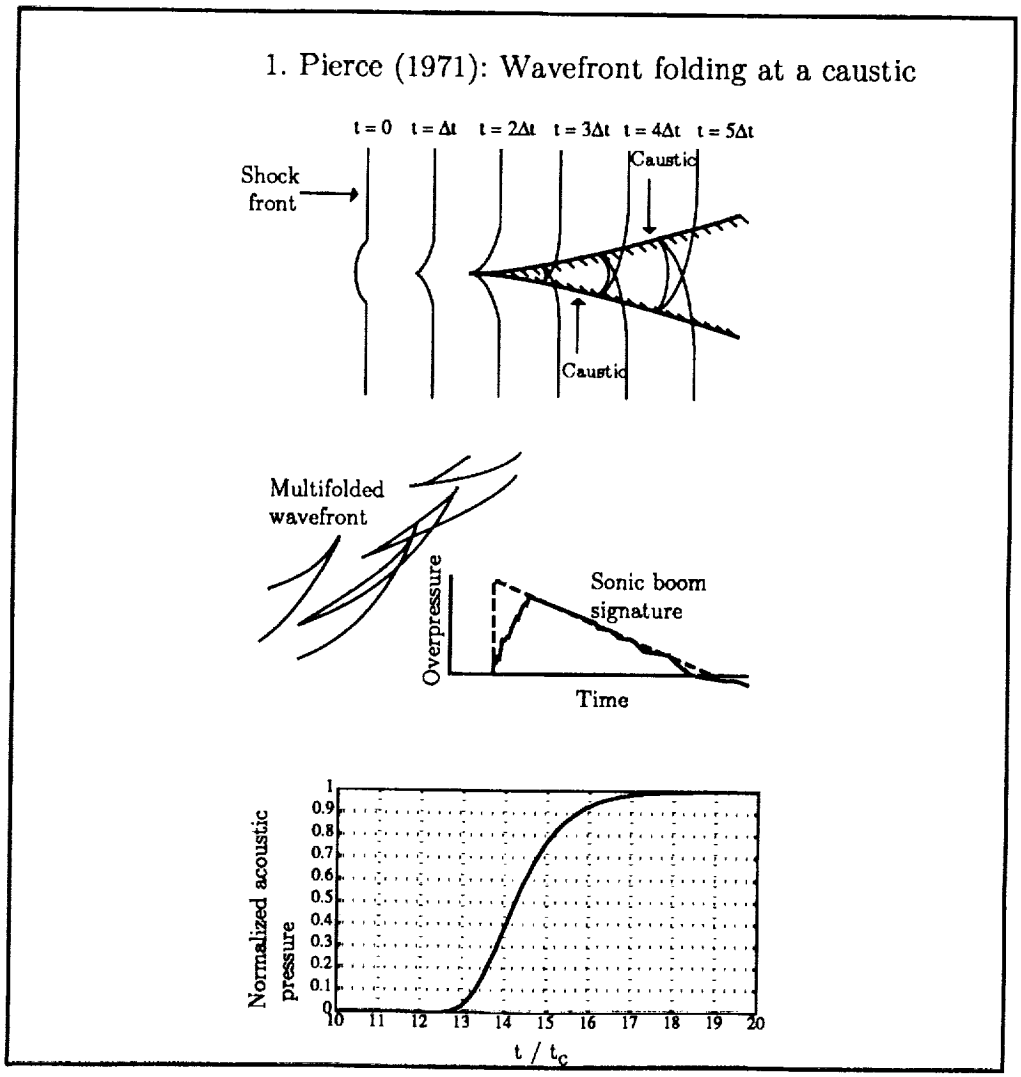

The mean waveform is expressed as a function of Crow's critical time t_c. The parameters E and b_1 are dependent on the structure of the atmospheric turbulence.

Again, the individual waveforms of the model experiment are shifted in order that times corresponding to 50 % of peak pressure coincide. The plot compares Pierce's prediction for the mean waveform and the computed mean of the shifted individual waveforms. A good agreement is reached.

In order to confirm this correlation, we performed an experiment at five different jet nozzle velocities. The comparison between Pierce's prediction and the measurements is fairly accurate. A maximum discrepancy of about 30 % is observed for a nozzle velocity of 31.3 m/s.

- mean waveform

$$\frac{\langle p(t) \rangle}{\Delta p_0} = \exp\left\{-E\hat{t}^{-1/6}e^{-b_1\hat{t}^{7/6}}\right\} \qquad \hat{t} = t/t_c$$

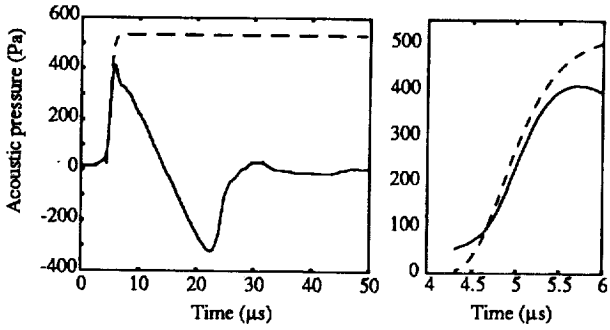

jet nozzle velocity (m/s)	charact. time (μs)	τ_{Pierce} (μs)	$\tau_{meas.}$ (μs)
12.4	0.23	0.554	0.685
18.3	0.32	0.769	0.745
22.7	0.37	0.889	0.922
26.6	0.41	0.984	1.061
31.3	0.46	1.091	1.308

Kulkarny and White (Ref. 5) and White (Ref. 6) developed a model for the plane wave propagation through a 2-D and 3-D, random, isotropic medium. The model is based on geometric acoustics. The results shown here are for a 3-D, random medium. White derived a uniform probability density function $p(t)$ for the occurence of a first caustic. The parameter t is a nondimensional variable. The only information needed about the random medium is its correlation function. Once this information is known, the scaling variable γ is calculated. The graph shows the probability density curve. It is observed that the most likely position for the occurence of a first caustic is at $t = 1.3$. In the table, values for the most likely position of a first caustic and the mean distance to a first caustic are shown. As is noticed, it is possible that an N wave will pass through a caustic. However, it is unlikely that the wave will pass through more than one caustic.

White and Kulkarny: plane wave propagation through a 3-D, isotropic, random medium (geometric acoustics)

- probability density function p(t) for the occurence of a first caustic

$$p(t) = \frac{a_1}{t^4} e^{-a_2 t^{-3}} \qquad t = \gamma^{2/3} s,$$

$$\gamma^2 = 2 \int_0^\infty \left(\frac{1}{r}\frac{\partial}{\partial r}\right)^2 R(r) dr$$

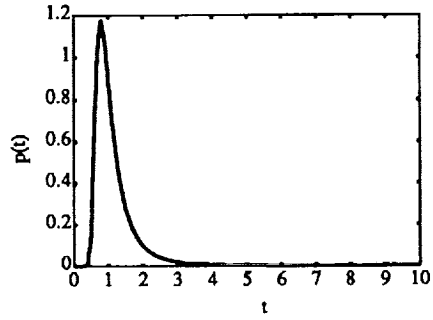

jet nozzle velocity (m/s)	most likely pos. caustic m	mean distance first caustic m
12.4	1.038	1.373
18.3	0.798	1.056
22.7	0.694	0.918
26.6	0.619	0.818
31.3	0.556	0.735

Plotkin and George (Ref. 7) developed a model based on second order scattering theory. They derived a Burgers equation in which the absorption term is a function of the turbulence characteristics. L_0 is the integral length scale, a measure of the eddies of permanent character, and $\epsilon_T = \left\langle \left(\Delta c + \Delta u_{\|}\right)^2 \right\rangle / c_0^2$ is an effective turbulence Mach number. The rise time is determined by the balance between nonlinear steepening and scattering by turbulence. An expression for the rise time is obtained. Plotkin (Ref. 2) compared results from their model with measurements and obtained a good correlation. It is, however, difficult to obtain accurate estimates of the integral length scale and the turbulence Mach number of the atmosphere. A controversy still exists as to whether travel time variations are accounted for correctly or not.

2. Plotkin and George (1972): Second order perturbation theory

$$\frac{\partial P}{\partial t} + \frac{c_0(\gamma+1)}{2\gamma}\frac{P}{p_0}\frac{\partial P}{\partial \xi} = \frac{L_0}{c_0}\left\langle \left(\Delta c + \Delta u_{\|}\right)^2 \right\rangle \frac{\partial^2 P}{\partial \xi^2}$$

$$p = p^N + p_1^S + p_2^S$$

$$P = p - p_1^S$$

$$\tau = \frac{16\gamma}{\gamma+1}\frac{p_0}{\Delta p_0}\frac{\left\langle \left(\Delta c + \Delta u_{\|}\right)^2 \right\rangle L_0}{c_0^3}$$

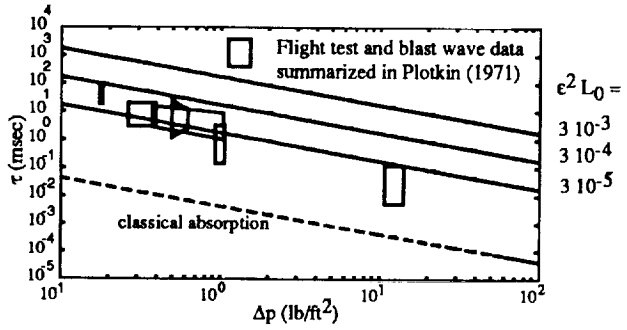

- Problem: travel time variations accounted for?

In order to compare Plotkin's prediction with measurements, we computed the mean waveform in two different ways. First, we computed the mean waveform by shifting the time origins in a similar way as described before and we call this the time shifted mean. Second, we calculated the stochastic mean waveform without any correction for the arrival time of each individual waveform and we call this the stochastic mean. The graph shows an example of the difference for the two computed mean waveforms. As is seen, the stochastic mean presents an insignificant upper bound to the rise time of the time shifted mean.

Again we compare results for five different nozzle velocities. It is noticed that Plotkin and George's prediction has a better correlation with the stochastic mean than with the time shifted mean. A conclusion that seems apparent from the results is that travel time variations of individual waves are not accounted for correctly in Plotkin and George's model.

$$\tau = \frac{16\gamma}{\gamma+1}\frac{p_0}{\Delta p_0}\frac{\left\langle \Delta u_{\parallel}{}^2 \right\rangle L_0}{c_0^3} \qquad \epsilon_t = \frac{\left\langle \Delta u_{\parallel}{}^2 \right\rangle^{1/2}}{c_0}$$

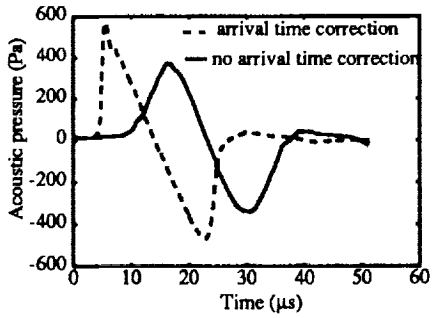

jet nozzle velocity (m/s)	charact. time (μs)	τ_{Plotkin} (μs)	stoch. mean $\tau_{\text{meas.}}$ (μs)	time shifted $\tau_{\text{meas.}}$ (μs)
12.4	0.23	1.13	2.767	0.685
18.3	0.32	2.49	3.867	0.745
22.7	0.37	3.78	4.840	0.922
26.6	0.41	5.34	4.833	1.061
31.3	0.46	7.37	5.528	1.308

The last model is that of Ffowcs Williams and Howe (Ref. 8) (FfW & H). In their paper FfW & H mention that the Burgers equation derived by Plotkin and George represents the stochastic mean. FfW & H warn about possible misinterpretation of the results of the Burgers equation as an energy loss, while in reality it describes the loss of coherence of the mean wave because of the random convection of the shock fronts. The model by FfW & H is based on a multiple scattering theory. A diffusion equation is obtained that describes the acoustic energy $\mathcal{E}$ in wavenumber space as a function of the turbulence Mach number m and a length scale Δ related to the Taylor microscale. An expression for the shock thickness δ is derived as a function of the incident shock thickness δ_0 and the integrated scattering diffusivity μ. FfW & H found at most an increase of 30 % in the rise time and concluded in their paper that molecular relaxation must be the cause of the large rise times of booms. Plotkin (Ref. 9) argued that since his model does not yield an acoustic energy loss but just a spatial relocation, one would not expect a change in rise time according to the definition employed by FfW & H.

3. Ffowcs Williams and Howe (1973): Multiple scattering

- Plotkin's approach describes stochastic mean properties of boom

- Multiple scattering theory: diffusion equation for distribution of acoustic energy in wavenumber space

$$\frac{\partial \mathcal{E}(\mathbf{k})}{\partial t} + c_0 \frac{\partial \mathcal{E}(\mathbf{k})}{\partial x_{\parallel}} = \frac{c_0 m^2 k^2}{2\Delta} \nabla_{\perp}^2 \mathcal{E}(\mathbf{k})$$

$$\frac{1}{\Delta} = \frac{\pi}{2u^2} \int_0^{\infty} \kappa E(\kappa) d\kappa$$

$$\delta = \delta_0 \left[1 + \mu(x)\right]$$

$$\mu(x) = 2 \int_0^x \frac{m(\xi)^2}{\Delta(\xi)} d\xi$$

- At most a 30 % increase in rise time

- Molecular relaxation is responsible for large rise time

- Problem: phase scrambling is not accounted for

The upper graph presents a comparison of the energy spectrum of an ideal N wave, its rise time and duration equal that of the spark-produced N wave, with the averaged spectrum of 200 N waves recorded in the absence of turbulence. The energy spectrum of the spark-produced N waves closely resembles that of an ideal N wave. The troughs and peaks of the measured spectrum are more rounded than that of the ideal N wave.

The middle graph shows a comparison of the averaged energy spectrum of 200 N waves recorded in the absence of turbulence with that of 200 N waves measured after propagation through the plane jet turbulence. Again, both spectra are very similar, and troughs and peaks are more rounded for the N waves that propagated through the turbulent medium. However, no significant redistribution of acoustic energy is observed in the spectrum, as was predicted by Ffowcs Williams and Howe.

The table presents a comparison between the prediction of Ffowcs Williams and Howe and the measured values for the rise time. Ffowcs Williams and Howe's model clearly yields values for the rise time that are much smaller than the measured ones.

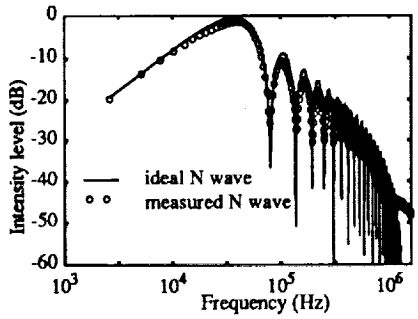

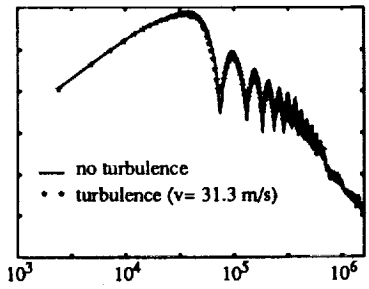

jet nozzle velocity (m/s)	μ	τ_{F-H} (μs)	$\tau_{meas.}$ (μs)
12.4	0.0027	0.687	0.685
18.3	0.0047	0.688	0.745
22.7	0.0067	0.690	0.922
26.6	0.0090	0.691	1.061
31.3	0.0116	0.693	1.308

A new model has been developed for plane wave propagation through a statistically random, isotropic medium (Ref. 3). The random medium consists of a turbulent velocity field. A linear acoustic wave equation (Ref. 2) is derived in which first and second order turbulence effects are included. A perturbation scheme is used to solve the wave equation up to second order.

The turbulent velocity field model was developed by Karweit *et al.* (Ref. 10). Von Kármán's model for incompressible, isotropic turbulence is used to obtain an expression for the 3-D turbulence energy density spectrum. The spectrum is characterized by two length scales. L_0 is an outer length scale, and η is the Kolmogorov microscale.

The 1-D energy spectrum of the plane jet was measured by hot-wire anemometry. If we assume the turbulence is isotropic, the 3-D energy spectrum can be derived. A good agreement is reached between the model and the measurement.

New numerical model for plane wave propagation through a statistically random, isotropic medium

- Turbulent velocity field model
- Linear acoustic wave equation, second order turb. effects
- Perturbation solution
- Results

1. Turbulent velocity field model (Blanc-Benon, Comte-Bellot, 1991)

- Von Kármán's model for incompressible, isotropic turbulence

$$\mathbf{E}(k) = \frac{55}{9}\frac{\Gamma(5/6)}{\sqrt{\pi}\Gamma(1/3)}\frac{u'^2}{L_0^{2/3}}\frac{k^4}{\left(k^2+L_0^{-2}\right)^{17/6}}\exp\left(-2.25(\eta k)^{4/3}\right)$$

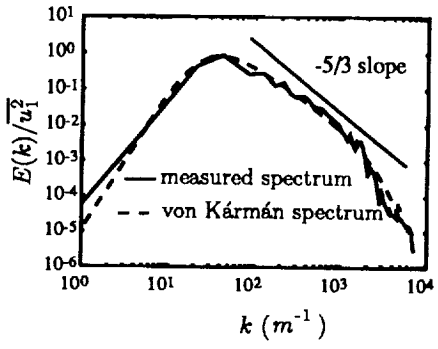

The turbulent velocity field consists of a sum of discrete Fourier velocity modes that are randomly oriented in space. The wave vector geometry of a single Fourier velocity mode is shown in the first graph. The angles θ and ϕ determine the orientation of the wavevector $\mathbf{k}$. The probability density function of both angles are chosen in order to ensure statistical entropy with respect to $\mathbf{k}$. With each turbulence wave vector, a velocity vector $\mathbf{a}(k)$ is associated. Because the turbulent velocity field is incompressible, the velocity vector lies in a plane perpendicular to $\mathbf{k}$. The random angle ψ determines the direction of $\mathbf{a}(k)$. The amplitude of $\mathbf{a}(k)$ is defined by von Kármán's spectrum. A random phase angle γ is attributed to each Fourier mode. A final expression for the turbulent field is obtained as a sum over all the modes.

Wave vector geometry of a single Fourier velocity mode

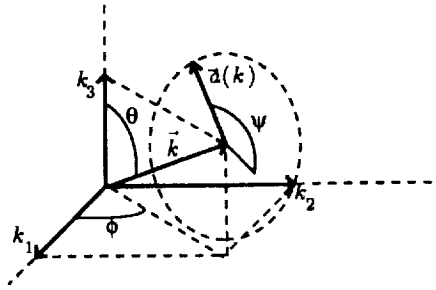

- wavenumber $\mathbf{k}$ is randomly oriented: $P(\theta) = \sin\theta/2$ and $P(\phi) = 1/2\pi$
  statistical isotropy with respect to $\mathbf{k}$

- velocity vector $\mathbf{a}(k)$ -> in plane perpendicular to $\mathbf{k}$
  ψ is random
  $\mathbf{a}(k) \sim \sqrt{\mathbf{E}(k)\Delta k}$
  phase γ of $\mathbf{a}(k)$ is random

- $\mathbf{u}_T(\mathbf{x}) = \sum_{j=1}^{N} |\mathbf{a}_j| \cos(\mathbf{k}_j \cdot \mathbf{x} + \gamma)$

A linear acoustic wave equation is derived. First and second order turbulence effects are retained in the wave equation. We assume that the wave propagation is lossless (isentropic) and that the turbulence is frozen. We only consider velocity fluctuations and do not include thermal fluctuations. ϵ_a is the acoustic Mach number and ϵ_T is the turbulence Mach number.

A regular perturbation scheme in the turbulence Mach number is employed to solve the wave equation. The N wave generated at the focus of the mirror is the boundary condition and it is represented as a sum of its Fourier components.

2. Linear acoustic wave equation

- lossless wave propagation
- the turbulence is frozen
- only turbulent velocity field is present
- wave equation

$$\Box^2 p = -\frac{2}{c_\infty^2}\mathbf{u}_T \cdot \nabla \frac{\partial p}{\partial t} - 2\frac{\partial u_{Ti}}{\partial x_i}\frac{\partial}{\partial x_j}(\int \nabla p dt)_i \qquad \epsilon_a \epsilon_T$$

$$+ 2\frac{\partial u_{Ti}}{\partial x_i}\frac{\partial}{\partial x_j}(\int (\mathbf{u}_T \cdot \nabla) \int \nabla p dt dt)_i \qquad \epsilon_a {\epsilon_T}^2$$

$$+2\frac{\partial U_{Ti}}{\partial x_i}\frac{\partial}{\partial x_j}(\int (\int \nabla p dt \cdot \nabla)\mathbf{u}_T dt)_i - \frac{1}{c_\infty^2}(\mathbf{u}_T \cdot \nabla)(\mathbf{u}_T \cdot \nabla p) \qquad \epsilon_a {\epsilon_T}^2$$

$$+\frac{1}{c_\infty^2} p \nabla \cdot ((\mathbf{u}_T \cdot \nabla)\mathbf{u}_T) \qquad \epsilon_a {\epsilon_T}^2$$

3. Perturbation scheme

$$p = p_0 + \epsilon_T p_1 + {\epsilon_T}^2 p_2 + \ldots$$

$$\text{B.C.} \quad p(0,t) = p_N(t)$$

$$p_N(t) = \sum b_n \sin n\omega_0 t$$

Results from the first order solution are shown here. Each graph represents the sum of the incident N wave and the first order pressure perturbation after propagation through a single realization of the turbulent velocity field. As one observes, the first order pressure perturbation is responsible for the distortion of the N waves. Variations in waveform from peaked to rounded are noticed. Double-peaked and multiple-peaked waveforms are also shown. In some cases (e.g., the rounded waveform), the rise time of the waveform is changed, in other cases it is unaltered. However, the arrival time of each wave is the nominal arrival time (i.e., that of the incident wave). A calculation of the second order pressure perturbation is necessary.

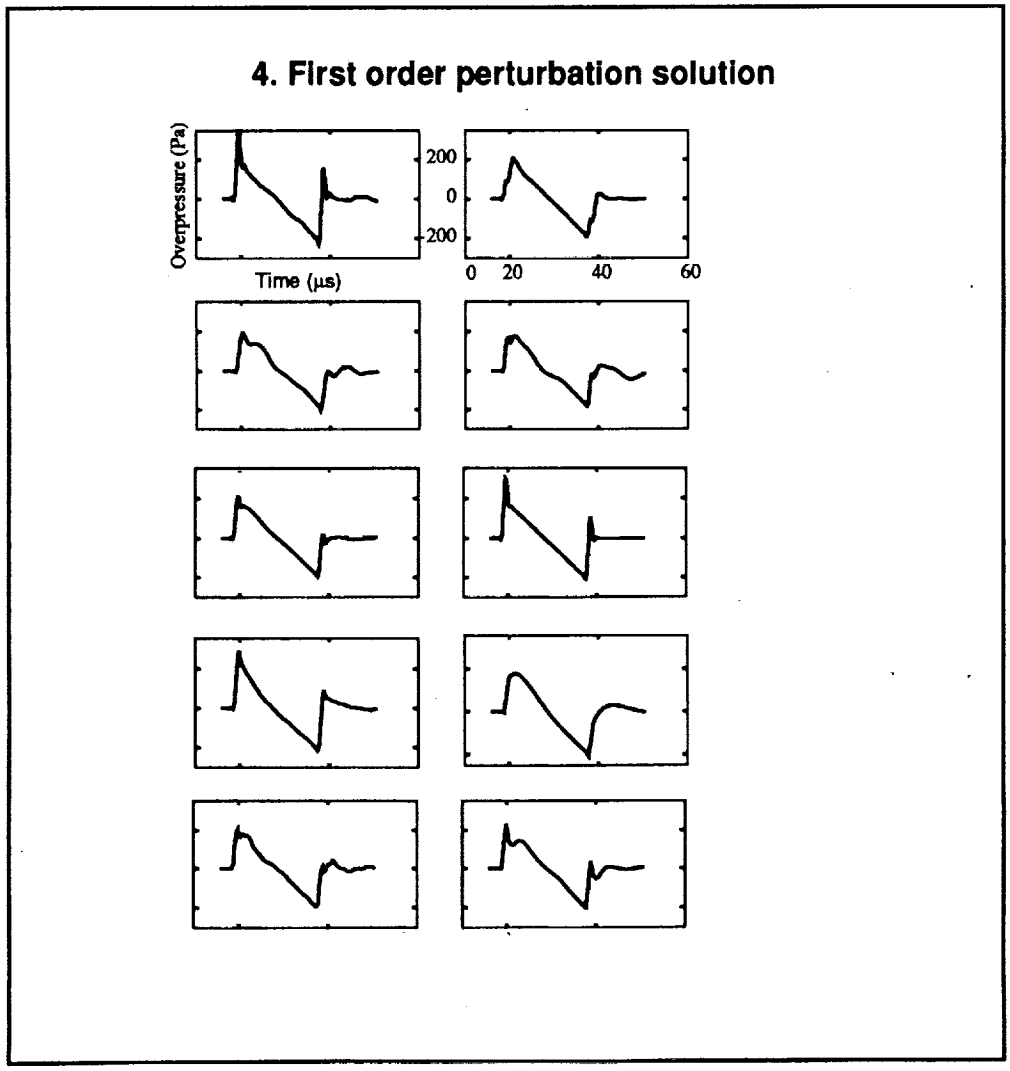

The second order equation that has to be solved contains two secular terms and regular terms. A solution for the second order pressure perturbation is obtained.

The total solution consists of the incident wave, the first order pressure perturbation, and the second order pressure perturbation due to the secular and regular terms. A renormalization technique is used to strain the z-coordinate. The straining of the z-coordinate is used to remove one of the singularities. The final solution is then written as a sum of the Fourier components of the N wave. The second order singularity introduces changes in the phase speed. At second order, the phase speed becomes dependent on the turbulence characteristics.

5. Second order perturbation solution

$$\Box^2 \epsilon_T{}^2 p_2 = (\alpha - \beta - \gamma) \sin n\omega_0\left(t - \tfrac{z}{c_\infty}\right) - \delta \cos n\omega_0\left(t - \tfrac{z}{c_\infty}\right), \quad p_2(0,t) = 0$$

+ regular terms

$$\epsilon_T{}^2 p_2 = -\frac{(\alpha - \beta - \gamma)c_\infty}{2n\omega_0} z \cos n\omega_0\left(t - \tfrac{z}{c_\infty}\right) + \frac{\delta c_\infty}{2n\omega_0} z \sin n\omega_0\left(t - \tfrac{z}{c_\infty}\right)$$

+ regular terms

6. Total solution

$$p = b_n \sin n\omega_0\left(t - \tfrac{z}{c_\infty}\right) + \epsilon_T p_1$$
$$-\frac{(\alpha - \beta - \gamma)c_\infty}{2n\omega_0} z \cos n\omega_0\left(t - \tfrac{z}{c_\infty}\right) + \frac{\delta c_\infty}{2n\omega_0} z \sin n\omega_0\left(t - \tfrac{z}{c_\infty}\right)$$

+ regular terms of order $\epsilon_T{}^2$ or higher

Renormalization technique (strained coordinate)

$$z = s(1 + \epsilon_T{}^2 \omega_1 + \ldots)$$

Final solution $$p = \sum_n (1 + \epsilon_T{}^2 \omega_2 z) \sin n\omega_0\left(t - \frac{z}{c_\infty(1 + \epsilon_T{}^2 \omega_1)}\right) + \epsilon_T p_1$$

- $\epsilon_T p_1$ is first order perturbation solution
- $\epsilon_T{}^2 \omega_1 = -\dfrac{(\alpha - \beta - \gamma)}{2b_n\left(\frac{n\omega_0}{c_\infty}\right)^2}$
- $\epsilon_T{}^2 \omega_2 = \frac{\delta c_\infty}{2n\omega_0}$

Results from the numerical simulations that incorporate the second order effects are shown. The phase speed is a function of the turbulence characteristics, and the actual phase speed is different from the nominal phase speed. Small variations in arrival time are observed. It is seen that a combination of first and second order effects of the turbulent velocity field is needed to fully explain the waveform distortion and the change in rise time.

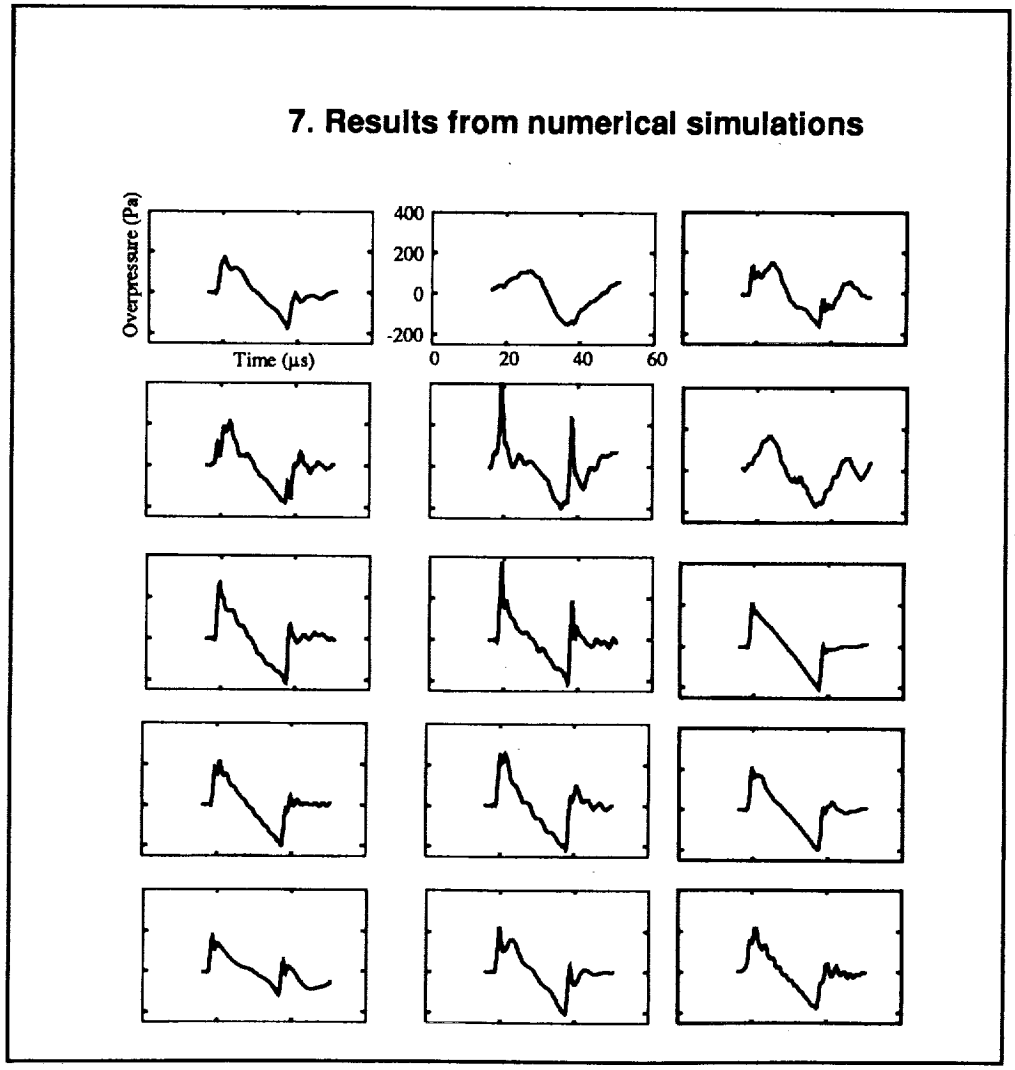

In order to make a convincing statement that the theoretical model is capable of simulating the propagation of plane N waves through a turbulent medium, we compared computed waveforms of the theoretical model with actual measured waveforms of the model experiment. The upper traces represent waveforms computed by the theoretical model, while the lower traces show waveforms from the model experiment.

Two examples are given of a spiked waveform, and two examples of a rounded waveform. As one notices, the waveforms from the theoretical model exhibit the same distortion and change in rise time as that of the model experiment.

8. Comparison of numerical simulations and measured waveforms

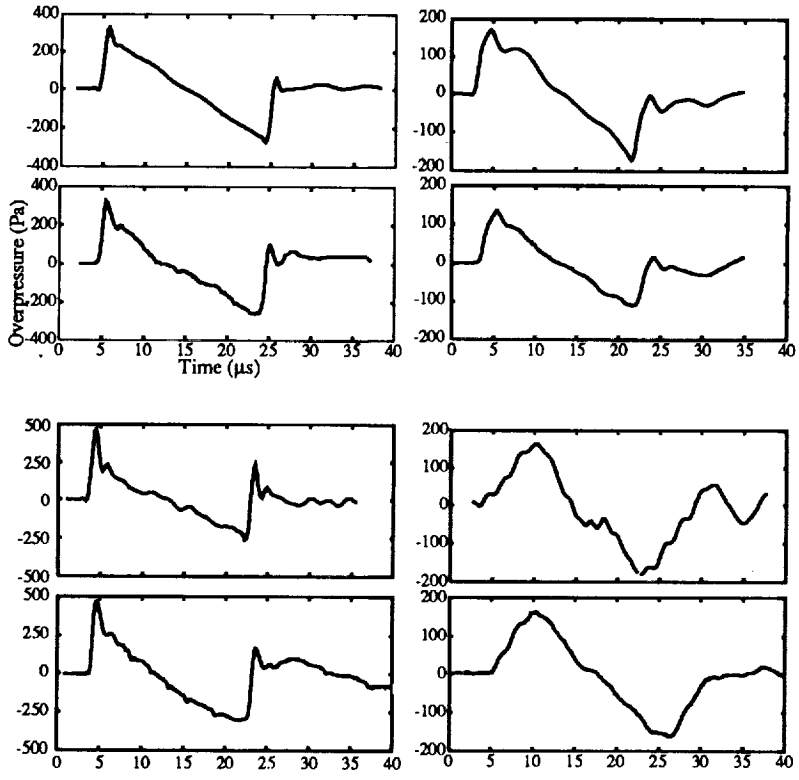

Comparisons of double-peaked waveforms are shown, and also a comparison of a U-shaped waveform and a rounded waveform is presented.

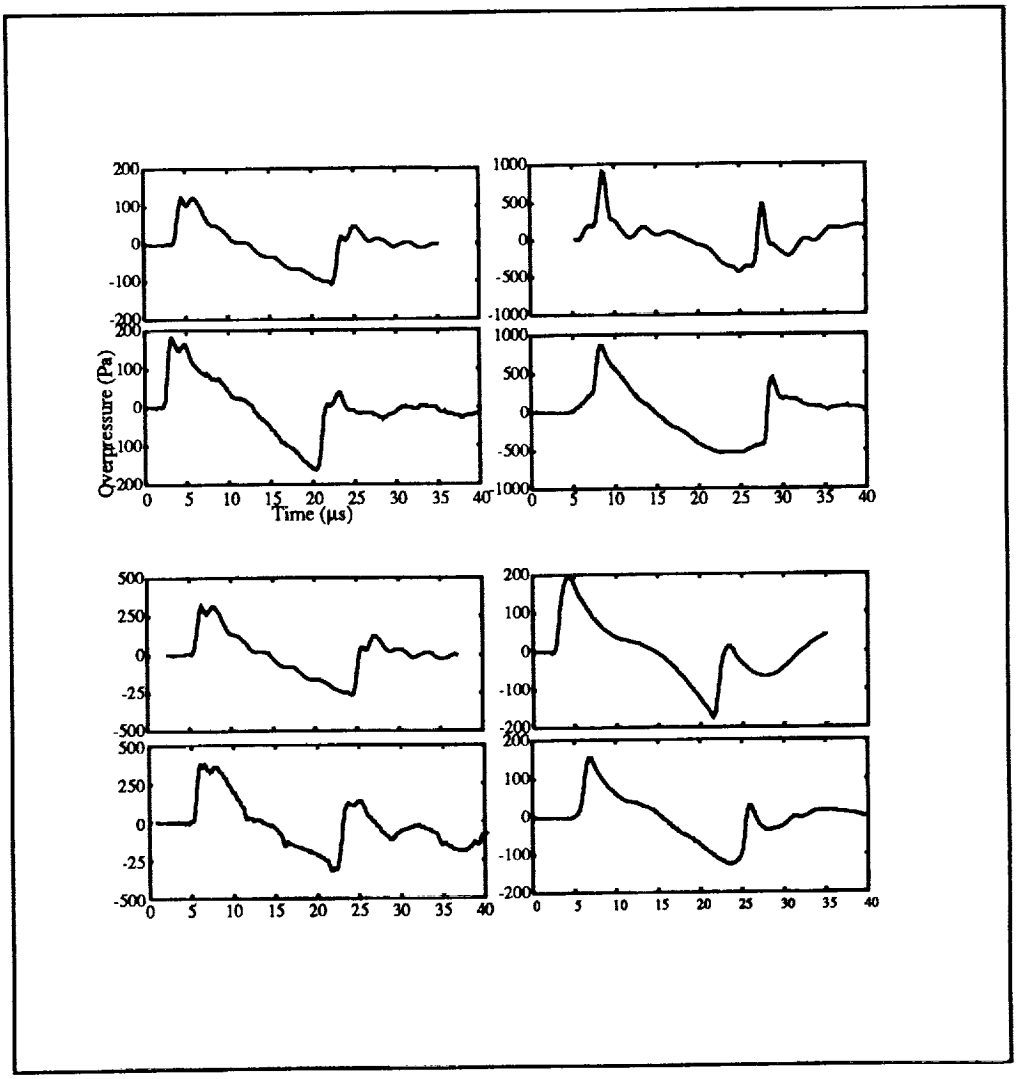

We showed that a model experiment can be successful in simulating the propagation of sonic booms through atmospheric turbulence.

We also reviewed sonic boom models and compared the data from the model experiment with the results from the models. We found that only Pierce's wavefront folding model is fairly accurate and that results from other models are not confirmed by the model experiment data.

A new theoretical model is developed in which plane waves propagate through single realizations of a turbulent velocity field. The wave equation is solved by a perturbation method. The first order pressure perturbation creates the distortion of the N wave, and at second order a singularity occurs. The second order singularity introduces changes in the phase speed. The results from the theoretical model are confirmed by comparison with measured waveforms from the model experiment.

Conclusion

- model experiment is successful

- reviewed sonic boom models
  - only Pierce's model is fairly accurate
  - others are not confirmed by model exp. data

- developed new theoretical model
  - waves are propagated through single realizations of turbulent velocity field
  - second order solution introduces a dispersion effect
  - waveform distortion and change in rise time is caused by dispersion effect
  - results are confirmed by comparison with measured waveforms

Bibliography

1 Crow, S. C. (1969). " Distortion of sonic bangs by atmospheric turbulence," *J. Fluid. Mech.* **37**, 529-563.

2 Plotkin, K. J. (1971). *The effect of atmospheric inhomogeneities on the sonic boom,* Ph. D. Thesis, Cornell University.

3 Lipkens, B. (1993). *Experimental and theoretical study of the propagation of N waves through a turbulent medium,* Ph. D. Thesis, The University of Texas at Austin.

4 Pierce, A. D. (1971). "Statistical theory of atmospheric turbulence effects on sonic boom rise times," *J. Acoust. Soc. Am.* **49**, 906-924.

5 Kulkarny, V. A., and White, B. S. (1982). "Focusing of waves in turbulent inhomogeneous media," *Phys. Fluids* **25**, 1770-1784.

6 White, B. S. (1984). "The stochastic caustic," *SIAM J. Appl. Math.* **44**(1), 127-149.

7 Plotkin, K. J., and George, A. R. (1972). "Propagation of weak shock waves through turbulence," *J. Fluid. Mech.* **54**(3), 449-467.

8 Ffowcs Williams, J. E., and Howe, M. S. (1973). "On the possibility of turbulent thickening of weak shock waves," *J. Fluid. Mech.* **88**, 563-583.

9 Plotkin, K. J. (1989). "Review of sonic boom theory," AIAA 12th Aroacoustics Conference, AIAA-89-1105, April 10-12, San Antonio, TX.

10 Karweit, M., Blanc-Benon, Ph., Juvé, D., and Comte-Bellot, G. (1991). "Simulation of the propagation of an acoustic wave through a turbulent velocity field: a study of phase variance," *J. Acoust. Soc. Am.* **89**(1), 52-62.

ON THE AGING OF SONIC BOOMS

Kenneth J. Plotkin
Wyle Laboratories
2001 Jefferson Davis Highway
Arlington, Virginia 22202

May 1993

Slide 1 —

This is the familiar formulation of sonic boom propagation. The near-field signature strength is defined by the F-function. There is an amplitude factor, the inverse of root-B, which is a generalization of cylindrical spreading. Nonlinear steepening appears as an adjustment to arrival time. This definition of the age parameter is very convenient, since once it's been computed for given flight conditions it can be applied to any F-function.

SONIC BOOM AMPLITUDE AND AGING

$$\delta p = \frac{p_o}{\sqrt{B}} F(\tau)$$

$$\frac{1}{\sqrt{B}} = \frac{\gamma M^2}{(2\beta r_a)^{1/2}} \left(\frac{\rho_o a_o^3 A_a}{\rho_a a_o^3 A} \right)^{1/2}$$

$$\tau = \underbrace{t - \int_o^s \frac{ds}{a_o}}_{\text{Acoustic Propagation}} + \underbrace{\frac{\gamma+1}{2\gamma} \int_o^s \frac{ds}{a_o \sqrt{B}} F(t)}_{\text{Nonlinear Steepening}}$$

Age Parameter:

$$\Lambda(s) = \frac{\gamma + 1}{2\gamma} \int_o^s \frac{ds}{a_o \sqrt{B}}$$

Signature at τ advances by $\Lambda(s)\ F(\tau)$

Slide 2 —

The kind of F-function we're most interested in is a shaped minimized one. This is George's F-function for a minimum-shock boom. (For simplicity, I'm only discussing the forward half, hence George's original form rather than the George/Seebass or Seebass/George extension to front and rear shocks.) As it ages, the initial delta-function impulse (Jones's asymptotic optimum) ages as an N-wave, while the isentropic compression behind follows. Everything is a very simple function of age parameter.

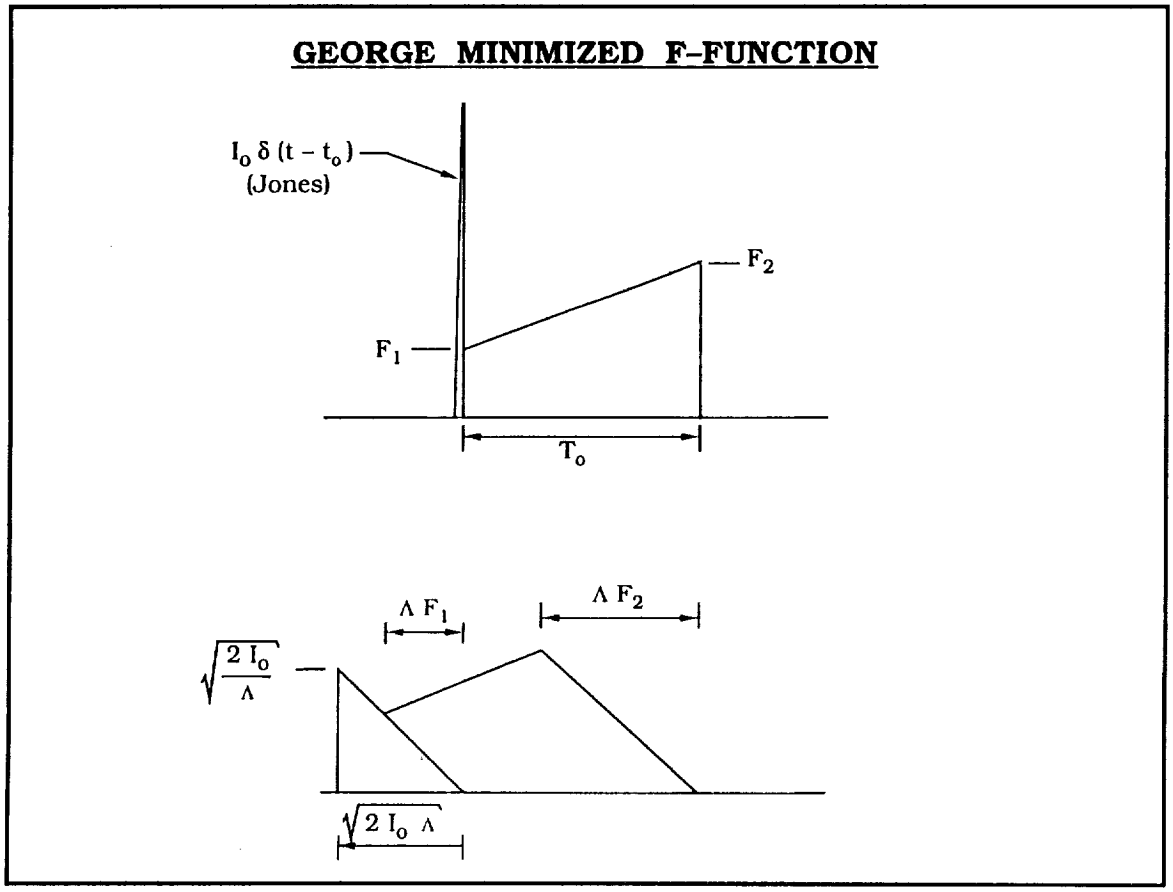

Slide 3 —

The target ground boom occurs when the N-wave from the impulse just coalesces into the ramp, and the ramp still has some rise time which is slow enough to be not audible. Everything — including the matching value of the initial impulse — is related in simple ways. It's worth looking at the age for which the ramp turns into a shock, as well as the age for the design condition.

FINAL MINIMUM SHOCK BOOM

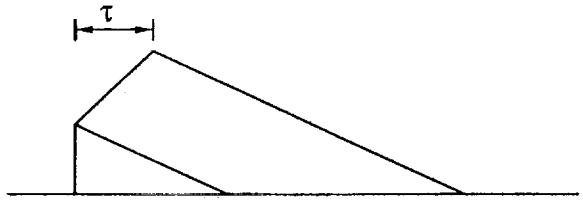

Target τ at Design Condition:

$$\Lambda F_2 - \Lambda F_1 = T_0 - \tau$$

$$\Lambda = \frac{T_0 - \tau}{F_2 - F_1}$$

$$\frac{\Lambda(\tau)}{\Lambda(0)} = \frac{\Lambda}{\Lambda_{shock}} = \frac{T_0 - \tau}{T_0}$$

Bow Shock Blends at Design Condition:

$$\sqrt{2 I_0 \Lambda} = \Lambda F_1$$

$$I_0 = \frac{\Lambda F_1^2}{2}$$

Slide 4 —

These values are idealizations of the various low-boom designs which have been discussed over the past few years, for minimum boom Mach 1.6 to 1.8 and flight altitude of 40 to 50 kfeet. I've idealized the duration and slope of the isentropic compressions, and assumed a perfectly matched nose impulse. The design age parameter is about 0.8, with full shock coalescence occurring around 1.3. For this signature's initial and target ramp durations, if the signature ages by perhaps 30 to 60 percent more than the optimum age it will degenerate into a very noisy full shock. Lesser degrees of "overaging" will not increase its loudness as drastically.

The 50 msec ramp is somewhat arbitrary. With Leatherwood, Sullivan, and Shepherd's excellent results from NASA—Langley's boom box experiments, it would be appropriate to establish formal target values for the ramp slope based on optimizing loudness.

TYPICAL VALUES

$M = 1.7$

$T_o = 0.12$ sec ($L \approx 200$ ft)

$F_1 = 0.06 \sqrt{ft}$, $F_2 = 0.15 \sqrt{ft}$

$\tau = 0.05$ sec

Resultant Design Condition:

$\Lambda = 0.8$ sec $\sqrt{ft}$

Shock Coalescence Condition:

$\Lambda_{shock} = 1.3$ sec $\sqrt{ft}$

Slide 5 —

In a uniform atmosphere, the age parameter grows as the square root of distance. A convenient model for parametric analysis is an isothermal exponential atmosphere, with straight ray paths and fairly simple complete expressions. The real atmosphere can reasonably be approximated by a scale height in the range indicated. The isothermal-exponential atmosphere age parameter has an asymptotic limit, which equals the uniform atmosphere value at a radius (in the uniform atmosphere) which is about a scale height. This asymptote leads to the concept of freezing.

AMPLITUDE AND AGE PARAMETERS

Uniform Atmosphere:

$$\frac{1}{\sqrt{B}} = \frac{\gamma M^2}{\sqrt{2\beta r}}$$

$$\Lambda_u = \frac{(\gamma+1) M^3}{2\sqrt{2\beta}\,\beta a_a} 2 r^{1/2}$$

Isothermal, Exponential Atmosphere:

a_o = constant

$\rho_o = \rho_g e^{-z/H}$; H = 20,000 ft—30,000 ft

$$\frac{1}{\sqrt{B}} = \frac{\gamma M^2}{\sqrt{2\beta r}} e^{-r/2H}$$

$$\Lambda_i = \frac{(\gamma+1) M^3}{2\sqrt{2\beta}\,\beta a_a} \sqrt{2\pi H}\ \mathrm{erf}\left(\sqrt{r/2H}\right)$$

Freezing: $\Lambda_i(\infty) = \Lambda_u(\pi H/2)$

Slide 6 —
Here are uniform and isothermal-exponential atmosphere age parameters at Mach 1.7. The asymptotic "frozen" limits are indicted on the right edge. Notice that these limits are not reached, or even approached, until very high altitudes — perhaps double the 40 to 60 kfeet of interest for HSCT. The term "freezing" has been used fairly often, and this familiarity has led to some common misconceptions. Atmospheric gradients clearly slow the aging process — to the point that McLean's midfield signature concept is practical — but we are not close to the freezing regime. The isothermal-exponential age parameters in this figure, in the altitude range of interest, look like diminished versions of the uniform age parameter.

Having the correct age parameter is essential even for predicting N-wave sonic booms. The overwhelming success of that endeavor suggests that there is no need to conduct elaborate experiments to prove that we know how sonic booms age, and certainly no need to become obsessed with asymptotic freezing.

What certainly does need attention is determining whether mid-field signature aircraft designs are practical, and whether the signatures will survive under real-world conditions. Wind tunnel tests confirming configuration concepts have been successful, but wind tunnels are not large enough to allow aging to the midfield. Flight tests using RPVs and modified existing aircraft are being planned, and are necessary. The rest of this paper concentrates on proper scaling, with regard to age parameter, of these reduced-scale flight tests. Some phenomena which do not scale are identified, and emphasis is placed on pre-test analysis of elements which may not be intuitively obvious.

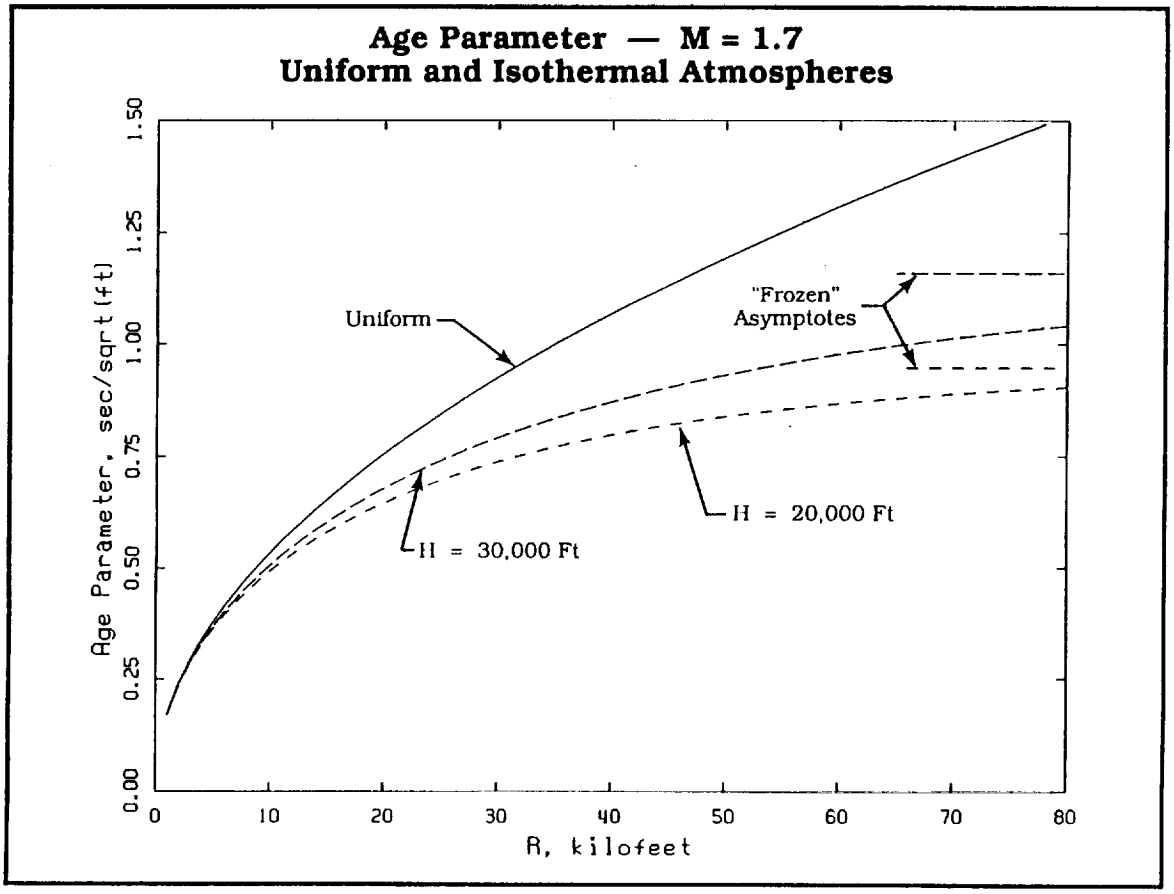

Slide 7 —

This is an age parameter chart similar to the previous one, except that it is at Mach 2.0. Differences between this chart and the previous one exhibit the importance of using the correct Mach number. That the age parameter is bigger at Mach 2 than at 1.7 illustrates one of the reasons why boom minimization is easier at low Mach numbers.

The age parameter for the real atmosphere is somewhat more complicated, depending on both the flight altitude and the ground altitude, rather than just the difference. Flight test design must use the real atmosphere. However, the isothermal-exponential model is adequate for the purposes of the current discussion.

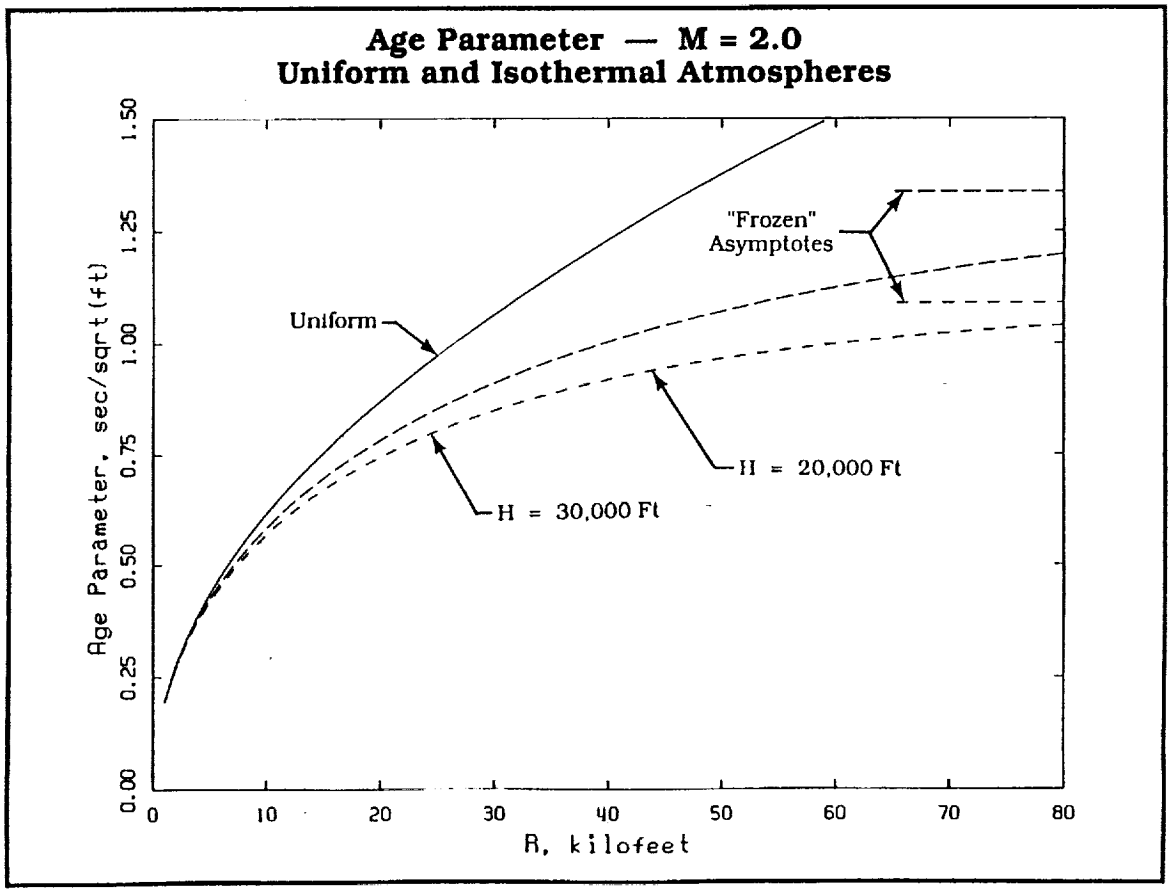

Slide 8 —

A real-world consideration is that the age parameter is larger off track than on. This is the relation for the isothermal-exponential atmosphere. At an azimuth of 45 degrees, the age parameter is about 15 percent bigger, and at 60 degrees it is about 40 percent bigger. There is a favorable benefit with the amplitude factor, but care must be taken to allow a margin before shock formation. In a flight test of an axisymmetric vehicle, on- and off-track measurements can be used to obtain several ages per flight.

OFF-TRACK AGING

- On-Track: $\phi = 0$, $r = z$.
- Off-Track, Isothermal Model:
  - $r = z/\cos\phi$
  - $H_{effective} \rightarrow H/\cos\phi$

$$\Lambda = \frac{(\gamma+1)\,M^3}{2\sqrt{2\beta}\;\beta\,a_a}\sqrt{2\pi\,H/\cos\phi}\quad \mathrm{erf}\left(\sqrt{z/2H}\right)$$

$$\Lambda_\phi = \Lambda_{\phi=0}/\sqrt{\cos\phi}$$

Slide 9 —

The first detail to consider for scaling flight test experiments is how the source scales with size. This is a simple representation of the volume and lift components of the F-function. The volume component always remains the same. Increasing the aircraft altitude at fixed weight increases the F-function, as well as the age parameter due to increased distance. Flying at an optimum lift coefficient keeps F fixed, and there is some recovery from the reduced amplitude factor at higher altitudes, so long as the increased aging does not lead to serious shock coalescence. This is why mission profiles with increasing altitude as fuel burns off tend to not show loudness increases, but rather decreases.

For model scaling purposes, it is reasonable to assume that the boom is dominated by volume, or that full-scale lift coefficient will be replicated. The entire F-function then behaves like volume boom.

F-FUNCTION FOR VOLUME AND LIFT (FIXED M)

$$F(x) = \underbrace{\frac{1}{2\pi}\int_0^x \frac{A''(\xi)}{(x-\xi)^{1/2}}\,d\xi}_{\text{Volume}} + \underbrace{\frac{\beta\cos\phi}{\rho_\infty u_\infty^2}\,\frac{1}{2\pi}\int_0^x \frac{L'(\xi)}{(x-\xi)^{1/2}}\,d\xi}_{\text{Lift}}$$

- Volume F-Function Fixed by Geometry.
- Lift Component:
  - Increases if Raise Altitude at Fixed L (Off-Design Condition)
  - Decreases if L Decreases at Fixed Altitude (Fuel Burn-Off at Fixed Altitude)
  - Stays Constant at Fixed C_L (Optimized Cruise Profile)

Slide 10 —

For geometrically similar models, the F-function scales as the square root of length. A model less slender than full scale (larger f) increases F, which would in turn require a smaller propagation distance to retain the same relative aging.

SCALING OF VOLUME BOOM

$$F_v(x) = \frac{1}{2\pi} \int_0^x \frac{A''(\xi)}{(x - \xi)^{1/2}} \, d\xi$$

Let

$$A(x) = f^2 \, l^2 \, \tilde{A}(x/l)$$

l = length

f = fineness ratio

$\tilde{A}(x/l)$ = nondimensional shape

$$F_v = f^2 \sqrt{l} \, \tilde{F}_v(x/l)$$

Slide 11 —

To achieve proper scaling in a uniform atmosphere simply requires altitude proportional to model length. In a real atmosphere, where the rate of growth of the age parameter is slower at larger distances, a model experiment requires flight altitudes which are smaller than obtained by using the model to full-scale ratio. If, for some reason, the model flight altitude must be proportional to model length, then the model must have a more slender fineness ratio.

MODEL FLIGHT TEST

- Require $(\Lambda F)_{model} = \frac{1}{L}(\Lambda F)_{full\ scale}$
- $F \propto \sqrt{1/L}$, so need $\Lambda \propto \sqrt{1/L}$
- Uniform Atmosphere: $\Lambda \propto \sqrt{r}$, So Scale $r_{model}/r_{full} = 1/L$
- Real Atmosphere: Λ tapers off $\Rightarrow r_{model}/r_{full} < 1/L$

Slide 12 —

This table shows the scaling for three size models: full, one-third, and one-tenth. This roughly covers the range of proposed tests. The quantity shown as F is the nominal full-scale F-function at the end of the ramp, which was 0.15 in our example. The age parameter is that required so that age times F will scale proportionately to model length; for full scale, the age parameter for 50,000 feet is shown. The value of z shown for the models is the corresponding altitude in the real atmosphere. The altitude ratio is always less than the model size ratio, and for the smallest scale is about half. The model age parameter is also proportionately more sensitive to altitude errors than full scale. It is straightforward to calculate required altitude precision, and the test plans must address this.

The final parameter in the table is the duration of the ramp. A nominal 50 msec full-scale ramp is expected to be clearly discernible. The corresponding model ramp durations are very close to the 3 to 10 msec range normally encountered for shock wave rise times. If we expect shocks to have their typical "full-scale N-wave" rise times, the smaller scale tests are somewhat dubious.

RELATIVE SCALES FOR ONE-THIRD AND ONE-TENTH MODEL TESTS

Scale	F	Λ	Z	Z/Z_{full}	τ
1.0	0.15	0.84	50,000	1.0	50 msec
1/3	0.087	0.48	9,500	0.19	17 msec
1/10	0.047	0.27	2,600	0.05	5 msec

Slide 13 —

Rise times may not, however, be as long as they are at full scale. Bass, Layton, and Bolen (*JASA*, July 1987) measured projectile shock waves which were considerably thinner than expected from steady theory. The reason was that propagation distances were sufficiently short that they had not had time to reach steady state. At last year's sonic boom workshop, Raspet discussed "healing times" and suggested that even full-scale N-wave shocks might not be steady. If full-scale shocks have not achieved steady thickness, then model shocks must certainly be investigated.

The current HSR team has developed several models which are suitable for calculating the evolution of shock structures. This is the time to use them.

POTENTIAL FOR THIN SHOCKS

- Unsteady Shock Formation Over Short Distances (Bass, Layton, and Bolen – *JASA*, July 1987).
- Healing Time of Weak Shocks (Raspet, 1992).
- Current Analysis Tools Available to Predict.

Slide 14 —

As a final element, I'd like to show some "anything can happen" data. This is of interest because this could mask results of an "aging" flight test, and also because it provides an example of turbulence effects which do not fit into the usual expected pattern.

We recently performed what should have been a very dull Boomfile test protocol on an aircraft not yet in the data base. Tests were conducted in the early morning, under overcast skies, so there was no convective turbulence. There was virtually no surface wind. The weather had been changing (it snowed overnight, and was clearing during the tests) and a rawindsonde at a site about 100 miles away indicated wind shears at about 15 to 20 kft and 20 to 25 kft MSL. The site was at about 5 kft MSL.

SUPPLEMENTAL BOOMFILE FLIGHT TEST

- Documentation of Steady Boom for an Aircraft Not Previously Measured.
- Flight Parameters: 10k, 18k, 25k AGL, at Mach 1.2, 1.25, 1.30.
- Recorded On and Near Centerline by USAF BEAR Systems.
- Early Morning, Calm Surface Conditions.
- Rawindsonde During Test, About 100 Miles Away.

Slide 15 —

Here is a typical good measurement. In this test, which yielded about 25 valid recordings from ten passes, about half the records were of this quality. The rest had significant distortion. The next three slides are particularly interesting.

25 kft, M = 1.3

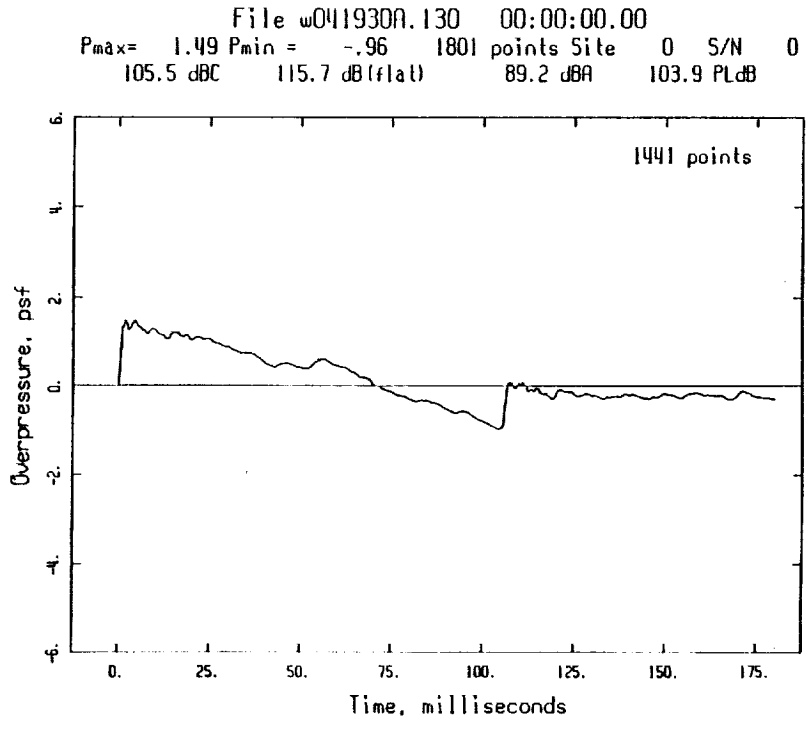

Slides 16, 17, 18 —

These are distorted measurements at 25, 18, and 10 kfeet AGL, respectively. Overpressures and durations were as expected. There was considerable distortion, and rise times were very long. These three booms have a particular characteristic that they look very much like minimum-shock shaped booms. Slides 15 and 16 are the same flight condition, so the nice minimum shock shape in 16 is anomalous.

Through most of this paper I have discussed simulation issues that could lead to what the statisticians call Type I errors — failing to confirm a phenomenon that exists. These three booms raise the possibility of Type II errors — detecting an effect that is not there.

These measurements are also interesting because they have features not fully consistent with the usual characteristics of distorted booms. Distortion was more common for the higher altitude runs, while the low-altitude runs yielded a higher percentage of clean booms. Surface layer turbulence would affect all altitudes. There was a considerable amount of noise after the booms — the kind that sounds like the echoing of distant thunder. This tended to persist for several seconds. Each BEAR would typically record three or four records per boom, with the first being the N-wave and the rest being noise. This was much more than observed during the 1987 Boomfile tests at Edwards AFB.

The site was flat, so the distortion and aftershocks had to be a combination of scattering and multiple paths. The long aftershocks and the substantial distortion are consistent with scattering from the shear layers and weather at higher altitudes, i.e., not in the surface and mixed layer as normally expected. Anecdotal reports of "echoing" in NASA's JAPE II sonic boom propagation experiment should be re-examined in terms of multi-path propagation from higher altitude atmospheric structures.

These measurements underscore that individual test conditions can obscure fine details such as would be seen in model tests of midfield signatures. Both Type I and Type II errors are possible. Care must be taken to design the initial round of shaped boom flight tests so as to avoid these conditions. It is also clear that atmospheric conditions occur which lead to distortions somewhat different from those seen in summertime desert tests. It would be prudent to extend propagation investigations into other geographical areas and atmospheric conditions.

18 kft, M = 1.25

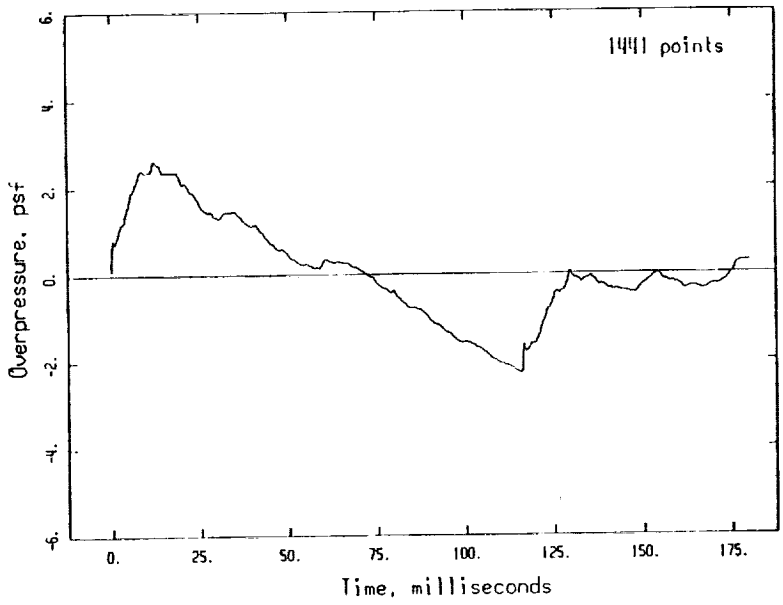

25 kft, M = 1.3

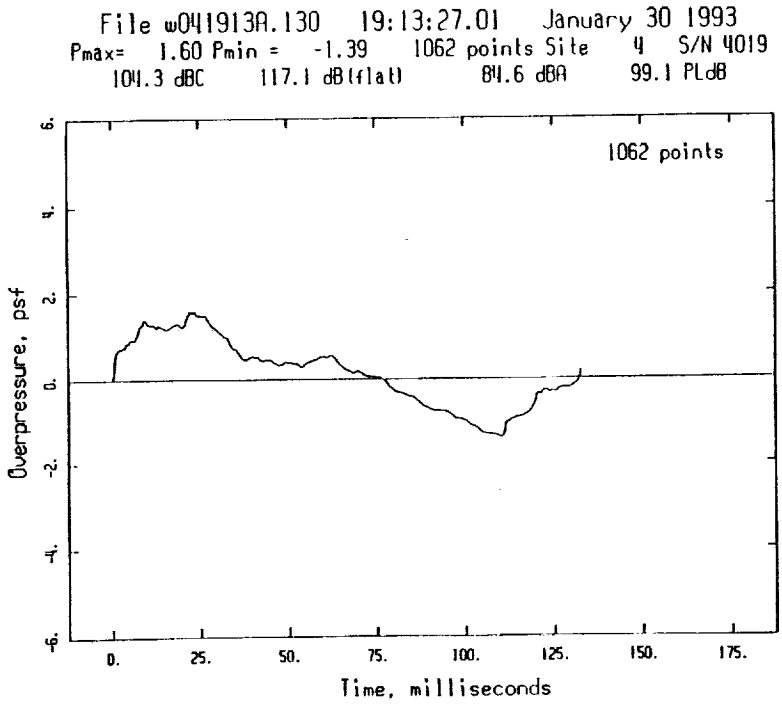

12.5 kft, M = 1.2

File w0420170.130 20:17:15.18 January 30 1993
Pmax= 2.21 Pmin = -1.80 1266 points Site 4 S/N 4019
106.2 dBC 121.1 dB(flat) 88.1 dBA 102.4 PLdB

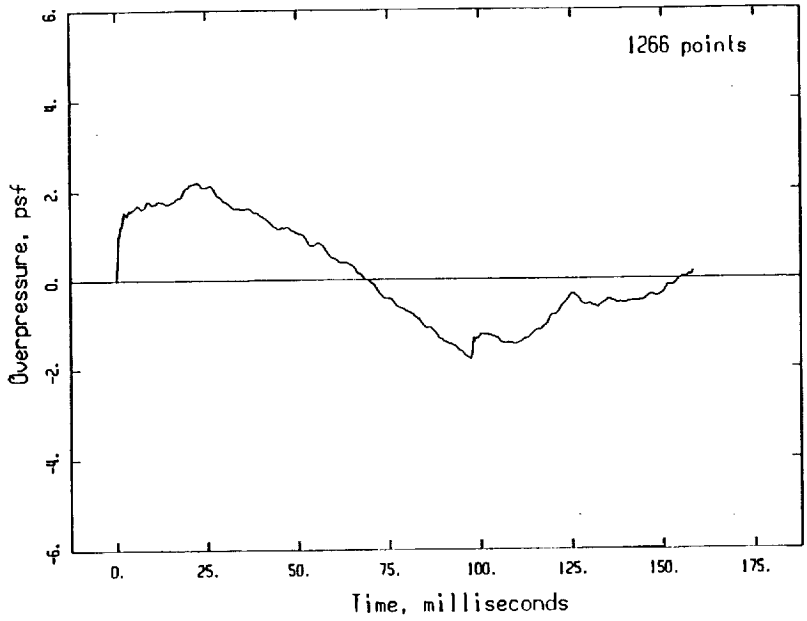

EXPERIMENTAL STUDIES OF LOUDNESS AND ANNOYANCE RESPONSE TO SONIC BOOMS

Brenda M. Sullivan
Lockheed Engineering and Sciences Company
Hampton, Virginia

Jack D. Leatherwood
NASA Langley Research Center
Hampton, Virginia

Presentation at NASA HSR Sonic Boom Workshop
NASA Ames Research Center
May 12–14, 1993

The purpose of this paper is to summarize the latest three sonic boom laboratory studies performed at NASA-Langley using the Sonic Boom Simulator. The first used synthesized idealized outdoor boom shapes which were filtered to represent booms heard inside a house. The test explored the efficacy of various metrics in assessing both loudness and annoyance responses to these booms. The second test investigated the effects of adding single reflections to idealized boom signatures, and the third compared booms recorded from real aircraft with idealized boom signatures to determine if subjects rated the real booms differently. In these studies, as in previous studies performed at NASA-Langley, there was a continuing effort to evaluate metrics for predicting the subjective effects of sonic booms.

OBJECTIVES

- Summarize recent lab studies
  - — Quantify indoor/outdoor subjective effects
  - — Determine effects of ground reflections
  - — Quantify loudness response to recorded booms
  - — Evaluate metrics

The tests were conducted using the NASA-Langley sonic boom simulator. The simulator is a person-rated, airtight, loudspeaker-driven booth capable of accurately reproducing user-specified waveforms with peak pressures of up to 138 dB. Signals are preprocessed to compensate for non-uniformities in the frequency response of the booth and sound reproduction system. The system is fully described in reference 1. Although tests using the Simulator cannot completely replicate conditions in real life, they allow listeners to evaluate sonic booms under controlled conditions.

SONIC BOOM SIMULATOR

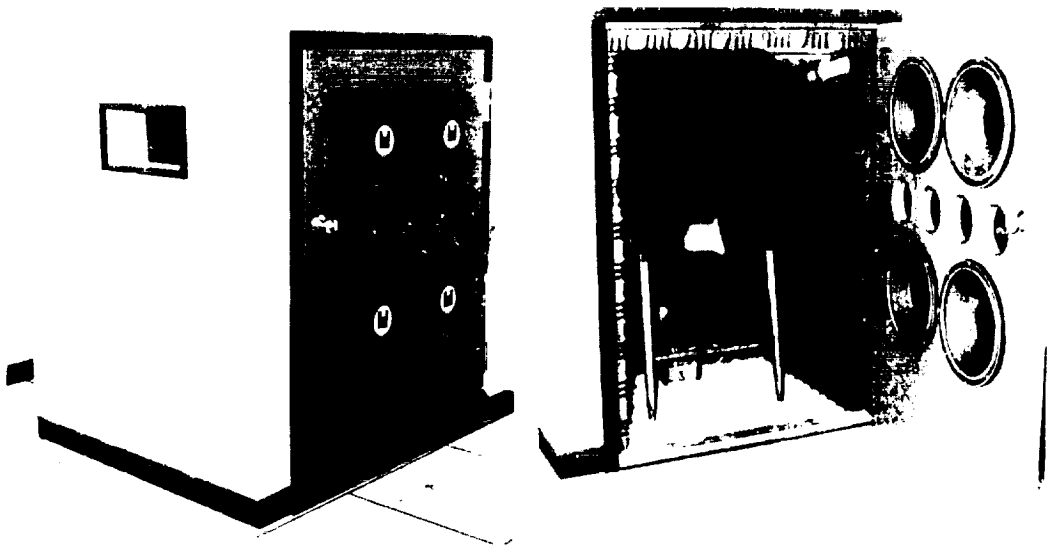

A total of 168 subjects took part in the three tests: 72 in test 1, 48 in test 2 and 48 in test 3. Tests 2 and 3 were run concurrently and used the same subjects. Magnitude Estimation Scaling was the psychometric methodology used. In this methodology, one boom was selected as a reference and given a score of 100. Subjects were asked to compare all other booms to this reference on a ratio basis. The wave shapes used in the tests included simulations of the N-waves, front-shock minimized (shaped) booms, composite booms (that is, an original N-wave or minimized boom waveform, to which was added a single delayed copy of the original), and recorded booms, which were digitally recorded and modified for reproduction in the simulator.

EXPERIMENTAL APPROACH

- Three experiments
- Magnitude estimation scaling
- 168 test subjects
- Signature shapes
  - N-waves
  - Shaped
  - Composite (original + reflected)
  - Recorded

Five metrics have been studied in these and previous tests run at Langley. These were unweighted sound exposure level (SEL), A-weighted sound exposure level (SEL_A), C-weighted sound exposure level (SEL_C), perceived level (PL) using the Stevens' Mark VII procedure, and Zwicker loudness level. Considering the results of all tests run in the Simulator to date, PL has proved to be the most effective metric for predicting subjective reactions to sonic booms. Therefore the results of the three tests in the present paper are reported in terms of PL. Full details on the calculation procedures are given in reference 2. Previous tests are described in references 3, 4 and 5.

METRICS

- Five metrics considered
  - — SEL (unweighted)
  - — SELA
  - — SELC
  - — Perceived Level (Stevens' Mark VII)
  - — Zwicker Loudness Level
- All studies have evaluated metric performances
- Perceived Level selected as best metric for general use

The objectives of the first experiment were to investigate whether people respond differently to sonic booms heard indoors as compared with booms heard outdoors, to determine whether there would be a difference if they were asked to rate loudness or annoyance, and to validate the PL metric. Tests in the booth cannot be true simulations of reactions in the home, as there is no rattle, no fear of property damage, and the subjects' sole activity is to sit and listen to the booms. Hence this test could only compare loudness and annoyance responses in the lab. The test results do provide a basis for determining which descriptor was more appropriate and for evaluating which metrics predicted people's reactions most accurately. This test used two groups of 36 subjects each; one group was asked to rate the booms based on annoyance and the other was asked to judge loudness. Both groups heard the same signals played at the same levels; both used the same reference boom with a score of 100. The calculated metric levels were unchanged between the two parts of the test; only the subjective ratings differed.

EXPERIMENT 1 OBJECTIVES

- Quantify loudness and annoyance of simulated indoor and outdoor booms
- Determine appropriate subjective criterion measure
- Verify PL metric

The signatures used in this study were based on three shapes: an N-wave, a front-shock minimized boom with a ratio of front shock to peak overpressure of 0.75 and a front-shock minimized boom with a ratio of front shock to peak overpressure of 0.5, as shown in the figure. The front-shock minimized (FSM) booms had a secondary rise time of 60 msec. All booms had a duration of 300 msec, and for all three shapes front-shock rise times of 2, 4 and 8 msec were used. Thus a total of nine waveforms comprised the outdoor signals.

NOMINAL OUTDOOR SIGNATURES

(All durations = 300 msec)

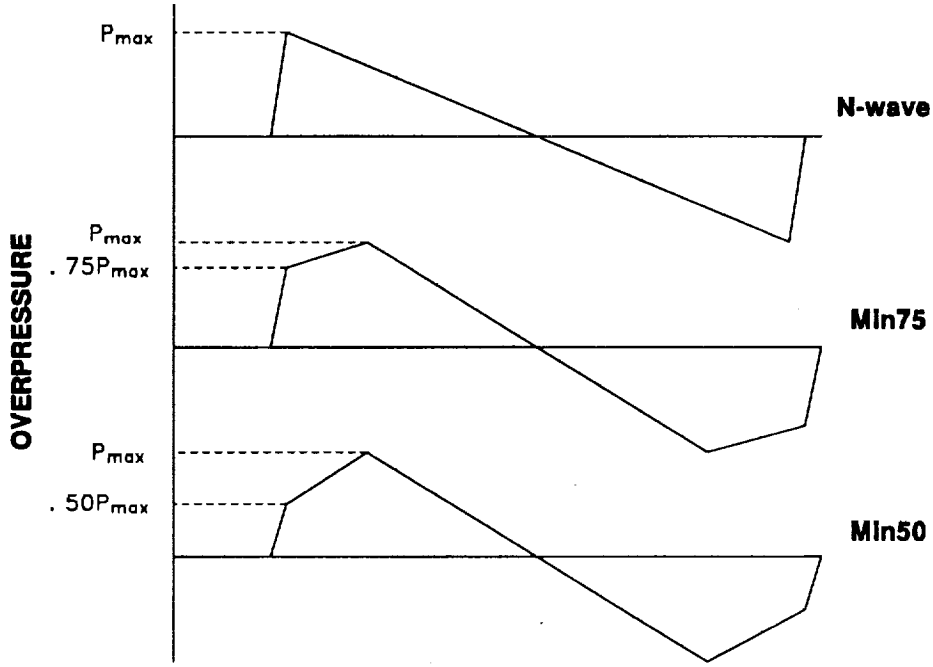

Each outdoor shape was digitally filtered using two filters, one representing the attenuation through a typical house wall with windows open and the other with windows closed. Both gave no attenuation below 10 Hz, which is considered the simplest reasonable assumption in view of the lack of data at these frequencies. Above 60 Hz, these shapes were mathematical curves based on measured data. For both filters, the effect was to remove high frequency energy, more of which was removed by the "windows closed" filter than by the "windows open" filter.

HOUSE FILTERS

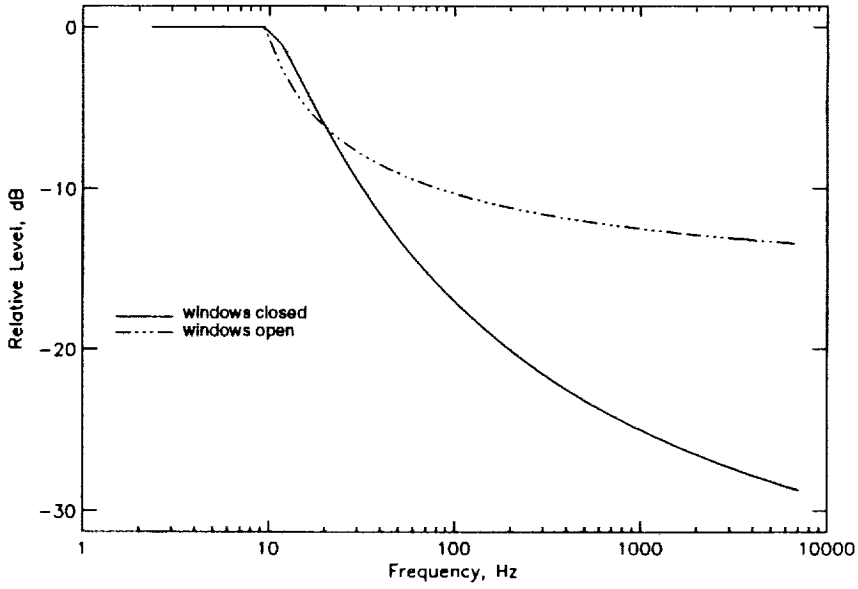

This chart shows simulated indoor and outdoor booms, as measured within the simulator, for cases where the outdoor booms had rise times of 2 msec. Differences between the N-wave and the FSM booms can still be seen in the filtered shapes, but the high frequency, sharp corners of the originals have been greatly reduced. The nine original shapes were each presented to the subjects in the original form (the "outdoor" booms) as well as in the two "indoor" forms ("windows open" and "windows closed"). Measurements of sonic booms inside real houses would show more complex signatures, because of phase changes which were not simulated. However, these changes do not alter the frequency content of the boom. No reverberation effects were included in these simulations.

OUTDOOR AND INDOOR SIGNATURES

(rise time = 2 msec)

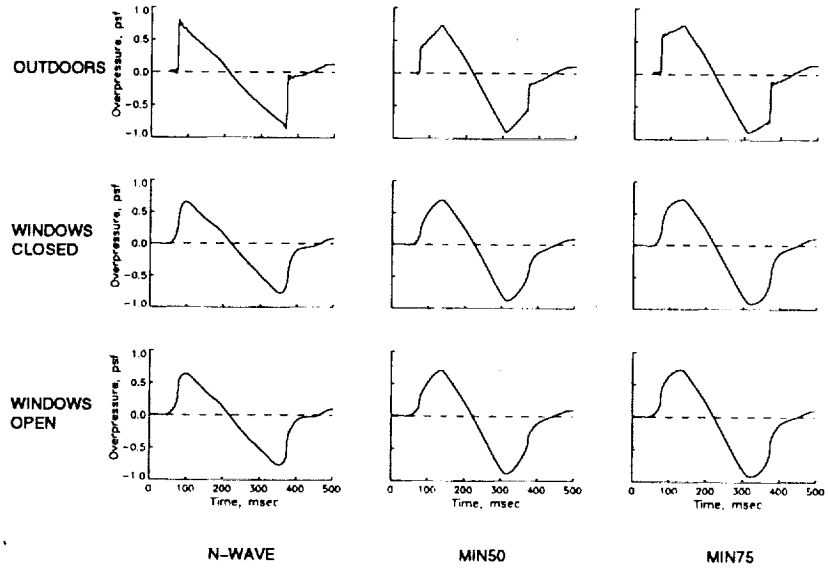

Results obtained in the first experiment are summarized in this chart which displays plots of the logarithm of the geometric means of the subjective ratings versus Perceived Level. The geometric mean is the appropriate central tendency measure for data obtained using the Magnitude Estimation psychometric method. For the outdoor booms, the results (displayed in the plot on the left) show no difference between loudness and annoyance responses, which agrees with previous studies. However, differences between loudness and annoyance scores were found for the indoor booms. For both simulated indoor conditions, the annoyance responses where higher than loudness responses. The plot on the right shows the results for the "windows closed" condition. The "windows open" results were similar, except that the differences between loudness and annoyance responses were smaller. This is reasonable since the "window open" filter had less effect on the boom than the "windows closed" filter. Statistically the slopes are not significantly different for either pair of lines. At the levels used in this test, the low frequencies were dominant in the indoor booms. Thus it could be inferred that they caused an increase in annoyance greater than their contribution to loudness. Based upon these results it is recommended that studies of indoor booms use annoyance rather than loudness as the judgement criterion, as the use of loudness may underestimate the booms' unacceptibility.

LOUDNESS AND ANNOYANCE RESPONSE

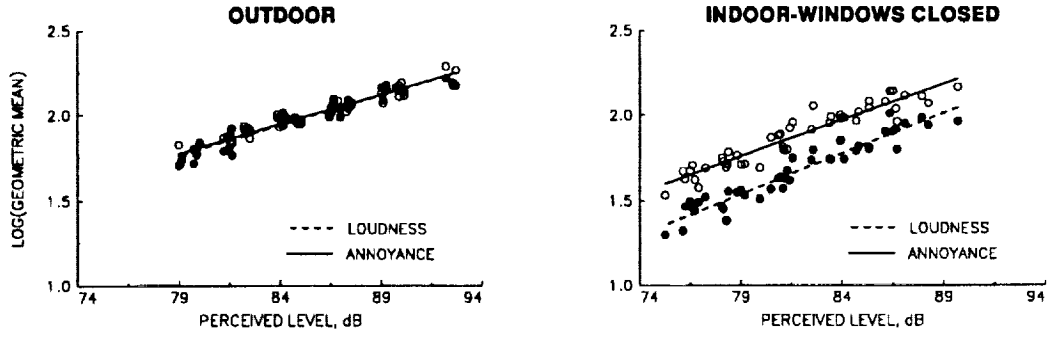

The performance of PL for judgements of loudness (left plot) and annoyance (right plot) for each simulated listening condition is shown in this figure. For a given PL value, the indoor booms were rated lower in loudness than the outdoor booms. The "windows open" condition lies between the outdoor and the "windows closed" loudness results. However, the indoor and outdoor booms of the same PL level were rated equally annoying. In both plots, the slopes of the regression lines for the indoor boom results differ significantly from those for the outdoor boom results. Results for SELA or the other metrics investigated (not shown) clearly indicate that PL predicted more accurately the annoyance for the combined data set of indoor and outdoor booms.

PL METRIC PERFORMANCE

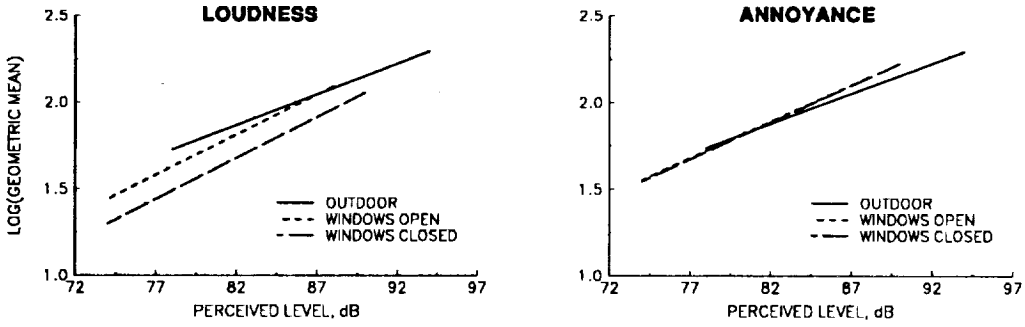

Field measurements of sonic booms are usually made with flush-mounted microphones, in which case a single reflection is present in the recording with a zero time delay between the direct boom and the reflected boom. However, outdoor listeners will usually receive a direct boom followed by a reflection off the ground having a finite delay, of the order of 8 msecs. In the second experiment, the objective was to evaluate the effects of different delay times on subjective response and to find a metric that accounted for these effects. To investigate this, single "reflections" were added to idealized boom shapes. Delay time between the "direct" boom and the "reflected" boom was a variable in this study. As only outdoor boom shapes were used, subjects were asked to rate loudness.

EXPERIMENT 2 OBJECTIVES

- Quantify loudness of sonic booms containing reflections (direct + single reflection)
- Determine delay time effects
- Verify PL metric

This chart demonstrates the effect of adding to an idealized N-wave shape (the "direct" boom) a single time-delayed version of the same shape (the "reflected" boom). The combined wave form is called a "composite" boom. No phase change or attenuation was introduced into the delayed wave. If the delay is zero, the result of combining the direct and reflected booms is a doubling of overpressure while the rise time remains unchanged. If the delay is equal to the rise time, the resulting wave has a rise time twice that of the original, while the overpressure is nearly double the original. Other delay times result in composites having complex, multi-segmented pressure increases.

COMPOSITE BOOM SIMULATION

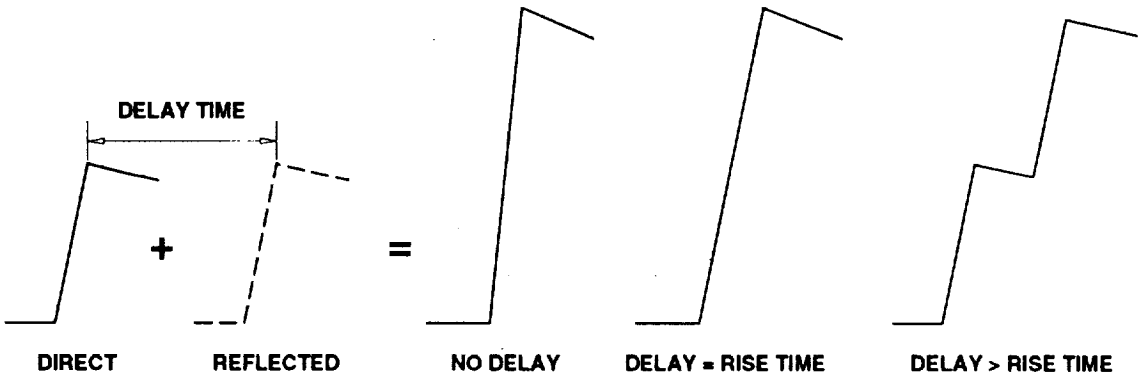

DIRECT + REFLECTED = COMPOSITE

The basic shapes considered were an N-wave and a front-shock minimized boom with a ratio of front shock overpressure to peak over pressure of 0.5. For both shapes rise times of 3, 6 and 9 msec were used, which resulted in six waveforms for the "direct" booms. For each direct boom, six values were selected for the delay time. Delays of 0 msecs and 12 msecs were used for each direct boom. A value of delay equal to the front shock rise time was also selected, together with rise time + 1 msec and rise time − 1 msec. The sixth value of the delay was 3 msecs, except for the booms with 3 msec rise times, where a value of 8 msec was used.

EXPERIMENTAL WAVEFORMS

- Six direct boom waveforms
  - — 3 N-waves (rise times = 3, 6, 9 msecs)
  - — 3 shaped (front shock rise times = 3, 6, 9 msecs)

- Six reflection delay times for each direct boom

The composite waveforms that resulted when a 6–msec N-wave was used as the original waveform are illustrated here. In these idealized plots, the direct boom has an overpressure of 1 psf. The delay time between the "direct" boom and the "reflection" was varied between 0 and 12 msec. The zero delay results in a waveform with a rise time of 6 msec, but a peak overpressure of 2 psf. When the delay equals 6 msec, the composite wave has a peak overpressure of almost 2 psf, but the rise time has been doubled to 12 msec. The other delays produce other more varied waveshapes.

COMPOSITE WAVEFORMS

(N–wave, τ = 6 msec)

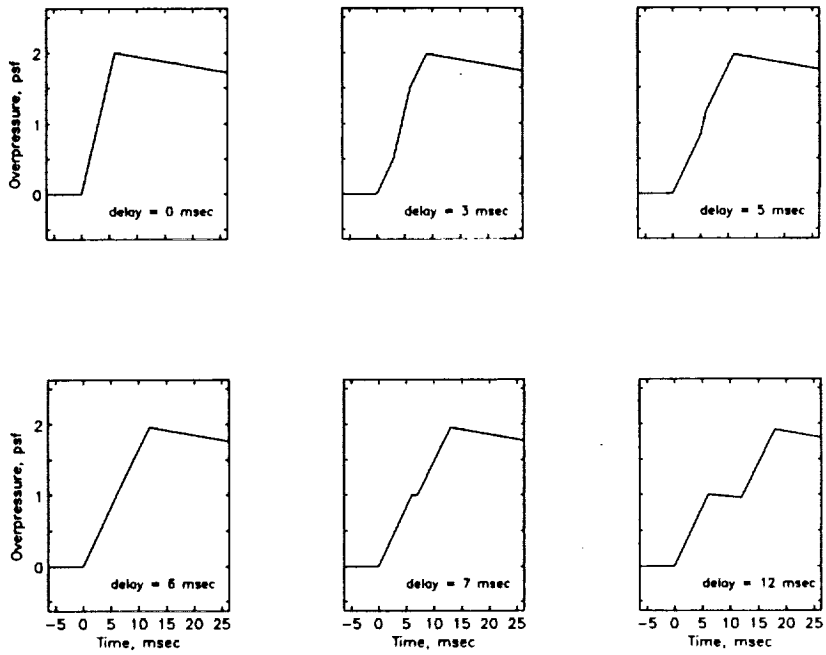

The effects of varying the delay for booms with a range of rise times were predicted using the PL metric. This chart shows the predicted PL values for N-waves with rise times ranging from 0.1 msec to 12 msec, and delays from 0 to 14 msec. The curves show a maximum at zero delay, and a minimum for most cases when the delay equals the rise time. Some of the irregularities in these curves are due to the fact that they were calculated using 1/3 octave bands. As the delay time changes, there are subtle changes in the spectrum, which cause energy to shift in frequency. As it shifts from one band to another, there are changes in the calculated values. If a continuous algorithm is used, such as that used for SELA, these irregularities are removed. SELA shows the minimum when the delay exactly equals the rise time, but for the short rise times PL shows the minimum at somewhat greater delays. This is probably an artifact of the calculation procedure.

PREDICTED DELAY TIME EFFECTS

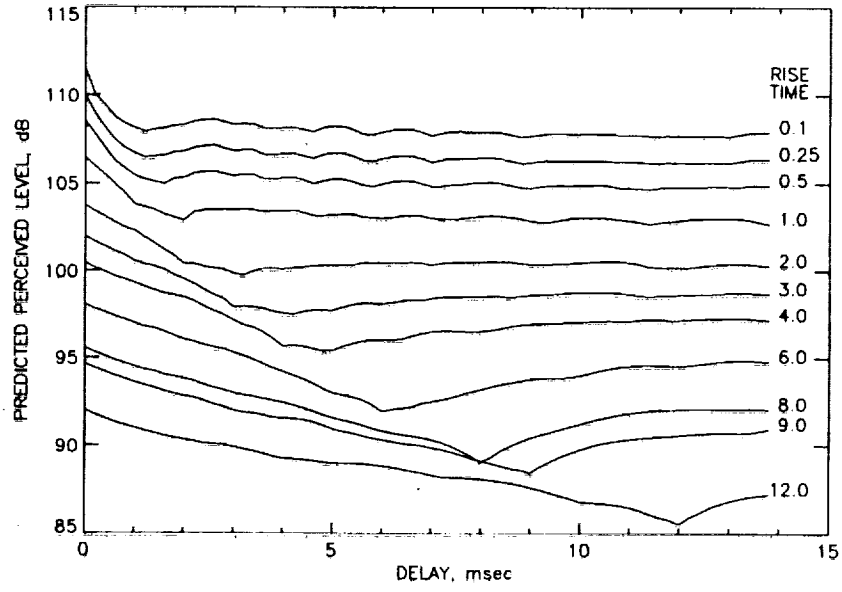

This chart shows the results obtained for the six basic waveforms, each with six different delay times. The solid lines show the subjective responses, converted to equivalent PL, while the dashed lines show PL calculated from the measured data. The results are normalized to 0 dB at a delay time of zero. In general there is good agreement between PL calculated from measurement and PL derived from the ratings. The ratings all show a minimum when the delay time is equal to the boom front shock rise time. Predicted PL and PL based upon measurements also gave minima when delay time equals front shock rise time except for the 3 msec booms which have a minimum at a 4 msec delay.

Most sonic boom measurements are made with flush-mounted microphones, for which there is zero delay between the direct wave and the ground-reflected wave. Hence, these measurements will yield loudness levels that are conservative compared to outdoor situations, where the listener will experience a ground reflection with a delay typically of the order of 8 msec. In an enclosed situation, there could be more than one reflection, and more complex wave forms could result.

DELAY TIME EFFECT

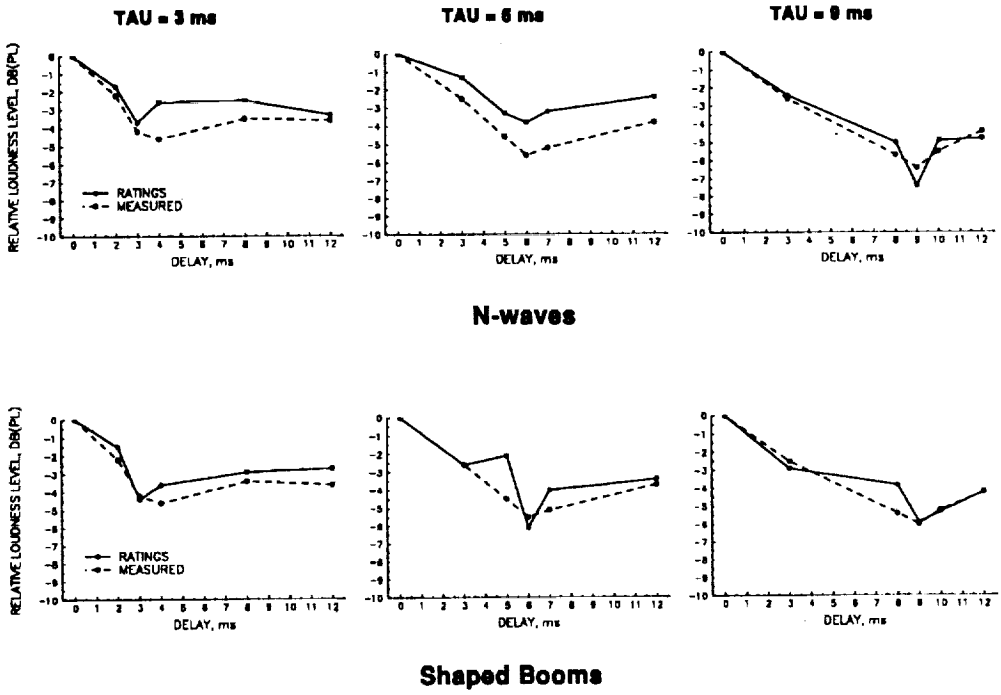

The figure shows a plot of subjective ratings as a function of PL calculated from measured data for the set of composite booms containing reflections with zero delay and for the set containing reflections with non-zero delays. There is no statistically significant difference between the two lines, and PL can be said to account for the effects of delay on loudness.

DELAY EFFECT - PL METRIC

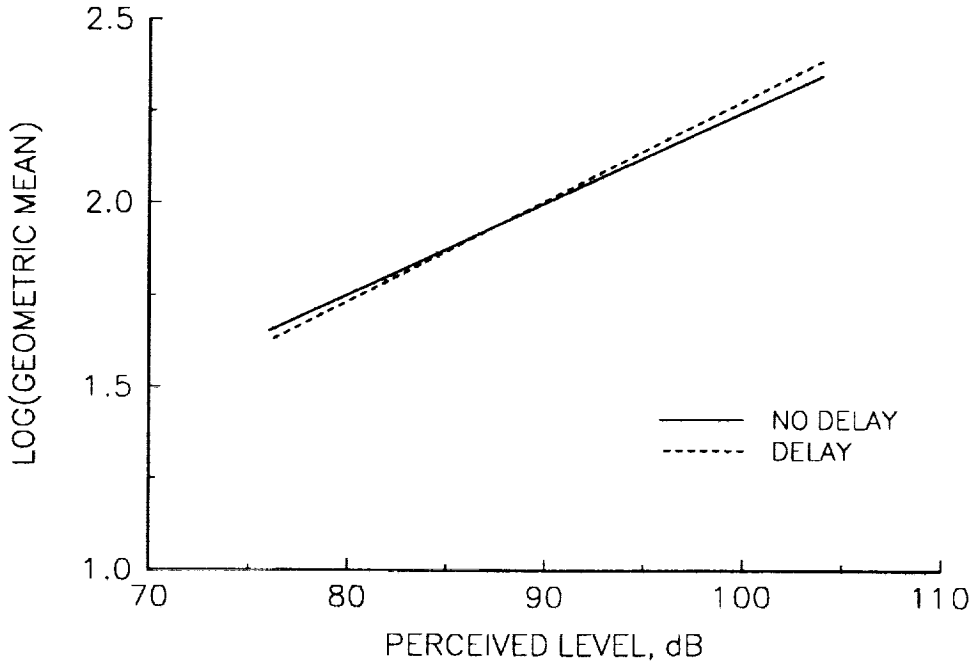

The third experiment used real sonic boom recordings made at White Sands Missile Range from T38 and F15 flyovers. The objective of the test was to determine if people reacted differently to real booms as compared to idealized booms, and to assess metric performance for predicting the loudness of real booms that have been distorted by propagation through the atmosphere. The recordings were made using the United States Air Force's BEAR (Boom Event Analysis Recorder) systems using a 8 kHz sample rate. Seven hundred recorded signatures were scanned and thirteen booms selected that fitted into four major categories of sonic boom shape:

1. N-wave
2. Rounded
3. Peaked
4. U-shaped

The recorded booms were digitally edited to remove some of the background noise and to increase the time between their front and rear shocks to 300 msec, which is more representative of a HSCT. The front and rear shocks were not altered by this procedure. Three idealized N-waves and two boom shapes based on predictions for HSCT from various CFD codes were also included, resulting in a total of 18 signals. The waveforms based on the CFD predictions were simplified, but both contained more than two pressure peaks. Because of the existence of extra shocks between the front and rear shocks, these were designated "intermediate" booms. All the signals, recorded and idealized, were preprocessed to account for the booth frequency response.

EXPERIMENT 3 OBJECTIVES

- Quantify loudness of recorded signatures
- Compare with results for idealized booms
- Verify PL metric

This chart presents some of the results from this test, together with three examples of the recorded waveforms as reproduced in the simulator. These data show that responses to the four categories of real booms did not differ from responses to the idealized N-waves when plotted against PL calculated from measured signals. Thus PL accounted for any differences between the waveforms. These booms were not played at the same levels as they were heard at White Sands, nor even at the same relative levels; instead they were adjusted to cover the same range of SEL_A values.

RESPONSE TO WHITE SANDS BOOMS

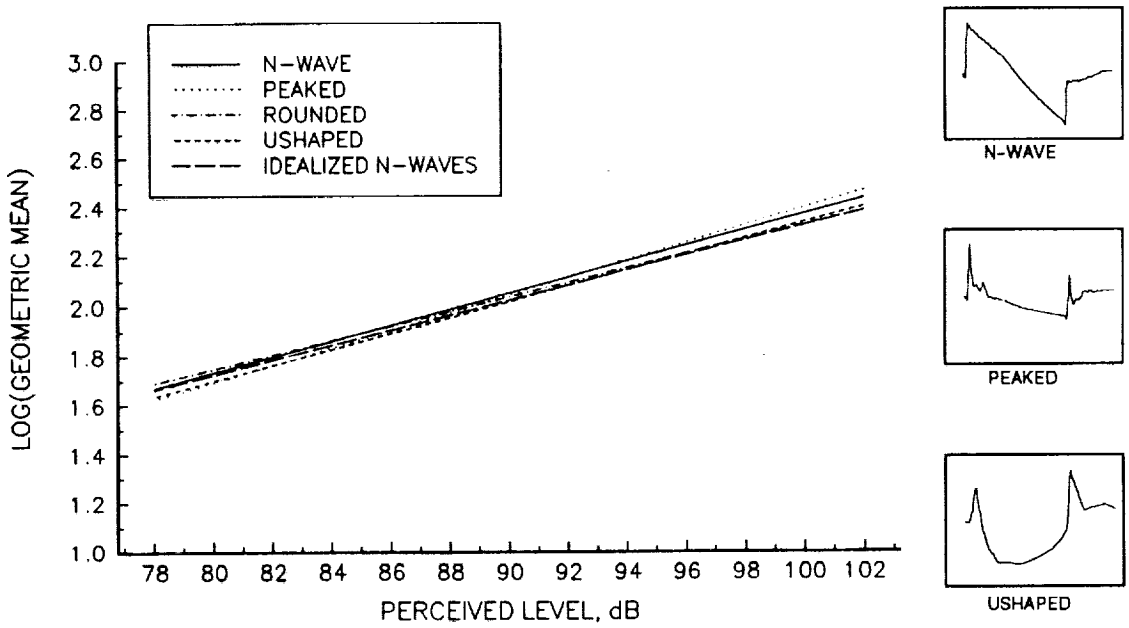

The only category of boom that stood out in this study were the "intermediate" booms. Time histories of these waveforms measured in the simulator are shown on the right of this chart. The plot displays the same judgement data as the previous chart, but the results for the two intermediate booms have been added separately. The intermediate boom results fall somewhat below those for the other boom categories, indicating that the subjects rated them as having lower loudness than the PL metric predicted. The slopes of the regression lines for the intermediate boom results differ from those for the other booms. Boom asymmetry is a possible contributing cause, though a previous study on asymmetry (reference 3) would predict little effect for Intermediate 1 and none at all for Intermediate 2. The multiple peaks may have some masking effect on each other. Further study is needed to understand these results, which were based on only two samples.

RESPONSE TO INTERMEDIATE BOOMS

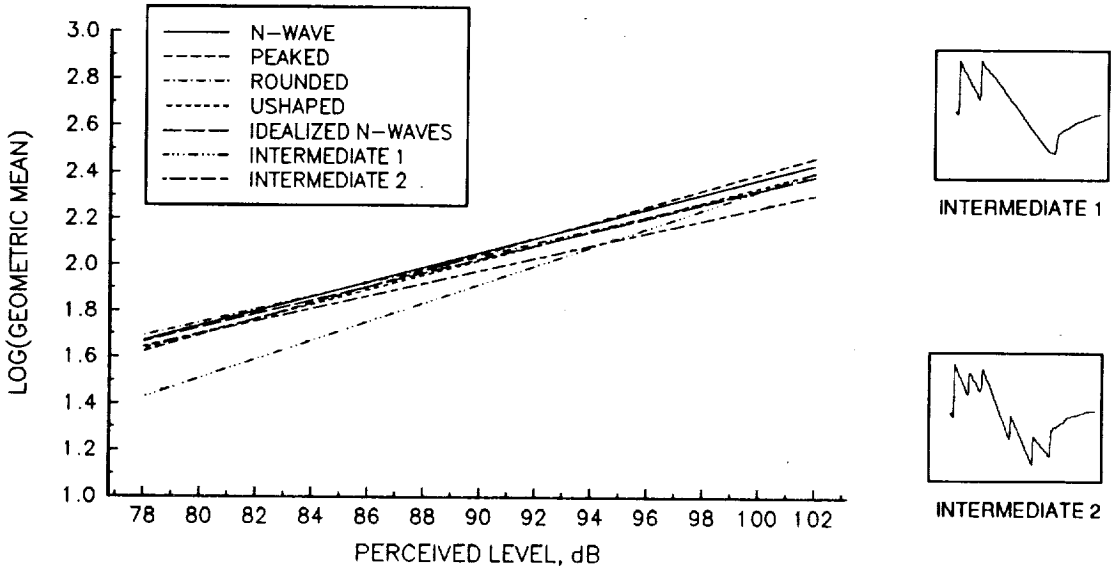

In summary the findings of the three studies showed that loudness and annoyance gave equivalent results for outdoor booms but differed for indoor booms. Annoyance is therefore recommended as the most appropriate criterion for indoor boom judgements. For booms containing a single reflection, the loudness ratings were higher when the delay between the direct and reflected booms was zero than when the delay was greater than zero . Hence loudness values calculated from flush-mounted microphone measurements will be conservative. Subjects did not judge recordings of real booms any differently from idealized booms. The PL metric was validated for annoyance ratings, for indoor and outdoor booms, for booms with reflections and for real booms compared with idealized simulations.

SUMMARY

- Loudness and annoyance are:
  - — equivalent for outdoor booms
  - — not equivalent for indoor booms
- Annoyance most appropriate criterion
- Booms with single reflections are
  - — less loud for nonzero delay times
  - — Hence measurements with flush-mounted microphones are conservative
- Real booms not judged differently from idealized booms
- PL metric validated

References

1. Leatherwood, Jack D.; Shepherd, Kevin P.; and Sullivan, Brenda M. : "A New Simulator for Assessing Subjective Effects of Sonic Booms" : NASA TM 104150, Sept. 1991.
2. Shepherd, Kevin P.; and Sullivan, Brenda M. : "A Loudness Calculation Procedure applied to Shaped Sonic Booms" : NASA TP-3134, Nov. 1991.
3. Leatherwood, Jack D.; and Sullivan, Brenda M. : "Effect of Sonic Boom Asymmetry on Subjective Loudness" : NASA TM 107708, Dec. 1992.
4. Leatherwood, Jack D.; and Sullivan, Brenda M. : "A Laboratory Study of the Effects of Sonic Boom Shaping on Subjective Loudness and Acceptability" : NASA TP-3269, Oct. 1992.
5. McDaniel, Scott; Leatherwood, Jack D.; and Sullivan, Brenda M. : "Application of Magnitude Estimation Scaling to the Assessment of Human Subjective Loudness Response of Simulated Sonic Booms" : NASA TM 107657, Sept. 1992.

Comparison of Methods of Predicting Community Response to Impulsive and Nonimpulsive Noise

Sanford Fidell and Karl S. Pearsons
BBN Systems and Technologies
A Division of Bolt Beranek and Newman Inc.
21120 Vanowen Street
Canoga Park, California 91303

Presentation at NASA HSR Sonic Boom Workshop
NASA Ames Research Center
May 12-14, 1993

Comparison of Methods of Predicting Community Response to Impulsive and Nonimpulsive Noise

Abstract

Several scientific, regulatory and policy-coordinating bodies have developed methods for predicting community response to sonic booms. The best known of these is the dosage-response relationship of Working Group 84 of the National Academy of Science's Committee on Hearing, Bioacoustics and Biomechanics (Galloway, 1981). This dosage-response relationship between C-weighted Day-Night Average Sound Level and the prevalence of annoyance with high energy impulsive sounds was derived from limited amounts of information about community response to regular, prolonged, and expected exposure to artillery and sonic booms.

U.S. Army Regulation 201 adapts this approach to predictions of the acceptability of impulsive noise exposure in communities. This regulation infers equivalent degrees of effect with respect to a well known dosage-response relationship for general (nonimpulsive) transportation noise. Differences in prevalence of annoyance predicted by various relationships lead to different predictions of the compatibility of land uses with sonic boom exposure. An examination of these differences makes apparent several unresolved issues in current practice for predicting and interpreting the prevalence of annoyance due to sonic boom exposure.

BACKGROUND

Any systematic approach to predicting and interpreting community response to noise exposure requires solutions to four fundamental problems:

1) Definition of community response;

2) Characterization of noise exposure;

3) Derivation of a predictive relationship between "community response" and noise exposure; and

4) Inference of regulatory policy from one or more predictive relationships

Finding practical answers to these questions requires detailed attention to issues such as the ease and cost of measuring selected quantities, the desired accuracy and precision of predictions, and relationships among alternate metrics of noise exposure, community response, and land use compatibility.

Most of the debate about compromises and assumptions needed to predict and interpret community response to transportation and other non-impulsive noise was conducted in the 1970s. To make a long story short, a collection of federal agencies (FICUN) adopted a common approach - based in large part on the work of Schultz (1978) - built on the following assumptions:

1) that "community response" can be usefully treated for most purposes (and in particular, for the airport neighborhood case) as the proportion of a residential community annoyed to a consequential degree by noise exposure[1];

2) that a cumulative measure of outdoor A-weighted sound levels in residential neighborhoods incorporating a so-called nighttime penalty (the Day-Night Average Sound Level, or DNL, as developed in the Environmental Protection Agency's 1974 "Levels Document"), suffices for characterizing noise exposure;

3) that a dosage-response relationship between the prevalence of annoyance and DNL, derived from a curve fitting exercise, is adequate for predictive purposes; and

4) that regulatory policy can be based on interpretations of land use compatibility made in acoustic terms alone.

The basic notion in any dosage-response relationship is that whatever quantity is plotted on the abscissa as the predictor variable is uniquely responsible for whatever quantity is plotted on the ordinate. In this case, the proportion of a community highly annoyed by noise is assumed to be determined not by individually notable noise events, but solely by some integration of outdoor neighborhood noise levels over a prolonged period of time.

"Land use compatibility guidelines" were subsequently developed by interpreting predictions about the prevalence of annoyance derived from the dosage-response curve. "Compatibility" was treated as an issue of noise exposure rather than one of noise effects, as though land use compatibility were somehow a property of noise exposure per se.[2]

The compromises and assumptions of the 1970s are not the only ones that could have been made, nor are they necessarily the most appropriate for all purposes. However, they provide the basis for the most widely understood and applied approach to assessing impacts of non-impulsive noise exposure on communities.

DERIVATION OF DOSAGE-RESPONSE RELATIONSHIPS

The data set on which Schultz based his original (1978) synthesis of the community noise literature contained 161 data points. One recent update of the so-called "Schultz Curve" (Fidell, Barber and Schultz, 1991) is based on more than 400 data points, while FICON (1992) has developed another dosage-response relationship based on a subset of these points. Each data point represents a field observation of a pairing of an exposure value and a percentage of social survey respondents describing themselves as highly annoyed. The percentage of social survey respondents is treated as an index of the stable, steady state prevalence of a consequential degree of long term annoyance in the community at large.

The utility of Schultz's approach to assessing community response to non-impulsive noise exposure quickly led to efforts to apply similar methods to the case of high energy impulsive noises[3]. Working Group 84 of the Committee on Hearing, Bioacoustics and Biomechanics (Galloway, 1981) of the National Research Council of the National Academy of Science made the initial (and still best known) effort to adapt the methods developed by Schultz (1978) to the case of impulsive noise.

CHABA Working Group 84 preserved Schultz's definition of community response; modified reliance on DNL as a noise metric only to the extent of substituting C-weighted for A-weighted sound levels[4]; and developed a dosage-response relationship from an eyeball fit to a small number of social survey observations about the annoyance of impulse noise.[5]

The resulting dosage-response relationship for impulsive noise (Galloway, 1981), illustrated in Figure 1, is as follows:

$$\% \text{ Highly Annoyed} = 100/(1 + \exp(11.17 - 0.153L_{Cdn})) \quad \text{Eq. 1}$$

where L_{Cdn} is the C-weighted Day-Night Average Sound Level created by sonic booms.

The form of this dosage-response relationship is a sigmoid given by a logistic fitting function. The sigmoidal shape is a reasonable one, given the need for asymptotes in the relationship in the vicinities of 0 and 100%. The prediction equation reflects a negotiated consensus of engineering judgments, and is intended as an approximate curve fit rather than the product of a formal statistical analysis.

INTERPRETATIONS OF DOSAGE-RESPONSE RELATIONSHIPS

The CHABA Working Group 84 relationship is derived from a considerably smaller data set than any of the relationships for non-impulsive noise. Of a total of fourteen data points, five represent observations of the annoyance associated with exposure to artillery fire, while the remaining nine are all derived from the only extensive study ever conducted of community response in an urban area subjected to sonic booms over a prolonged period.

For six months in 1964, residents of this city were exposed to a maximum of 8 booms a day at overpressures of 1 to 2 psf. Figures 2 and 3 are linear regressions between the prevalence of annoyance and A-weighted and C-weighted exposure values, respectively, for this data set, as described by Galloway (1981). The former (C-weighted) regression accounts for 94% of the variance in the annoyance data, while the latter (A-weighted) regression accounts of 87% of the variance.

The circumstances of impulsive noise exposure in the artillery and Oklahoma City studies which are summarized in the CHABA relationship are noteworthy: they were all familiar, expected, predictable and of long duration. In the case of artillery noise, respondents were residents of neighborhoods near fixed firing points. Daily artillery noise was a familiar part of the noise exposure environment in these respondents' neighborhoods. In the case of the sonic boom exposure in Oklahoma City, advance schedules for the numbers and times of occurrence of sonic booms were well advertised, and the aircraft producing the booms flew a single flight track for the entire half year study period.

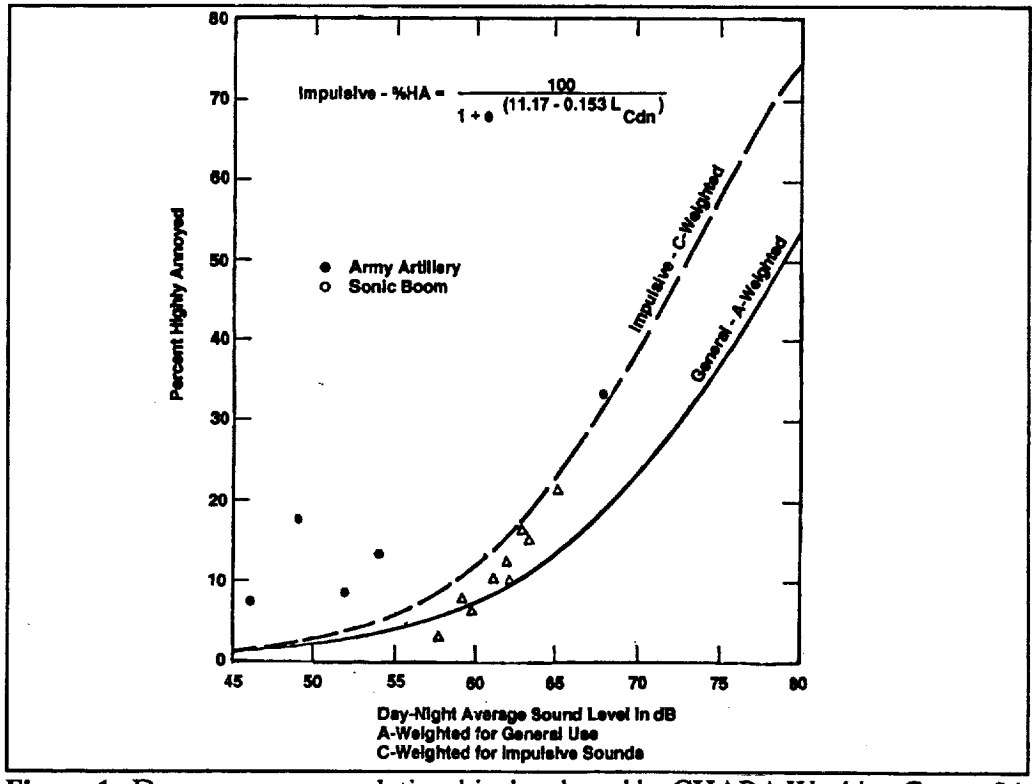

Figure 1: Dosage-response relationship developed by CHABA Working Group 84

The most common form of community exposure to sonic booms today is that produced in the vicinity of military supersonic operations areas. Caution is required in predicting community response and land use compatibility in such circumstances. Sonic booms are generally experienced at unpredictable and relatively infrequent times as short duration daytime noise intrusions of widely varying level. There is no agreement comparable to that for the case of urban noise about the most useful approach to predicting the annoyance of this type of noise exposure.

Use of DNL or CDNL to predict the prevalence of annoyance is based on the "equal energy hypothesis". The equal energy hypothesis expresses the notion that the number, level and duration of noise events are fully interchangeable determinants of annoyance as long as their product (energy summation) remains constant. In other words, quantification of noise exposure in DNL for purposes of predicting annoyance reflects a tacit theory: that people are indifferent between the annoyance of small numbers of very high level noise events of short duration and the annoyance of large numbers of compensatingly lower level noise and/or longer duration noise events.

This hypothesis is the underpinning of a convenient method for measuring noise exposure for purposes of predicting annoyance. When used as a predictor variable in a dosage-response relationship such as that synthesized by Schultz, DNL accounts for about half of the variance in a set of field observations about the annoyance of general transportation noise. This demonstrates that the equal

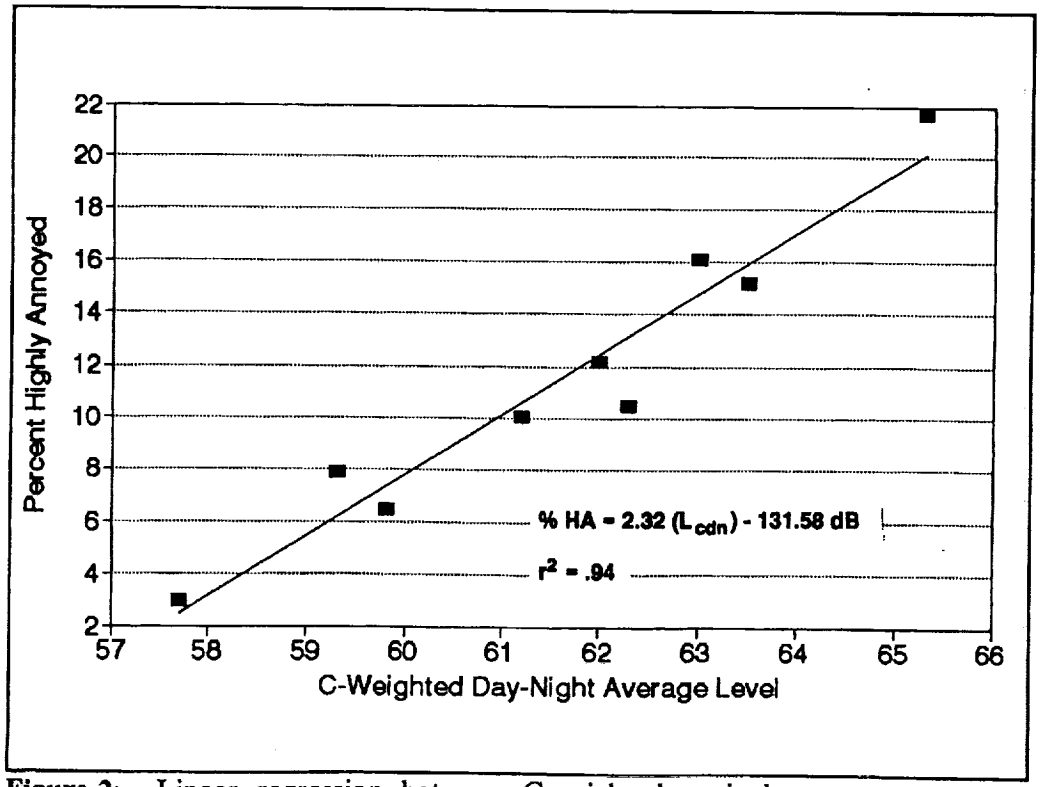

Figure 2: Linear regression between C-weighted sonic boom exposure and prevalence of annoyance in Oklahoma City (data from Galloway, 1981)

energy hypothesis can provide a useful account of the data over a range of at least 20 dB, from values of about 55 to 75 dB.

There is, however, little empirical evidence on which to base extrapolations of predictions of annoyance at the low values of CDNL associated with infrequent exposure to sonic booms. For example, all of the data summarized by Galloway (1981) at low values of CDNL represent reactions to artillery fire, not sonic booms.

ASSESSING LAND USE COMPATIBILITY WITH IMPULSIVE NOISE EXPOSURE

The notion that environmental noise impacts can be construed for global purposes in terms of land use compatibility may be traced through a chain of noise metrics and prediction methods four decades long to the pioneering work of Rosenblith and Stevens (1953). The latest embodiment of this approach may be found in the Appendix to ANSI Standard S12.40-1990.

The U.S. Army has adopted the clearest guidelines among federal agencies for land use compatibility with high energy impulsive noise exposure. Chapter 7 of U.S. Army Regulation 200-1, "Environmental Noise Abatement Program" (dated 23 April 1990) addresses land use compatibility issues with respect to impulse noise exposure. The recommendations in this regulation are based on an equivalence of

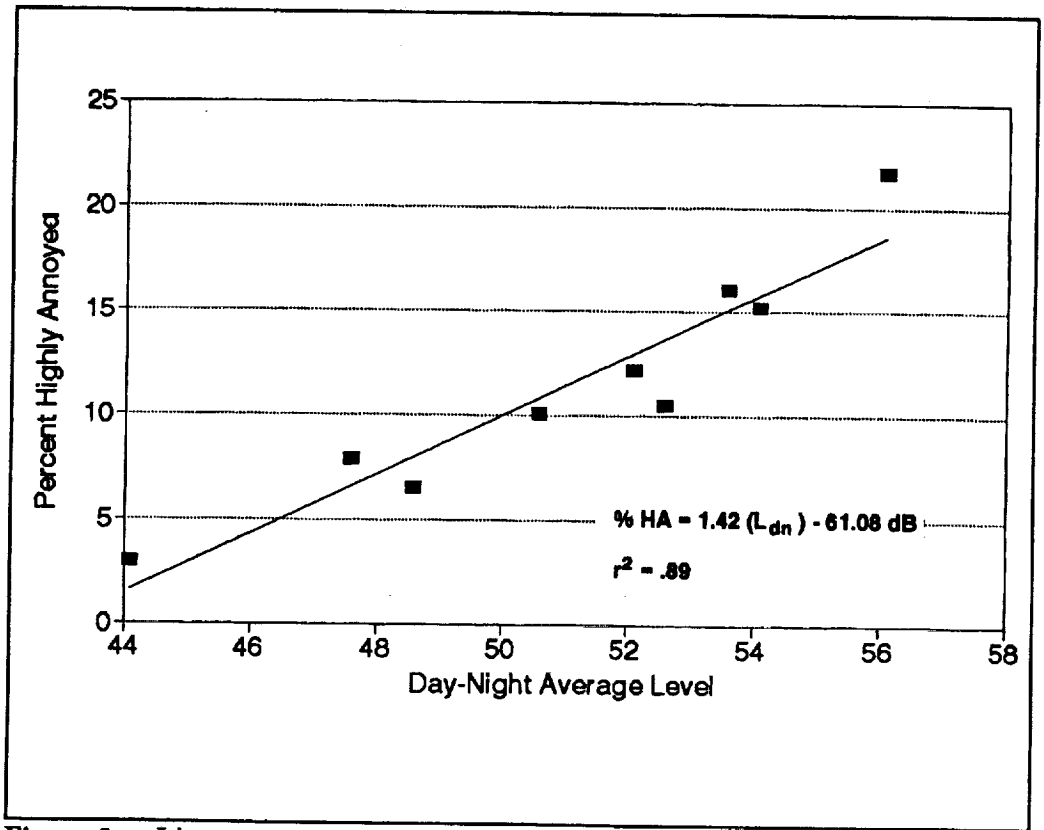

Figure 3: Linear regression between A-weighted sonic boom exposure and prevalence of annoyance in Oklahoma City (data from Galloway, 1981)

exposure of C-weighted to A-weighted cumulative exposure units. This equivalence is made not in terms of exposure levels, but rather in terms of the prevalence of annoyance implied by the FICUN (1980) and ANSI S12.40-1990 guidelines.

Equivalent exposure is inferred in the Army regulation through comparisons of annoyance predictions of Schultz's original (1978) dosage-response relationship for general transportation noise and CHABA's (Galloway, 1981) dosage-response relationship for high energy impulsive noise. Table 1 compares the prevalence of annoyance predicted by Schultz's and other relationships.

Table 2 examines the implications of drawing land use compatibility inferences on the basis of these equivalences. In the range of interest, differences in the slopes of the logistic fitting functions described by Galloway (1981) give rise to an approximate 5 dB difference in the criterion levels as expressed in A- and C-weighted cumulative exposure units. The net effect is to increase the difference between A- and C-weighted units associated with the same prevalence of annoyance. Thus, whereas Army Regulation 200-1 relies on the dosage-response relationship developed by Schultz (1978) to equate an A-weighted DNL of 65 dB with a C-weighted DNL of 62 dB, the equivalence developed from FICON's (1992) dosage-response relationship is to a C-weighted DNL of 60 dB. Even greater differences are apparent if the analysis is restricted to sonic boom data only.

Table I. Percentage of Community Highly Annoyed ("%HA") Predicted by Several Dosage-Response Relationships over a Range of DNL/CDNL Values.

FITTING FUNCTION	55 dB	60 dB	65 dB	70 dB	75 dB
$\%HA = 0.8553L_{dn} - 0.0401L_{dn}^2 + 0.00047L_{dn}^3$ [Schultz (1978)]	3.9%	8.5	15.3	24.6	36.9
$\% HA = 100/(1 + \exp(10.43 - .132L_{dn}))$ [USAF logistic fit to Schultz data]	4.0%	7.5	13.6	23.3	37.0
$\% HA = 0.0360L_{dn}^2 - 3.2645L_{dn} + 78.92$ [Fidell, Schultz, and Barber (1991)]	8.3%	12.7	18.8	26.8	36.6
$\% HA = 100/(1 + \exp(11.13 - .141L_{dn}))$ [USAF logistic fit to subset of Fidell, Schultz and Barber (1991)]	3.3%	6.5	12.3	22.1	36.5
$\%HA = 100/(1 + \exp(11.17 - .153L_{Cdn}))$ (CHABA WG 84 [Galloway, 1981])	2.9%	6.0	22.7	38.7	57.6
$\% HA = 2.324\ L_{Cdn} - 131.6$ (Linear regression through Oklahoma City data)	n/a	7.8	19.4	31.1	42.7

Table 3 shows some examples of predicted consequences of several sorts of sonic boom exposures. Note that even small numbers of relatively modest booms (for example, four booms at 1 psf per day) can lead to a prediction of noise exposure inconsistent with single family residential use.

Although there is little alternative to relying on such predictions on an interim basis, a larger body of direct evidence about the annoyance of sonic boom exposure is clearly needed. It is possible, for example, that the time constants of arousal and decay of annoyance with impulsive noise exposure may differ from those for non-impulsive noise. People living near future overland supersonic flight corridors might react more quickly or more vigorously to the novel experience of sonic boom exposure than to more familiar forms of noise exposure.

CONCLUSIONS

Confidence in predictions and interpretations of the effects on communities of high energy impulses in general and sonic booms in particular is not as great as for the case of general transportation noise. Small differences in assumptions and procedures may lead to large differences in assessments of the effects of impulsive noises on exposed populations. Some of these assumptions and procedures that have not been revisited for a decade could benefit from further scrutiny.

The circumstances of noise exposure produced by sonic booms of en route aircraft

Table II. Land use compatibility guidance inferred from equivalent prevalence of annoyance for A-weighted and C-weighted Day-Night Sound Levels for alternate impulsive dosage-response relationships.

Compatibility with Single and Multiple Family Residential Land Uses (per ANSI S12.40-1990)	Percent Highly Annoyed	(A-Weighted) Day-Night Average Sound Level*	C-weighted Day-Night Average Sound Level**	C-weighted Day-Night Average Sound Level***
Normally compatible	1.7 %	50 dB	46 dB	57.4
Marginally compatible with single family, extensive outdoor use	3.3	55	51	58
Marginally compatible with multiple family, moderate outdoor use and with multi-story, limited outdoor use	6.5	60	55.6	59.4
Compatible with insulated multi-story use; incompatible with single and multiple family use	12.3	65	60.2	61.9
Incompatible with any residential land use	36.5	75	69.4	72.3

* % Highly Annoyed = $100 / [1 + \exp(11.13 - 0.141L_{dn})]$ (FICON, 1992)

** % Highly Annoyed = $100 / [1 + \exp(11.17 - 0.153L_{Cdn})]$ (Galloway, 1981)

*** % Highly Annoyed = 2.324 LCdn - 131.6 (Oklahoma City data)

are inherently more difficult to treat than those of airport neighborhoods. Sonic boom exposure produced by military operations is generally sporadic rather than regular, highly variable and difficult to predict accurately (due to the vagaries of long range acoustic propagation and uncertain flight tracks), and likely to be associated with nonlinear physical effects. Regular exposure to sonic booms near future overland flight corridors may be somewhat easier to predict.

Not only are there more complications and loose ends in dealing with impulsive exposure than with general transportation noise, but there are far fewer data about exposure effects. Although several DoD and NASA-sponsored laboratory and field studies on the annoyance of sonic booms have begun to contribute new information, the body of information available for analysis is still considerably smaller than for the case of general transportation noise.

Laboratory work, although useful for understanding how individuals' immediate annoyance is affected by various aspects of impulsive signals, does not directly produce the sorts of information needed to generate and interpret impacts at the community level. Controlled field studies of longer term individual reactions can serve as a bridge between laboratory and community studies, but are difficult to design and conduct in ways that can test basic assumptions about the applicability of the equal energy hypothesis to relatively infrequent sonic booms.

New technology, new assumptions, and new analyses are needed to identify and test improved means of predicting the effects of sonic booms on exposed individuals and communities.

Table III. Relationship between numbers of sonic booms and land use compatibility. (Calculations performed for N-waves with 0.5 ms rise time and a duration of 350 ms, as described by Shepherd and Sullivan, 1991.)

No. of 0.5 psf daytime booms/day	No. of 1 psf daytime booms/day	CDNL*	% HA (Galloway, 1981)	% HA (Oklahoma City)
1		48 dB	2.1%	n/a
2		51	3.3	n/a
4		54	5.2	n/a
8		57	8.0	0.9
	1	54	5.2	n/a
	2	57	8.0	0.9
	4	60	12.0	7.8
	8	63	17.8	14.8
1	1	55	6.0	n/a
2	2	58	9.1	3.2
4	4	61	13.7	10.2
8	8	64	20.1	17.1

*Constructed from computed CSEL values

C-3.

REFERENCES

American National Standards Institute, "Sound Level Descriptors for Determination of Compatible Land Use", ANSI S12.40-1990 (ASA 88-1990, Revision of ANSI S3.23-1980), 2 August 1990.

Environmental Protection Agency, "Public Health and Welfare Criteria for Noise", NCD73.1, July 27, 1973, pp. 3-4, Washington, D.C.

Federal Interagency Committee on Noise Final Report, Airport Noise Assessment Methodologies and Metrics, August, 1992.: FICON

Federal Interagency Committee on Urban Noise (1980). Guidelines for Considering Noise in Land Use Planning and Control. Washington, D.C.: FICUN

Fidell, S., "Interpreting Findings About Community Response to Environmental Noise Exposure: What Do the Data Say?", Euronoise '92, London, September 1992.

Fidell, S., Barber, D., and Schultz, T. J., "Updating a Dosage-Effect Relationship for the Prevalence of Noise-Related Annoyance", Journal of the Acoustical Society of America, January 1991.

Galloway, W.J. (1981). "Assessment of Community Response to High Energy Impulsive Sounds." Report of Working Group 84, Committee on Hearing, Bioacoustics and Biomechanics: The National Research Council. Washington, D.C.: National Academy Press. (CHABA).

Pearsons, K., Tabachnick, B., Howe, R., Ahuja, K. and Stevens, J., "A Study of the Effects of Sonic Boom Waveform Modification on Annoyance", BBN Report 7770, March, 1993.

Rosenblith, W.A., K.N. Stevens and the Staff of Bolt Beranek and Newman Inc., *Handbook of Acoustic Noise Control, Vol. 2: Noise and Man*, WADC TR-52-204, Wright Air Development Center, Wright-Patterson Air Force Base, Ohio, 1953, pp. 181-200.

Schultz, T.J., "Synthesis of social surveys on noise annoyance", J. Acoust. Soc. Am., Vol. 64, No. 2, August, 1978.

Shepherd, K., and Sullivan, B., "A Loudness Calculation Procedure Applied to Shaped Sonic Booms", NASA Technical Paper 3134, November, 1991.

ENDNOTES

1. The term "exposure" is commonly used in two ways. One use of the term implies the time integral of intensity, while the other use implies the average sound intensity over a specific time period. Intensity is the rate of flow of sound energy per unit area per second. At distances from sound sources that are of interest in environmental analyses, sound intensity is directly proportional to the square of sound pressure. Thus, sound exposure is usually represented as the time integral of squared sound pressure. This process is often referred to informally as "energy summation". Magnitudes are reported in logarithmic terms. For example, sound exposure level is 10 times the logarithm to the base 10 of the ratio of sound exposure to a reference exposure of 400 μPa^2-seconds. In this logarithmic form, squared sound pressure is called sound level and expressed in units of decibels. Sound level in decibel notation is often expressed as an average (equivalent) sound level over a specified time interval (usually 1 hour or 24 hours). Single events are often described by their sound exposure level (SEL) with a reference time interval of one second.

2. This definition of "land use compatibility" does not deal directly with effects of noise exposure on people. Furthermore, certain of the remedies commonly used in airport neighborhoods to treat incompatible land uses (e.g., re-zoning land, insulating residences, purchasing avigation easements) are inappropriate in the case of en route exposure to sonic booms. Fidell (1992) contains additional discussion of the standard approach to dealing with the compatibility of aircraft noise and land use.

3. According to Galloway (1981), "High-energy impulsive sounds of concern for community response are ... those for which the C-weighted sound exposure level... in any 2-second period is greater than 85 decibels (or greater than 75 decibels at night) and is 10 decibels greater than the C-weighted sound exposure level due to other sources in any contiguous 2-second period. These levels correspond to peak overpressures greater than approximately 105 decibels (95 decibels at night), that is, greater than approximately 0.1 pounds per square foot.

4. The C-weighting network was selected in lieu of the A-weighting network in a noise metric intended to characterize high energy impulsive noise because two impulsive sounds with very different low frequency energy content may have the same A-weighted sound pressure level. This follows equally from the insensitivity of the A-weighting network to energy at frequencies below about 50 Hz, and from the fact that the spectral peaks of common impulsive noises are often two octaves yet lower in frequency.

Approximate equivalences between C-weighted measurements and A-weighted measurements of a class of sounds (such as sonic booms) may nonetheless be established in several ways. One such equivalence (between A-weighted and C-weighted SEL values for sonic booms) is as follows:

$$CSEL = 0.68(SEL) + 40.5 \text{ dB}$$

This relationship is derived from A- and C-weighted measurements of actual sonic

booms made outdoors (Galloway, 1981) and of recordings of simulated sonic booms made indoors (Pearsons, Tabachnick, Howe, Ahuja, and Stevens, 1993). It is appropriate primarily for estimating A-weighted levels for characteristic sonic booms with well-formed N shapes, but may also work reasonably well for sonic booms which have propagated long distances through the atmosphere, or for sonic booms occurring near the lateral cutoff distance.

5. It was tacitly accepted in preserving Schultz's assumptions that for purposes of predicting community response due to impulsive noise exposure, startle was fully accounted for by annoyance. It was likewise tacitly assumed that annoyance associated with secondary emissions was fully accounted for by substitution of the C-weighting network for the A-weighting network. ("Secondary emissions" are indoor rattling sounds produced by nonlinear re-radiation of low frequency impulsive energy from household contents.)

VARIABILITY OF MEASURED SONIC BOOM SIGNATURES

Study Performed Under NASA Langley Research Center
Contract NAS1 - 19060 ; Dr. K. Shepherd Technical Monitor

by

K.R. Elmer and M.C. Joshi

McDonnell Douglas Aerospace - Transport Aircraft Long Beach, CA

Presentation at NASA HSR Sonic Boom Workshop

NASA Ames Research Center

May 12-14, 1993

Atmospheric Turbulence

The propagation of sonic booms through the real atmosphere can have a pronounce effect on the signature received on the ground. It has been well established that turbulence in the lower part of the planetary boundary layer known as the mixing layer is a significant contributor to the distortion of sonic booms, as illustrated in this figure. The changes in the atmospheric conditions during a day and from day to day results in a large variation in the sonic boom signature measured on the ground for an aircraft flying at a nominal operating condition at different times of the day. The objective of this study is to evaluate the variability in the loudness of the booms due to these propagation effects.

ATMOSPHERIC TURBULENCE EFFECT

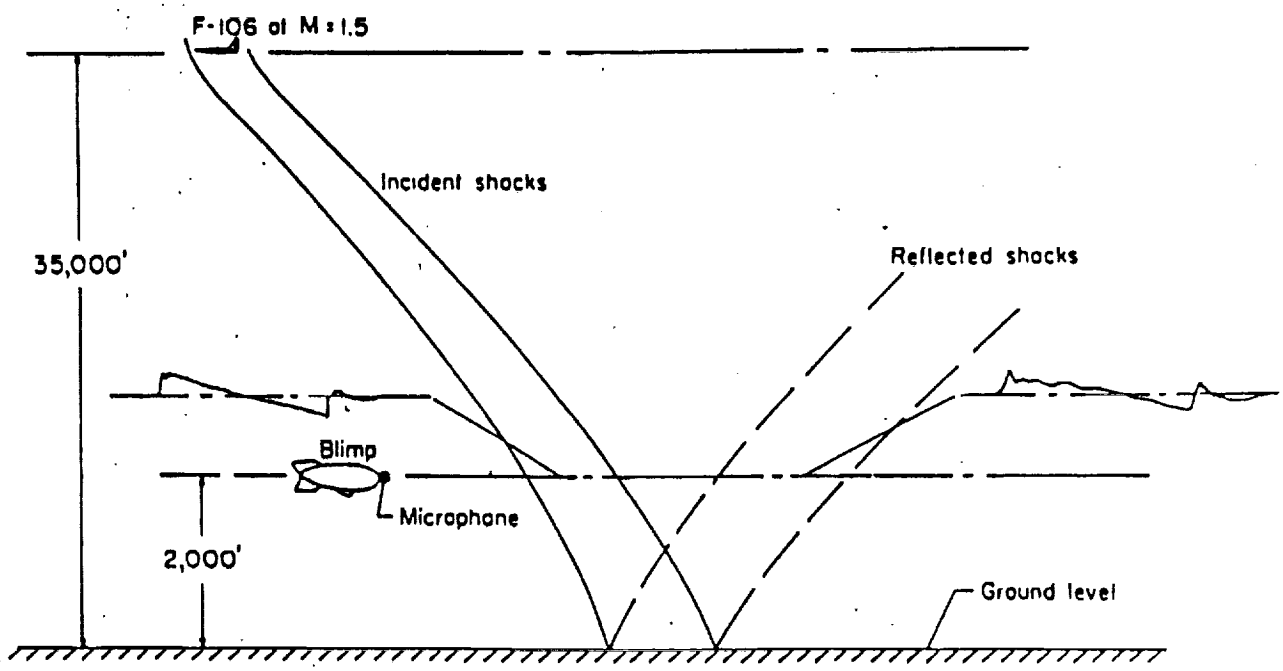

BOOMFILE Database Descriptions

The BOOMFILE database contains overpressure distributions for 43 passes of the several types of aircraft previously mentioned. This data was collected using Boom Event Analyzer Recorders (BEAR) and modified Larson Davis LD700 Personal Dosimeters. These devices were arranged in a linear array of 13 microphones located perpendicular to the flight path at sideline distances ranging from 0 miles (i.e., directly under the flight path) to roughly 20 miles as shown in the figure. The aircraft flew across the microphone array with steady flight conditions which were achieved several miles prior to reaching the microphones. BOOMFILE also contains aircraft tracking data which consists of altitude, Mach number, climb angle, acceleration, heading, and lateral and longitudinal position with respect to a reference microphone. This data is provided at one second intervals for most of the aircraft overflights. Limited atmospheric data was also collected during the BOOMFILE tests. This data consisted of ground station wind speed and direction, air pressure, and air temperature measured just prior to each set of flyovers. Upper atmosphere rawinsonde data recorded at nearby weather stations on the test days are also provided. This consists of wind speed and direction, sound speed, relative humidity, dew point, temperature and pressure at 1,000 foot altitude intervals ranging from roughly 2,500 to 100,000 feet above mean sea level (Reference 1).

BOOMFILE MICROPHONE ARRAY

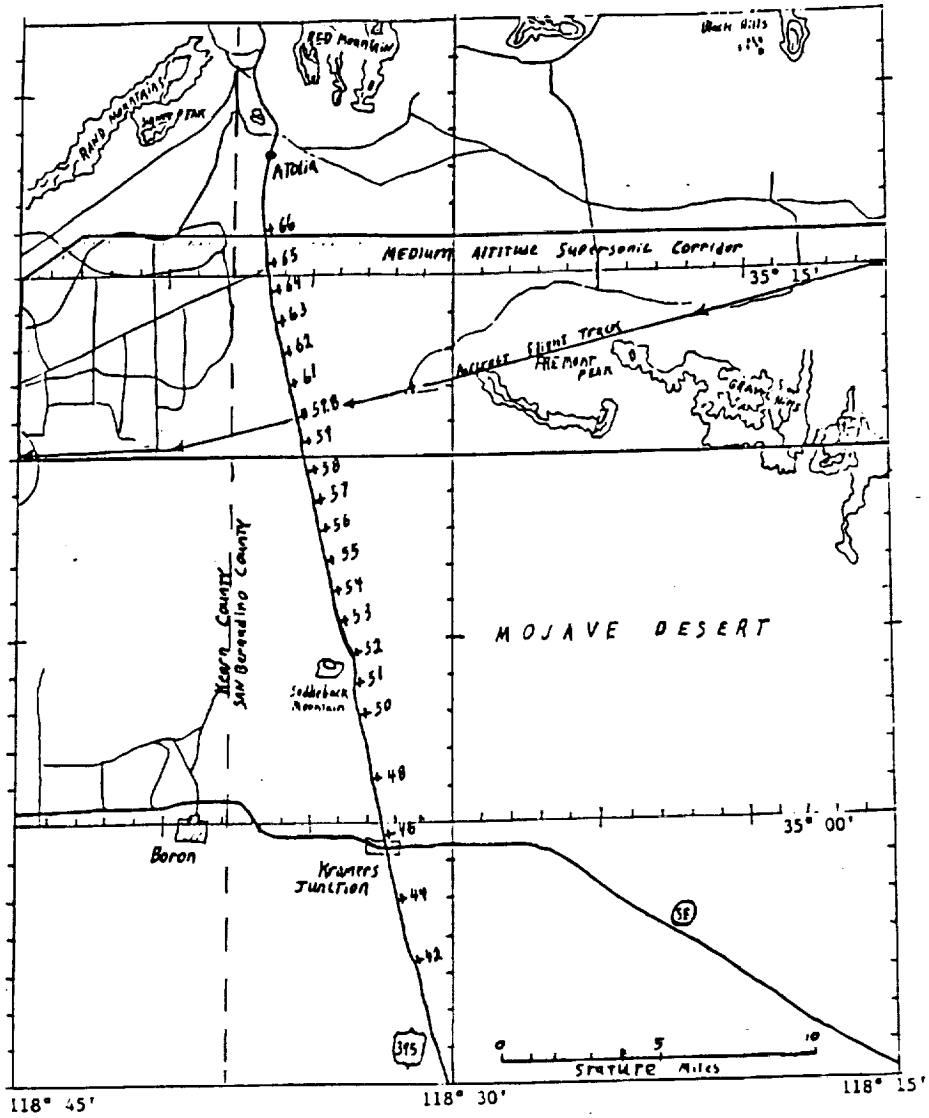

BOOMFILE Flight Conditions

The BOOMFILE flight conditions are listed in this table. The range of conditions is large from Mach 1.0 to 3.0 and altitude 13,000 ft to 70,000 ft with 9 different aircraft. However, repeat runs of the same aircraft at similar flight conditions are limited.

BOOMFILE Flight Conditions Summary

DATE	AIRCRAFT	FLIGHT TRACK INTERSECTION	MACH NUMBER	ALTITUDE (Ft MSL)	BOOM AT SITE 00 (Local Time)
31 JUL 87	F-4 *	57.8	1.20	16000	08:41:20
03 AUG 87	F-4	60.1	1.24	29200	07:48:33
	F-4	60.6	1.29	29300	07:58:33
	F-4	53.6	1.10	13000	08:08:04
	F-4	59.2	1.10	14400	10:29:59
	F-4	61.3	1.37	44400	10:43:22
	T-38	58.6	1.00	13600	10:05:35
	T-38	56.0	1.10	13000	10:12:15
	T-38	59.5	1.11	29600	12:28:18
	T-38	60.5	1.05	21200	12:38:17
04 AUG 87	AT-38	60.0	1.17	41400	07:19:41
	AT-38	60.0	1.12	32300	07:30:09
	AT-38	63.0	1.15	16700	07:36:46
	AT-38	59.6	1.20	30300	09:14:06
	AT-38	59.0	1.10	14000	09:23:15
	F-15	61.5	1.38	41400	07:56:42
	F-15	60.3	1.20	29700	08:04:06
	F-15	60.6	1.10	12500	08:10:13
	F-15	60.0	1.13	15200	10:46:15
	F-15	59.0	1.28	31000	11:02:18
	F-15	64.0	1.42	45000	11:11:28
	F-15	60.0	1.40	45500	11:34:21
05 AUG 87	F-16	57.0	1.25	29500	09:06:05
	F-16	60.0	1.43	46700	09:33:54
	F-16	58.8	1.17	19300	09:44:51
	F-16	59.5	1.13	14400	11:44:24
	F-16	60.6	1.12	13800	11:54:39
	F-16	60.5	1.25	30000	12:04:46
	SR-71	60.8	2.50	64800	09:26:12
	SR-71 *	59.8	3.00	73000	10:55:12
	SR-71	59.4	1.23	32400	11:08:38
	SR-71	62.0	1.70	52000	12:35:51
06 AUG 87	F-18	60.0	1.30	30000	07:44:12
	F-18	59.6	1.40	44700	07:57:05
	F-18	58.0	1.10	14200	08:10:36
	F-18	59.8	1.30	30000	10:22:47
	F-18	59.8	1.43	45000	10:34:14
	F-18 *	59.8	1.10	13000	10:48:38
	F-14	56.2	1.20	31500	08:28:45
	F-14	62.0	1.27	16500	10:43:43
	F-111D	59.8	1.20	14000	11:48:18
	F-111D	59.8	1.40	45000	12:04:44
07 AUG 87	F-111D	58.3	1.25	29900	10:50:26

For each of these flights, except where noted by an asterisk, tracking data are provided

XB-70 Database Descriptions

The XB-70 database (Reference 2) consists of frequency spectra and overpressure time histories for 39 flights (51 runs) of the XB-70 aircraft. The data was collected at several ground stations using a microphone, tuning unit, d.c. amplifier, and FM tape recorder setup played back into a recording oscillograph. The oscillograph plots were then digitized using an optical scanning system. In this test program the microphones were arranged in one of two configurations, either three ground and one pole or six ground and two pole microphones all located within a 200 foot by 200 foot grid pattern shown in the figure. The location of the measurement site with respect to the aircraft flight path for different runs ranged from directly overhead to a sideline distance of over 15 miles. Each run is considered as one flight over one cluster of 4 or 8 microphones. Atmospheric data for the XB-70 database consists of digitized trace plots for temperature and wind speed parallel and perpendicular to the flight path for all runs. The National Oceanic and Atmospheric Association provided pressure, temperature, wind, and relative humidity vs altitude profile rawinsonde data at 12:00 and 24:00 hours. They also provided limited test site climatological data consisting of temperature, wind speed and direction, cloud cover description, and dew point within an hour of each run. This database has more repeat runs than BOOMFILE, however, the sideline distance to the microphone cluster varied significantly from run to run (Reference 2).

XB-70 MICROPHONE CLUSTER ARRANGEMENTS

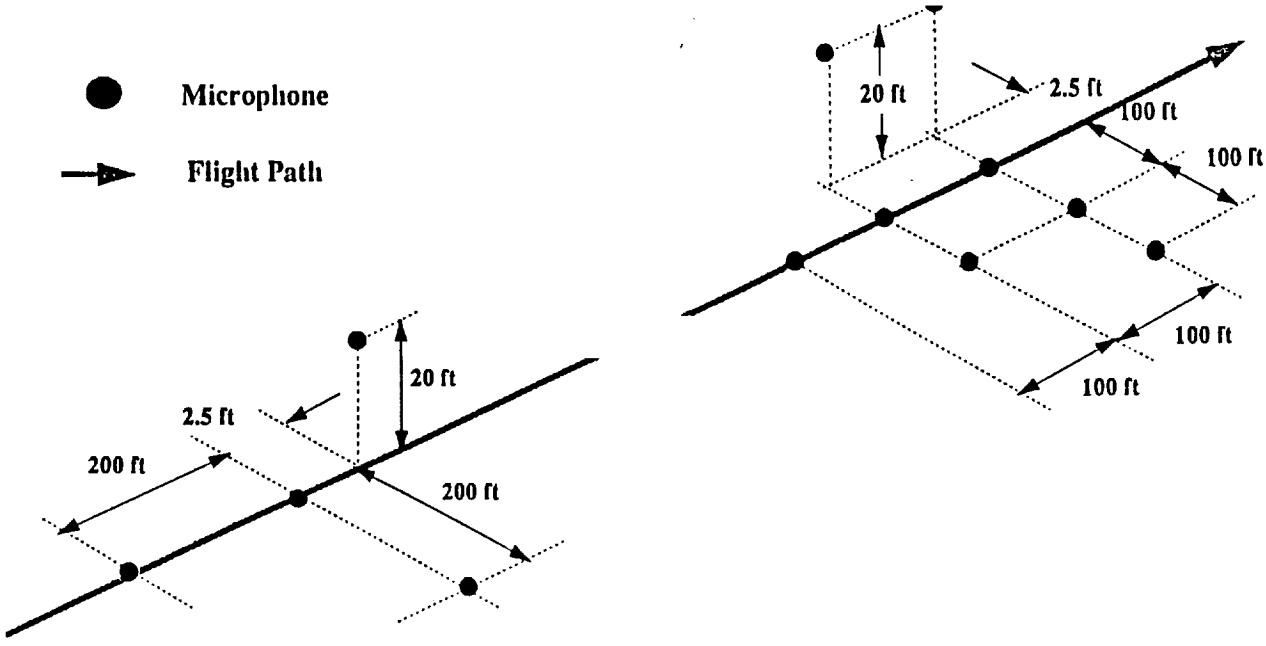

The flight conditions of the XB-70 database are listed in this table.

XB-70 SONIC BOOM LOG

(for flights of March 4, 1965 through May 27, 1966)

DJM File#	Date	A/C#-Flt #	T/O Time	T/O Gr.Wt.	Flt. Time	Boom Time	Boom Mach	Boom Alt	Boom Gr.Wt.	Land Gr.Wt.
1	3-4-65	1-7	1018	480K	1:37	1114	1.83	50500	337K	297K
2	4-20-65	1-10	1113	510K	1:42	1213	1.80	48000	350K	300K
3	7-1-65	1-14	0650	510K	1:44	0800	2.60	66000	310K	285K
4	7-27-65	1-15	0707	510K	1:43	0732	1.23	32000	423K	300K
5	8-10-65	2-2	0700	470K	1:27	0740	1.38	42300	357K	310K
6	8-18-65	2-3	1220	490K	1:58	1330	1.40	46000	381K	305K
7	8-20-65	2-4	1115	493K	2:04	1159	1.42	42500	387K	295K
8	9-22-65	1-16	1200	510K	1:57	1225	1.50	33800	456K	300K
9	9-29-65	2-6	1147	495K	2:04	1220	1.35	33000	440K	295K
10	10-5-65	2-7	1213	495K	1:40	1243	1.42	31000	438K	295K
11	10-11-65	2-8	1310	515K	1:55	1332	1.51	34000	423K	298K
12	10-14-65	1-17	0906	510K	1:47	0936	1.76	41000	433K	300K
13	10-16-65	2-9	0912	520K	1:43	1027	1.40	50000	313K	295K
14	11-2-65	2-11	1126	520K	1:54	1255	1.80	50500	317K	295K
15	11-4-65	1-18	1019	515K	2:04	1105	1.87	41500	357K	300K
16	11-18-65	1-21	1233	515K	2:02	1336	1.61	41500	348K	300K
17	11-30-65	1-22	0900	515K	1:59	1010	1.82	53000	325K	295K
18	12-1-65	2=13	0902	525K	2:02	1030	2.31	60000	328K	297K
19	12-2-65	1-23	0915	515K	1:59	1040	1.79	54000	317K	300K
20	12-3-65	2-14	0906	520K	1:55	1030	2.48	65500	329K	300K
21	12-10-65	1-25	1230	515K	2:18	1315	1.55	30500	436K	--
			(2nd run)		----	1400	1.25	38000	371K	295K
22	12-11-65	2-15	0858	520K	2:03	0918	1.50	37000	454K	--
			(2nd run)		----	1020	2.90	70000	321K	300K
23	12-21-65	2-16	1307	510K	1:49	1427	2.92	70000	321K	300K
24	1-3-66	2-17	0901	520K	1:52	1020	2.91	69800	317K	295K
25	1-11-66	1-31	0702	447K	1:35	0750	1.80	44900	369K	295K
26	1-12-66	2-18	0855	525K	1:48	1018	2.05	66000	297K	290K
27	1-15-66	1-33	1108	450K	1:27	1153	1.78	45100	373K	290K
28	3-4-66	1-36	1055	523K	2:27	1140	1.75	41000	446K	--
	(2nd station-same run)				----	1140	1.82	42000	445K	293K
29	3-7-66	1-37	1402	520K	2:19	1532	1.17	41000	344K	--
	(2nd station-same run)				----	1532	1.17	40000	343K	295K
30	3-15-66	2-24	0909	535K	1:59	1030	2.66	68500	310K	--
	(2nd station-same run)				----	1030	2.66	69300	310K	293K
31	3-17-66	2-25	0847	535K	1:52	1015	2.74	66000	308K	--
	(2nd station-same run)				----	1015	2.74	66000	308K	297K
32	3-19-66	2-26	1040	530K	1:57	1210	2.84	70300	305K	--
	(2nd station-same run)				----	1210	2.84	70300	304K	291K
33	3-28-66	1-40	0950	520K	1:41	1053	1.80	51000	319K	--
	(2nd station-same run)				----	1053	1.80	51000	319K	300K
34	3-29-66	2-29	1027	530K	1:51	1137	1.56	44000	314K	--
	(2nd station-same run)				----	1137	1.56	44000	314K	--
	----------(2nd run)				----	1152	1.36	36400	304K	--
	(2nd station-2nd run)				----	1152	1.36	36400	304K	300K
35	4-6-66	1-42	1026	520K	2:01	1138	1.55	52000	334K	295K
36	4-21-66	1-45	1539	524K	2:02	1646	2.26	53000	338K	290K
37	4-23-66	2-35	1120	525K	2:01	1140	1.11	32000	468K	--
	(2nd station-same run)				----	1140	1.18	32000	467K	--
	----------(2nd run)				----	1255	2.20	64000	362K	--
	(2nd station-2nd run)				----	1255	2.20	64000	362K	310K
38	5-16-66	2-38	0900	520K	2:09	1040	1.30	44300	321K	300K
39	5-27-66	2-42	1100	520K	2:08	1240	1.24	39800	310K	300K

Total number of sonic boom flights = 39

Total number of sonic boom runs = 51

Analysis Progression

This figure shows the organization for the remainder of the presentation, beginning with a description of the variables calculated in what will be referred to as the extended database. The analysis of these calculated parameters with respect to the aircraft flight conditions and flight times is reviewed. The analysis then is focused on time of day variations. This is followed by further analysis in terms of lateral cutoff and morning vs afternoon comparisons.

OUTLINE

- EXTENDED DATABASE
- VARIABILITY IN OVERPRESSURE, RISE TIME, AND LOUDNESS WITH FLIGHT CONDITIONS
- SONIC BOOM VARIABILITY IN REPEAT FLIGHTS
- VARIABILITY WITH TIME OF DAY
- VARIABILITY IN BOOM SYMMETRY
- STATISTICAL DISTRIBUTION BY LATERAL DISTANCE
- STATISTICAL DISTRIBUTION BY TIME OF DAY

Extended Database

Several noise metrics and various categories of rise time were determined for each point in the BOOMFILE and XB-70 databases. These quantities, listed in the figure, are available in tabular and digital format. An example of this extended database is shown.

ANALYSIS PARAMETERS

- MAXIMUM OVERPRESSURE, P_{max}
- STEVENS MARK VII PERCEIVED NOISE LEVEL, PLdB
- A-WEIGHTED SOUND EXPOSURE LEVEL, ASEL
- C-WEIGHTED SOUND EXPOSURE LEVEL, CSEL
- RISE TIME FROM 10% TO 90% P_{max}
- RISE TIME TO 50% P_{max}
- RISE TIME TO 75% P_{max}
- RISE TIME TO 100% P_{max}

Prediction Method

The noise metrics for the measured boom signatures were compared to metrics for signatures predicted using Carlson's simplified method (Reference 3) option of the sonic boom analysis program MDBOOM (Reference 4). In this technique, a simple F-function input is scaled to the local conditions. The scaling factors used are the lift parameter, K_L determined from the aircraft Mach number, weight, length, and local pressure, and the shape parameter, K_S determined from the aircraft type and K_L as shown in the figure. K_S is then used to scale the simple F-function of the figure by the factor shown. The signature is then evolved to the microphone (far field), resulting in a change of amplitude. An aging or steepening calculation is then performed to arrive at the signature propagated through a non-turbulent atmosphere (ideal N-wave).

SIMPLIFIED SONIC BOOM PREDICTION PROCEDURE

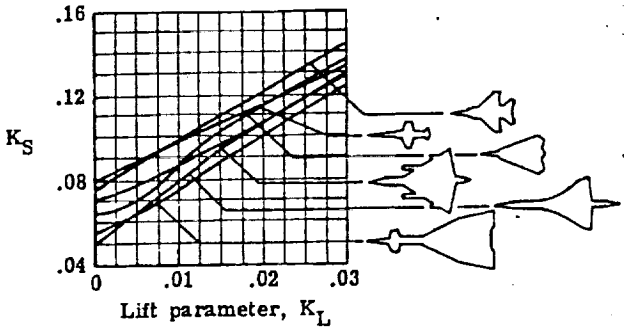

Enter lift parameter K_L

$$K_L = \frac{\sqrt{M^2 - 1}\ W}{1.4 p_v M^2 \ell^2}$$

Select shape factor K_S

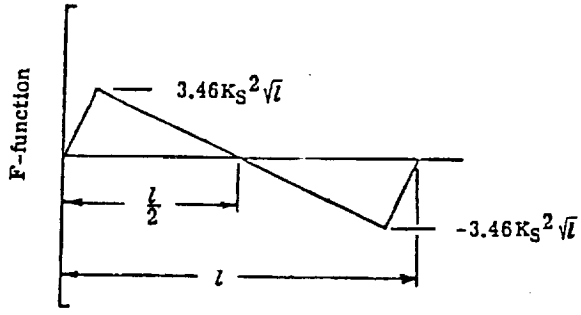

Flight Condition Groups

For sonic boom variability analysis the BOOMFILE and XB70 data were each divided into four groups based on aircraft altitude and Mach number values. The range of flight conditions for these groups are shown in the figure.

FLIGHT CONDITIONS
BOOMFILE DATABASE

RANGE	GROUP 1	GROUP 2	GROUP 3	GROUP 4
Altitude (feet)	10,000 - 20,000	25,000 - 35,000	40,000 - 50,000	50,100 - 80,000
Mach number	1.05 - 1.30	1.10 - 1.40	1.10 - 1.50	1.50 - 3.50
Sideline Distance (feet)	0 - 45,000	0 - 55,000	0 - 80,000	0 - 60,000

XB70 DATABASE

RANGE	GROUP 1	GROUP 2	GROUP 3	GROUP 4
Altitude (feet)	30,000 - 40,000	40,100 - 50,000	50,100 - 60,000	60,100 - 72,000
Mach number	1.17 - 1.55	1.17 - 1.87	1.55 - 2.31	2.05 - 2.92
Sideline Distance (feet)	0 - 50,000	0 - 80,000	0 - 70,000	0 - 80,000

Overpressure Variability Dependence on Flight Conditions

Comparisons between measured and calculated data were made for the various metrics and rise times as they varied with sideline distance. The high altitude / high Mach number group, bottom figure, shows very good agreement between measured maximum overpressures and predicted maximum overpressures (assuming uniform non-turbulent atmosphere). For the low altitude / Mach number group, upper figure, the comparison is relatively poor. While the measurements in both groups include the effects of propagation through the lower layer of turbulent atmosphere, the high altitude / high Mach number group represents flights where measurements are well within the lateral cutoff, where the boom has already propagated an adequate distance so that the shock is in an equilibrium state prior to entering the lowest 5,000 feet of the atmosphere, and where the propagation through the atmosphere is more vertical than the low altitude / low Mach number flights. These can be expected to reduce variability in measurements and improve theory - data agreement. These plots include morning as well as afternoon flights.

OVERPRESSURE VARIABILITY

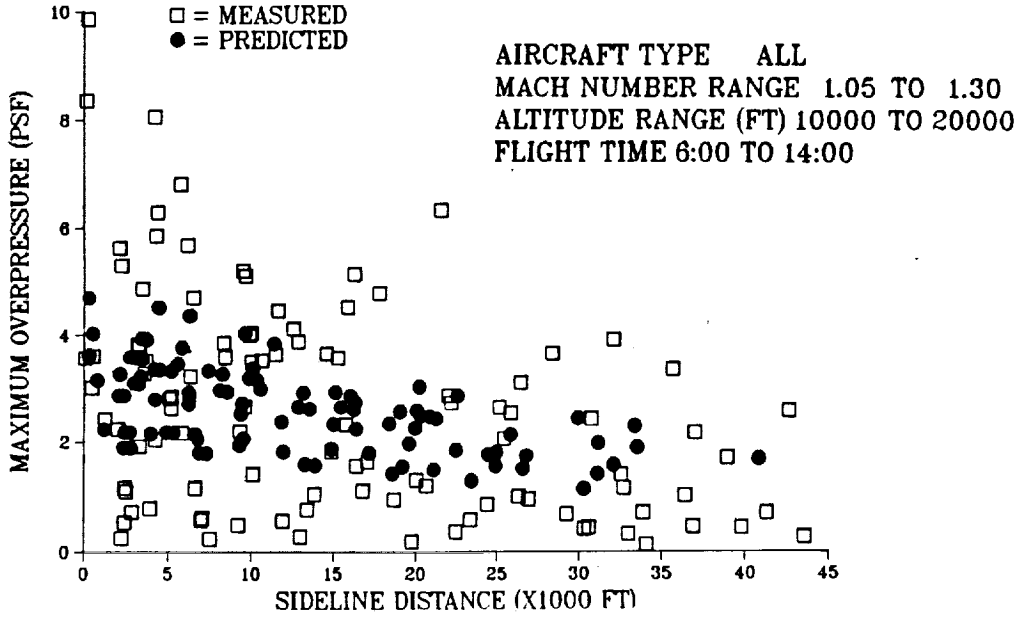

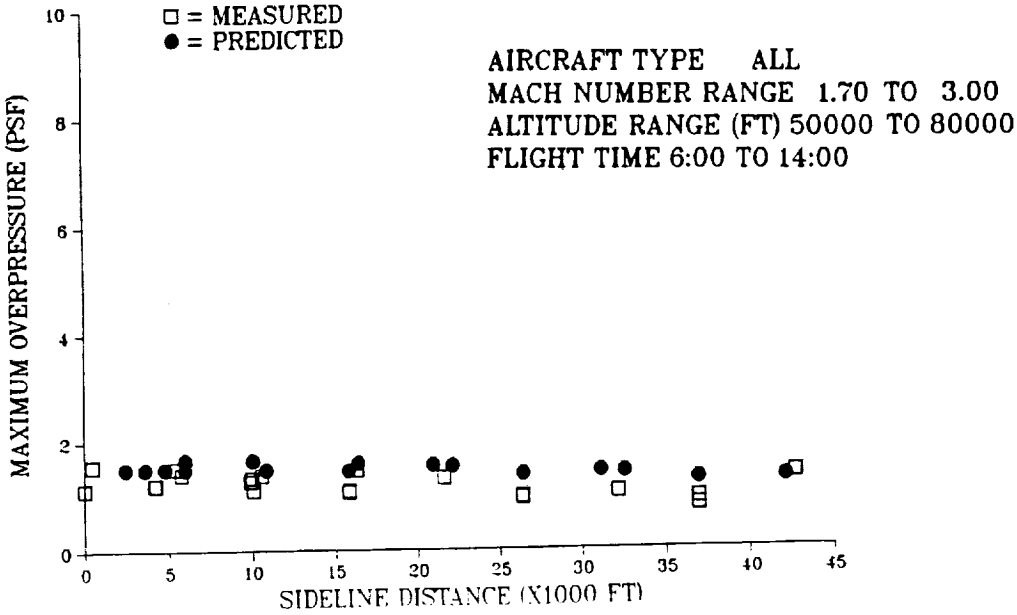

Rise Time Variability Dependence on Flight Conditions

The variability in the rise times (measured from 10% to 90% P_{max}) for two groups of measurements is plotted in these figures. Again, the low altitude / low Mach number group (top figure) shows a wider range of values (up to 50.3 msec) compared to the smaller variation (up to 11.8 sec) for the high altitude / high Mach number group (bottom figure).

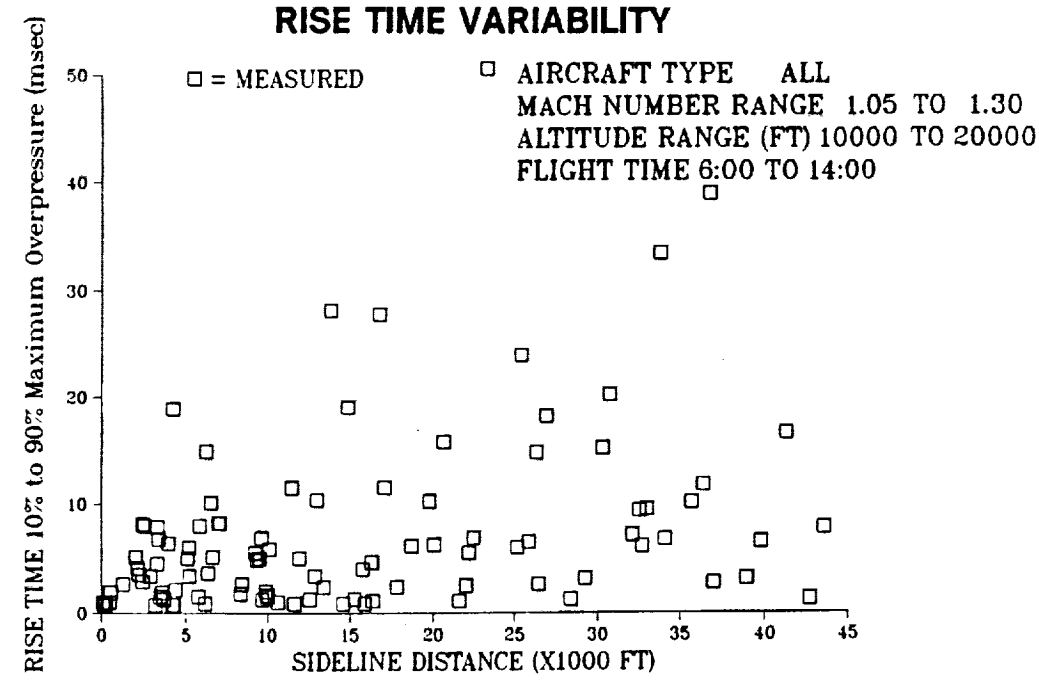

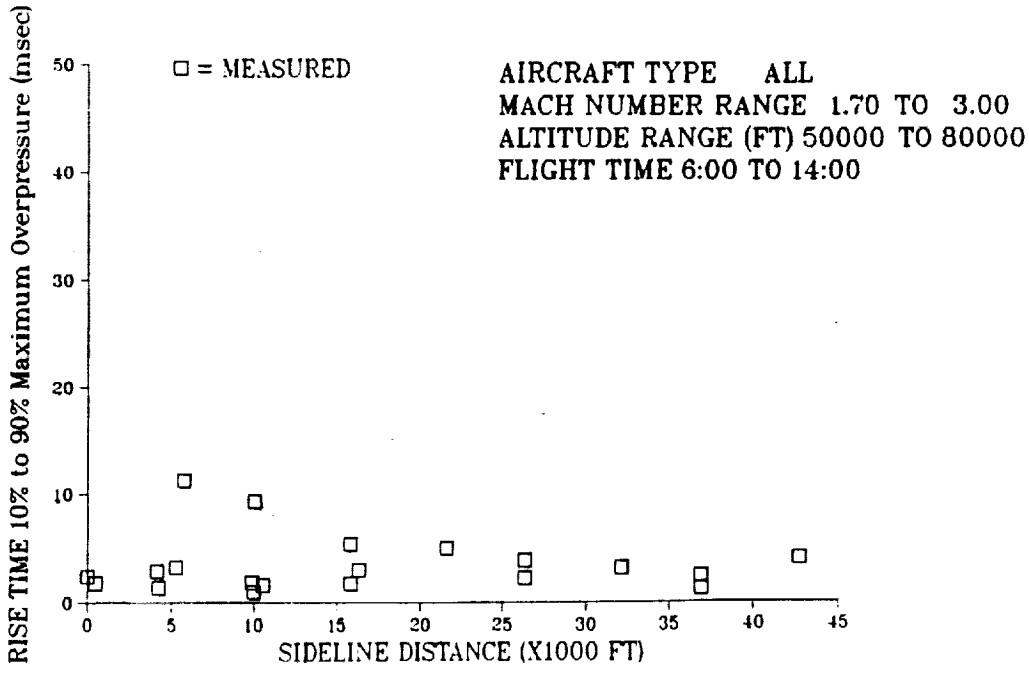

Loudness Variability Dependence on Flight Conditions

These figures illustrate that, as would be expected based on the observations of previous figures, the loudness of the measured and predicted booms are in good agreement for the high altitude / high Mach number flight groups (bottom figure). For the low altitude / low Mach number altitude group the loudness values of the measured booms are scattered around the predicted boom loudness values (top figure). For the other frequency domain metrics, ASEL and CSEL, similar comparisons were noted.

LOUDNESS VARIABILITY

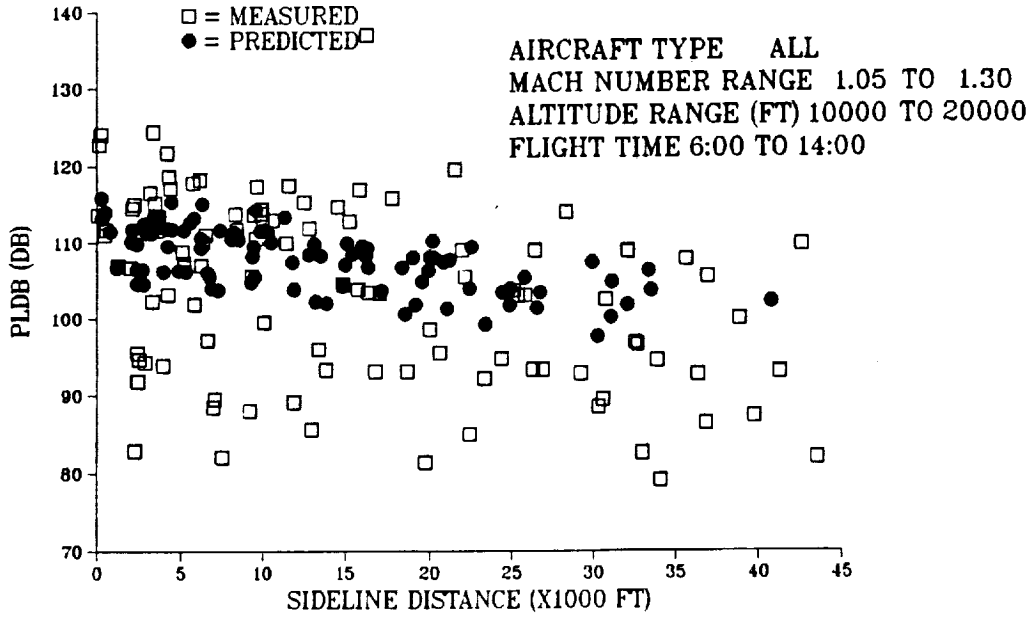

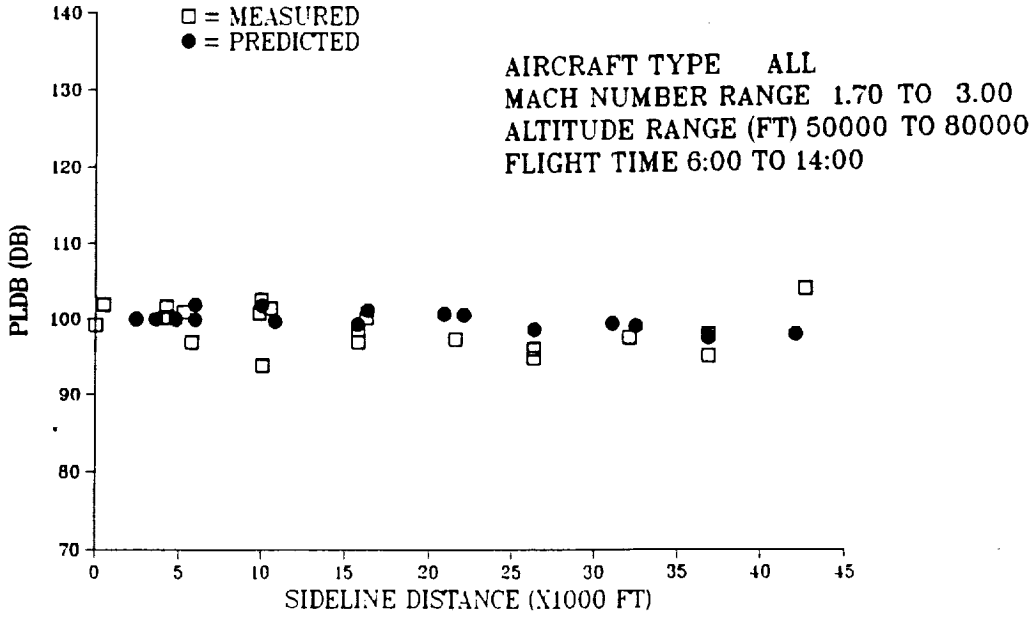

Sonic Boom Variability in Repeat Flights

The BOOMFILE database has a limited number of repeat flights (i.e., same aircraft at nominally the same flight conditions). Analysis of measurements from two such sets are shown. The first set consists of two flights of F16 aircraft at an altitude of 14,000 feet. The second set consists of two flights of F15 aircraft at a higher altitude of 45,000 feet. In each case, the repeat flights were made within a few minutes of the first flight. These plots thus provide a real representation of the variability in sonic boom measurements due to propagation effects. It can be noticed that the lower altitude runs (top figure) show a greater variability in sonic boom maximum overpressure compared to the higher altitude runs (bottom figure).

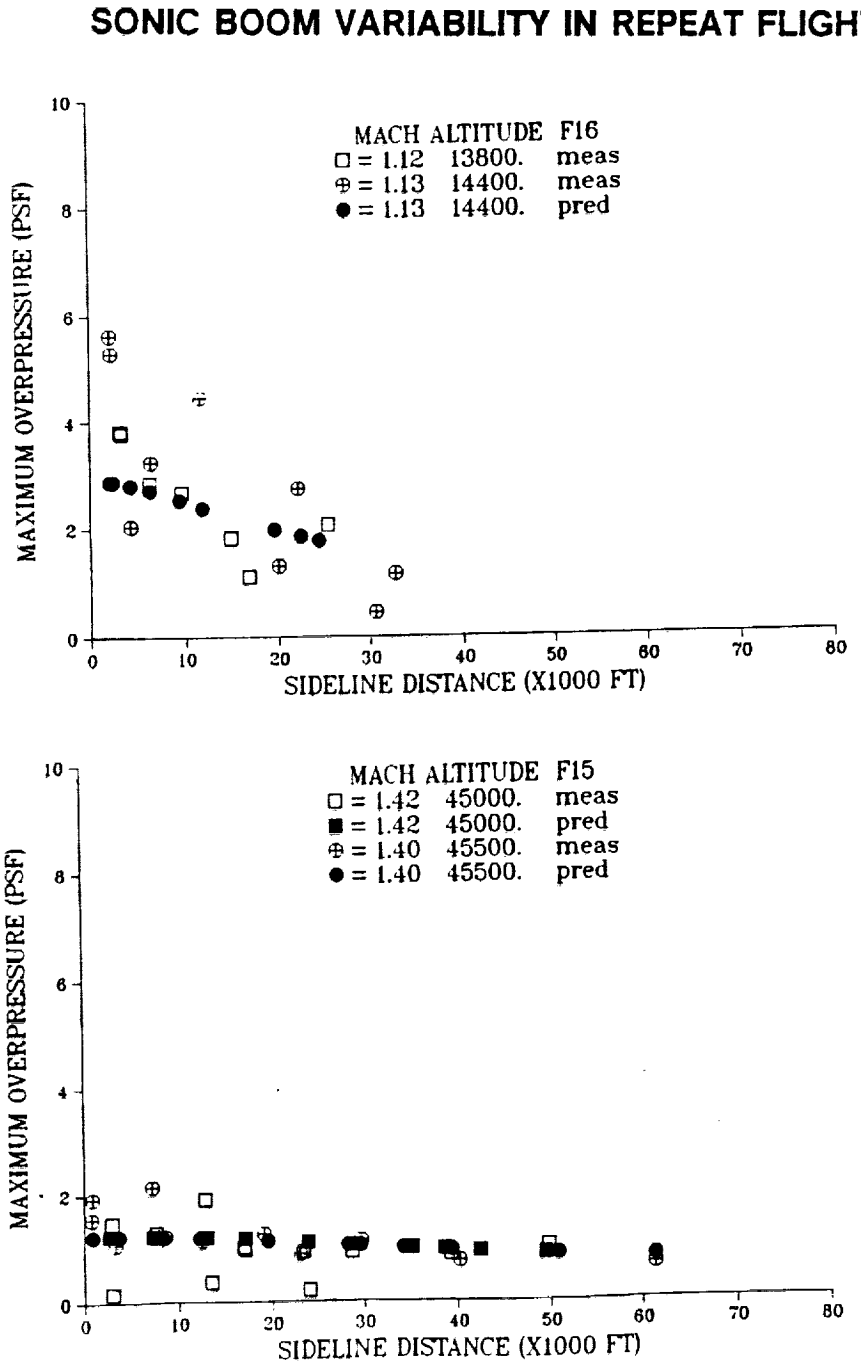

Sonic Boom Variability in Repeat Flights

These plots show that the lower altitude runs (top figure) have greater variability rise time compared to the higher altitude runs (bottom figure).

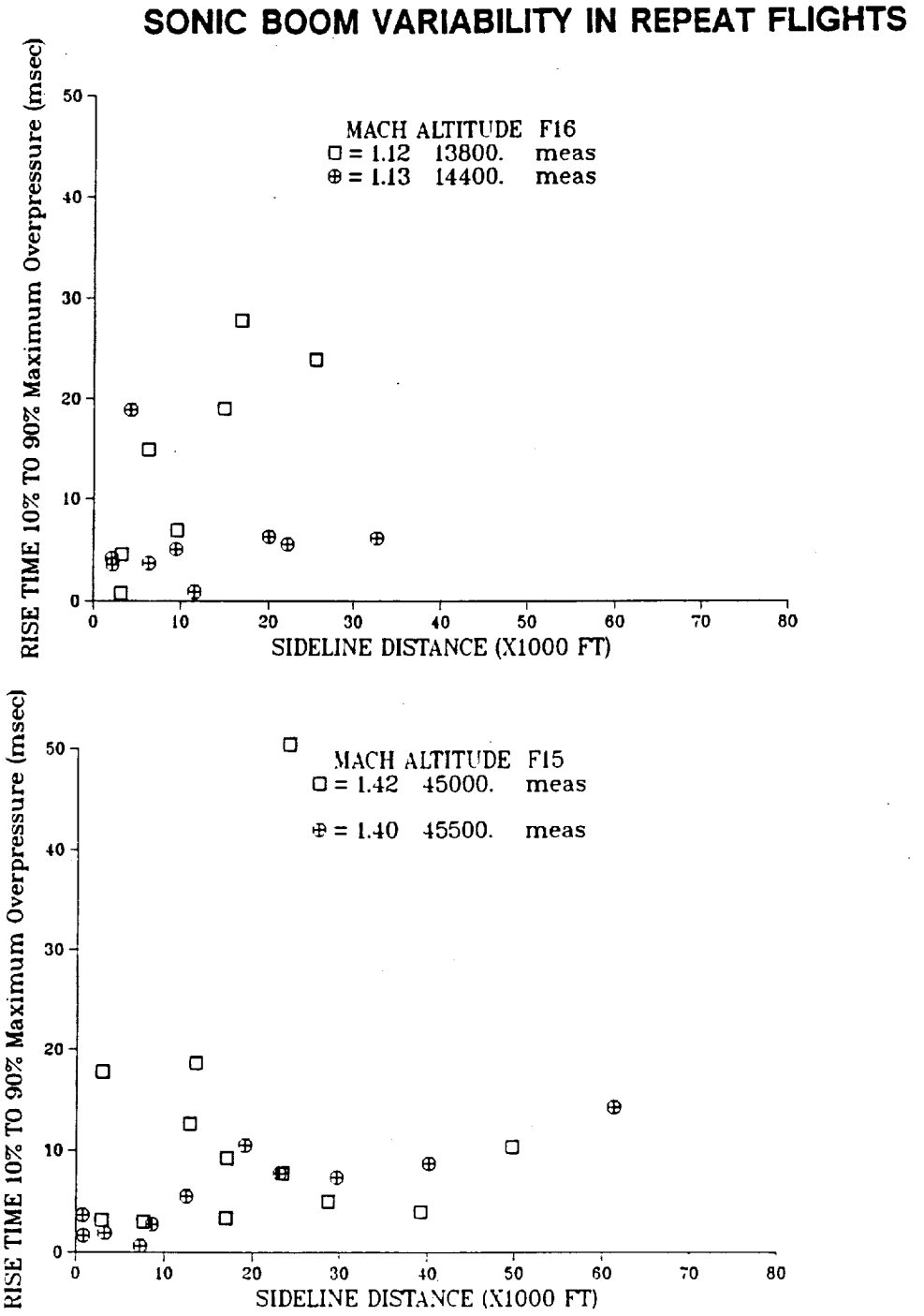

Sonic Boom Variability in Repeat Flights

These plots show that the lower altitude runs (top figure) have greater variability in loudness compared to the higher altitude runs (bottom figure).

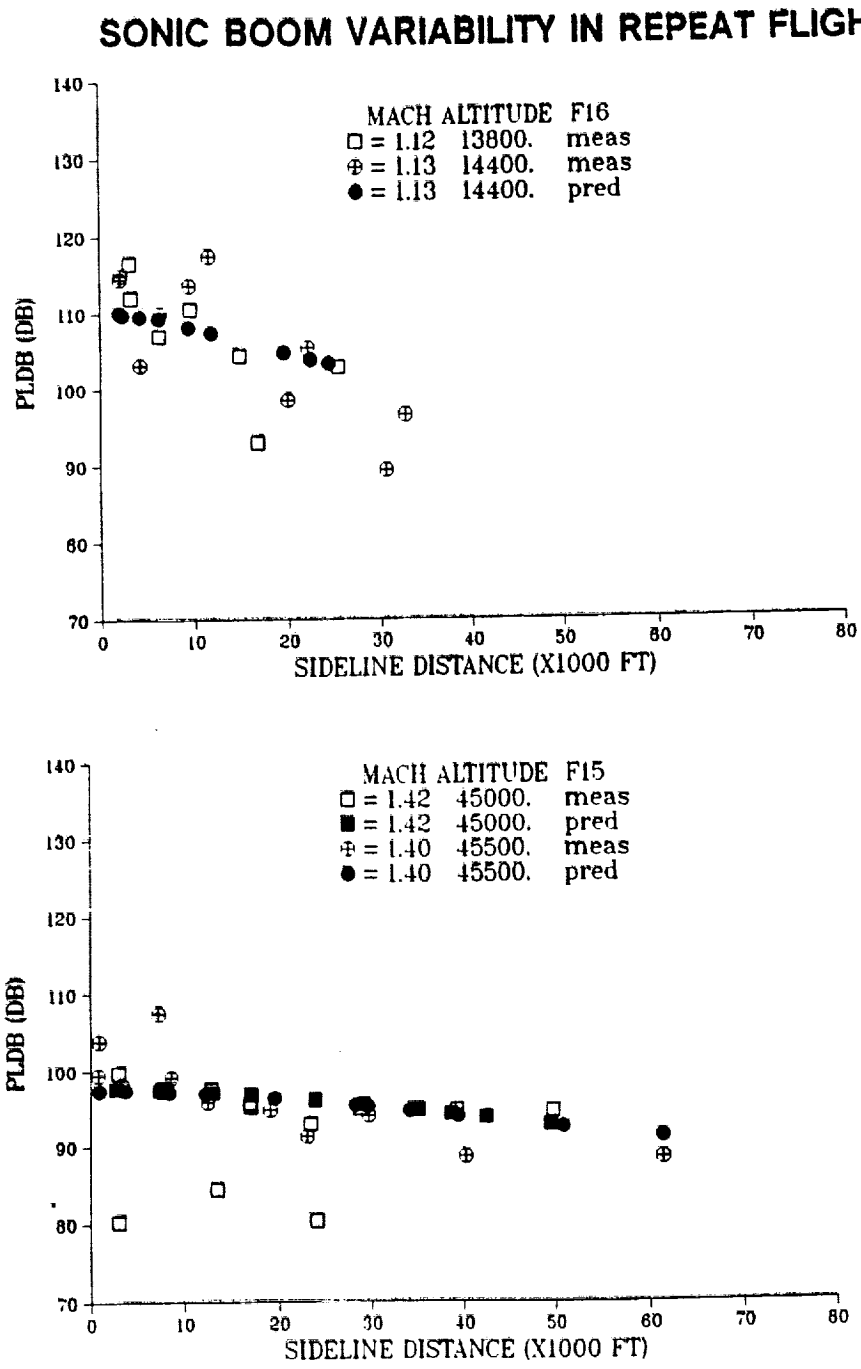

Sonic Boom Variability in a Repeat Data Point

Data from two different flights at similar flight conditions roughly 10 minutes apart show the effect propagation through the atmosphere has on sonic booms. The overpressure plots show that the 11:44 flight resulted maximum overpressure of 5.19 psf and a rise time of 5 ms whereas the 11:54 flight yielded a maximum overpressure of 2.66 psf with a rise time of 6.875 ms. The difference in loudness between these two booms was 3.1 PldB. The spectra plot shows that the 11:44 flight had less low frequency noise (below 200 Hz) and more high frequency noise (above 200 Hz) than the 11:54 flight.

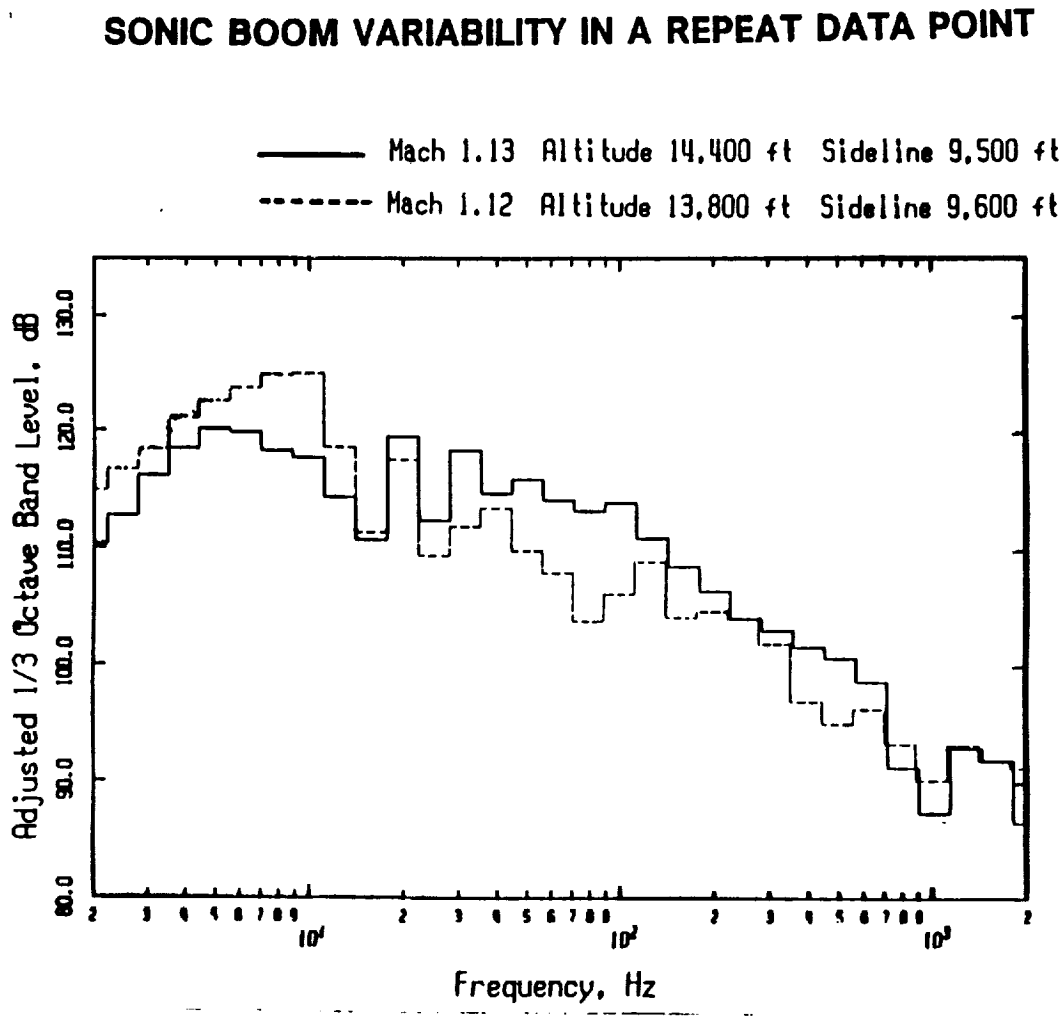

Variability with Time of Day

The measurements set up in the XB-70 database used either a three or six ground microphone cluster in a 200 by 200 foot square. Only minor variations are expected from one microphone to the other in the absence of significant propagation effects. Atmospheric turbulence and thus the propagation are expected to vary with the time of the day. The figure examines the variation in maximum overpressure with time of day. The data points are for flight conditions Mach = 1.17 to 1.87 and altitude = 40,000 ft to 50,000 ft (identified as Group 2 previously). The variation in values from one cluster to another is due to differences in operating conditions and sideline distances but the variations within a cluster are due to propagation differences. It can be noticed in this figure that the variability in maximum overpressure is very small for morning flights (prior to 11AM). Around noon and in the afternoon this variability increases a little.

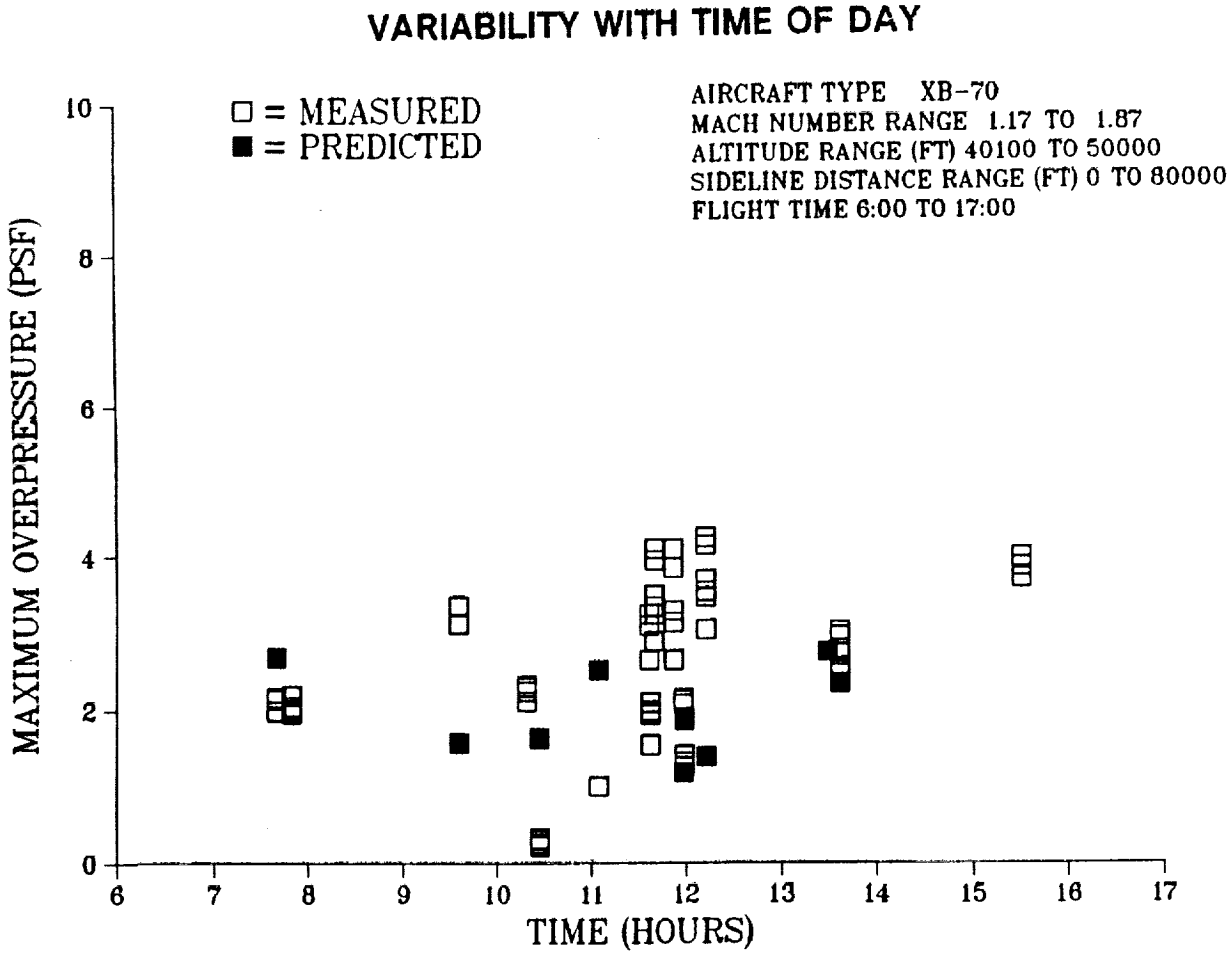

Variability with Time of Day

This figure shows the variation in rise time with time of day. The data points are for flight conditions Mach = 1.17 to 1.87 and altitude = 40,000 ft to 50,000 ft (identified as Group 2 previously). The variation in values from one cluster to another is due to differences in operating conditions and sideline distances but the variations within a cluster are due to propagation differences. The rise time shows a large increase in variability in the afternoon.

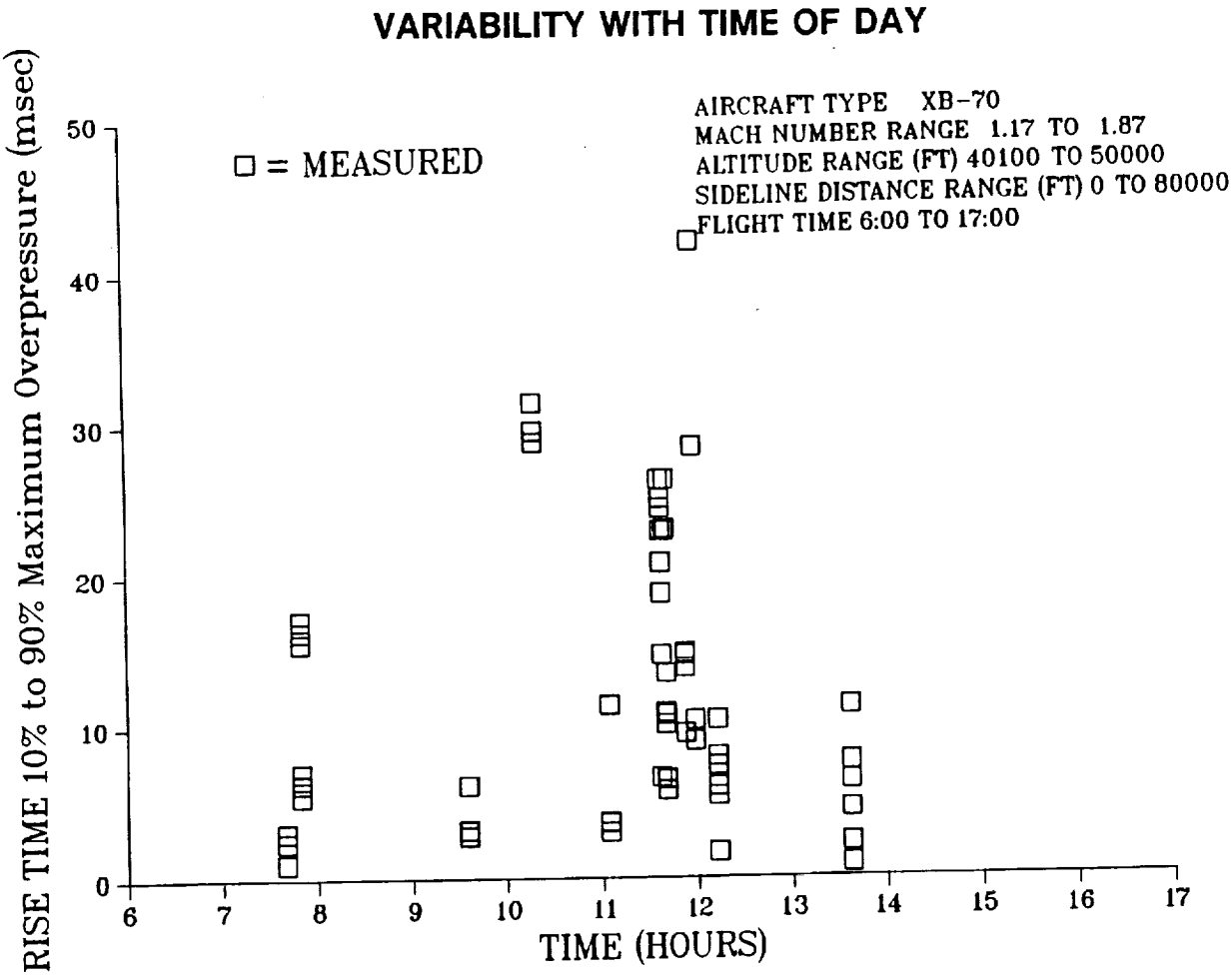

Variability with Time of Day

This figure examines the variation in loudness with time of day. The data points are for flight conditions Mach = 1.17 to 1.87 and altitude = 40,000 ft to 50,000 ft (identified as Group 2 previously). The variation in values from one cluster to another is due to differences in operating conditions and sideline distances but the variations within a cluster are due to propagation differences. It can be noticed in this figure that the variability in loudness can be as much as 10 PLdB in the measured data. Similar variability in loudness was noticed in groups 1,3, and 4 of the XB-70 database with the higher altitude runs generally having slightly lower variability.

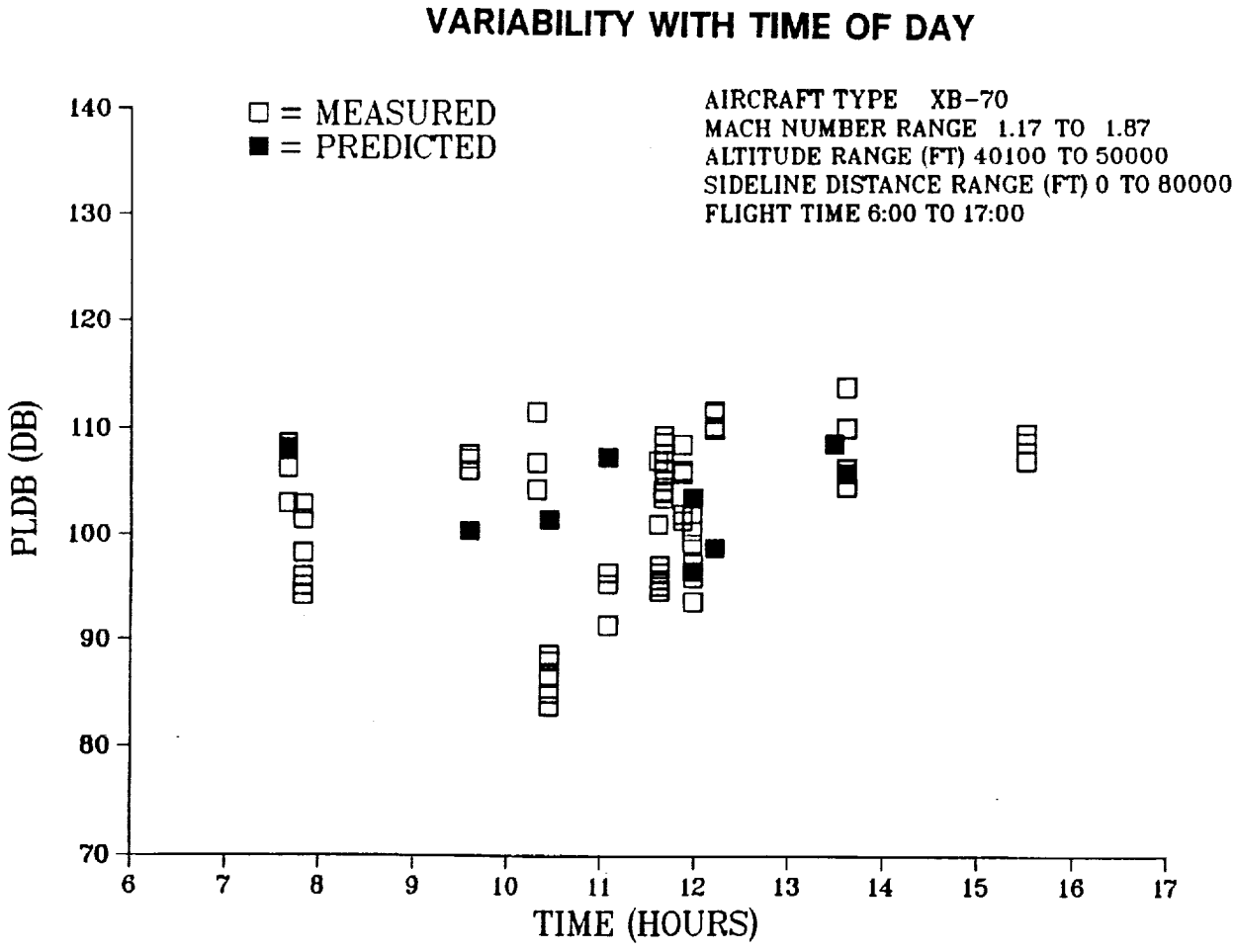

Variability in Boom Symmetry

Sonic boom asymmetry was determined by the difference between overpressure, PLdB, ASEL, or CSEL calculated separately for the compression portion and the expansion portion of the sonic boom signature. The variability in Δ overpressure for the lower altitude / lower Mach number group of flights (top figure) is slightly greater than the high altitude / high Mach number group of flights (bottom figure). The lower values and smaller variability in Δ overpressure (front shock) for the higher altitude / higher Mach number group is consistent with the near N-wave signatures and reduced atmospheric effects associated with these signatures in this altitude group.

VARIABILITY IN BOOM SYMMETRY

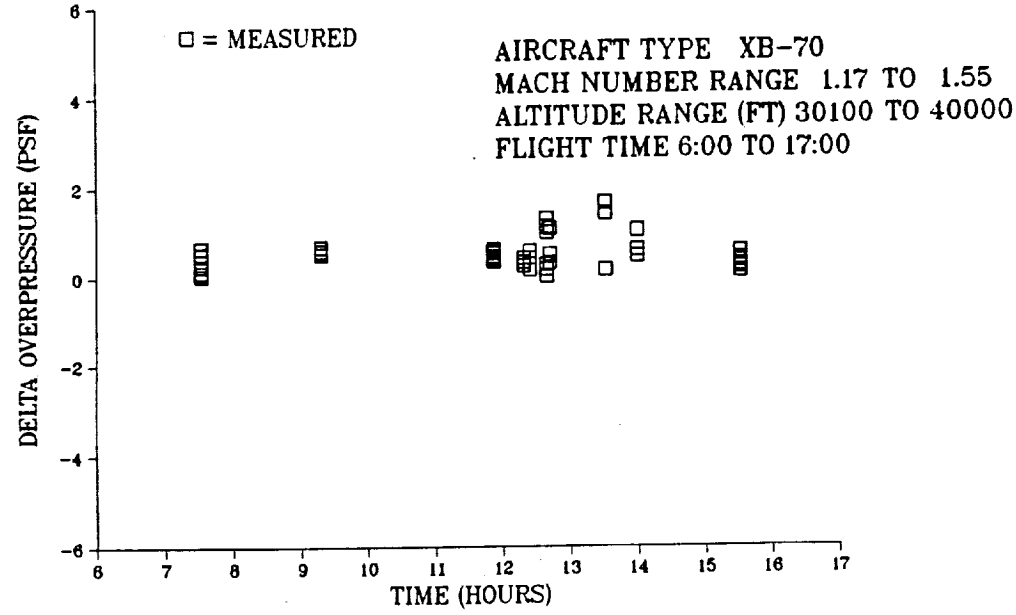

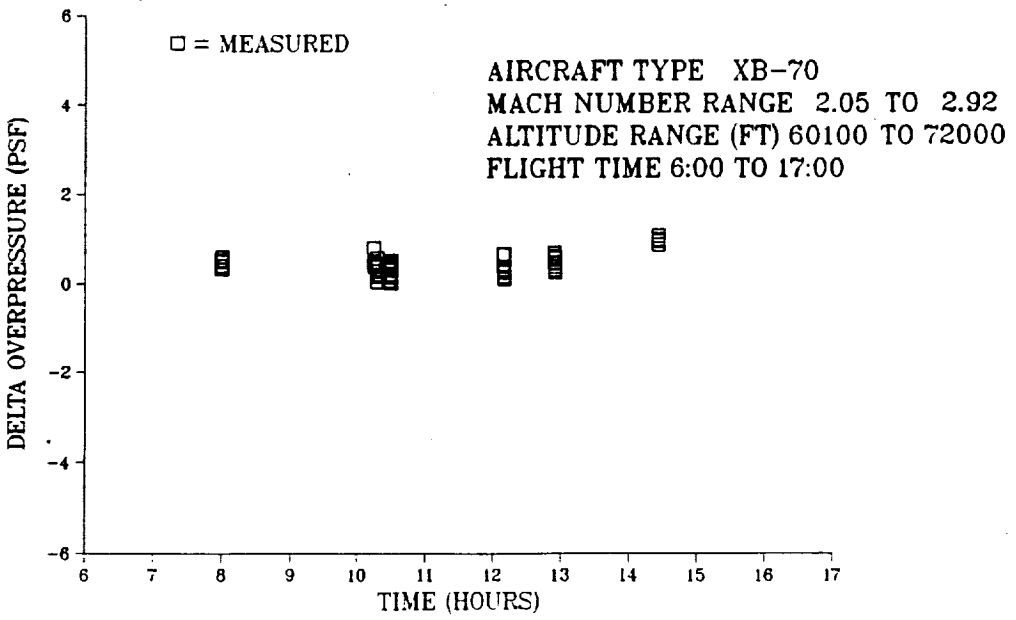

Variability in Boom Symmetry

Sonic boom asymmetry was determined by the difference between overpressure, PLdB, ASEL, or CSEL calculated separately for the compression portion and the expansion portion of the sonic boom signature. The variability in Δ PLdB in the lower altitude / lower Mach number group of flights (top figure) is slightly greater than the high altitude / high Mach number group of flights (bottom figure). In the "afternoon hours", the asymmetry in loudness has a greater variability than the asymmetry in overpressure (previously shown). This is an indication of the larger effect of atmospheric turbulence on rise time.

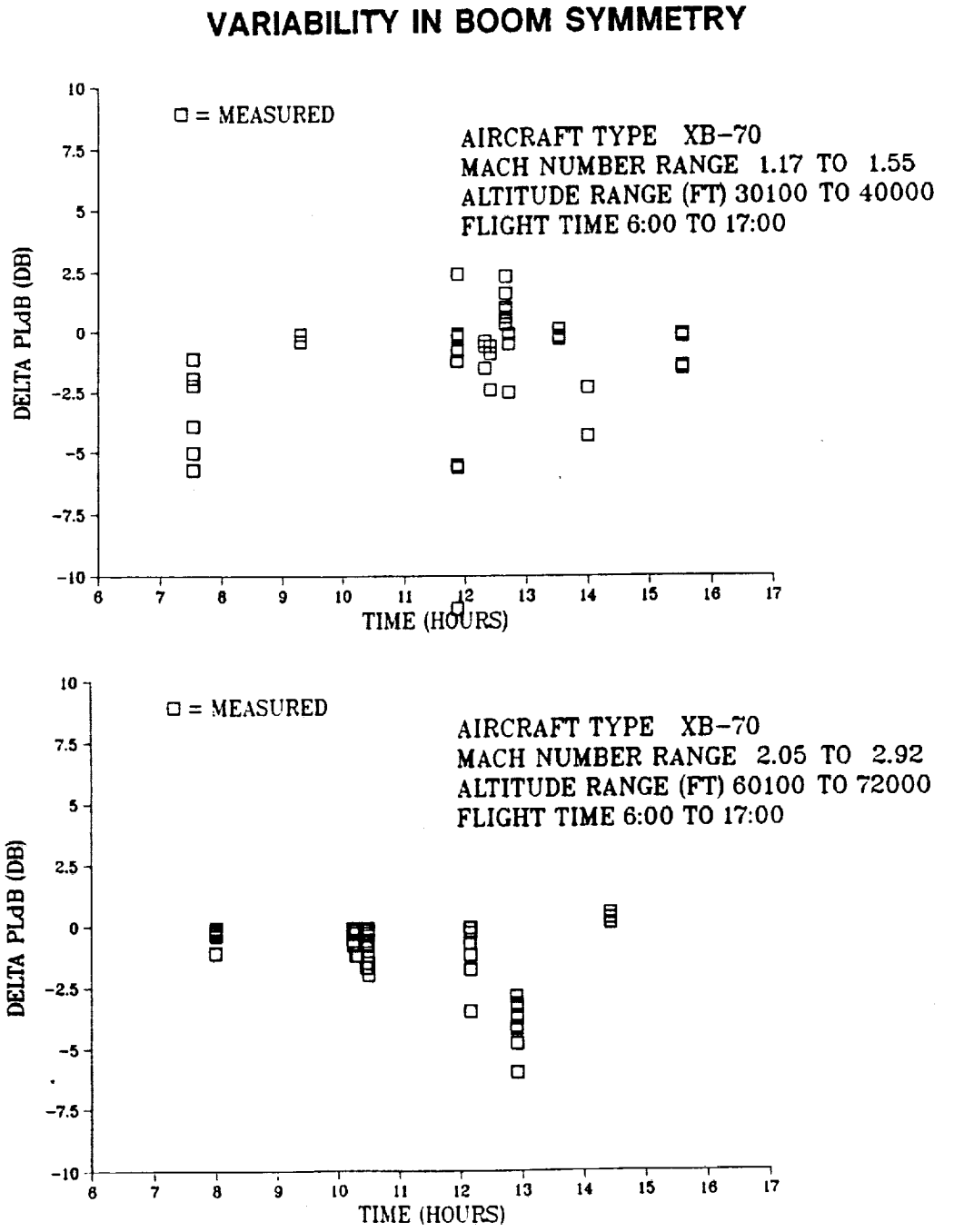

Statistical Distribution

The XB-70 database was divided into two data groups - those within 50 percent of the calculated lateral cutoff distance (dyc) and those outside of this boundary. Such a grouping has been used in Reference 5 in the analysis of BOOMFILE data. The histograms these figures represent the distribution of measured maximum overpressure values (normalized by the corresponding calculated uniform atmospheric maximum overpressure) in the database for these two groups. It can be seen that for the below 50% dyc group (bottom figure) maximum overpressure distribution is nearly symmetric and has approximately a normal distribution shape with shorter skirts (smaller variance) away from the mean value. By comparison, the above 50% dyc group (top figure) shows a large variability in measured maximum overpressure.

STATISTICAL DISTRIBUTION

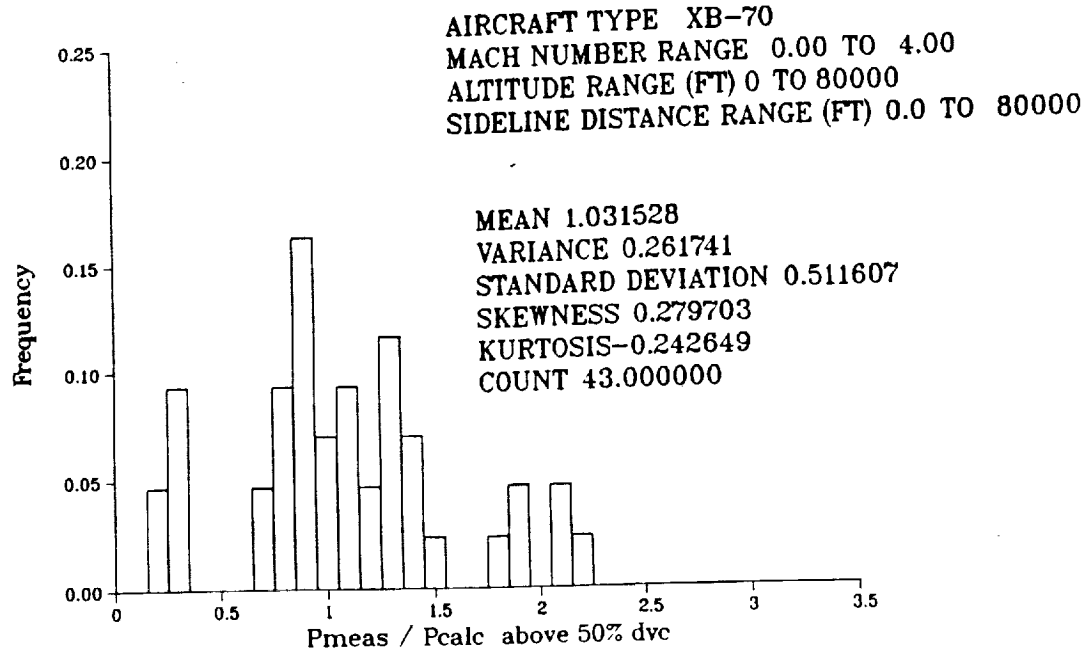

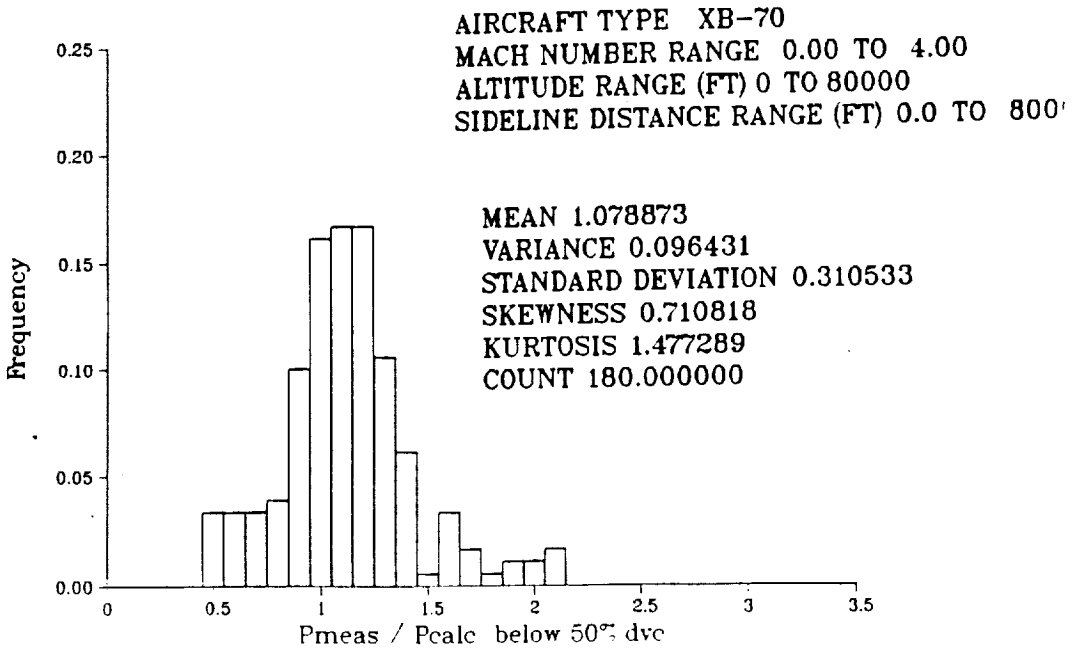

Statistical Distribution

The XB-70 database was divided into two data groups - those within 50 percent of the calculated lateral cutoff distance (dyc) and those outside of this boundary. Such a grouping has been used in Reference 5 in the analysis of BOOMFILE data. The histograms in these figures represent the distribution of the difference between measured and calculated (uniform atmosphere assumed) loudness in the XB-70 database for these two groups. The below 50% dyc group (bottom figure) has a symmetric distribution with a -0.15 dB mean for $PL_{meas} - PL_{calc}$ whereas the above 50% dyc group (top figure) has a bi-modal type distribution with a -1.7 dB mean and larger variance about the mean.

STATISTICAL DISTRIBUTION

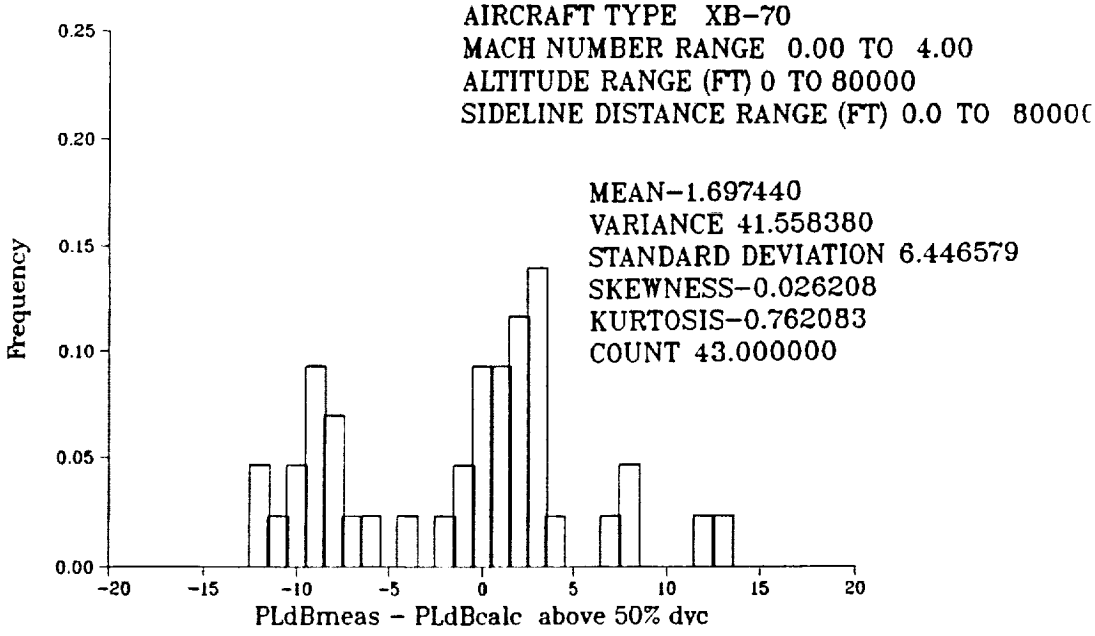

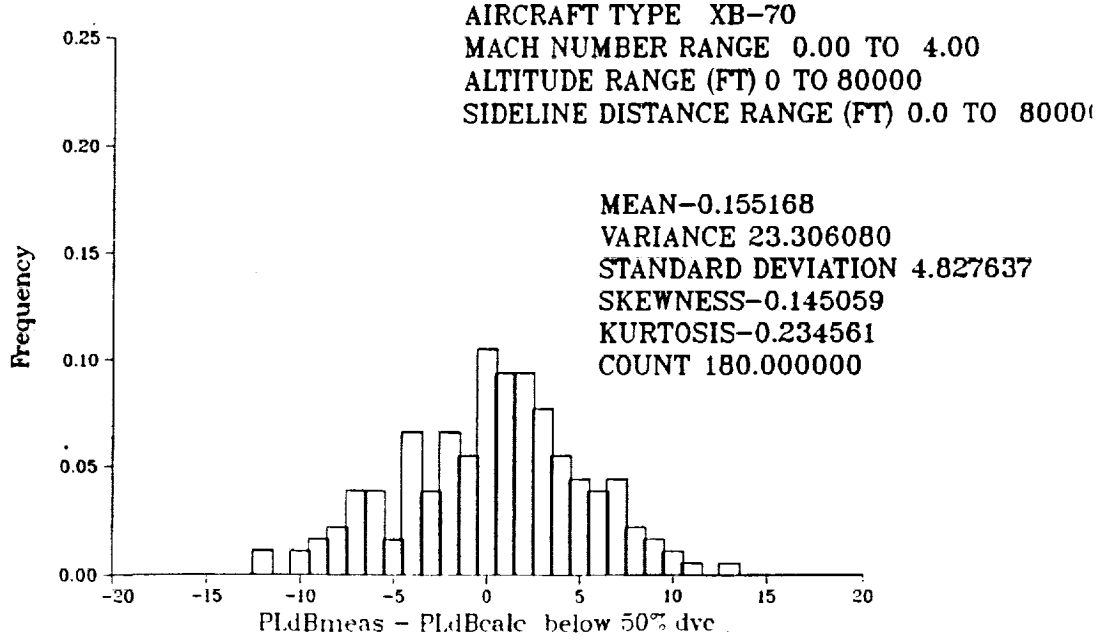

Statistical Distribution by Time of Day

The variability of measured maximum overpressure in the below 50% dve group was further analyzed in terms of the time of day to statistically quantify the turbulence effects. The histogram in top figure shows that the maximum overpressure measurements for the morning (before 11am) flights have a smaller variability than for flights which occur after 11am (bottom figure). While the mean values of maximum overpressure in the two plots are not very different, the mean values occurs more frequently before 11am than after 11am (i.e., the afternoon distribution has a larger variance). This trend was also observed in the sonic boom measurement program at White Sands Missile Range (Reference 6).

STATISTICAL DISTRIBUTION BY TIME OF DAY

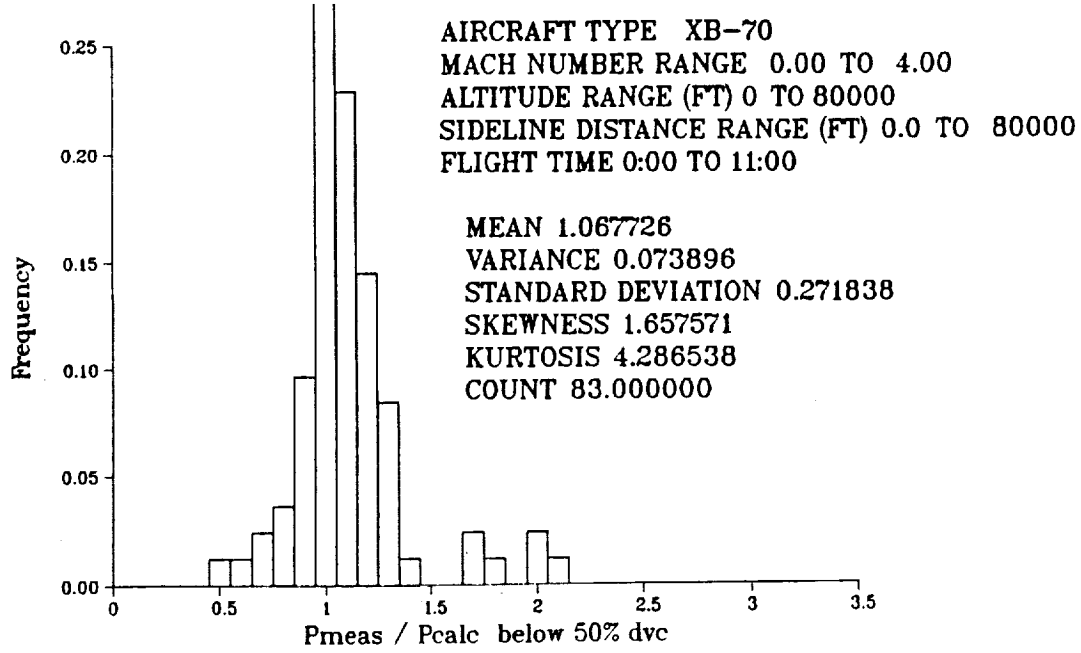

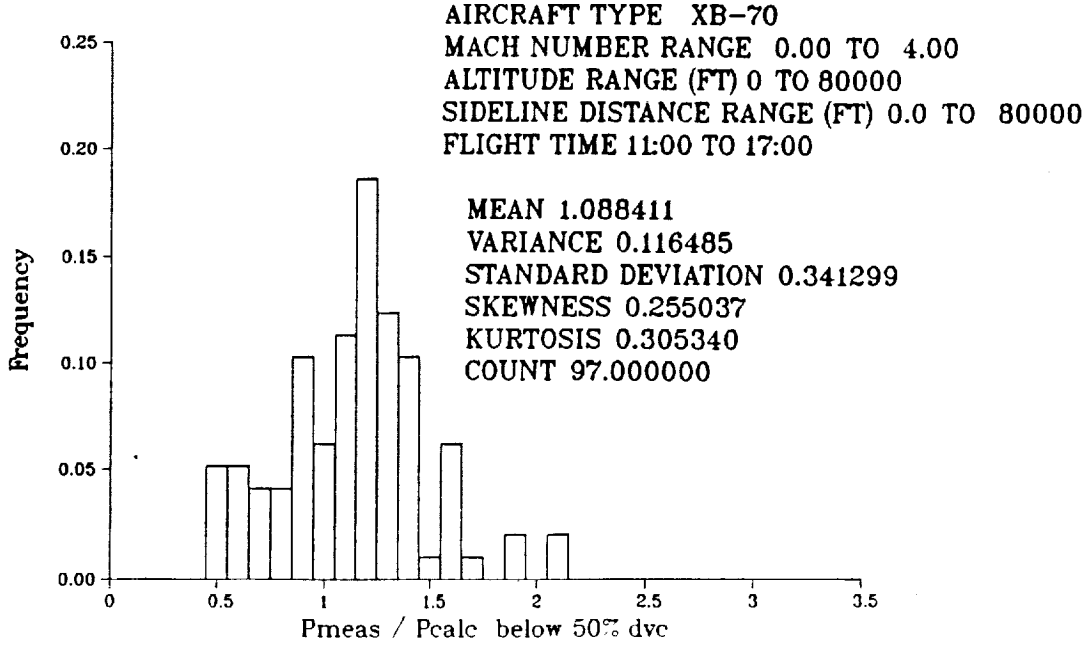

Statistical Distribution by Time of Day

The variability of measured loudness in the below 50% dvc group was further analyzed in terms of the time of day to statistically quantify the turbulence effects. The histogram in top figure shows that the loudness measurements for the morning (before 11am) flights have a smaller variability than for flights which occur after 11am (bottom figure).

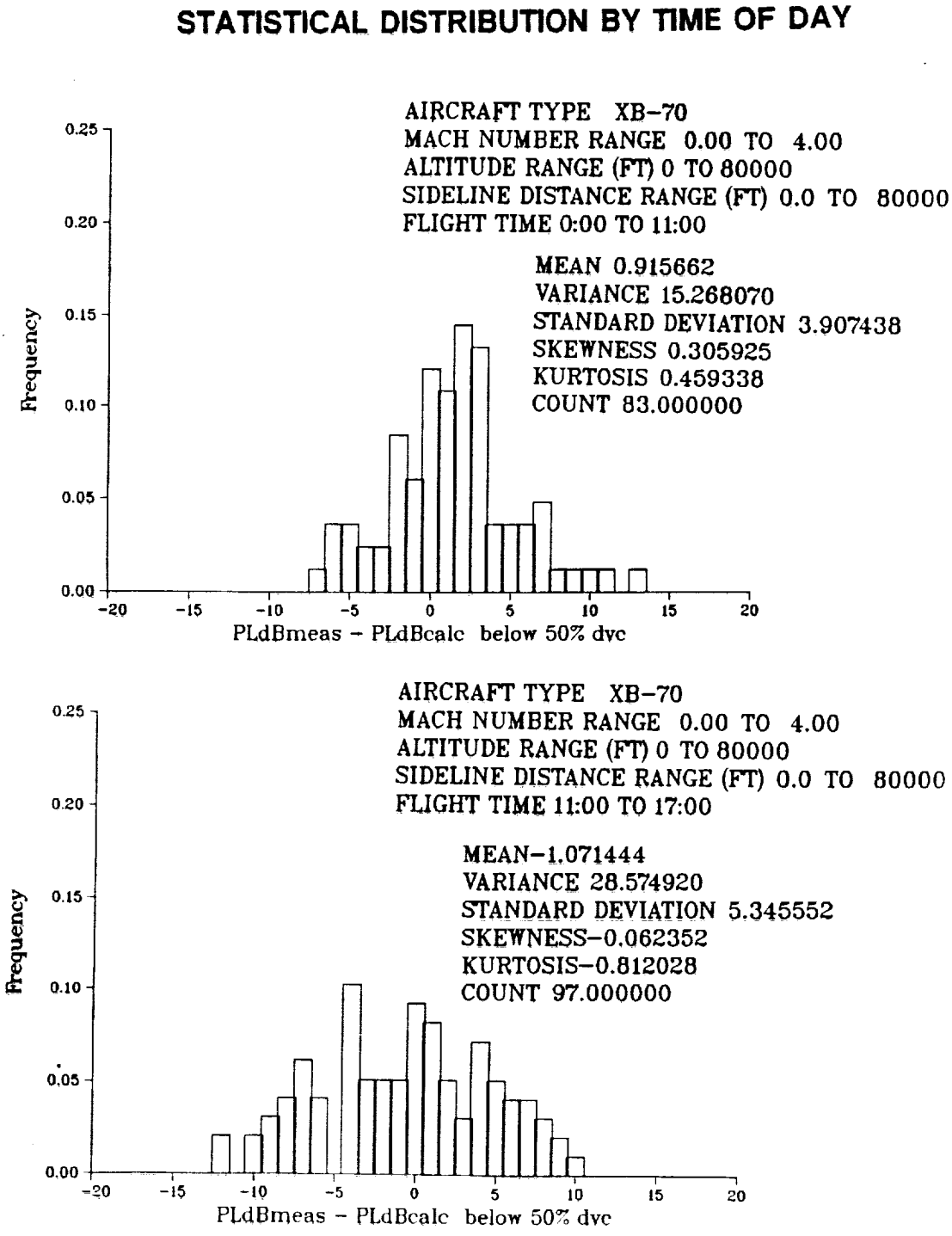

Summary

The BOOMFILE and XB70 databases were analyzed in various calculated metrics and rise times which are available in electronic format. The variation in boom loudness was observed to be as much as 10 PLdB with larger variation occurring in the lower altitude / lower Mach number flights, afternoon flights, and outside the carpet semi-span. Analysis of asymmetry showed that differences of up to 12 dB occurred and was greater for lower altitude / lower Mach number flights.

SUMMARY

- **ANALYZED VARIABILITY IN SONIC BOOM SIGNATURE PARAMETERS AND METRICS (DUE TO ATMOSPHERIC PROPAGATION) USING BOOMFILE AND XB-70 DATABASES**
- **10 dB VARIABILITY IN BOOM LOUDNESS POSSIBLE**
- **GREATER VARIABILITY OBSERVED IN**
  - **LOWER ALTITUDE / LOWER MACH NUMBER FLIGHTS**
  - **AFTER MID-MORNING FLIGHTS**
  - **MEASURMENTS OUTSIDE 50% OF SONIC BOOM CARPET SEMI-SPAN**
- **UP TO 12 dB ASYMMETRY OBSERVED**
- **VARIABILITY IN BOOM ASYMMETRY GREATER FOR LOWER ALTITUDE / LOWER MACH NUMBER FLIGHTS**

References

1. Lee, R. A. and Downing, J. M., "Sonic Booms Produced by United States Airforce and United States Navy Aircraft: Measured Data", Armstrong Laboratory Report AL-TR-1991-0099, 1990.

2. Maglieri, D. J. et al, Summary of XB-70 Sonic Boom Signature Data for Flights During March 1965 Through May 1966", NASA Contract Report 189630, 1992.

3. Carlson, H. W., "Simplified Sonic Boom Prediction", NASA Technical Paper 1122, 1978.

4. Plotkin, K. J., "MDBOOM and MDPLOT Computer Programs for Sonic Boom Analysis", WYLE Research Report WR 88-7, 1988.

5. Downing, J. M., "Lateral Spread of Sonic Boom Measurement From US Air Force BOOMFILE Flight Tests", NASA CP 3172, 1992.

6. Willshire Jr., W. L. and Devilbiss, D. W., "Preliminary Results from the White Sands Missile Range Sonic Boom", NASA CP 3172, 1992.

7. Panofsky H. A. and Dutton, J. A., Atmospheric Turbulence , pp.119-174, 1984.

Sonic Booms and Marine Mammals: Informational Status and Recommendations

William C. Cummings
Oceanographic Consultants

Presentation at NASA HSR Sonic Boom Workshop
NASA Ames Research Center
May 12 - 14, 1993

Figure 1

Outline of presentation.

SONIC BOOMS AND MARINE MAMMALS

Bill Cummings
Oceanographic Consultants

INTRODUCTION TO MARINE MAMMALS
- Baleen Whales
- Toothed Whales
- Seals & Sea Lions
- Sea Otter
- Polar Bear
- Manatees

MARINE MAMMAL HEARING
- Baleen Whales
- Toothed Whales
- Seals & Sea Lions

NOISE EFFECTS
- Explosives
- Other

SONIC BOOMS
- In Air (understood)
- In Water

SONIC BOOM EFFECTS ON MARINE MAMMALS
- Real Stimulus
- Simulated Stimulus

PREDICTIONS
- Submerged or Swimming
- Hauled Out (Pinnipeds)

RECOMMENDATIONS
- Contact With NRC, NMFS and MM Commission
- Symposium (with SMM)
- SSB Tests on Captive Porpoises & Pinnipeds
- Habituation Tests

Figure 2

Examples of baleen (blue whale, top) and toothed (bottlenose dolphin, bottom) whales.

Balaenoptera musculus

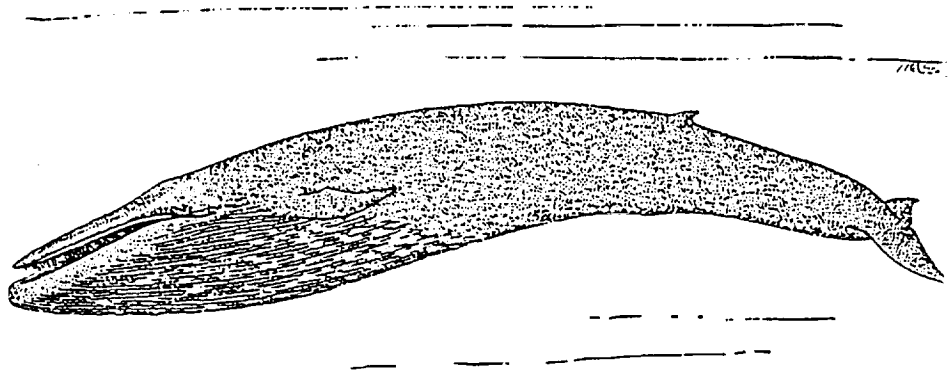

Tursiops truncatus

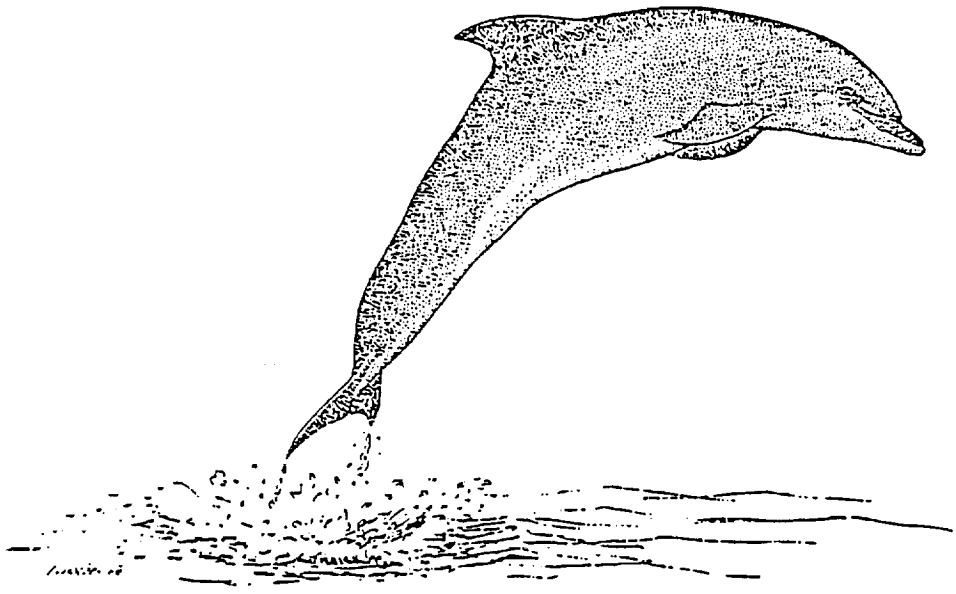

Figure 3

Examples of pinnipeds: harbor seal (top), California sea lion (bottom).

Phoca vitulina

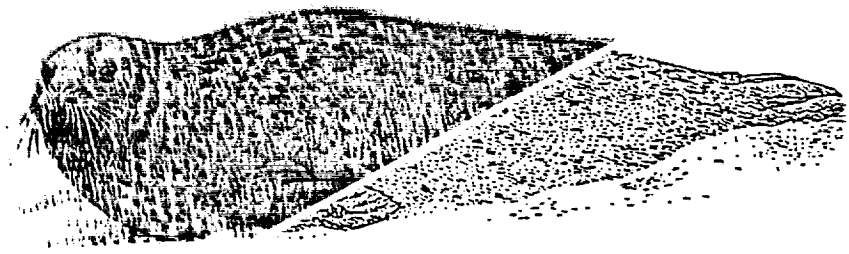

Zalophus californianus

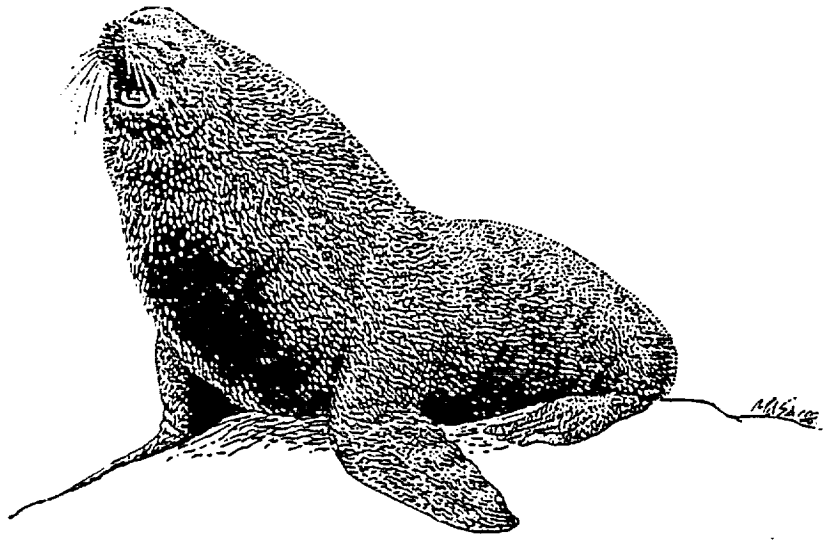

Figure 4

Examples of other marine mammals: Amazon manatee (top), sea otter (bottom).

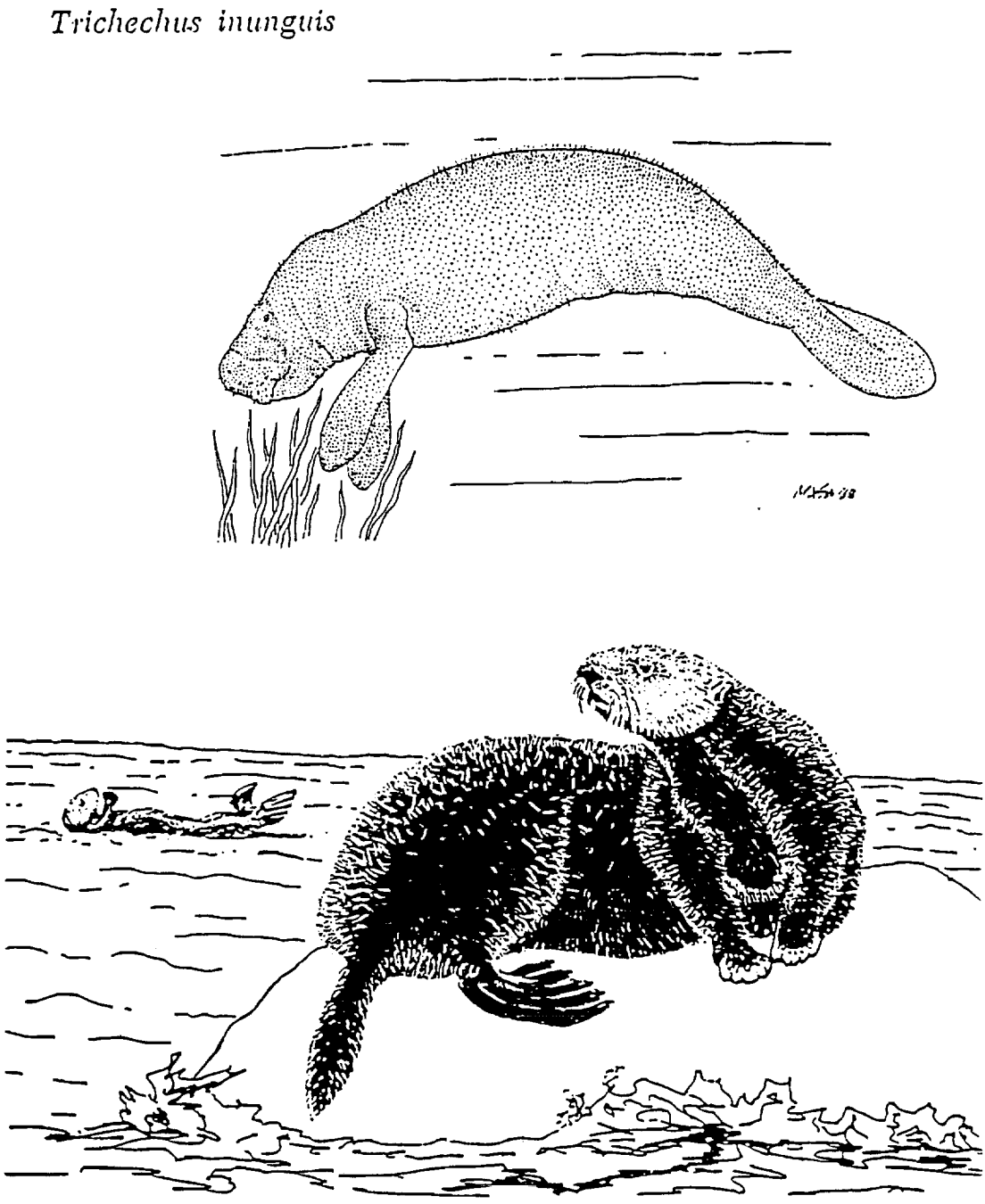

Figure 5

Estimated population sizes of selected large whales (from Gaskin).

WHALE	POPULATION SIZE
Sperm Whale	over 567,800
Bowhead Whale	about 2,500
Right Whale	about 3,500
Gray Whale	between 7,000-15,000
Humpback Whale	between 3,000-5,000
Blue Whale	between 7,000-13,000
Fin Whale	about 88,000
Sei Whale	about 130,000
Bryde's Whale	over 80,000
Minke Whale	between 113,000-646,780

THE BEST ESTIMATES OF LARGE WHALE POPULATION SIZES (DATA FROM GASKIN 1982).

Figure 6

Sound source levels of selected species of marine mammals (various sources).

MARINE MAMMAL SOUND SOURCE LEVELS	dB re 1 µPa, 1m
Baleen Whales	131 - 189
Toothed Whales	135 - 200
Seals	95 - 180
Sea Lion, Walrus	157 - 172

Figure 7

Audiograms of five toothed whale species (from indicated sources).

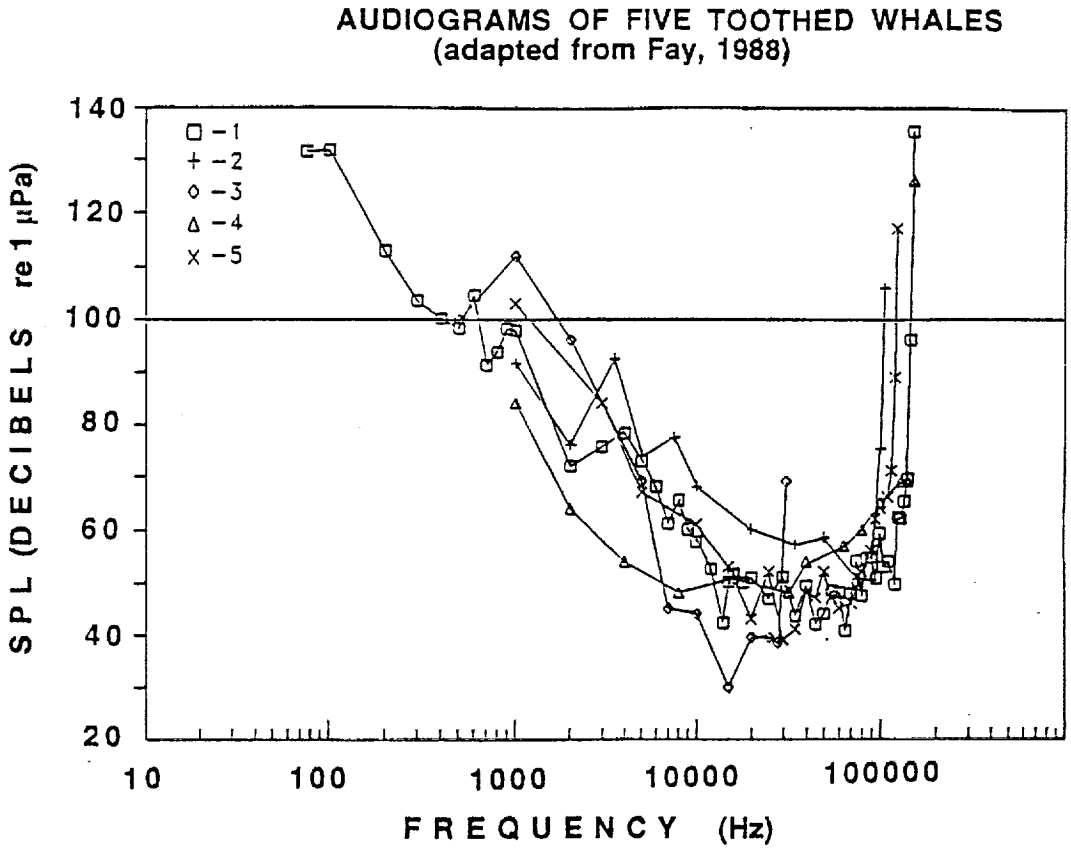

1- Bottlenose dolphin (Johnson)
2- Amazon River dolphin (Jacobs & Hall)
3- Killer whale (Hall & Johnson)
4- Harbor porpoise (Andersen)
5- Beluga whale (White et al.)

Figure 8

Audiograms of five pinnipeds (from indicated sources).

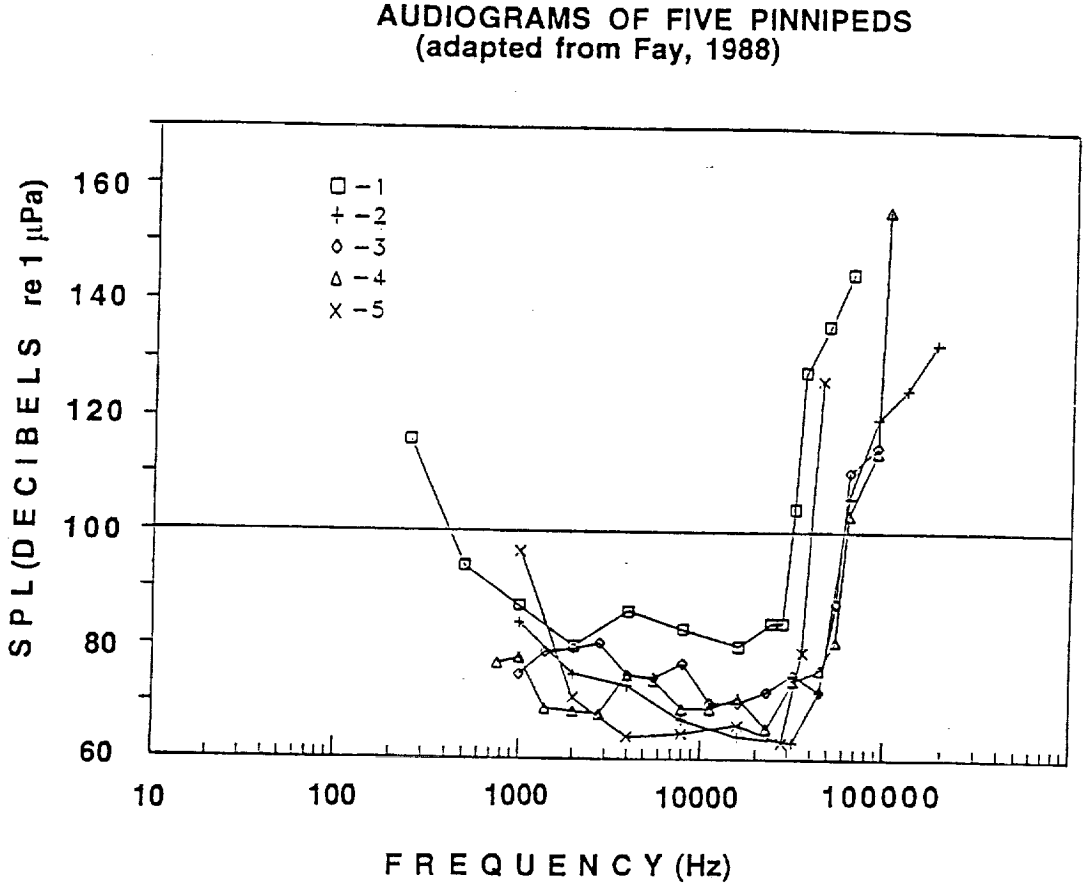

1- California sea lion (Schusterman et al., 1972)
2- Harbor seal (Mohl, 1968)
3- Ringed seal (Terhune & Ronald, 1975)
4- Harp seal (Terhune & Ronald, 1972)
5- Northern fur seal (Schusterman & Moore, 1978)

Figure 9

Sound spectra from a sonic boom at the water's surface and at depths indicated, compared to spectra of typical, low and high oceanic ambient noise (after Cook).

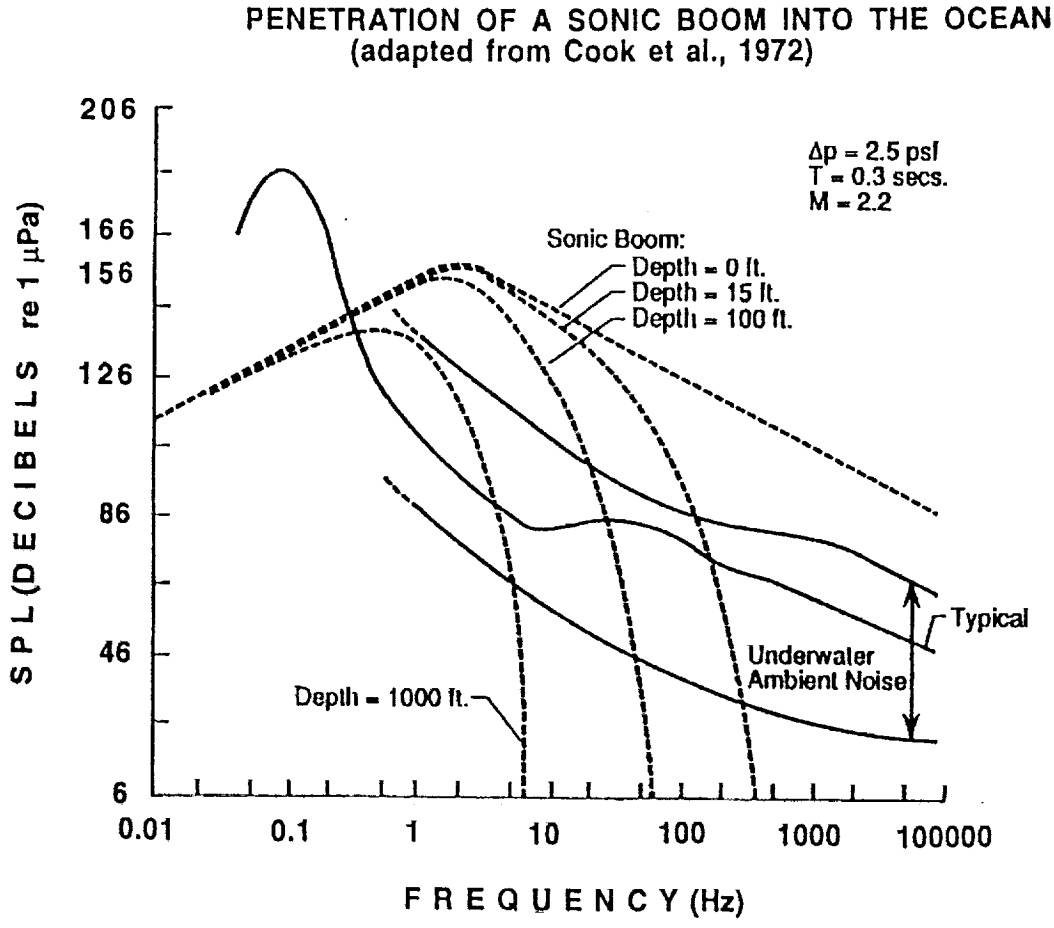

Figure 10

Sound spectrum of a sonic boom as measured at 15 ft depth, compared to average hearing curves of selected pinniped and toothed-whale species.

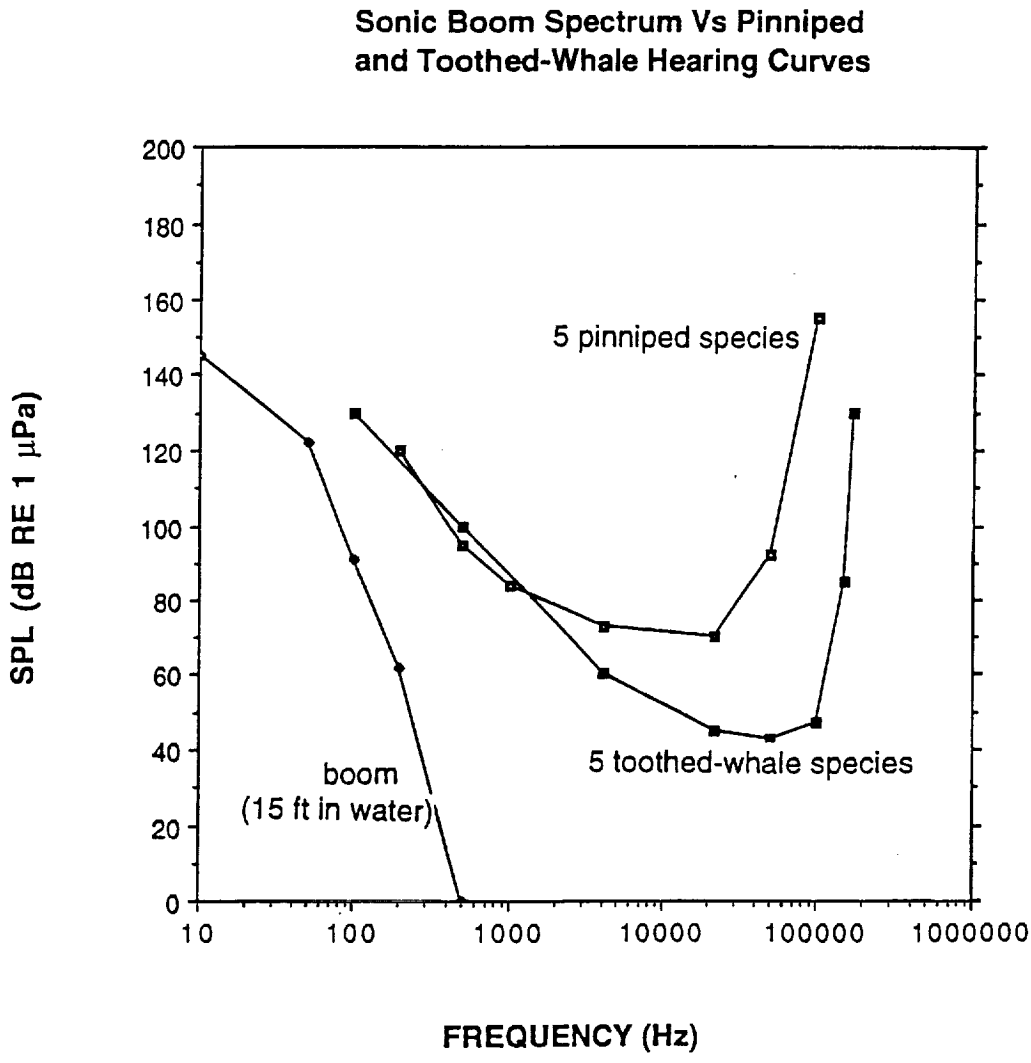

Figure 11

This study showed that marine mammal distributions will coincide with SS aircraft sonic booms. Depending upon the species and location, marine mammals will sense, not sense, or questionably sense sonic booms. Marine mammals probably will not be harmed physically. It is not probable that whale or swimming pinniped behavior will be significantly affected by sonic booms. Hauled out pinnipeds may or may not be affected by booms possibly depending upon species, age, and behavior at the time of the boom. There is little doubt that marine mammals will habituate to some extent.

CONCLUSIONS

COINCIDENCE +

SENSATION + - ?

DIRECT PHYSICAL HARM -

BEHAVIORAL EFFECTS

- Whales -
- Swimming Pinnipeds -
- Hauled-Out Pinnipeds + - ?

HABITUATION + ?

Figure 12

There has only been one experimental study (Sea World) on one species of pinniped using simulated sonic booms and none based upon real booms. No studies have been undertaken on the effects of sonic booms on any other marine mammals. I recommend early contacts with the National Research Council and Acoustical Society of America committees, with the regulatory authorities at the National Marine Fisheries Service, and with the Marine Mammal Commission. Low cost, comparatively easily facilitated studies may be undertaken on captive porpoises and pinnipeds using simulated booms for the purpose of determining any effects or habituation. However, regulatory authorities may not require such studies. A marine mammal permit should be applied for well before any decision is made regarding technical feasibility of the overall program.

RECOMMENDATIONS

EARLY CONTACTS (NRC, ASA, NMFS, MM COMMISSION

CONDUCT SYMPOSIUM (CONJUNCTION WITH SMM)

SSB TESTS ON CAPTIVE PORPOISES & PINNIPEDS
(ONLY IF REQUIRED BY NMFS)

HABITUATION TESTS
(ONLY IF REQUIRED BY NMFS)

REPORT DOCUMENTATION PAGE

Form Approved
OMB No. 0704-0188

1. AGENCY USE ONLY (Leave blank)	2. REPORT DATE	3. REPORT TYPE AND DATES COVERED
	February 1994	Conference Proceedings

4. TITLE AND SUBTITLE

High-Speed Research: Sonic Boom, Volume I

5. FUNDING NUMBERS

537-03-21

6. AUTHOR(S)

Thomas A. Edwards, Editor

7. PERFORMING ORGANIZATION NAME(S) AND ADDRESS(ES)

Ames Research Center
Moffett Field, CA 94035-1000

8. PERFORMING ORGANIZATION REPORT NUMBER

A-94045

9. SPONSORING/MONITORING AGENCY NAME(S) AND ADDRESS(ES)

National Aeronautics and Space Administration
Washington, DC 20546-0001

10. SPONSORING/MONITORING AGENCY REPORT NUMBER

NASA CP-10132

11. SUPPLEMENTARY NOTES

Point of Contact: Thomas A. Edwards, Ames Research Center, MS 230-2, Moffett Field, CA 94035-1000; (415) 604-4465

12a. DISTRIBUTION/AVAILABILITY STATEMENT

Unclassified — Unlimited
Subject Category 02

12b. DISTRIBUTION CODE

13. ABSTRACT (Maximum 200 words)

The second High-Speed Research Program Sonic Boom Workshop was held at NASA Ames Research Center May 12–14, 1993. The purpose of this workshop was to provide a forum for government, industry, and university participants to present and discuss progress in their research. The workshop was organized into three sessions dealing with atmospheric propagation, acceptability, and configuration design. Attendance at the workshop was by invitation only.

Volume I includes papers on atmospheric propagation and acceptability studies. Significant progress is noted in these areas in the time since the previous workshop a year earlier. In particular, several papers demonstrate an improved capability to model the effect of atmospheric turbulence on sonic booms. This is a key issue in determining the stability and, ultimately, the acceptability of shaped sonic booms. In the area of acceptability, the PLdB metric has withstood considerable scrutiny and is validated as a loudness metric for a wide variety of sonic boom shapes. The differential loudness of asymmetric sonic booms is better understood, too.

14. SUBJECT TERMS

Sonic boom extrapolation, Sonic boom acceptability, Sonic boom minimization

15. NUMBER OF PAGES

238

16. PRICE CODE

A11

17. SECURITY CLASSIFICATION OF REPORT	18. SECURITY CLASSIFICATION OF THIS PAGE	19. SECURITY CLASSIFICATION OF ABSTRACT	20. LIMITATION OF ABSTRACT
Unclassified	Unclassified		